LA-8047-T
Thesis

C.3

A Statistical Model Investigation of Nuclear Fission

LOS ALAMOS SCIENTIFIC LABORATORY
Post Office Box 1663 Los Alamos, New Mexico 87545

This thesis was accepted by the University of Wisconsin, Madison, Wisconsin, in partial fulfillment of the requirements for the degree of Doctor of Philosophy in Nuclear Engineering. It is the independent work of the author and has not been edited by the Technical Information staff.

UNITED STATES
DEPARTMENT OF ENERGY
CONTRACT W-7405-ENG. 36

LA-8047-T
Thesis

UC-34c
Issued: October 1979

A Statistical Model Investigation of Nuclear Fission

Richard Edwin Pepping *

*Associated Western Universities, Inc., Graduate Student.
Present address: Sandia Laboratories, Fuel Cycle Risk Analysis, Organization No. 4413, Albuquerque, NM 87185.

CONTENTS

A STATISTICAL MODEL INVESTIGATION OF NUCLEAR FISSION

by

Richard Edwin Pepping

ABSTRACT

To assist in the improvement of fission product yield data libraries, the statistical theory of fission has been investigated. Calculation of the theory employs a recent nuclear mass formula and nuclear density of states expression. Yields computed with a simple statement of the theory do not give satisfactory results. A slowly varying empirical parameter is introduced to improve agreement between measured and calculated yields. The parameter is interpreted as the spacing between the tips of the fragments at the instant of scission or as the length of a neck in the fissioning nucleus immediately prior to scission. With this spacing parameter semi-quantitative agreement is obtained between calculated and measured mass chain yields for six cases investigated, $^{233}U(n_{th},f)$, $^{235}U(n_{th},f)$, $^{239}Pu(n_{th},f)$, $^{235}U(n+14,f)$, $^{238}U(n+14,f)$, and $^{252}Cf(sf)$. An indication of the source of mass asymmetry in fission is presented.

The model developed predicts a mass and energy dependence of some of the parameters of models currently in use in data generation. A procedure for the estimation of the fission product yields for an arbitrary fissioning system is proposed.

INTRODUCTION

Reliable nuclear data is required for both civilian and military applications of nuclear energy. In reactor operation, fission product buildup affects reactivity and fuel burnup through neutron absorption. The fission products themselves are sources of decay heat which must be taken into account in the design of safety systems. After leaving the reactor, shielding and cooling requirements of the spent fuel again demand that the composition be known in order to insure safe handling. In some cases of importance accurate measurements have been made to determine these sources. For less frequent fission events and for less well measured fissioning systems, modeling has been employed to estimate the yields of the various fission products. It is the object of this work to improve upon the method of yield estimation through the use of a reasonable physical model.

In selecting a model for use here, there are basically two schools of thought. By computing from first principles the dynamic behavior of a heavy nucleus as it proceeds from its original state to two fission fragments one may expect to understand the entire fission process in addition to understanding the probability of the formation of a given pair of fission fragments, the fission fragment yield. Such a calculation is possible, in principle, but is tedious and prohibitively expensive in practice. Alternatively, one may make a simplifying assumption that renders the exact details of the fission process of little importance and concentrates

upon the fission yields. Such a simplifying assumption would be to assume that the entire process is statistical, completely determined by the properties of the final state. This assumption appears to have been first made by Fong.[1]

That the fission process may indeed be statistical is indicated by examining the available data on fission yields. The distributions of product mass vary slowly between fissioning systems, differences which appear being understood through simple conservation laws. The mass yields also vary slowly with particle energy in particle-induced fission. Again, the final state appears to be the important factor in determining yields.

The application of statistical models to the fission process is not a new idea. Fong[1] presented the idea over 20 years ago and has written prolifically on the subject since then. More recently, calculations have been presented by other authors.[2,3] Most recently, Wilkins, et al.[4] gave an extensive treatment of the topic giving qualitative agreement with observations of many fissioning systems. It shall be the object of this work to investigate the statistical model to determine its validity in a quantitative sense for possible use in improving fission product data libraries.

As an aid to the reader, the following is a brief guide to the organization of the presentation that follows. The fission process is briefly reviewed in order to qualitatively describe the process and establish some of the language to be used to describe it. The theory is then cast quantitatively to demonstrate the

nature of the assumptions necessary to make the theory calculable. It should be kept in mind that a large number of things must be assumed, any one of which, if in error, is of sufficient consequence to change any conclusions dramatically. Given a set of assumptions, a number of things may be computed, in addition to the yields, as diagnostics and are discussed in the section "The Yield and Its Moments." Following this section, three sets of assumptions to be used in calculations are described and motivation given for their selection. After specifying some expressions necessary to the evaluation in the section titled "The Densities," the calculation may proceed.

The first yield calculation is performed for several reasons. It employs the density expression most similar to the other statistical model evaluations mentioned and gives historical continuity to this work. It also allows some experimentation with the masses and single-particle energy treatments. Most importantly, it is used to demonstrate the equivalence of two of the sets of assumptions, thereby simplifying the calculation. This particular calculation is performed with extreme computational care in order to insure that none of the conclusions made are the results of numerical artifacts.

Having become somewhat more at ease with the calculation and the various input quantities, a new density expression is introduced, a feature which, along with the mass formula, sets this

work apart from previous calculations. With this expression and the mass formula the model is completely free of adhoc parameters other than those explicitly appearing. After establishing the computational technique to be used with the new density, a set of sample yields is computed and discussed.

To obtain quantitative agreement, some parameterization is necessary in order to achieve overall agreement between measured and computed values of the chain-yields, prompt neutron number, total gamma energies, and total kinetic energy. In describing independent yields, the model employed when data is poorly known requires the use of some empirically determined parameters. Working backward, one may extract the values of these parameters from both the published yields and calculated yields. Comparing these values reveals some small differences. Possible reasons for these discrepancies are discussed.

Finally, observations of potential practical use by way of simple models and scaling relations are discussed. The various physical models necessary for the calculation are briefly discussed in several appendices. Any one of these subjects is, by itself, deserving of a thorough treatment. The appendices, however, describe only the features necessary for this calculation and their methods of implementation.

FISSION REVIEW

If one examines the familiar plot of binding energy per nucleon for stable nuclei,[5] it may be seen that nuclei near mass number 60

are most tightly bound with about 8.5 MeV of binding energy per nucleon. With increasing mass number the binding energy per nucleon decreases. For a sufficiently heavy nucleus it may then be energetically favorable for the nucleus to split into two lighter nuclei. To do this the heavy nucleus must deform and elongate to such a degree that the repulsive Coulomb force is sufficient to overcome the attractive nuclear force. At this point, the nucleus may split, or fission, rather than return to its ground state shape.

In order to describe the nucleus as it elongates, one must be able to describe its behavior as it proceeds along some trajectory in a multi-dimensional space of shape coordinates. Shapes that have been useful in describing the behavior specify such general quantities as elongation, mass asymmetry, axial asymmetry, and neck formation of the deformed nucleus. Initially, the heavy nucleus may resist deformation such that an elongation of its shape is accompanied by the increase in the potential energy of the system. At larger deformations the potential energy may actually begin to decrease, a manifestation of shell effects in the deformed nucleus. These shell effects depend strongly upon the shape of the nucleus. In the multidimensional shape space the potential energy surface may have many local maxima and minima. The minima are associated with so called shape-isomerism in heavy nuclei, metastable states of the deformed nucleus. At some point the Coulomb repulsion becomes sufficiently strong that it overcomes the nuclear attraction. The nuclear potential energy then decreases with further elongation. In general, any of the local

maxima define saddle-points in the potential energy. In the discussion that follows, the term "saddle-point" shall be used to refer to that shape at which the Coulomb repulsion and nuclear attraction exactly cancel.

As the nucleus proceeds beyond the saddle-point deformation, the shape may begin to resemble that of a dumbell with two lobes, the nascent fragments, connected by a neck. The Coulomb force may drive the elongation further until the nuclear restoring force is no longer able to hold the system together. The neck snaps and fission occurs. At this instant, called the scission-point, the system consists of two separate nuclei.

During the descent from saddle to scission the fragments may accelerate in the Coulomb field such that at the scission-point the fragments possess some translational kinetic energy associated with the motion of their centers of mass. Depending upon the exact nature of the descent and snap, they may also be rotating and their shapes vibrating. Beyond the scission-point the fragments may further accelerate in the Coulomb field. The energy associated with translational kinetic energy at the scission-point and the energy obtained from the Coulomb repulsion may be measured in the lab as the fragment total kinetic energy. The energy associated with rotation, shape vibration and deformation, and any internal excitation gained during the descent provides energy for prompt neutron and gamma ray emission. The distinction shall be made between fission <u>fragments</u> and fission <u>products</u>, the fragments being

the two nuclei immediately following scission and the products resulting after prompt neutron emission from the fragments.

THE THEORY

During the descent from saddle to scission, the nuclear shape is driven to further elongation, the nascent fragments acquiring translational kinetic energy, under the influence of Coulomb repulsion. Depending upon the nature of the nuclear Hamiltonian, the collective degrees of freedom may be coupled to internal degrees of freedom such that the collective motion is damped, some of the energy gained during the descent being converted into internal heat. At the scission-point an amount of energy, G, is released,

$$G = M^{*} - m_1 - m_2 - C$$

Here, M^{*} is the mass of the fissioning nucleus, m_i is the mass of the i^{th} fragment, and C is the Coulomb interaction energy. As a result of the strong Coulomb repulsion, the fragments may be deformed such that their masses are increased by the amount D relative to the ground-states values, m_{io}. Denoting collectively by $\vec{\alpha}$ any parameters assumed to describe the fragments' geometry at scission, G may be written,

$$G(\vec{\alpha}) = M^{*} - m_{1o} - m_{2o} - D_1(\vec{\alpha}) - D_2(\vec{\alpha}) - C(\vec{\alpha}) \quad .$$

This energy may appear as fragment excitation energy or rotational,

vibrational, and translational kinetic energy. Energies associated with rotation and vibration are neglected, justification of which is offered in Appendix C. The energy at the scission-point is assumed to be partitioned between intrinsic degrees of freedom, or heat, and collective translational kinetic energy degrees of freedom.

Formally, the decay width is given by the Fermi Golden Rule,[6]

$$\Gamma(A,Z,\vec{\alpha}) = |\langle f|H_{fiss}|i\rangle|^2 \rho(G) \quad ,$$

Here, A and Z specify the mass and charge of the light fragment, the mass and charge of the heavy fragment given by conservation laws, H_{fiss} is the perturbing Hamiltonian causing the decay, $|i\rangle$ denotes the initial state, the fissioning nucleus, and $|f\rangle$ denotes the final state, two fragments of specified mass, charge, and any other parameters, $\vec{\alpha}$, assumed to describe the scission configuration. Herein lies the problem.

Specification of the mass and charge division alone does not adequately describe the scission-point. Until the $\vec{\alpha}$-parameters are given, the calculation can not begin. These parameters are given by H_{fiss}, making it an extremely important quantity. This may be illustrated with regard to the nuclear shapes by assuming the phase-space density to be given by a constant temperature Boltzman expression,

$$\rho(G) = \exp(G/T) \quad ,$$

and H_{fiss} to be a constant for all possible final states. The most probable scission configuration is that for which G is a maximum. Wilets[7] has determined this configuration, in the limit of the liquid-drop behavior, to be two infinitely long nuclear needles of vanishing diameter. In a real nucleus, this limit is not attainable. The conclusion is similar, however, that the overriding factor is the Coulomb energy driving the shape to one of extreme elongation, a shape that may be attained with sufficiently many degrees of freedom.

For more modest deformations of the fragments another problem arises. The energy, G, to be partitioned must be positive. It has been suggested[1] that at the scission-point the fragments are tangent. Even for the largest deformations which the mass formula allows (Appendix A), positive values of G can not be obtained without introducing a spacing parameter, δ, to be interpreted as the distance between the tips of the fragments. Introduction of this parameter allows the Coulomb energy to be reduced sufficiently to allow positive values of G. As the parameter increases, G increases such that the most probable scission configuration corresponds to fragments at infinite separation with $C = D_1 = D_2 = 0$.

It would then appear that the nature of H_{fiss} is quite important since it is the only factor remaining which can prohibit these configurations so strongly favored through the phase-space term. Proceeding from first principles, one must then compute the behavior of the fissioning system as it descends from the saddle-

point to the scission-point, the end of the fission process, keeping track of all energies, coordinates, and quantum numbers. Having determined the scission-point shapes, separations, matrix elements, and energy partition, an important quantity to be discussed later, for all possible final states, the phase-space term may be computed for each and the yield of a given mass and charge given by integrating over the uninteresting variables.

The descent has only been calculated for a few nuclei, and then only in the context of a simplified model. Rather than attempt to solve this problem here, the Golden Rule shall be used with existing fission product yield data[8] to view the fission process in hope that the nature of H_{fiss} may be extracted. Clouding this view will be other assumptions and model limitations necessary to make the calculation possible.

THE YIELD AND ITS MOMENTS

It shall be assumed that, apart from determining the scission-point energy partitions and shapes, the matrix element is a constant. The shapes are presumed to be given by some distribution, $f(\vec{\alpha})$. The yield of a given fragment charge and mass is then proportional to the sum over $\vec{\alpha}$ of the decay widths,

$$y(A,Z) \propto \sum_{\vec{\alpha}} f(\vec{\alpha}) \cdot \Gamma(A,Z,\vec{\alpha}) = \sum_{\vec{\alpha}} \rho\,[G(\vec{\alpha})] \cdot f(\vec{\alpha}) \quad ,$$

with the definition,

$$I_y(A,Z) = \sum_{\vec{\alpha}} \rho[G(\vec{\alpha})] \cdot f(\vec{\alpha}) \quad .$$

The yield is given by normalizing,

$$y(A,Z) = \frac{I_y(A,Z)}{\sum_{A,Z} I_y(A,Z)} \quad .$$

To evaluate $\rho[G(\vec{\alpha})]$, thermal equilibrium shall be assumed between the intrinsic degrees of freedom and the collective translational kinetic energy degrees of freedom. Supressing the $\vec{\alpha}$ argument,

$$\rho(G) = \int_0^G \rho(k) \int_0^{G-k} \rho_1(E_1)\rho_2(E_2=G-k-E_1)\,dE_1\,dk \quad ,$$

where $\rho(k)$ is the density of states of translational kinetic energy, k, and $\rho_i(E_i)$ is the density of states of the i^{th} fragment at excitation energy E_i.

In addition to the yield integral, two moments of interest shall be computed,

$$I_E(A,Z) = \sum_{\vec{\alpha}} f(\vec{\alpha}) \int_0^G \rho(k) \int_0^{G-k} E_1 \rho_1(E_1)\rho_2(G-k-E_1)\,dE_1\,dk \quad ,$$

$$I_k(A,Z) = \sum_{\vec{\alpha}} f(\vec{\alpha}) \int_0^G k\rho(k) \int_0^{G-k} \rho_1(E_1)\rho_2(G-k-E_1)\,dE_1\,dk \quad .$$

With respect to the $\vec{\alpha}$-parameters, weighted averages may be computed for any quantity, Q,

$$I_Q(A,Z) = \sum_{\vec{\alpha}} Q(\vec{\alpha}) \cdot f(\vec{\alpha}) \cdot \rho[G(\vec{\alpha})] \quad .$$

Then the average value of any quantity is given by

$$\langle Q \rangle = \frac{I_Q(A,Z)}{I_y(A,Z)} \quad .$$

Of particular interest are the quantities <D>, <C>, <k>, $\langle E_1 \rangle$, and $\langle E_2 \rangle = \langle G \rangle - \langle k \rangle - \langle E_1 \rangle$.

These moments may be used as checks on the various parameters and assumptions. For example, after normalization, the moments, <k>, <C>, $\langle E_i \rangle$, and $\langle D_i \rangle$ may be compared to experimental values of the total fragment kinetic energy, <TKE>, and the decay energy for prompt neutron and gamma ray emission, X_i,

$$\langle C \rangle + \langle k \rangle = \langle TKE \rangle \quad ,$$

$$\langle D_i \rangle + \langle E_i \rangle = \langle X_i \rangle \quad .$$

With a table of neutron separation energies, an upper bound on the number of prompt neutrons may be determined from X_i.

In making comparisons between measured and computed yields, some of the terminology that shall be used is as follows:

1) Independent yield: the A and Z dependent yield, y(A,Z).

2) Mass-chain yield, mass yield, or chain-yield: the yield of a given mass, independent of charge,

$$y(A) = \sum_{Z} y(A,Z) \quad .$$

3) Charge yield: the yield of a given charge, independent of mass,

$$y(Z) = \sum_{A} y(A,Z) \quad .$$

Energies and diagnostic terms weighted by the independent yields and summed are referred to as integral values.

Within a fixed mass chain, the independent yields may be devided by the chain yield to form the fractional independent yield, fiy(A,Z),

$$fiy(A,Z) = \frac{y(A,Z)}{y(A)}$$

THE SCISSION CONFIGURATION

Before the calculation can begin, the parameters, $\vec{\alpha}$, describing the scission configuration must be specified. Since the fragments are neutron-rich, unstable, and highly deformed, experimental knowledge of their masses is not available. A mass formula must then be used to estimate the mass and its shape dependence. Seeger and Howard[9] give such a formula, described in Appendix A, with two parameters specifying the shape. These are the Nilsson parameters, ε and ε_4, used to describe the single-particle potential well of the nucleus. They describe axially symmetric shapes, only. Some

of the shapes considered are shown in Figure 1. Approximate values of the coefficients of a collective radial expansion in Legendre Polynomials corresponding to these shapes appear in Table 1. The charge is assumed to be uniformly distributed throughout the nuclear mass. Only multipoles of even order appear in a multipole expansion of the Coulomb interaction energy since only even order multipoles appear in nuclear potential. The scission configuration is then specified by four shape parameters and the spacing parameter, δ, which shall initially be held constant for all masses, charges, and shapes.

The distribution of shape parameters, $f(\vec{\alpha})$, is given by H_{fiss}. As an example of such a distribution, it has been proposed that the fissioning nucleus is extremely dissipative and that the descent from saddle to scission is so slow as to be quasi-static. If this is the case, it is argued,[1] the nucleus may follow a minimum potential energy trajectory on its way to scission. The energy release, G, is equivalent to the negative of the potential energy. Then a consistent method exists to define a scission-point configuration, which shall be called the GMAX configuration,

$f(\vec{\alpha}) = 1.$ $\quad G(\vec{\alpha})$ = maximum

$f(\vec{\alpha}) = 0.$ $\quad$ all other $\vec{\alpha}$.

More detailed investigations of the behavior of viscous liquid-drops reveal that the presence of high viscosity causes the trajectory to deviate considerably from that of minimum potential energy for the case of symmetric mass splits. It may then be anticipated that the view of the scission-point may be somewhat obscured

by computing yields at the GMAX shapes. Two other shape distributions, $f(\vec{\alpha})$, shall also be considered. Within the space of allowed shape combinations in the fragments, the yield integrals may be evaluated at all points and a yield surface determined for a given A and Z. Assuming $f(\vec{\alpha}) = 1.$ for all $\vec{\alpha}$, the yield is given by summing over all $\vec{\alpha}$, defining the SUM method. Having the yield surface, the shape combination at which it takes on maximum value defines the YMAX configuration and the YMAX shape distribution,

$$f(\vec{\alpha}) = 1. \qquad \rho[G(\vec{\alpha})] = \text{maximum} \quad ,$$

$$f(\vec{\alpha}) = 0. \qquad \text{all other } \vec{\alpha} \quad .$$

The interest in these three configurations may be seen in the following. Assume for the time being a constant temperature form for the phase-space term,

$$\rho(G) = \exp(G/T) \quad ,$$

The yield surface peaks at the GMAX configuration and may be approximated as a Gaussian about this point. The SUM method is then approximately the integration of a Gaussian, the result of which is the product of the peak value, the GMAX value, and a width parameter. To the extent that the yield surface is approximately Gaussian and the width parameter smoothly varying with mass and charge, the GMAX and SUM yields are identical, the width parameter entering as an overall constant which drops out of the yield expression upon normalization. Comparison of the two yields should indicate the validity of these assumptions.

In fact, the phase-space term is not of a constant temperature form. In addition to the G-dependence single-particle terms in the fragments affect the yield. It is for this reason that the YMAX yield is greater than that of the GMAX yield. Again, the SUM yield may be compared with the YMAX yield to test the validity of the assumption of Gaussian behavior about the YMAX configuration and the smoothness of the width parameter.

A practical problem arises with the YMAX and SUM yields, namely that the yield integrals must be evaluated at all combinations of the shape parameters. When possible, this is done. In the larger shape space ultimately to be considered, this is too tedious and a restricted area in the vicinity of GMAX is explored to find the YMAX configuration. The SUM method is too expensive to be applied in this case.

THE DENSITIES

A. The Kinetic Energy Density

The density of linear momentum states for a two-particle system of reduced mass, μ, in a volume, V, is given by,

$$\rho(k) = \frac{d}{dk} N(k) \quad ,$$

where k is the translational kinetic energy and N(k) is the total number of translational states of kinetic energy less than or equal to k,

$$N(k) = \frac{V}{h^3} \int_0^{p_{max}} d^3p$$

$$= \frac{4\pi V}{3h^3} p^3_{max}$$

$$= \frac{4\pi V}{3h^3} (2\mu k)^{3/2}$$

Hence,

$$\rho(k) = \frac{4\pi V}{h^3}\sqrt{2\mu^3 k}$$

The reduced mass of the two particles of approximate mass A_1 and A_2 is

$$\mu = \frac{A_1 A_2}{A_1 + A_2} \text{ mass units} \quad .$$

As only proportionalities are important, the expression used for $\rho(k)$ is taken as.

$$\rho(k) = \sqrt{(A_1 A_2)^3 k} \quad .$$

In later cases, the A_1 and A_2 terms are dropped, these being slowly varying quantities.

B. The Nuclear State Density

The density of states for a nucleus of N neutrons and Z protons at excitation energy E is formally defined as the inverse Laplace transform of the partition function, $\Omega(\alpha_N, \alpha_Z, E)$, for the system,

$$\rho(N,Z,E) = \frac{1}{(2\pi i)^3} \oint\oint\oint \exp[\Omega(\alpha_N, \alpha_Z, \beta) - \alpha_N N - \alpha_Z Z + \beta E] \, d\alpha_N d\alpha_Z d\beta \quad .$$

The partition function is computed separately for the neutron and proton systems,

$$\Omega(\alpha_N,\alpha_Z,\beta) = \Omega_N(\alpha_N,\beta) + \Omega_Z(\alpha_Z,\beta) \quad .$$

The contour integral may be well approximated at reasonable excitation energies by the saddle-point method,

$$\rho = \frac{e^S}{(2\pi)^{3/2} D^{1/2}} \quad ,$$

where S is the entropy,

$$S = \Omega - \alpha_N N - \alpha_Z Z + \beta E \quad ,$$

and D is the 3x3 determinant of the matrix of second derivatives of Ω with respect to α_N, α_Z, and β. Through the saddle-point approximation, the quantities α and β take on the identities of the chemical potential and reciprocal temperature of the system. All quantities are to be evaluated at the saddle-point, defined by the location of the peak of the integrand,

$$N = \frac{\partial\Omega}{\partial\alpha_N} \qquad Z = \frac{\partial\Omega}{\partial\alpha_Z} \qquad E = -\frac{\partial\Omega}{\partial\beta} \quad .$$

The partition function has been determined for a system of Fermions with a residual pairing interaction by Sano and Yamasaki.[11] Densities computed with this partition function have been investigated by Moretto[12] and Huizenga, et al.,[13-15] and are the basis for yields computed later. The formalism and its implementation are described in Appendix D.

By assuming the single-particle states to be uniformly spaced an analytical density expression may be obtained. The expression was first proposed by Bethe[16] and was later modified by several others[17-21] in order to improve agreement between predicted and measured neutron resonance spacings. The form of the density in the constant spacing limit is given by

$$\rho(E) = \frac{\sqrt{\pi}}{12} \frac{\exp(2\sqrt{aU})}{a^{1/4} U^{5/4}} ,$$

where U is the excitation energy and a is the "density parameter". It is upon the density parameter that effort has been concentrated since it allows the introduction of empiricism to account for the shortcomings of the constant single-particle spacing assumption. This expression is described in Appendix E.

The analytical expression is significant since it was the only expression available before fast electronic computers allowed the implementation of the more realistic method proposed by Moretto and Huizenga. It is still in use[22] and has been used by Fong to compute fission product yields.[1] Yields based on both methods will be presented in this work.

A SAMPLE YIELD CALCULATION BASED ON AN ANALYTICAL DENSITY FORMULA

As an example of the method of evaluation, yields are computed for $^{235}U(n_{th},f)$ assuming the nuclear density of states expression to be given by the analytical expression of Gilbert and Cameron.[17] This formula is discussed at length in Appendix E. The expression is written in two pieces and describes the density of states at

excitation energy, E,

$$\rho_H(E) = \frac{\sqrt{\pi}}{12} \frac{\exp(2\sqrt{aU})}{a^{1/4} U^{5/4}} \qquad E > E_x$$

$$\rho_L(E) = \frac{1}{T} \exp\left(\frac{E-E_o}{T}\right) \qquad E < E_x$$

The subscripts, L and H, refer to the value of E relative to a transition energy, E_x, L (low) for energies less than E_x and H (high) for energies above E_x. The two formulas are required to join smoothly at E_x, a condition which defines the two parameters appearing, T, the temperature, and E_o,

$$\frac{1}{T} = \sqrt{\frac{a}{U}}\Bigg|_{E_x} - \frac{5}{4U}\Bigg|_{E_x}$$

$$E_o = E_x - T \log [T \rho_H(E_x)] \quad .$$

The excitation energy in the high excitation energy form is written as U and is related to the excitation energy argument, E, by

$$E = U + P \quad .$$

P is the pairing energy of the nucleus. This particular statement accounts for the fact that there is a residual interaction, pairing, in the ground state of the nucleus. Its effect is to cause an overall shift of the energy axis. The transition energy, E_x, is actually given in terms of U_x,

$$U_x = E_x - P$$

where

$$U_x = 2.5 + 150/A$$

This result was determined empirically by Gilbert and Cameron.[17] The fit expression reproduces the data to approximately ± 200 keV. As shown in Appendices E and F, use of this formula also requires a single-particle shell energy, S, which enters through a, the density parameter. The density parameter is usually the object to be modeled when using this formula, as discussed in Appendix F.

Depending upon the value of E relative to the cross-over energy, E_x, three types of integrals are encountered in the yield calculation,

$$I_1 = \int k^{n/2} \int E^m \rho_L^{(i)}(E) \rho_L^{(j)}(G-k-E)\, dE\, dk$$

$$I_2 = \int k^{n/2} \int E^m \rho_L^{(i)}(E) \rho_H^{(j)}(G-k-E)\, dE\, dk$$

$$I_3 = \int k^{n/2} \int E^m \rho_H^{(i)}(E) \rho_H^{(j)}(G-k-E)\, dE\, dk \quad ,$$

where, for the yield, n = 1, m = 0, for the mement, $\langle I_E \rangle$, n = 1, m = 1, and for the moment $\langle I_k \rangle$, n = 3, m = 0. The subscripts refer to the form of the Gilbert and Cameron density, low excitation (L) or high excitation (H), and the superscripts index the single-particle parameters appropriate to that fission fragment. I_1 may be evaluated analytically. The order of integration in I_2 may be reversed and one integration performed analytically, the second

integration performed numerically. Both integrations in I_3 must be performed numerically.

For this first example, it is desired that the integrals be evaluated sufficiently accurately that numerical errors may confidently be ignored. Any choice of computational method must satisfy this requirement. To determine the method of numerical evaluation of the integrals, fragment data were scanned to determine extreme and median values of the energies, S, P, E_x, and T. Test cases were then chosen and the integrals evaluated by a standard adaptive Newton-Cotes Quadrature Rule[23] with a relative computational error of 10^{-9}. These same test integrals were then evaluated using Gauss-Legendre and Gauss-Laguerre Quadrature Rules[23] and compared to the Newton-Cotes values. Ultimately, combinations of 12-point Gauss-Legendre and Gauss-Laguerre Rules were chosen giving values that deviated by less than 7 parts in 10^4 from those of the Newton-Cotes. The Gauss Quadrature Rules are generally faster than the Newton-Cotes Rule making them more desirable.

Modeling of the density parameter, $\underline{a}$, is discussed in Appendix F. For this example, simple model forms shall be used. The model itself accompanies a set of single-particle shell and pairing energies, S and P, and is of the form,

$$a/A = p_1 - p_2 S \quad ,$$

where A is the mass number and p_1 and p_2 are constants. An older set of single-particle energies is that of Cook et al.[18] Values of p_1 and p_2 they give are

$p_1 = 0.120$

$p_2 = 0.00917$.

In order to compute the mass formula of Appendix A, S, and P values are again calculated, the results differing from those of Cook. Determining a model for the density parameter based upon these values gives,

$p_1 = 0.1624$

$p_2 = 0.0131$.

As mentioned in the Appendix A, the standard deviation of the computed and measured masses using the mass formula is about 700 keV. This is a rather large error on a term which appears in an exponential. The Garvey-Kelson recursion relations[24] give standard deviations between computed and measured masses of only 157 keV, but the relations do not give the deformation dependence of the mass. One may envision a mass formula which gives a ground-state mass according to Garvey-Kelson and a shape dependence according to the mass formula of Appendix A. While the two mass expressions differ by less than 2 MeV, on the average, it shall be shown that the effect upon the yields computed is quite pronounced. of the possible combinations of single-particle energies and masses, three combinations have been selected,

1) S and P values and ground-state masses taken from the mass formula of Appendix A.
2) Cook S and P values and Garvey-Kelson ground-state masses.
3) Garvey-Kelson ground-state masses and S and P values taken from the mass formula of Appendix A.

As with the Garvey-Kelson masses, the mass formula of Appendix A is used to determine the deformation dependence of the Cook shell and pairing energies. For all of these cases, a constant value of the spacing parameter, δ, was chosen with $\delta = 3$ fm. Also in this example, fragment shape degrees of freedom were restricted somewhat by not allowing ε_4 to vary freely. The shapes allowed were those of Figure 1 with ε_4 assuming the value for a given ε corresponding to the midline of the grid, i.e., ε_4 usually equal to zero.

The integrals must be evaluated at every combination of the shape parameters in each fragment. The YMAX configuration is that combination of shapes at which the yield integral is maximum and the GMAX configuration is that combination which maximizes G, which may be determined prior to actual evaluation of the integrals. At each point in the space of shape parameters, the energies essential to G, the Coulomb energy, the masses, the shell and pairing energies, must be computed. These may be recorded as diagnostics. Other quantities recorded for later reference are such things as the scission-point elongation of the fragments, the deformation energies, the parameters of the density of states expression, T, E_x, and E_o, or any combination of any of these quantities deemed of interest. The computed yields provide the weighting function for computing averages of these quantities. Of particular interest are two quantities averaged over all charges and masses, the total kinetic energy (TKE) of the fragments and the energy appearing in

prompt de-excitation, <D> + <E>. Assuming a simple neutron emission model, described in Appendix J, an estimate is made of the number of prompt neutrons, ν_p, and prompt gamma energy, E_γ. Experimental values of these quantities are[25]

$\nu_p = 2.40$

$E_\gamma = 6.96$ MeV

TKE = 169.6 MeV .

The yields obtained for each of the three cases for the GMAX, YMAX, and SUM methods are shown in Figures 2-10. For reference, the chain yields from ENDF/B[8] for this reaction are shown in Figure 11. The total kinetic energies, prompt neutron numbers, and total gamma energy appear in Table 2. Overall agreement is reasonable, the prompt neutron number being a little too high. This may be a result of the fact that the computed chain yield, the weight function for computing these averages, is displaced somewhat from the measured mass-chain yield.

Regarding the mass yield plots, the location of the fragment mass peaks seems least sensitive to the choice of masses and single-particle energies. The peaks are determined by the quantity,

$$G - P_1 - P_2$$

since, in the saddle-point approximation, the yield integral is proportional to

$$\exp[2\sqrt{(a_1 + a_2)(G-P_1-P_2)}]$$

where a_1 and a_2 are constants. The plot in Figures 12 shows

this quantity for the case of S and P values and masses as given by Seeger. The source of the peak is the shell correction term to the binding energy, shown in Figure 13.

Experimentally[8] the mass distribution rises smoothly to mass 90, is fairly flat from mass 90-100, peaking at 95, and drops into a valley about symetric mass splits. The ratio of the yields at mass 95 and 118 is about 600. The computed mass peaks are then 5 to 6 units too close to symmetry as compared to data. Still, the results are encouraging in light of the simplicity of the model.

The valley is well defined for yields computed assuming that the ground-state masses are given by the Garvey-Kelson formula. However, the Seeger mass formula, of Appendix A, gives a much more shallow valley in the YMAX and SUM cases and a third peak in the GMAX case. This serves as an illustration of the sensitivity of the calculation to the input quantities. As a general rule, it is not advisable to correct one mass formula with another. Since only the Seeger formula allows direct evaluation of the mass of nuclei in shapes other than that of the ground-state and has been tested for agreement with neutron-rich mass measurements in a few cases, as discussed in Appendix A, it is more desirable. It should not be surprising, however, if mass asymmetric yields are not easily achieved.

As mentioned in previous discussion, the hope here is to demonstrate the equivalence of either the YMAX or GMAX methods with the SUM method. The chain yield plots are qualitatively similar,

especially the results of the SUM and YMAX methods. The SUM method is dominated by the YMAX term, by definition. The variables over which the sum is performed are the shape variables describing the fragments at the scission-point so that the yield may be seen as a surface in the shape variables. If this surface is sharply peaked at the YMAX configuration, the SUM method may be seen as an integration over a sharply peaked surface. To the extent that this surface is Gaussian, the result is the YMAX value multiplied by some term typical of the width of the Gaussian. To the extent that the width variable is a constant or a slowly varying quantity between fragments, this term drops out of the yield expression upon normalization. The extent to which the YMAX and SUM yields are the same is then a measure of the constancy of this width parameter. There is one complicating factor.

The space of allowed shapes is somewhat limited in that in all of the three cases considered, the GMAX shape required that the heavy fragment assume the shape of maximum prolateness. The YMAX case had a prolatness corresponding to about 0.1 less than maximum value of ϵ, i.e., $\epsilon \simeq 0.6$ for GMAX vs $\epsilon \simeq 0.5$ for YMAX. With the distribution peaked so close to the edge of the shape grid, there may be some terms missing in the SUM method, all of the major contributing terms not appearing within the space of allowed shapes (Figure 1).

The problem may be cast somewhat more quantitatively in the following. Denoting by α the fractional elongation of the symmetry axis of the fragment relative to that of spherical fragment, the

effect upon the G energy of an elongation is given by the relationships,

$$D \propto \alpha^2 \qquad C \propto 1/R \qquad R \propto R_o \alpha \qquad R_o = r_o A^{1/3} \qquad r_o = 1.2254 \text{ fm}$$

where R is the fragment center-to-center distance. About the GMAX configuration, G is approximately parabolic in the α variables for each fragment, α_{light} and α_{heavy}. Then

$$G(\alpha) \simeq G_{max} + \sum_{\substack{i = light, \\ heavy}} \frac{1}{2}\left(\frac{\partial^2 G}{\partial \alpha_i^2}\right)_o (\alpha_i - \alpha_{o,i})^2$$

$$\simeq G_{max} - \left\{ \frac{D_{light}}{\alpha^2_{o,light}} + C\left[\frac{R_{o,light}}{R}\right]^2 \right\} (\alpha_{light} - \alpha_{o,light})^2$$

$$- \left\{ \frac{D_{heavy}}{\alpha^2_{o,heavy}} + C\left[\frac{R_{o,heavy}}{R}\right]^2 \right\} (\alpha_{heavy} - \alpha_{o,\,heavy})^2$$

From the average values of the yields computed, the necessary quantities are C = 166 MeV, R = 19 fm, D_{light} = 2 MeV, D_{heavy} = 15.5 MeV, A_{light} = 102, and A_{heavy} = 134. These values are representative of the three cases. Then,

$$G \simeq G_{max} - \left(\frac{\alpha_{light} - \alpha_{o,light}}{0.153}\right)^2 - \left(\frac{\alpha_{heavy} - \alpha_{o,heavy}}{0.093}\right)^2$$

In terms of the α-coordinates, the space of allowed shapes is limited to values of $\alpha \leq 0.43$. For the YMAX case, the average values are $\alpha \simeq 0.3$ in both fragments. To the extent that the width of the

SUM distribution about the YMAX configuration is measured by the values of the second derivatives of G about GMAX, the edge of the grid is too close to assure inclusion of all of the dominant contributing terms in the SUM method. Errors may be introduced into the YMAX and SUM comparisons as a result of this also. Comparison of the computed mass-chain yields between the YMAX and SUM results shows values in error by a multiplicative factor of 1.57 on the average with extreme values of 0.6 and 3.1 for the three cases considered. This type of error is compatible with those anticipated based upon limitations of the shape grid. The YMAX yield may then be assumed to be typical of the SUM yield, maximum error being a multiplicative $3^{\pm 1}$.

YIELD CALCULATIONS BASED ON THE MORETTO DENSITY FORMULA

To evaluate the yield and interest moments, three integrals must be evaluated,

$$I_y = \int_0^G \int_0^{G-k} k^{1/2} \rho_1(E_1) \rho_2(G-k-E_1)\, dE_1 dk$$

$$I_E = \int_0^G \int_0^{G-k} E_1 k^{1/2} \rho_1(E_1) \rho_2(G-k-E_1)\, dE_1 dk$$

$$I_k = \int_0^G \int_0^{G-k} k^{3/2} \rho_1(E_1) \rho_2(G-k-E_1)\, dE_1 dk \quad .$$

Integral I_y is the unnormalized yield, I_E is the excitation energy moment, and I_k is the translational kinetic energy moment. The

quantities in the integrands are $\rho_i(E_i)$, the density of states of the i^{th} fragment at excitation energy E_i, G, the energy released at the scission point, and k, the prescission translational kinetic energy. In this case, $\rho(E)$ is assumed to be given by the Moretto density expression[12] developed in Appendix D. By this method the thermodynamic functions necessary to determine the density of states are evaluated as sums over realistic single-particle states. In Appendix D, spline fits are determined to the required functions in terms of the temperature, T, of the excited nucleus. Recall the definition,

$$\beta_i = \frac{1}{T_i} = \frac{d\ell n \rho_i(E_i)}{dE_i}$$

Having these analytical expressions, the integrals may be evaluated employing the numerical techniques used to evaluate the integrals over the analytical density expressions. However, with little loss of accuracy, these integrals may be evaluated by the saddle-point technique. Very simply, this means that the integrand is approximated as a Gaussian completely described by a width and a peak value. The integration limits are extended to $\pm \infty$ with the following expression resulting,

$$I = \iint f(x,y)dx\ dy = 2\pi f(x_o,y_o)\ \frac{1}{D^{1/2}} \quad .$$

D is the determinant of 2^{nd} partial derivatives of $\ell n\ [f(x,y)]$

evaluated at the saddle-point, $x_o y_o$. The saddle-point is defined by the solutions to

$$\frac{\partial \ell nf}{\partial x} = 0 \qquad \frac{\partial \ell nf}{\partial y} = 0 \quad .$$

Applying these conditions to the yield integral, I_y, the following equations must be solved

$$T_1(E_{1o}) = T_2(E_{2o})$$

$$k_o = 0.5T_{1o}$$

$$G - k_o - E_{1o}(T_1) - E_{2o}(T_2) = 0 \quad .$$

The second derivatives are, denoting $f_y = \ell n[k^{1/2}\rho_1\rho_2]$

$$\frac{\partial^2 f_y}{\partial k^2} = \frac{-1}{2k_o^2} + \left.\frac{\partial \beta_2}{\partial E_2}\right|_o \qquad \frac{\partial^2 f_y}{\partial E_1^2} = \left.\frac{\partial \beta_1}{\partial E_1}\right|_o + \left.\frac{\partial \beta_2}{\partial E_2}\right|_o$$

$$\frac{\partial^2 f_y}{\partial k \partial E_1} = \left.\frac{\partial \beta_2}{\partial E_2}\right|_o \quad .$$

Since $E_i = E_i(\beta \text{ only})$, $\frac{\partial \beta_i}{\partial E_i} = \frac{d\beta_i}{dE_i}$. Hence, in addition to the splines determined in Appendix D, splines are also needed for $E_i(T_i)$ and $\frac{d\beta_i}{dE_i}$. This derivative was computed exactly, but it was found that the spline approximation to $E_i(T_i)$ was so good that the spline itself could be differentiated to give this quantity with better than 1% agreement to the exact evaluation.

For the integral, I_E, the saddle-point is given by

$$T_2 = (E_1 T_1)/(E_1 + T_1)$$

$$k_o = 0.5 T_2$$

$$G - k_o - E_1(T_1) - E_2(T_2) = 0 \quad .$$

Letting $f_E = \ell n[E_1 k^{1/2} \rho_1 \rho_2]$, the second derivatives are

$$\frac{\partial^2 f_E}{\partial k^2} = \frac{-1}{2k_o^2} + \frac{\partial \beta_2}{\partial E_2}\bigg|_o \qquad \frac{\partial^2 f_E}{\partial E_1 \partial k} = \frac{\partial \beta_2}{\partial E_2}\bigg|_o$$

$$\frac{\partial^2 f_E}{\partial E_1^2} = \frac{-1}{E_{1o}^2} + \frac{\partial \beta_1}{\partial E_1}\bigg|_o + \frac{\partial \beta_2}{\partial E_2}\bigg|_o$$

For the integral I_k, the saddle-point is given by

$$T_1 = T_2$$

$$k_o = 1.5\, T_1$$

$$G - k_o - E_1(T_1) - E_2(T_2) = 0 \quad .$$

Letting $f_k = \ell n[k^{3/2} \rho_1 \rho_2]$, the second derivatives are

$$\frac{\partial^2 f_k}{\partial k^2} = \frac{-3}{2k_o^2} + \frac{\partial \beta_2}{\partial E_2}\bigg|_o \qquad \frac{\partial^2 f_k}{\partial E_1^2} = \frac{\partial \beta_1}{\partial E_1}\bigg|_o + \frac{\partial \beta_2}{\partial E_2}\bigg|_o$$

$$\frac{\partial^2 f_k}{\partial E_1 \partial k} = \frac{\partial \beta_2}{\partial E_2}\bigg|_o \quad .$$

Hence, the saddle-point approximation yields simple plug-in formulas by which all integrals may be evaluated. The accuracy of the approximation must be determined.

To test the validity of the saddle-point approximation, assume the density of the states to be given by

$$\rho(E) = \exp\left(2\sqrt{aE}\right) .$$

For this experiment, the a-parameter shall be assumed to be given by

$$a = A/9.5\ \text{MeV}^{-1}$$

where A is the mass number, and empirically observed result[26]. To span the range of values anticipated, values of A_1 assumed were A_1 = 75, 95, and 118 with A_2 given by 236 - A_1. The integrals were evaluated using a standard 7-point Newton-Cotes Quadrature Rule[23] and the results compared to the saddle-point approximation for values of G ranging from 1 to 65 MeV. The Newton-Cotes evaluation was carried out to a relative computational error of 10^{-4}. The approximation for I_y reproduced the Newton-Cotes value to within 25% at 1 MeV, the error dropping to 2% at 5 MeV and increasing monotonically to 10% at G = 65 MeV. This monotonic error indicates a small systematic error in the saddle-point approximation, but its smallness make the expression acceptable. In the case of the integral, I_E, the saddle-point expression reproduced the Newton-Cotes values very well with an error of 5% at 1 MeV and a monotonically decreasing error with increasing G. The k-moment integral, I_k, was consistently low by about 10% relative to the Newton-Cotes value.

The small value of k predicted by this theory, $k \simeq 1$ MeV, makes this error of little consequence.

A SAMPLE YIELD BASED ON THE MORETTO DENSITY FORMULA

Consider the prediction of yields for the reaction $^{235}U(n_{th},f)$ using the spline fit expressions for the thermodynamic functions required to evaluate the density of states expression according to the Moretto prescription[12] (Appendix D). As an example, assume the spacing parameter, δ, to be a constant for all mass and charge splits, $\delta = 3$ fm, and allow both shapes of freedom, ε and ε_4 in each fragment. Two cases are considered, described previously, the GMAX and YMAX cases. The YMAX method is modified somewhat by requiring the YMAX configuration to lie in the vicinity of the GMAX configuration. This is done by exploring the shape combinations about GMAX until the local maximum is found. This is necessary due to the size of the space of possible shape combinations. With 39 shapes possible in each fragment, there are 39 x 39 combinations for which the yield integral would have to be evaluated. This is simply too expensive. Recall that the interest in the YMAX configuration comes from the possibility that single-particle effects may displace the centroid of the shape distribution from that expected by assuming a minimum potential energy configuration. Masses are taken from the Seeger and Howard[9] mass formula. There are no explicit single-particle energies, S or P.

In Figure 14, the GMAX and YMAX yields are shown. Both yields rise rapidly to about mass 90 and then more slowly toward symmetry.

The GMAX shows a local minimum at mass 102. Both yields favor even mass numbers. The energy to be partitioned is shown for both cases in Figure 15. The behavior is similar to the yield with the obvious pairing effect. The source of the GMAX dip in the yield at mass 102 is apparent in the GMAX G. The dip is suggested in the YMAX G but is totally absent in the YMAX yield. To explain this, the effect of single-particle corrections upon the density of states must be investigated. In the YMAX case, the single-particle shell correction energies for the fragments sum to -1.5 MeV in the vicinity of mass 102 whereas the same energies sum to +0.5 MeV in the GMAX case. This may be understood in the context of the analytical density formulation, namely, that the nuclei with the smaller shell corrections have the larger level densities.

This calculation was repeated for 6 values of δ such that the yield and configuration parameters were scanned through values of $1 \text{ fm} \leq \delta \leq 7 \text{ fm}$. Similar yields were obtained and, based on this fact alone, it is concluded that the statistical model of fission based on the assumption of fixed scission-point tip-to-tip separation is not very good. One point is noteworthy and has implications regarding the analytical density formulation. In Figure 16 are plotted the values of the spectrum averaged values of the single-particle shell energies for the fragment (light) and compliment (heavy). These plots seem to support the observation of Gilbert and Cameron[17] regarding the effect of the shell correction energy upon the density.

A caveat is in order here. In computing the YMAX and GMAX yields, the shapes of the fragments at the scission-point was recorded. For the earlier yield calculation based on the analytical density model, mention was made of the fact that the scission configuration usually occurred at maximum values of the ε shape parameter, $\varepsilon = 0.6$. In the case of yields based on the Moretto density with two shape degrees of freedom, ε and ε_4, the problem with ε is diminished. However, the values of ε_4 now assume the prolate maximum (see Figure 1). It would be a tedious but straightforward process to extend the space of allowed shapes in the ε_4 degree of freedom. To do so, however, would be to admit some rather unphysical shapes, shown in Figure 17, with surface ripples and sharp corners. Looking at the fragment elongations for the two cases in this yield example, α_{light} and α_{heavy},

	$\alpha_{,light}$	$\alpha_{,heavy}$
GMAX	0.504	0.494
YMAX	0.441	0.504

With both ε and ε_4 degrees of freedom available, the maximum elongation is 0.613. In the case of ε only varying, the maximum elongation is 0.432 (Appendix H and Table 1). It may be seen that while the maximum value of ε was not attained, a greater elongation was attained. This is a manifestation of the effect described in the discussion of the scission configuration: as more shape degrees of freedom are added to the collective shape description, the GMAX configuration assumes shapes of greater elongation until, with

infinitely many degrees of freedom, the shape is that of an infinitely long needle.[7] Of course, before that limit is attained, the description of the nucleus via the mass formula breaks down completely.

SEMIQUANTITATIVE AGREEMENT

The yields computed for fixed values of δ bear little resemblance to experimental data. The yield integrals are quite sensitive to δ through the energy release, G. Allowing δ to become a free variable depending upon such things as mass, charge, and incident neutron energy, it may be possible to parameterize the yield in terms of δ in a way which varies smoothly between fissioning systems.

In any comparison made between computed scission-point yields and measured fission product yields, a treatment of prompt neutron emission is necessary. The emission of prompt neutrons appears to be post-scission phenomenon, the neutrons emitted from highly excited fission fragments. Models have been developed to treat the general problem of the decay of highly excited nuclei. These are, in general, too expensive considering the large number of nuclei for which such calculations would be performed. Two simple treatments are presented in Appendix J. These are proposed as methods of estimation of the number of prompt neutrons which may be emitted from the fragments.

To further minimize the effect of prompt neutrons, a parameterization is attempted in terms of the fragment charge. While

the charge yield is not affected by the emission of prompt neutrons, it may be affected by any beta-decay contamination in the data. That such contamination may be present is indicated by the fact that the yield for a given charge is not necessarily equal to that of the complimentary charge in the accepted data set.[8] In the absence of better information, the yield of a given fragment charge is assumed to be the average of the yields of that charge and its compliment.

Yields are computed, y_c, for all masses and charges for seven values of δ, 1 fm $\leq \delta \leq$ 7 fm, giving a set of $y_c(A,Z,\delta)$. These values are then lumped according to charge to give the charge yield, $y_c(Z,\delta)$,

$$y_c(Z,\delta) = \sum_A y_c(A,Z,\delta) \quad .$$

For a given Z, $\log[y_c(Z,\delta)]$ is a smooth function of δ allowing cubic spline interpolation for intermediate values. Assuming some δ_o and Z_o, the solution of

$$\frac{y_c(Z,\delta)}{y_d(Z)} = \frac{y_c(Z_o,\delta_o)}{y_d(Z_o)} \quad ,$$

for all Z, where y_d is the measured (data) yield of a given charge, gives a family of $\delta(Z;Z_o,\delta_o)$ which reproduces the charge yields. To make the final comparison, the logarithms of the computed yields, $y_c(A,Z,\delta)$, are also interpolated using cubic splines in δ. Figure

18 shows the smooth behavior of both charge and independent yields integrals.

As an example, yields for $^{235}U(n_{th},f)$ were computed for both the YMAX and GMAX cases for seven values of δ. Assuming $Z_o = 46$ and $\delta_o = 2$ fm, the family of $\delta(Z)$ shown in Figure 19 results. Using these $\delta(Z)$, the yields were redetermined and are shown in Figures 20 and 21. The two treatments of prompt neutrons described in Appendix J give the final fission product yields shown in Figures 22 and 23. In general, the YMAX yields are smoother and more satisfactory than the GMAX yields and the simple cascade treatment of prompt neutrons is better than the 2T model. Small discrepancies in the computed and measured charge yields, Figure 21, are apparent. This is due to the fact that, in spite of the smooth behavior predicted in Figure 18, the computed yield has some small discontinuous variation as G, increasing with δ, allows other terms to "turn on" and contribute to the total charge yield.

Other integral quantities are of interest here, the total number of prompt neutrons, ν_p, and the total energy available for gamma-ray emission, E_γ, computed from the two neutron models, the prescission kinetic energy, k, the Coulomb energy at the scission point, C, and the average cooling energy, the total energy of de-excitation taken away by emitting a neutron, E_{cool},

	CASCADE		2T	
	GMAX	YMAX	GMAX	YMAX
γ_p	3.96	4.21	3.52	3.77
E_γ	5.43	5.01	7.66	7.41
E_{cool}	7.32	7.45	7.70	7.72
k	1.42	1.38	1.42	1.38
C	158.	157.	158.	157.

All energies are given in MeV. Energy accounting is very good with ν_p x cooling + E_γ, the energy in prompt de-excitation channels, agreeing to within 0.5 MeV for the two neutron treatments for both the YMAX and GMAX cases. Again, the Simple Cascade Model prompt neutron treatment fission product spectra (Figure 23) agrees better with the experimental yields. The total number of prompt neutrons for this case is high by about 1.5 while the total gamma energy is only about 1 MeV low. It then appears that the total fragment excitation energy is high by 10-12 MeV, rather than improperly distributed, on the average, between neutron and gamma decay. Note also that the total fragment kinetic energy, k + C, is low by about 10 MeV.

Up to this point it has been assumed that all of the energy, G, is to be partitioned. From this example, however, it appears that 10 MeV or so of the G energy should be constrained to remain in the translational kinetic energy degree of freedom, i.e., $G = k_o + E_1 + E_2 + k$, with $k_o \approx 10$ MeV. Then $G - k_o$ is the energy to be partitioned. Note that the postulated slow, quasi-static descent from saddle-to-scission[1] is incompatible with the apparent

requirement of a high prescission kinetic energy to achieve overall agreement with experimental observation. A scission configuration which nearly satisfies experimental observed values of the total fragment excitation energy, translational kinetic energy, and yield distribution may be achieved by carefully choosing an amount of energy to be shifted into a constant k_o coupled with the $\delta(Z)$ determination.

In the process of determining the $\delta(Z)$, the energies relevant to determining any energy to be shifted into k_o may also be determined as functions of Z and $\delta(Z)$ and interpolated with cubic splines in δ. The energies of interest are G, the energy released at the scission-point, the scission-point Coulomb energy, C, and the scission-point energy of deformation, D. All quantities used are the spectrum-averaged values. Assuming $Z_o = 46$ and examining these energies as functions of the value of δ_o, the following results are obtained from the GMAX case:

δ_o	<G>	<C>	<D>
2	21.9	158.	14.03
3	32.2	152.	9.57
4	41.6	145.	7.16
5	49.4	138.	6.40
6	56.9	133.	4.36
7	63.3	129.	3.06

All energies are in MeV. For the case of $\delta_o = 2$ fm, the GMAX yield gives $\nu_p = 3.96$ and an average neutron cooling energy of 7.32

MeV/neutron. For this case, the value, <G> = 21.9 MeV, yielded 6 or 7 charges for each mass, similar to ENDF/B.[8] This value may be taken as a lower bound on <G> with lower values giving to few charges. The prompt neutron yield is governed by the sum of the excitation and deformation energies, <E> + <D>. For the purpose of this exercise, it shall be assumed that <E> $\simeq$ <G> since <k> is generally small. The value of ν_p is high by about 1.5 in the δ_o = 2 fm case.[8] At 7.32 MeV cooling energy, the indication is that <G> + <D> is high by about 1.5 x 7.32 MeV $\simeq$ 11.0 MeV. The amount of energy necessary for the desired number of prompt neutrons is then about (21.9 + 14.03) - 11.0 $\simeq$ 25.0 MeV. By increasing the value of δ_o, the energy, G, in excess of about 22.0 MeV may be arbitrarily moved into the prescission kinetic energy degree of freedom and, after adding the Coulomb energy, compared to the experimental value. At the same time, the sum of the deformation energy and G may be compared to the value needed for the prompt neutrons and gammas, 25.0 MeV. Defining the energy which may be shifted, Δ, as

$$\Delta = \langle G \rangle - 21.9 \text{ MeV} \quad ,$$

the total kinetic energy is given by <k> + <C> + Δ. The energy for prompt neutrons and gammas is <E> + <D> = <G> + <D> - <k> - Δ $\simeq$ <G> + <D> - Δ . The following results are obtained:

δ_o	Δ	$\langle C \rangle + \Delta$	$\langle G \rangle + \langle D \rangle - \Delta$
3	10.3	162.3	31.47
4	19.7	164.7	29.06
5	27.5	165.5	28.03
6	35.0	168.0	26.26
7	41.4	170.4	24.96

Recalling the k is of the order of 1 MeV and that the gamma ray energy was low by about 1 MeV, some δ_o between 5 and 6 fm should give acceptable results.

Assuming $\delta_o = 5$ fm and $Z_o = 46$, the computed G-energy is arbitrarily shifted by 27.5 MeV. The yield integrals are evaluated at 5, 6, and 7 fm and quadratic splines used to interpolate intermediate values of δ. Fitting gives the family of $\delta(Z)$ shown in Figure 24. Using these values, the yields were recomputed. In Figures 25 and 26 the fragment mass and charge distributions resulting are shown. Assuming the simple cascade treatment (Appendix J) of the prompt neutrons, the fission-product distribution shown in Figure 27 results. Again, YMAX yields are somewhat better than GMAX yields.

Energy accounting may be performed. The spectrum averaged energies of interest are

	GMAX	YMAX
ν_{pl}	1.223	1.067
ν_{ph}	1.586	1.948
$E_{\gamma l}$	2.338	2.230
$E_{\gamma h}$	2.412	2.890
$cool_l$	7.401	7.427
$cool_h$	7.073	7.162
C	141.3	139.4
k	28.33	28.28

Again, energies are in MeV. Where appropriate, the terms are listed separately for the light(l) and heavy(h) fragment. Experimental values are available[8,25] for ν_p, E_γ, and total kinetic energy, $\overline{TKE}$, a bar over the quantity denoting an experimental value,

$\overline{\nu}_p$ = 2.40

$\overline{E}_\gamma$ = 6.96 MeV

$\overline{TKE}$ = 169.6 Mev

The computed number of neutrons is high and the gamma energy low. With the average cooling energy available for each emitted neutron, ΔE_ν may be defined,

$$(\nu_{pl} + \nu_{ph} - \overline{\nu}_p) \times \left[\frac{\nu_{pl} \times Cool_l + \nu_{ph} \times Cool_h}{\nu_{pl} + \nu_{ph}} \right] = \Delta E_\nu \quad .$$

Here, ΔE_ν is the estimate of the excess excitation energy in the neutron decay channel. For the gamma decay channel, a similar

quantity may be defined,

$$(E_{\gamma l} + E_{\gamma h} - E_{\gamma}) = \Delta E_{\gamma} \quad .$$

Then the total excitation energy excess may be defined,

$$\Delta E_{\nu} + \Delta E_{\gamma} = \Delta E \quad .$$

In making this definition, any excess energy in either channel may be compensated by an energy deficit in the other. Recalling that gamma competition has been ignored in this simple neutron treatment, it is likely that the available energy has been improperly partitioned between these channels. The following table results:

	$(\nu_{pl} + \nu_{ph} - \overline{\nu}_{p})$	ΔE_{ν}	ΔE_{γ}	ΔE
GMAX	0.41	2.95	-2.21	0.74
YMAX	0.62	4.46	-1.84	2.62

The resulting ΔE values indicate a little excess excitation energy in the fragments although the original estimate of 25 MeV was not too bad.

The total kinetic energy in this model is given by the Coulomb energy and the constrained and computed prescission kinetic energies,

	TKE	TKE-$\overline{\text{TKE}}$
GMAX	169.6	0.
YMAX	167.7	-1.9

Adding these errors to those in the excitation energy, the GMAX results appear consistent, within the accuracy of the mass formula,

with the 5 fm scission configuration. The YMAX case could perhaps be improved by shortening the separation by a few tenths of a fm.

In Figure 24 it should be noted that $\delta(Z)$ has not been determined for $Z \leq 27$. The experimental data extend to $Z = 23$. The yields computed for these charges is zero because the value of G is negative after the k_o energy is removed. Even by reducing k_o to zero, $\delta(Z)$ can not be determined for $Z = 23$ and 24 without extending the current allowed maximum value of the parameter, $\delta_{max} = 7$ fm. This would then admit extremely large scission separations. While it may not be unreasonable to expect k_o to vary with mass and charge, introduction of such a variation without theoretical guidance or experimental evidence for such behavior reduces to further paramaterization. Considering that the computed and measured charge yields agree well over 5 orders of magnitude (Figure 26), concern over the behavior of these low probability events is not warranted and shall not be addressed here.

Note that in the analysis of the various scission-point energies, only GMAX quantities were considered. The additional shape degree of freedom in the YMAX configuration introduces a random variation making it difficult to determine the configuration which simultaneously satisfies all constraints. It was observed empirically that the YMAX quantities computed from a scission configuration determined by GMAX energies generally gave acceptable agreement. This same procedure was used in the determination of all subsequent scission-point configurations.

It is not out of place at this time to compare the empirically determined scission configuration to that given by calculation of the dynamic behavior of viscous liquid-drops. These calculations describe symmetric fission only and vary depending upon the nature of the assumed potential energy and viscosity.[10,27-30] Typically, results indicate k_o to be in the region of 20 to 30 MeV and values for the spacing parameter, δ_o, and elongation (with $\varepsilon_4 = 0$) parameter may be inferred giving $\delta_o = 3.5 - 7.5$ fm and $\varepsilon = 0.35 - 0.55$.[31] The scission parameters determined empirically, $\delta_o = 5$ fm and $k_o = 27.5$, are not out of line with these predictions.

The method described above has been applied to five other fissioning systems with similar results. In each case, Z_o is chosen to correspond to the value of the charge for symmetric splits and δ_o was chosen to be 5 fm. The minimum value of G is chosen each time to correspond to that value given with $k_o = 0$ and $\delta_o = 2$ fm, that value always giving the desired 6-7 charges yielded for each mass. k_o is then determined by the value of G at 5 fm in excess of the value of G at 2 fm. The systems considered, the experimental energies to be obtained, and the values of k_o determined are here tabulated.[8,25]

		$\overline{\nu}_p$	$\overline{E}_\gamma$	$\overline{TKE}$	k_o
1.	$^{233}U(n_{th},f)$	2.49	7.60	167.4	28.0
2.	$^{239}Pu(n_{th},f)$	2.87	7.78	176.0	28.0
3.	$^{235}U(n+14MeV,f)$	4.37	6.96	169.6	25.0

		$\overline{\nu}_p$	$\overline{E}_\gamma$	$\overline{TKE}$	k_o
4.	$^{238}U(n+14MeV,f)$	4.43	6.26	170.0	25.2
5.	$^{252}Cf(sf)$	3.76	8.60	185.7	27.0

The $\delta(Z)$ and the yields computed with them are shown in Figures 28-47. Comparing prompt neutrons, prompt gamma energy, and total kinetic energy, as for the $^{235}U(n_{th},f)$ case, Table 3 is obtained. As expected, the predicted charge yields agree well with measured values. The YMAX yields are, in general, smoother than the GMAX yields. The comparisons in Table 3 show the energies agreeing within a few MeV, the most noticeable error coming from the improper partitioning of energy between neutron and gamma decay channels due to the simplistic neutron treatment. The six sets of $\delta(Z)$ parameters are shown in Figures 48 and 49. Apart from the even-odd variation, all vary rather smoothly as the charge deviates from the symmetric split value, Z_{sym}. The spontaneous and 14 MeV neutron fission cases all tend to follow the same smooth trend. The Uranium thermal fissioning systems follow a parallel, but displaced, trend relative to these cases. Plutonium is somewhat peculiar in that it behaves as the thermal Uranium cases near symmetric splits and is more similar to the spontaneous and 14 MeV fission cases in the vicinity of the mass peaks and more asymmetric regions, about five charge units from Z_{sym} in this case. The rise in $\delta(Z)$ values moving away from symmetric splits seems to be related to the magnitude of the peak-to-valley ratio. The thermal systems, having the largest values of this ratio, have $\delta(Z)$ rising

most rapidly, smooth behavior followed after reaching the yield peaks, five to seven charge units away from Z_{sym}.

INDEPENDENT YIELDS

Having a model which qualitatively reproduces the measured mass yields, the question of independent yields, the distribution of charges yielded for a given mass, may be addressed. For fixed mass, the yield of a given charge has been observed to be given by a Gaussian about some peak value, Z_p,[32]

$$y(A,Z) = \frac{y_p(A)}{\sigma\sqrt{2\pi}} \exp[-(Z-Z_p)^2/2\sigma^2]$$

More recently, pairing effects have been observed,[33-35] superimposing an even-odd fluctuation onto the Gaussian. The model, for fixed mass, is then characterized by three parameters, Z_p, σ, and Δ_z, the pairing term. Empirically, Z_p is known to differ by about one charge unit from that value predicted by Unchanged Charge Distribution (UCD),

$$Z_{p,UCD} = (Z_o/A_o)\ A \quad ,$$

where Z_o and A_o characterize the fissioning system. The value of σ used to determine yields when data is poorly known is[35]

$$\sigma = 0.56 \pm 0.06 \quad .$$

Pairing enhancements have been reported to cause fluctuations of about 23% about Gaussian behavior for $^{235}U(n_{th},f)$[35] depending upon whether or not the fragment charge is even or odd. A similar effect is anticipated with regard to neutron pairing, however, prompt neutron emission is expected to wash-out this effect. The

value reported is about 4%.[35] In any case, this is a small effect to expect to see with a 10% calculation. Other errors resulting from the $\delta(Z)$ parameterization are also expected to affect computed quantities. All computed yields are nevertheless examined to extract model predictions of these quantities. The yield expressions are evaluated and fit, within a given mass chain, to a Gaussian in Z,

$$\log[y(Z)] = aZ^2 + bZ + c + (-)^Z\Delta_Z \quad .$$

Having determined these coefficients, the model parameters are given by

$$Z_p = -b/2a$$
$$\sigma = -1/2a$$

$$\text{even-Z enhancement} = \exp[(-)^Z\Delta_Z] - 1 \quad ,$$

then, $y_p = \exp(c - Z_p^2/2\sigma^2)$. Instead of listing the value of Z_p, its value relative to UCD is noted. All quantities are then computed for both the YMAX and GMAX configurations. The results for $^{235}U(n_{th},f)$ are typical and are shown in Figures 50 and 51. The averaged results are listed in Table 4.

Figures 50 and 51 show a great deal of noise, but some of the gross features may be understood. The value of Z_p is expected to be greater in the light fragment than that value predicted by UCD. This is a result of the behavior of the masses. For a given mass number, the masses of the members of that isobaric family exhibit

an approximately quadratic behavior in the charge or neutron number, Z or N, and make a small excess of charge in the light fragment an energetically more favorable split. The magnitude of the preferred excess is proportional to the difference between the masses of the light and heavy fragments. This behavior in Figure 50 is not as apparent in Figure 52, where $\delta(Z)$ is held constant at 5 fm. The effects of $\delta(Z)$ varying within a mass chain may be understood since the $\delta(Z)$ values are larger for lower Z members of the mass chain. This enhances their yields somewhat, drawing the peak of the distribution toward lower Z-values, closer to UCD. For the case of $^{235}U(n_{th},f)$ the $\delta(Z)$ values used appear in Figure 24. The variation of $\delta(Z)$ is most rapid in the vicinity of symmetric splits and is more pronounced in the GMAX case than in the YMAX case. Near symmetry the mass difference is small and the light mass preference for excess charge weak. In this vicinity the effect of $\delta(Z)$ varying may be seen as causing the Z_p value to become less than the UCD prediction in Figure 50. Also apparent is the smaller effect in the YMAX case than in the GMAX case.

The effect of prompt neutrons upon the deviation of Z_p from UCD may be understood by noting that the emission of neutrons reduces the mass while holding the charge constant. The resulting product is then less neutron-rich than the fragment, having a charge-to-mass ratio more than that of the fragment. The effect, to lowest order, is to shift the curve of Figure 50 uniformly to obtain that of Figure 51. In Table 4, comparison of the values of Δ_{ucd} shows that the magnitude of the shift ranges from 0.2 to 0.7

for the six cases considered, the shift being greater for the systems emitting the greater number of prompt neutrons.

In order to compare to data, ENDF/B[8] values were processed in the same manner to extract values of Z_p, σ, and the even-Z pairing enhancement. The Z_p values obtained are plotted in Figure 53 as deviations from UCD for $^{235}U(n_{th},f)$, a typical case. The difference in Z_p values between the calculation and ENDF/B are plotted in Figure 54. The calculated value is generally less than the ENDF/B value in the light mass region, the deviation being greatest about mass 110, where Z_p is close to UCD (Figure 51).

The widths of the Gaussian, σ, are shown for the fragments and products, as computed, and the ENDF/B data in Figures 55-57 for $^{235}U(n_{th},f)$. The value of σ appears to vary with mass, however, the variation appears to be random, no models indicated by the data. In each case considered, the behavior of σ is consistent with a constant value of σ for all product masses. Results appear for all six cases in Table 4. The value of σ extracted from the ENDF/B data for $^{235}U(n_{th},f)$ is 0.597, somewhat greater than the values indicated in Table 4. Note that in this regard, the prompt neutron treatment does not significantly increase the value of σ in the fission products over the value in the fission fragments. That the value is low is of some consolation since measurement error and a proper treatment of prompt neutrons, including gamma competition in the latter stages of decay, would tend to broaden the distribution over that occurring in the fission fragments.

The even-Z pairing enhancements are also computed and tabulated in Table 4. Due to the simplicity of the prompt neutron treatment and the anticipated errors in the evaluation of the yield integrals, a sizeable uncertainty is anticipated in these quantities. Nevertheless, the computed value for $^{235}U(n_{th},f)$ is about 55% which is close to the ENDF/B value of 46%. An estimate of the error in the pairing enhancement term is provided by the persistence of the pairing effect into the 14 MeV and spontaneous fission cases, where the pairing effect is expected to be completely washed out.[35] Examination of Table 4 then indicates an error perhaps as large as 20% in this quantity.

The values of Δ_{ucd} give some indication that the $\delta(Z)$ parameterization may not be the correct way to view the process. The presence of a Z-variation of δ within a mass chain, as mentioned above, is to enhance the low Z yields and draw the Z_p value toward Z_{ucd}. This effect is most prominent near symmetric mass splits where the value of Z_p becomes less than Z_{ucd}. That this effect is present in Figures 50 and 51, but not in Figure 53, the measured data values, indicates that the δ values should not vary within a given mass chain, other than perhaps an even-odd variation. Note also that the value of Δ_{ucd} is low in the case of $^{235}U(n_{th},f)$, even though the number of prompt neutrons computed is high, a process which causes the deviation from Z_{ucd} to increase. This gives another indication that the computed value of Z_p is too close to the Z_{ucd} value, as compared to the measured data. To

correct this situation, another parameterization without a Z-variation may be preferable.

A PARAMETERIZATION IN THE MASS NUMBER, A

In order to remove the effects of a Z-varying δ within a given mass chain, values of δ averaged over the mass chain may be extracted from the computed yields and used to recompute yields. To extract these parameters, the six sets of $\delta(Z)$ parameters, plotted simultaneously in Figures 48 and 49 for the GMAX and YMAX cases and listed in Table 5, were examined to estimate the average even-odd Z behavior in the parameters which appears on top of an otherwise smooth variation with Z. To be sure that such behavior was, in fact, the case, each set of $\delta(Z)$ parameters occurring for the six cases considered were examined for both the GMAX and YMAX cases. In each case, the $\delta(Z)$ were modeled, as described in Appendix F, to determine coefficients of the following proposed model,

$$\delta(Z) = f(Z - Z_o) + (-)^Z g(Z - Z_o) \quad ,$$

where Z_o is the value of the charge corresponding to a symmetric charge split and f(Z) and g(Z) are polynomials in Z. Results of this modeling indicate that such a decomposition is possible, model values deviating from input values by 0.03 to 0.07 fm. Most importantly, for this exercise, in each case the model was consistent with the hypothesis,

$$g(Z-Z_o) = g_o = \text{constant},$$

i.e., the even-odd behavior was well described by a simple constant magnitude term of varying sign. The values of g_o encountered varied between - 0.05 and - 0.08 fm with average values of

g_o = - 0.059 fm GMAX

g_o = - 0.060 fm YMAX

To determine the average value of δ for a given mass chain, the smooth part of $\delta(Z)$ is then averaged over the fractional independent yields for that mass to obtain the $\delta(A)$ parameter,

$$\delta(A) = \sum_Z fiy(A,Z) \; [\delta(Z)-(-)^Z g_o] \quad ,$$

where

$$\sum_Z fiy(A,Z) = 1.0 \quad ,$$

Yields may then be recomputed, as previously described, using a δ parameter now depending upon both mass and charge

$$\delta(A,Z) = \delta(A) + (-)^Z g_o \quad .$$

The $\delta(A)$ values resulting appear in Figures 58 and 59, and are listed in Table 6. These are similar and are to be compared to the $\delta(Z)$ values appearing in Figures 48 and 49.

Recomputing yields with the new $\delta(A,Z)$ parameters gives mass-chain yields which differ little from those computed with the $\delta(Z)$

parameters. Again, $^{235}U(n_{th},f)$ is typical. Yields for this case are shown in Figures 60 through 62 and are to be compared to those shown in Figures 25-27. As expected, there is a noticeable loss in quality of agreement between measured and computed charge yields. Energy accounting was performed in all cases and the results appear in Table 7. Agreement is again comparable to that achieved with the $\delta(Z)$ parameters, shown in Table 3.

Of particular interest, having provided the motivation for this new parameterization, are the independent yield parameters of the Gaussian model. These appear in Table 8 and are to be compared with the values in Table 4 obtained with the $\delta(Z)$ parameters. For the case of $^{235}U(n_{th},f)$ the values of σ and Δ_{ucd} are plotted as functions of the mass number, A, in Figures 63 and 64. With the $\delta(A)$ parameters the Z_p values tend to be further from the UCD value than with the $\delta(Z)$ parameters, as anticipated. In Figure 65 the Z_p values are plotted relative to those extracted from ENDF/B[8] data. Agreement is improved over that indicated in Figure 54, the same plot for the $\delta(Z)$ parameters. However, discrepancies of about 0.4 still appear in the vicinity of the light mass peak. This behavior appears in all of the six cases considered.

Comparing Tables 4 and 8, shows that the value of the width parameter, σ, is not particularly sensitive to differences in the parameterization, the results being consistent with no change at all. The value of the even-Z pairing enhancement changes somewhat between the two parameterizations. If any conclusion is to be

drawn regarding this term, it is again an estimate of the error associated with the computed value, derived from the persistence of the pairing effect to the high energy systems. The indication here is that an error of about 35% in the GMAX case and 20% in the YMAX case may be anticipated. This feature is discussed further later.

At this point a "model's eye view" of the source of mass asymmetry in the fission process may be extracted. In Figure 66 are plotted three relevant parameters as functions of the fragment mass for $^{233}U(n_{th},f)$. The parameters D and S are the deformation and shell correction energies, respectively, averaged over all charges yielded for that mass. The parameter AA is the ratio of the fragment center-to-tip distance in the scission configuration to that of a spherical nucleus of the same mass number and is a measure of the fragment deformation. Examining Figure 66, the deformation energy is rising toward a large value in the vicinity of mass = 120 while at rather constant deformation, AA ≃ 1.5. By mass = 125, the fragment has assumed a nearly spherical shape, indicated by AA ≃ 1.1. In this region, the heavy fragment is passing through the vicinity of two closed spherical shells, 50 protons and 82 neutrons. This is evident from the large shell terms in this region. To understand the effect upon the yield, recall that the GMAX configuration is determined by

$$G = S - (D + C) + \text{constant} \quad .$$

At sufficiently large values of D, a lesser deformed shape becomes

more energetically favorable, even though the Coulomb energy is larger for that shape. To demonstrate that the shell effect is in fact driving the G energy and, through it, the yield in this vicinity, Figures 67 and 68 are to be examined. In Figure 67, the yield and G energy are shown as a function of mass for $^{233}U(n_{th},f)$. If shell corrections are the source of the asymmetry in both curves, the effect should be removed by subtracting the shell terms, S_1 and S_2. In Figure 68 the quantity $G - S_1 - S_2$ is plotted. While the plot is somewhat noisy, there is no indication of an asymmetric peak. Supporting evidence for this conclusion is obtained from plots similar to Figure 66 for other fissioning systems. The Coulomb energy is proportional to the product of the fragment charges, Z_1Z_2. In the vicinity of mass $\simeq$ 135 the heavy fragment charge is slowly varying with the complimentary charge, Z_1, taking on that value which conserves charge. The Coulomb energy in the vicinity of the mass peaks should then increase with the charge of the fissioning nucleus and a larger D energy should become necessary in order to overcome the difference between the deformed and the nearly spherical Coulomb energies. Examination of Figures 69 and 70 confirms the expectation.

This investigation may be carried one step further with interesting results. Combining the observed behavior of D for A 100 in Figures 66, 69, and 70, the following model approximates the deformation energy,

$$D_\alpha = 0.345A - 29.2 \text{ MeV} \quad ,$$

where the α-subscript denotes that this value is typical of a highly deformed shape. At the value of A corresponding to the change from deformed to nearly spherical shapes, the G-values must be equal, i.e.,

$$G_\alpha = G_o \quad ,$$

or

$$D_\alpha + C_\alpha = D_o + C_o \quad ,$$

where the o-subscript denotes quantities corresponding to a nearly spherical heavy fragment. Writing the Coulomb energy as,

$$C = Z_1 Z_2 f(\alpha) \quad ,$$

where $f(\alpha)$ contains all of the shape dependencies, the following relation is obtained,

$$\frac{D_\alpha - D_o}{Z_1 Z_2} = f_o - f(\alpha) \quad .$$

From the figures, $D_o \simeq 2.0$ and assuming D_α as given above,

$$\frac{0.345A_T - 31.2}{Z_1 Z_2} = f_o - f(\alpha) = \Delta f \quad ,$$

where A_T is the "transition mass," that mass at which the shape transition occurs. Examining the computed yields to determine the charges typical of the masses at which the shape transition occurs

and noting that the complimentary charge, Z_1 is given by conservation of charge, the following table is obtained,

	A_T	Z_2	Δf
$^{233}U(n_{th},f)$	122	48	0.00518
$^{239}Pu(n_{th},f)$	125	49	0.00543
$^{252}Cf(sf)$	128	50	0.00542

On the average, $\Delta f = 0.00535$ and $Z_2 = 49$. Using these results, the following formula is offered to estimate the location of the shape transition mass,

$$A_T = 0.759Z_o + 53.2 \quad .$$

Beyond this transition mass, the curves show a rapidly rising shell term which has been identified as the source of the asymmetric mass peak. The transition mass then locates that mass at which the mass yields rise rapidly to form the asymmetric peak and may be taken as an indication of the width of the symmetric valley, the valley extending a distance of $A_T - A_{sym}$ about that mass corresponding to symmetric splits, A_{sym}. This prediction may be checked by comparing the following predicted valley locations with the measured yields, Figures 25, 29, 33, 37, 41, and 45.

A_o	Z_o	A_T	Valley
234	92	123	111-123
236	92	123	113-123
240	94	125	115-125
239	92	123	116-123
252	98	128	124-128

The six cases considered show this prediction to be reasonably confirmed, the effect being somewhat more obscure in the 14 MeV fission cases where the valley is shallow.

This information may be added to the general observation that the heavy mass peak is relatively stationary for all of the fissioning systems considered, the peak extending approximately from mass 134 to mass 146. Except for the depth of the valley and the finer details of the shape of the peak, the location of the peaks and valley are given approximated by these general results.

SUMMARY OF PRECEDING WORK

With the simple model developed thus far, the fission process has been viewed through the Fermi Golden Rule with a simplifying assumption of thermal equilibrium in order to extract a view of the scission-point configuration of the fragments. The resulting parameterization has a simple interpretation in terms of the spacing of the fission fragments. Two configurations have been examined with regard to the shape degrees of freedom. While the YMAX configuration is more in keeping with the spirit of the thermal

equilibrium assumption (maximum phase-space), a special role has implicitly been given to the GMAX configuration (minimum potential energy) since it provides the starting point for the search for the YMAX configuration. Coming somewhat as a surprise was the observation that overall agreement with experimental measurement could be achieved only by constraining a large amount of energy to remain in translational degrees of freedom.

Semiquantitative agreement is achieved with measured mass chain yields. Parameters of the independent yields agree less satisfactorily, the Z_p and σ values being consistently low in spite of a slight excess of prompt neutrons computed, an error which should cause an over-estimation of these quantities. Even-Z pairing enhancements are consistently high with a possible systematic error indicated by their persistence to high energy fissioning systems. A potential source of error which directly affects these quantities is the treatment given to the prompt neutrons. An improved model would give some treatment of gamma competition while remaining simple enough to be applied to the hundreds of fission fragments encountered in this calculation.

CONCLUSIONS OF POTENTIAL USEFULNESS

A few things may be said regarding the general behavior of the computed yields which may be of use where data is sparse by way of simple dependencies and scaling laws. Before beginning this discussion, a few words are in order concerning the manner in which

errors in various quantities, input to the calculation, are propagated through to the yields. Of particular interest here are errors in the mass, the energy constrained to remain in translational degrees of freedom, k_o, and the δ-parameters. All of the quantities enter the calculation through the energy, G.

The yield is proportional to the integral, I,

$$I = \int_o^G \rho(k) \int_o^{G-k} \rho_1(E_1)\rho_2(G-k-E_1)dE_1 dk \quad .$$

All densities involved are assumed to be zero for argument zero so that,

$$\frac{dI}{dG} = \int_o^G \rho(k) \int_o^{G-k} \rho_1(E_1) \frac{d\rho_2(G-k-E_1)}{dG} dE_1 dk$$

With the definition of the temperature, T, this becomes,

$$\frac{dI}{dG} = \int_o^G \rho(k) \int_o^{G-k} \frac{\rho_1(E_1)\rho_2(G-k-E_1)}{T_2(G-k-E_1)} dE_1 dk \quad .$$

In making the saddle-point approximation to evaluate the integral,

$$T_1 = T_2 = T = \text{constant} \quad ,$$

so that

$$\frac{dI}{dG} = \frac{I}{T} \quad ,$$

or,

$$I(G) = I_o e^{G/T} \quad .$$

Errors in the mass formula (Appendix A) are estimated to be about

700 keV. Note however that newer investigations of the masses of neutron-rich nuclei, mentioned in Appendix A, reveal that this error may be as high as a few MeV. For saddle-point temperatures of the order of 1 MeV, this may give rise to an error of a factor of 7 or more from the mass terms alone.

An error in the k_o energy, of magnitude Δk_o, enters directly into the calculation through the G-energy as

$$I = I_o e^{\left(\frac{G-\Delta k_o}{T}\right)} = I\, e^{\left(\frac{-\Delta k_o}{T}\right)} .$$

The temperature is a quantity slowly varying across the chain-yield spectrum, making an error in k_o enter as an overall constant multiplier which drops out of the yield expression upon normalization.

Variations of the δ-parameters shall be treated more carefully. The yield of the i^{th} fragment or chain is given by,

$$y_i = \frac{I_i}{\sum_j I_j} .$$

The dependence upon the k^{th} δ-parameter, δ_k, is given by

$$\frac{dy_i}{d\delta_k} = \Delta_{ik}\left[\frac{\left(\frac{dI_k}{d\delta_k}\right)}{I_k}\right] y_k - \left[\frac{\left(\frac{dI_k}{d\delta_k}\right)}{I_k}\right] y_i y_k .$$

where the Kroneker delta has been written as Δ_{ik} to avoid confusion with the δ-parameters. Assuming a random error in δ_k of magnitude, σ_k, one would write the error in the i^{th} computed yield, σ_{yi}, as

$$\sigma_{yi}^2 = \sum_k (\Delta_{ik} y_k - y_i y_k)^2 \left(\frac{d\ell nI_k}{d\delta_k}\right)^2 \cdot \sigma_k^2 \quad .$$

Assuming the quantity $\left(\frac{d\ell nI_k}{d\delta_k}\right)^2 \cdot \sigma_k^2$ to be constant, the subscripts may be dropped giving,

$$\sigma_{yi}^2 = \left[\left(\frac{d\ell nI}{d\delta}\right)^2 \cdot \sigma^2\right] \sum_k (\Delta_{ik} y_k^2 - 2\Delta_{ik} y_i y_k^2 + y_i^2 y_k^2) \quad ,$$

or,

$$\sigma_{yi}^2 = \left[\left(\frac{d\ell nI}{d\delta}\right)^2 \cdot \sigma^2\right] (y_i^2 - 2y_i^3 + y_i^2 \sum_k y_k^2) \quad .$$

The sum, $\sum_k y_k^2$, may be bounded,

$$y_k^2 \leq \sum_k y_k y_{k,max} = y_{k,max} \quad ,$$

where $y_{k,max}$ is the largest y_k encountered, of the order of

$$y_{k,max} \simeq 0.1 \quad .$$

Hence,

$$\sum_k (\Delta_{ik} y_k - y_i y_k)^2 \leq y_i^2 (1.1 - 2 y_i) \quad .$$

The quantity $\frac{d\ell nI}{d\delta}$ may be determined by chain-rule differentiation, but a simpler estimate is given by examining Figure 18 and others like it giving,

$$\frac{d\log_{10}I}{d\delta} \simeq 2 \text{ to } 3.5 \text{ fm}^{-1} \quad ,$$

or,

$$\frac{d\ell nI}{d\delta} \simeq 4.6 \text{ to } 8.1 \text{ fm}^{-1} \quad .$$

Then,

$$\frac{\sigma_y}{y} \leq \sigma\alpha \quad ,$$

where α ranges from 5 to 9 fm^{-1}. To insure that $\frac{\sigma_y}{y} < 1$, the δ-parameters must then be specified to 0.1 to 0.2 fm. To do a 10% calculation, the δ-parameters must be specified to 0.01 to 0.02 fm. and one may justifiably argue whether or not the location of the nuclear surface may be specified to such small tolerances. The conclusion to be made here is that the computed quantities are quite sensitive to the model parameters. The fact that the degree of agreement achieved between computed and measured chain yields is so good indicates that some cancelation of errors has occurred. A better method of error estimation is not obvious.

Not addressed here for lack of an intelligent way to do so are errors introduced by incorrect specification of the nuclear

shapes at the scission-point. Since the assumption has been made that these are the shapes of either the GMAX or YMAX configuration, the errors may be assumed to be zero and the computed yields viewed as a test of these assumptions. The indication is that the YMAX assumption is the more valid. In view of the large error possible, the small errors remaining between the measured and computed mass-chain and charge yields are of diminished importance.

One prediction of the simple equidistant-spacing density of states model that is confirmed in this calculation regards the independent yield parameter, σ, the width of the Gaussian describing the distribution of charges yielded for fixed mass. According to this model, the yield, y, is proportional to

$$y \propto e^{2\sqrt{aG}} \quad ,$$

where $\underline{a}$ is the density parameter and, in simple models, is proportional to A_o, the mass of the fissioning system. It was previously noted that the G-energy is quadratic in the charge, Z, about some most probable value, Z_o,

$$G = G_o + G_z(Z-Z_o)^2 \quad ,$$

where G_z is the strength of the variation.

Then,

$$y(Z) \propto e^{2\sqrt{aG_o}\cdot\left[1 + \frac{G_z}{G_o}(Z - Z_o)^2\right]^{1/2}}$$

$$y(Z) \propto e^{\sqrt{\frac{a}{G_o}}\, G_z (Z - Z_o)^2} \quad .$$

The width of the parameter, σ, may be identified as

$$\sigma^2 = \frac{1}{2G_z}\sqrt{\frac{G_o}{a}} \quad .$$

The prediction here is that σ scales with the energy as $G^{1/4}$ and with the mass of the fissioning system as $A_o^{-1/4}$. For example, taking σ and G values from Tables 3 and 4,

		GMAX	YMAX
$^{235}U(n_{th},f)$	σ =	0.462	0.458
$^{235}U(n+14,f)$	σ =	0.521	0.508
$^{235}U(n_{th},f)$	G =	18.75	16.78
$^{235}U(n+14,f)$	G =	32.29	29.36

Scaling from the thermal (th) to the 14 MeV (14) cases, the prediction is,

$$\sigma_{14} = \sigma_{th}\left(\frac{G_{14}}{G_{th}}\right)^{1/4} \quad .$$

The predicted values of σ_{14} are,

$$\sigma_{14} = \begin{cases} 0.529 & \text{GMAX} \\ 0.527 & \text{YMAX} \end{cases} \quad .$$

Agreement is reasonable. Note that average values of G have been used rather than average values of the G_o. This should be acceptable if the charge distribution for fixed mass is sufficiently

sharp that the average value of G is a good approximation of G_o.

Encouraged by this result, the same argument may be applied to predict values of the width parameter for individual fragment masses for $^{235}U(n+14,f)$, $\sigma_{14}(A)$, in terms of the values for $^{235}U(n_{th},f)$, $\sigma_{th}(A)$,

$$\sigma_{14}(A) = \sigma_{th}(A)\left(\frac{G_{14}(A)}{G_{th}(A)}\right)^{1/4} .$$

Comparison of computed values of $\sigma_{14}(A)$ with the values predicted by this scaling relation reveal a small systematic error in addition to a small variance. The results are tabulated here for the GMAX and YMAX cases. Indicated are the average error, BAR, its standard deviation, VAR, and the maximum error observed, MAX,

	BAR	VAR	MAX
GMAX	0.015	0.029	0.065
YMAX	0.023	0.032	0.069

To compare values of σ between systems, one may write,

$$\sigma = \alpha\left(\frac{G}{A_o}\right)^{1/4} .$$

Solving for α in the six cases, again using Tables 3 and 4,

	G		σ		α	
	GMAX	YMAX	GMAX	YMAX	GMAX	YMAX
$^{233}U(n_{th},f)$	18.45	16.63	0.462	0.460	0.872	0.891
$^{235}U(n_{th},f)$	18.75	16.78	0.462	0.458	0.870	0.887
$^{239}Pu(n_{th},f)$	21.63	19.11	0.484	0.469	0.883	0.883
$^{235}U(n+14,f)$	32.29	29.36	0.521	0.508	0.857	0.855
$^{238}U(n+14,f)$	30.77	27.40	0.520	0.506	0.868	0.894
$^{252}Cf(sf)$	24.97	22.86	0.512	0.492	0.913	0.896

The indication is that

$$\alpha = \begin{cases} 0.877 \pm 0.018 & \text{GMAX} \\ 0.884 \pm 0.014 & \text{YMAX} \\ 0.881 \pm 0.016 & \text{overall} \end{cases}$$

The conclusion to be made here is that the model makes a definite prediction of the behavior of the charge width, σ, with the mass and excitation energy of the fissioning nucleus.

Lest too much faith be placed in the behavior of the yields as predicted by the equidistant model, the mass chain yields are to be investigated. Applying the model to individual chain-yields gives less satisfactory results as shall be shown here. In conjunction with the Gaussian model for charge widths, the chain-yields is given by,

$$y(A) \propto \exp(2\sqrt{aG})$$

where G is the charge-weighted value of the G-energy for that mass

chain. Knowing that the a-parameter varies somewhat between different fragments and having a set of chain-yields for one incident neutron energy, one may ask if this simple model may be used to estimate the yield at another energy. By solving for the a-parameter in the expression for the i^{th} yield,

$$y_i = \frac{\exp\ (2\sqrt{a_i G_i})}{\sum_j \exp\ (2\sqrt{a_j G_j})} \quad ,$$

the resulting set of a_i may be used to estimate the yield at the new value of the G-energy resulting from absorption of a neutron of different energy. Again, only ratios are known and one value of the a-parameter must be assumed. This value is denoted by a_o as is taken to be given by the empirically observed relationship between a_o and A_o, the mass number of the fissioning system,[26]

$$a_o = A_o/9.5$$

The remaining a_i are obtained by solving

$$y_i/y_o = \exp(2\sqrt{a_i G_i} - 2\sqrt{a_o G_o}) \quad .$$

The resulting a_j may then be used to estimate yields at some different energy, G', resulting from a different incident neutron energy. Using yields computed for $^{235}U(n_{th},f)$ to determine the a_i and using these a_i to estimate the yields for $^{235}U(n+14,f)$ gives ratios of the estimated to computed yields for this reaction of,

$$\frac{y_{i,est}}{y_{i,calc}} = \begin{cases} 1.013 \pm 0.781 & \text{GMAX} \\ 0.832 \pm 1.001 & \text{YMAX} \end{cases}$$

The predictions of the mass chain yields based upon the equidistant model are not sufficiently good that a reliable scaling relation is indicated.

PROCEDURE FOR AN ARBITRARY FISSIONING SYSTEM

The calculation of yields for an arbitrary system proceeds in four steps,

1) Generation of yield integrals with fixed δ and constrained k_o for use in interpolation.
2) Selection of δ-parameters.
3) Interpolation of the fixed δ intergral values at the desired δ values.
4) Empirical adjustment.

The average value of k_o over the six cases treated is 26.8 MeV. As mentioned previously, errors in the term do not introduce large errors into the yield calculation. From the cases considered, it appears that it is sufficient to evaluate fixed delta integrals at only three values of δ, 5, 6, and 7 fm. Although YMAX configurations give better agreement with measured yields, the GMAX configuration must be computed to begin the calculation and offers diagnostic information, being free of the shape variation of the YMAX configuration.

In figures 48, 49, 58, and 59, the six sets of δ are plotted. The same quantities are tabulated in Tables 5 and 6. As previously

discussed, the $\delta(A)$ and YMAX cases are recommended. It should be noted that it is the $\delta(Z)$ parameters which are determined from the yields, the $\delta(A)$ parameters determined from the $\delta(Z)$ after an assumption concerning the magnitude of the even-odd Z term is made. One could in principle use another even-odd term from Table 5 to redetermine the $\delta(A)$. The peak-to-valley ratio is determined by the rapidity of the rise in δ values near symmetry. This may be seen in Figures 48, 49, 58, and 59 as the thermal neutron -induced fission cases, all with large peak-to-valley ratios, rise most rapidly moving away from symmetry. Information available regarding the peak-to-valley ratio may dictate a best set of δ-parameters to use. In the absence of this information, averaging may be performed with the six sets. The results of such averaging may be presented more simply by fitting the δ's to a simple form,

$$\delta(x) = f(x-x_o) + (-)^Z g(x-x_o) \quad ,$$

where x is Z or A and x_o is the value at symmetry. f and g are assumed to be polynomials in $x-x_o$. The polynomials were determined as described in Appendix F with the same form resulting in all cases,

$$\delta(x) = f_o+f_2(x-x_o)^2+f_3(x-x_o)^3+f_4(x-x_o)^4+f_5(x-x_o)^5+f_6(x-x_o)^6+(-)^Z g_o \quad .$$

The values of the coefficients appear in Table 9 with the observed standard deviations. The standard deviations are large compared to that needed to insure a small error in the computed yields,

The six data sets, strictly speaking, should not be lumped together, however, as may be obvious in the figures, since such dissimilar behavior is exhibited by the various sets of δ-parameters. The formulas determined by the above fit then represent something of a best guess. As shown in Figure 71 for representative cases, use of this formula will introduce potentially large systematic errors.

To illustrate the utility of the polynomial formula for the δ-parameters, yields were recomputed with coefficients for the δ(A) parameters in Table 9. The results are shown in Figures 72-77 for a few cases. As expected, the chain and charge yields have suffered a loss in quality of agreement with the measured yields. Also, the peak-to-valley ratio is too small in the thermal cases, as expected, since the δ parameters used are not as rapidly increasing in the region of symmetry as those specific to this reaction, as may be seen in Figure 71.

Energy accounting may be done again for this set of δ-parameters, the results of which appear in Table 10 and show a small loss in agreement relative to those values in Table 7. In Table 11 the parameters of the independent yield Gaussian model appear. Comparing Table 8 and 11 shows that the Gaussian parameters have changed very little between the two cases, indicating that the main effect of the δ(A) is to determine chain yields.

Having a set of computed yields, several adjustments are possible by way of empirical fixes. For example, the width of the

Gaussian describing independent yields, σ, for $^{235}U(n_{th},f)$ is calculated to be

$$\sigma = 0.47 \quad ,$$

whereas extracting the same quantity from ENDF/B[8] for this reaction gives a value of

$$\sigma = 0.59 \quad .$$

The reason for this difference is not understood but may result from the simple prompt neutron treatment, the presence of gamma competition broadening the distribution somewhat. Another potential source of error is indicated by examining the yields in ENDF/B[8] and lumping them according to charge. It was the charge-lumped yield data that were used to determine the original $\delta(Z)$ parameters. Examining the charge-lumped yields reveals an apparent violation of charge conservation since, in general,

$$y(Z) \neq y(Z_o - Z) \quad .$$

This fact indicates the presence of some combination of measurement error, beta-decay contamination, and modeling error in the data. It then seems reasonable to assume the computed and measured Gaussian widths to be related by an error term through

$$\sigma^2_{meas} = \sigma^2_{calc} + \sigma^2_{err} \quad ,$$

where the subscripts indicate the measured, calculated, and error terms, respectively. Using the $^{235}U(n_{th},f)$ results to determine

σ_{err} gives

$$\sigma_{err} \approx 0.36 \quad .$$

Hence, with the computed chain yields, a correction may be considered in which the Gaussian model is broadened in this fashion.

The computed Z_p values differ somewhat from the ENDF/B values as shown in Figure 65 for $^{235}U(n_{th},f)$. The result is nearly identical for the other cases considered, deviations being about -0.3 through the light mass peak and +0.2 through the heavy mass peak. Again, assuming that the chain yields are given, either by measurement or calculation, one may consider a small correction in the computed Z_p values as indicated in Figure 65. A further, smaller correction results from the fact that the computed number of neutrons is high by about 0.5. Examining Tables 7 and 8 shows that the Z_p value moves relative to UCD by about 0.16 for each neutron emitted (light-product only). This implies an additional correction of 0.08 to the Z_p value from the prompt neutron treatment alone.

The even-Z pairing enhancements, as computed, are to be used with extreme caution. Values computed with the original $\delta(Z)$-parameters of Table 5, appearing in Table 4, indicate errors consistently high by as much as 18% relative to the same quantities extracted from the ENDF/B[8] data, appearing in Table 12. In Table 8 the same quantities are again computed assuming the even-odd Z term in the δ-parameters to be -0.06. As indicated in Table 5,

the values of this parameter range from -0.05 to -0.09, the value of -0.06 being the average over the six cases. Examining the variation in the pairing term between Tables 4 and 8 and the deviation of the even-odd Z term from -0.06 for each case shows that the even-Z pairing enhancement changes by 0.1 for a change of about 0.01 fm. Thus, accurate determination of the enhancement requires an extremely small tolerance on the specification of the location of the nuclear surface, perhaps unphysically small.

To summarize, it appears that the model may be useful even in the complete absence of experimental information to predict chain yields, each piece of evidence that is available being useful in the selection of a better set of δ-parameters. Having a set of chain yields, either computed or measured, independent yields may be computed and adjusted empirically. In making any such adjustments, it is recommended that the adjustments be made in the fragments, rather than the products, to insure that charge conservation is not violated. This will, of course, affect small changes in the prompt neutron and total gamma energy computed. With a fairly complete set of yields for a particular excitation energy of the fissioning compound nucleus, yields at another excitation energy may be estimated by scaling the measured yields by the ratio of the computed yields at the two energies.

ACKNOWLEDGMENTS

A large number of people were helpful throughout the course of this work to whom my thanks are extended. My advisor, Dr.

Charles Maynard, originally proposed the idea of the investigation of this model for possible use in data generation. His advice and comments throughout have been of great help. His work with Drs. Donald Walker of the Associated Western Universities and Phillip Young, of the Los Alamos Scientific Laboratory, made it possible for me to come to Los Alamos to perform the calculation. Thanks to Drs. David Madland and Talmadge England of LASL, under whose guidance I worked most directly.

Help with the nuclear models employed came from Drs. Phillip Seeger and Ed Arthur, both of LASL. I would particularly like to thank Dr. Luciano Moretto and doctor-to-be Lee Sabotka of the Lawrence Berkeley Laboratory for their assistance and hospitality during my visit with them. Many enlightening discussions were held with Dr. Ray Nix, at LASL, whose advice was most helpful.

Numerical and computational techniques were developed for use in the calculation with the assistance of Carla McInteer and Drs. Richard Beckman, David Kahaner, Blair Swartz, and Wayne "Flash" Fullerton. Code development was assisted by the LASL consulting staff, Bob Frank, Chester Kazek, Mac Fraser, and Jim Engle. Without the help of these people the calculation would not have been completed.

My heartfelt thanks to Helen Holleman for typing the manuscript, and to Claire Baxman for her assistance throughout my visit to LASL.

APPENDIX A

The Mass

In order to determine G, the fragment masses must be known. As fission fragments are unstable, neutron-rich and highly deformed, their masses have not been measured, and a mass-formula must be used. The earliest mass formulas, such as proposed by Weisaecker,[36] were based on liquid-drop comparisons. Perhaps the best pure liquid-drop formula is that of Myers and Swiatecki.[37] Comparison of their computations with experimental measurements show that while smooth behavior with mass and charge is reasonably well given, deviations of several MeV are observed, presumably due to single-particle effects. These effects would be of little consequence were it not for the fact that in the region of interest, the light actinides, the energy release at the scission-point, computed from liquid-drop considerations alone, is nearly zero. Hence, in this computation, the small deviations are important and a better mass formula is needed.

Since single-particle effects seem to be the problem, a single-particle model would seem to be in order. Here, the problem is just the reverse. Fluctuations associated with shell and pairing effects are reasonably well predicted, but the bulk mass is difficult to obtain in a general sense. A useful formula must then combine these two models with the liquid-drop formula giving the smooth mass and charge dependence and the single-particle method giving the observed deviations about this smooth background.

Such a method was proposed by Strutinsky[38] and implemented by Seeger and Howard.[9] By this method, the nuclear mass may be written as

$$M = M_{1d} + \sum_{n,p} (\delta U + P) \quad ,$$

where M_{1d} is given by a liquid-drop formula, and δU and P are single-particle correction and pairing energies, respectively. The procedure presented here for determining δU and P is taken from References 9, 32, 39, and 40.

The corrections are determined by first assuming some single-particle potential. Seeger used a deformed Nilsson model[41] characterized by deformation parameters ε and ε_4. Single-particle levels were determined for each shape on a discrete grid of 20 values of ε ranging $-.35 \leqslant \varepsilon \leqslant .6$ and five values of ε_4 ranging $-.08 \leqslant \varepsilon_4 \leqslant .15$ with the grid turning upward in ε_4 for the larger values of ε, as shown in Figure 1. This grid was chosen after preliminary work with other grids such that the middle value of ε_4 corresponds roughly to the most probable value for a given ε on the grid.

In treating single-particle shell and pairing corrections, neutrons and protons are treated independently, corrections computed for each, as indicated by summing over n and p.

Having solved the Schroedinger Equation, a set of levels, indexed by j, with energy E_j, are given. These levels may then be filled with N particles to give the total energy of the system, E,

$$E = \sum_{j=1}^{N} E_j = \int_{-\infty}^{\lambda} Eg(E)dE \quad ,$$

where g(E) is the density of states,

$$g(E) = \sum_k \delta(E-E_k) \quad ,$$

and λ is the Fermi energy of the system, the energy of the last occupied state, defined by

$$N = \int_{-\infty}^{\lambda} g(E)\, dE \quad .$$

According to the Strutinsky prescription, everything is assumed to be separable into a smooth, average behavior, denoted by a tilda (~) over the quantity, to be associated with liquid-drop behavior, and a deviation resulting from shell corrections, i.e.,

$$E = \tilde{E} + \delta E \quad ,$$

$$g(E) = \tilde{g}(E) + \delta g(E) \quad .$$

The smooth Fermi energy is defined with respect to the smooth density by

$$N = \int_{-\infty}^{\tilde{\lambda}} \tilde{g}(E)\, dE \quad .$$

Then,

$$\tilde{E} = \int_{-\infty}^{\tilde{\lambda}} E\tilde{g}(E)\, dE \quad ,$$

and the quantity desired, δE, is given by

$$\delta E = \sum_{j=1}^{N} E_j - \int_{-\infty}^{\tilde{\lambda}} E\tilde{g}\,(E)\, dE$$

Hence, the problem reduces to one of separating the smooth behavior of the density, $\tilde{g}(E)$, from the actual density, $g(E)$.

The separation is performed by expanding the delta-function in Hermite Polynomials, H_m,

$$g(E) = \sum_k \delta(E-E_k) = \frac{1}{\gamma\sqrt{\pi}} \sum_k e^{-u_k^2} \sum_{m=0}^{\infty} c_m H_m(u_k) \quad ,$$

where $u_k = \frac{E - E_k}{\gamma}$, γ defines an arbitrary "smearing width," and c_m is given by

$$c_m = \begin{cases} \frac{(-)^{m/2}}{2^m(m/2)!} & m = \text{even} \\ 0 & m = \text{odd} \end{cases}$$

The sum over m may be split into two pieces,

$$g(E) = \frac{1}{\gamma\sqrt{\pi}} \sum_k e^{-u_k^2} \sum_{m=0}^{p} c_m H_m(u_k) + \frac{1}{\gamma\sqrt{\pi}} \sum_k e^{-u_k^2} \sum_{m=p+1}^{\infty} c_m H_m(u_k) \, .$$

The lower-order polynomials vary rather slowly and smoothly, whereas the higher-order polynomials vary rapidly and must be included to describe the rapid fluctuations associated with shell effects. The distrinction between smooth and fluctuating behavior is arbitrarily made by fixing p, the smooth, liquid-drop behavior represented by polynomials of order less than or equal to p, and the fluctuating shell behavior represented by the higher-order polynomials. The smooth density sought, $\tilde{g}(E)$, is given by

$$\tilde{g}(E) = \frac{1}{\gamma\sqrt{\pi}} \sum_k e^{-u_k^2} \sum_{m=0}^{p} c_m H_m(u_k) \quad ,$$

and the smooth energy, $\tilde{E}$, is given by

$$\tilde{E} = \frac{1}{\gamma\sqrt{\pi}} \sum_{k} \sum_{m=0}^{p} c_m \int_{-\infty}^{\tilde{\lambda}} E e^{-u_k^2} H_m(u_k) dE \quad .$$

The sum over k includes all levels of the Nilsson potential but, in practice, need extend only to a few shells above the highest occupied. Then the Strutinsky shell correction term, δU, is given by

$$\delta_U = \delta E = \sum_{j=1}^{N} E_j - \tilde{E} \quad .$$

As no physical significance is associated with the parameters, γ and p, results should be independent of their values. Such is the case if, as Seeger uses,

$$p = 6 \qquad \gamma = 1.2\ \hbar\omega_o \quad ,$$

where $\hbar\omega_o$ is the oscillator strength in the Nilsson Model. For oscillator strengths Seeger gives

$$\hbar\omega_{on} = 35.37\ \text{MeV}/A^{1/3} \qquad \hbar\omega_{op} = 31.08\ \text{MeV}/A^{1/3}$$

for neutrons and protons, respectively, where A is the mass number.

The pairing term is determined from the same set of levels used to compute the shell correction term. Using a BCS Hamiltonian, the nuclear ground state is given for an N-particle system by

$$E_{BCS} = E_{\text{odd-particle}} + \sum_{j=1}^{n} \left[1 + \frac{E_J - \tilde{\lambda}}{\sqrt{(E_j - \tilde{\lambda})^2 + \bar{\Delta}^2}} \right] E_j - \frac{\bar{\Delta}^2}{G} \quad ,$$

where the sum over j runs over the n levels used to determine the BCS ground-state, where n = N if N is even, and n = N + 1 if N is

odd. Any odd, unpaired particle is excluded from the sum and appears explicitly in the first term. The pairing strength, G, is related to the pairing gap, $\bar{\Delta}$, the smooth level density, and the smooth Fermi energy by

$$\frac{1}{G} = \tilde{g}(\tilde{\lambda}) \log \left\{ \left[\left(\frac{n}{\tilde{g}(\tilde{\lambda})\bar{\Delta}} \right)^2 + 1 \right]^{1/2} + \frac{n}{\tilde{g}(\tilde{\lambda})\bar{\Delta}} \right\} \quad .$$

For the gap parameter, Seeger uses the phenomenological result,

$$\bar{\Delta} = 10.5 \text{ MeV}/A^{1/2} \quad .$$

Having determined the energy of the nucleus without pairing from the shell model calculation above, the pairing energy is given by the difference between this energy and that of the BCS ground-state, E_{BCS},

$$P = E_{BCS} - E \quad .$$

Note that this is the total pairing energy, as opposed to a Strutinsky-type pairing correction. Hence, the parameters of the liquid-drop portion of the mass formula are determined by fitting an expression for BE_{ld} to

$$BE_{ld} = BE_{exp} - (\delta U + P) \quad ,$$

where BE_{exp} is the experimental binding energy.

The binding energy of the nucleus is then given according to Seeger and Howard by

$$BE = BE_{ld} + \delta U + P \quad ,$$

where

$$BE_{ld} = \alpha A - \beta \frac{(N-Z)^2}{A} \cdot \frac{1}{1 + \zeta B_S(\varepsilon_i)/A^{1/3}} - \gamma A^{2/3} B_S(\varepsilon_i)$$

$$+ \phi A^{1/3} B_k(\varepsilon_i) - E_c(\varepsilon_i) - 35 \frac{|N-Z|}{A} + 14.33 \times 10^{-6} Z^{2.39}$$

$$E_c(\varepsilon_i) = E_{dir} B_c(\varepsilon_i) + E_{exch} + E_{so}$$

$$E_{dir}(\varepsilon_1) = \frac{3}{5} \frac{Z(Z-1)e^2}{R} \cdot [1 + 18.0295 \left(\frac{a}{R}\right)^3 - 85.2330 \left(\frac{a}{R}\right)^4]$$

$$E_{exch} = \frac{1}{Z} E_{dir} - 3\left(\frac{3}{16\pi}\right)^{2/3} \frac{Z^{4/3} e^2}{R}$$

$$\cdot [1.-1.3356\left(\frac{a}{R}\right) + 7.127\left(\frac{a}{R}\right)^2 - 18.2104\left(\frac{a}{R}\right)^3]$$

$$E_{so} = (.0369A - .0805Z) \frac{Z}{R^3} [1+\pi^2 \left(\frac{a}{R}\right)^2]$$

$$R = r_o A^{1/3} \left[1 + \frac{5}{6} \pi^2 \left(\frac{a}{r_o A^{1/3}}\right)^2 - \frac{7}{24} \pi^4 \left(\frac{a}{r_o A^{1/3}}\right)^4\right] .$$

The values of the various constants are given as

$r_o = 1.2254$ $\qquad$ $a = 0.153$

$\alpha = 15.2568$ MeV

$\beta = 33.166$ MeV

$\gamma = 17.073$ MeV

$\zeta = 3.28$

$\phi = -0.76$ MeV .

The parameters ε_i appearing here denote a particluar point in the two-dimensional space of shapes considered. The B_s,B_c and B_k are the surface, Coulomb, and curvature shape dependencies of the liquid-drop terms as computed by Hasse.[42] These terms are normalized to unity for spherical shapes.

For a given nucleus, the binding energy formula may be evaluated at each point in the ε, ε_4 space. The ground-state of the nucleus corresponds to a maximum of the binding energy. In the vicinity of the maximum binding energy grid point, a biquadratic interpolation is used to determine the exact location of the ground-state. Comparison of the binding energies computed in this fashion with 1553 measure masses[43] gives a standard deviation of 704 keV.

The question of the validity of extrapolating the mass formula into neutron-rich regions must be addressed. Recent measurements of 52 neutron-rich masses have been made by Aleklett[44] and comparisons to two other mass formulas of the droplet-plus-corrections type[45,46] have been made. This study indicated the Seeger and Howard formula to be best, observed errors ranging from 0.3 to 1.0 MeV. Another recent measurement of the masses of neutron-rich rubidium and cesium isotopes has been made[47] showing deviations as large as 2.0 MeV from the predictions of the Seeger and Howard formula. It would then appear that the mass formula used, while not perfect, is as good as one may expect.

In general, mass recursion relations give better mass predictions near β-stability. This is to be expected since they contain many more parameters. One such set of relations has been determined by Janecke[24] giving a standard deviation of 157 MeV from measured

masses. The Janecke relations appear to work as well as the Seeger and Howard formula in the neutron-rich mass studies cited above. As a general rule, extrapolation of these relations into the neutron-rich region is not advised,[44,48,49] and the observed agreement may be happenstance. However ill-advised, some yields were computed assuming Janecke's values or, where available, experimental values[50] of the ground-state mass. The shape dependence, not given by the recursion relations, was then taken from the Seeger and Howard formula.

APPENDIX B

The Coulomb Energy

The two fission fragments are considered to be uniformly charged deformed spheres whose charge distributions may be characterized by a set of multipole moments. The fragments are assumed to be axially symmetric and their symmetry axes are assumed to be colinear. For such a system, the general expression for the Coulomb energy, taken from Hirschfelder, Curtiss, and Bird [51], reduces to a particularly simple form. Denoting the Coulomb energy by C,

$$C = \sum_{n_a n_b} \left[\frac{(n_a + n_b)!}{n_a! n_b!} \right] \cdot \left[\frac{Q_{n_a} Q_{n_b}}{r^{n_a + n_b + 1}} \right] ,$$

where r is the center-of-mass separation between the fragments and Q_{n_i} is n^{th} multipole moment of the i^{th} fragment,

$$Q_{n_i} = \int \rho_i(\vec{r}_i)\, r_i^{n_i}\, P_n(\cos\theta)\, d^3 r_i \quad .$$

In practice the assumed shapes are given in terms of the parameters of the Nilsson model, ε and ε_4. The multipoles may be determined numerically by using the expression of Nix [40] for the radius, R,

$$R(\theta) = R_o/\lambda \left[\frac{1 - \frac{1}{3}\varepsilon + \frac{2}{3}\varepsilon P_2(\cos\theta_t)}{1 - \frac{2}{3}\varepsilon P_2(\cos\theta_t) + 2\varepsilon_4 P_4(\cos\theta_t)} \right]^{1/2} ,$$

where

$$\cos\theta_t = \left[\frac{1 - \frac{2}{3}\varepsilon}{1 + \frac{1}{3}\varepsilon - \varepsilon\cos^2\theta} \right]^{1/2} \cdot \cos\theta \quad .$$

Assuming the charge density, ρ, to be a constant, this expression may be inserted into the integrand and the integration performed numerically. A standard Newton-Cotes quadrature rule [23] with a relative computational error of 10^{-9} was used to do this. The volume preserving factor, λ, was determined by requiring the monopole moment to be -Ze, where Z is the atomic number and e is the electron charge. The radius term, R_o, is given in terms of the mass number, A, by

$$R_o = r_o A^{1/3} \quad ,$$

with r_o taken from the mass formula of Appendix A,

$$r_o = 1.2254 \text{ fm.}$$

Since the Nilsson model employed in the mass formula employs only even-order deformation parameters, only even mutipoles appear in the charge expansion. The multipoles were evaluated through order 16 and the higher order terms were assumed to be zero. Defining a dimensionless multipole moment, dependent only upon shape parameters,

$$q_n = \frac{Q_n}{ZeR_o^n} \quad ,$$

the expression finally used to evaluate the Coulomb energy is given by

$$C = \frac{Z_1 Z_2 e^2}{r} \sum_{\substack{i,j=0 \\ \text{even}}}^{16} c_{ij} \left(\frac{R_{o1}}{r}\right)^i \left(\frac{R_{o2}}{r}\right)^j q_{i1} q_{j2} \quad .$$

The series expansion of the Coulomb energy is not of such a form that that an error bound may be made. Examination of the higher order multipole-multipole interaction terms for some test cases gives some indication of the magnitudes of the neglected terms. The interaction terms are proportional to the reciprocal of r raised to some power. The smallest value of r that occurs in this calculation corresponds to the case of tangent fragments. The largest value of an interaction term involving a 16^{th}-order multipole was 10^{-4} times the monopole-monopole interaction term. Separating the fragments such that the distance between their tips was about 2.4 fm. reduced this term to 10^{-6} times the monopole-monopole term. Hence, the first neglected term may be of the order of 100 eV. Assuming that the series does converge, this gives some indication of the error possible.

Also of interest for this calculation is that fraction of the Coulomb energy resulting from the multipole-multipole interactions other than monopole-monopole. For the most extreme deformation allowed, this fraction was less than 12% for the case of tangent fragments and less than 8.5% for fragments tips separated by 2.4 fm. At larger tip-to-tip distances this fraction, as well as the truncation error, should decrease.

The value of the nuclear radius constant, r_o, should be noted here. The value used universally in the calculation is that given by Seeger and Howard.[9] This value was determined in the mass

formula work by allowing it to be a free variable, determined by least-squares fitting. A more conventional value [30] is given by high energy electron scattering experiments,

$$r_o = 1.18 \text{ fm.}$$

Since the Coulomb energy scales with this parameter, use of the smaller value could increase the Coulomb energy by a few percent. Noting the errors reported in the yield calculations, this error is of little consequence and would be compensated by an adjustment in the scission-point separation.

APPENDIX C

The Neglect of Rotations and Vibrations

The presence of rotations and vibrations complicates the scission-point picture. These may simply be ignored or included in the list of assumptions about the scission-point. However, modes of vibration in the fissioning nucleus at its saddle-point have been identified which could give rise to rotations and vibrations in the fragments at scission.[52] It then seems preferable to attempt to estimate the effects of rotations and vibrations in the hope that they are of little consequence. Such shall be argued here.

Two effects result from the presence of these modes: both consume energy and both affect the density-of-states expression. The energy involved in rotation is given by

$$E_{rot} = \frac{J(J+1)\hbar^2}{2I_\perp} \quad ,$$

where J is the total angular momentum of the nucleus, $\hbar^2$ is the square of Planck's constant over 2π, and $I_\perp$ is the moment of inertia of the nucleus about an axis perpendicular to the nuclear symmetry axis. Approximating the nuclear shape as that of a pure ellipsoid described by a radius vector, $R(\theta)$,

$$R(\theta) = R_o[1+\alpha P_2(\cos\theta)] \quad ,$$

the appropriate value of $I_\perp$ is given by

$$I_\perp = (2/5)Am_nR^2\ (1_o + \alpha/10) \quad ,$$

where A is the mass number, m_n = mass unit = 931 MeV/c^2, R_o = radius of a spherical nucleus of mass A, $R_o = r_oA^{1/3}$, and r_o = 1.2254 fm. This is

the so-called "rigid body" moment of inertia and best characterizes the rotational behavior of excited nuclei.[53,54] The energy of rotation is then largest for small masses and deformations. For mass 70,

$$E_{rot} = 0.03\ J(J+1)\ \text{MeV} \quad .$$

Hence, J must be of the order of 5 or more in order to involve as much as 1 MeV of energy in rotation. Experimentally, fission product spins are observed to be of the order 7-10.[55,56] However, this is presumed to result from torques experienced as the deformed fragment accelerates in the strong Coulomb field of the complimentary fragment. As shown by Strutinsky,[57] the presence of a small deviation of the fragments' symmetry axes from colinearity can easily account for values of J as high as 20. Hence there is no experimental evidence for high scission-point rotation in binary fission that would be required to consume much energy.

In the presence of a stable deformation of the nucleus, a rotational band may be built upon each single-particle state characterized by a quantum number, Ω, specifying the projection of the total particle angular momentum on the nuclear symmetry axis. The density of states is enhanced by the presence of the rotational states. Huizenga et al.[15] have shown that this enhancement is given to good approximation by $\sigma_\perp^2$, where $\sigma_\perp^2$ is related to $I_\perp$ by

$$\sigma_\perp^2 = \frac{I_\perp T}{\hbar^2} \quad .$$

T is the nuclear temperature. While $\sigma_\perp^2$ may itself be large, its variation among the fission fragments is slow, varying as $A^{5/3}/G^{1/2}$, and may

be ignored as an overall constant, dropping from the yield expression upon normalization.

The presence of vibrations at the scission-point may also consume energy. In order to estimate these, simple harmonic motion shall be assumed. If the frequency of oscillation of the i^{th} mode is ω_i, the total energy involved in vibrations is given by

$$T_v = \sum_i n_i \hbar\omega_i = \sum_i \frac{\hbar\omega_i}{e^{\beta\hbar\omega_i} - 1} \quad .$$

For simplicity, only quadrupole and hexadecupole vibrators shall be considered. Also, for simplicity, liquid-drop inertial parameters, D_λ, shall be assumed,[58]

$$D_\lambda = (3/4\pi\lambda) \cdot A \cdot m_n R_o^2 \quad ,$$
$$\lambda = 2,4$$

To low order, the quadrupole (λ=2) shape may be associated with the Nilsson quadrupole parameter, ε, and the hexadeculpole (λ=4) with the ε_4 parameter. The oscillator strength is again assumed to be given by liquid-drop arguments[58]

$$C_\lambda = \frac{1}{4}(\lambda-1)(\lambda+2)\, b_{surf} A^{2/3} - \frac{3}{2\pi} \frac{\lambda-1}{2\lambda+1} \frac{e^2}{r_o} Z^2 A^{-1/3} \quad ,$$

where

b_{surf} = 17 MeV

r_o = Coulomb constant = 1.2254 fm

Z, A = nuclear charge and mass

The ground-state oscillator energies may be estimated,

$$\hbar\omega_{\lambda o} = \hbar(C_\lambda/D_\lambda)^{1/2} \quad .$$

Assuming Z to be given by Uniform Charge Distribution,

$$Z_{ucd} = (Z_o/A_o)A \quad ,$$

where Z_o and A_o describe the fissioning system, taken here to be ^{236}U. Then the ground-state oscillator energy is given by

$$\hbar\omega = \left[157.3 \frac{\lambda(\lambda-1)(\lambda+2)}{A} - 9.9 \frac{\lambda - 1}{2\lambda + 1}\right]^{1/2} \quad .$$

Some test cases are given here.

A	λ	$\hbar\omega_\lambda$ (MeV)
70	2	4.0
170	2	2.3
70	4	12.6
170	4	8.0

Assuming the temperature, T, to be of the order of 1 MeV, energies of the order of hundreds of kilovolts might be expected to appear in vibrational modes. This is a small amount of energy relative to that shown to be responsible for overall trends. It is, however, sufficiently large to effect small changes, and this result should be kept in mind.

The presence of vibrations also affects the density of states expression. This problem has been addressed by Moretto[12] and shown to introduce an overall multiplicative $T^{1/2}$-term to the density expression, where T is the nuclear temperature. The temperature is slowly varying across the mass yield spectrum. The main effect is then that of another overall multiplicative constant which drops out of the yield expression upon normalization.

APPENDIX D

The Moretto Density

Moretto [12] and others [13] have proposed a method of computing nuclear density of states functions numerically from the partition function assumed to describe the statistical properties of the nucleus. The partition function, Ω, is derived from a BCS Hamiltonian by Sano and Yamasaki [11] and is given by

$$\Omega = -\beta\sum_k (e_k - \lambda - E_k) + 2\sum_k \ell n[1 + \exp(-\beta E_k)] - \frac{\beta\Delta^2}{G} \quad .$$

where,

E_k = quasi-particle energy = $\sqrt{(e_k - \lambda)^2 + \Delta^2}$

e_k = energy of the k^{th} single-particle level

λ = a Lagrange multiplier, to be identified with the chemical potential, α, $\alpha = \beta\lambda$

β = a Lagrange multiplier, to be identified with the nuclear temperature, $\beta = 1/T$

Δ = $\Delta(\alpha,\beta)$ = the pairing gap

G = the pairing interaction strength, assumed constant.

In the presence of pairing, $\Delta \neq 0$, these quantities are related by the "Gap Equation",

$$\frac{2}{G} = \sum_k \frac{\tanh(\beta E_k/2)}{E_k} \quad .$$

These relations exist separately for the neutrons, N, and the protons, Z. The density-of-states is formally given as the inverse Laplace transform of the partition function. For N neutrons at excitation energy, E_N, the density of states $\rho(E_N,N)$, is given by

$$\rho(E_N,N) = \left(\frac{1}{2\pi i}\right)^2 \oint d\alpha_N \, d\beta_N \, \exp(S_N) \quad ,$$

where S_N is the entropy of the neutron system,

$$S_N = \Omega_N - \alpha_N N - \beta_N E_N \quad .$$

In the real nucleus with both neutrons and protons present, the two systems are assumed to be in equilibrium such that,

$$\beta_N = \beta_Z = \beta \quad .$$

The appropriate expressions for use are

$$\rho(E,N,Z) = \left(\frac{1}{2\pi i}\right)^3 \oint d\alpha_N \, d\alpha_Z \, d\beta \, \exp(S) \quad ,$$

$$S = \Omega - \alpha_N N - \alpha_Z Z + \beta E \quad ,$$

$$E = E_N + E_Z \quad ,$$

$$\Omega = \Omega_N + \Omega_Z \quad .$$

The contour integral may be evaluated exactly, as proposed by Ford [59], or by the computationally more simple saddle-point approximation, as proposed by Moretto. The saddle-point is defined by

$$N = \frac{\partial \Omega}{\partial \alpha_N} \qquad Z = \frac{\partial \Omega}{\partial \alpha_Z} \qquad E = -\frac{\partial \Omega}{\partial \beta} \quad .$$

Through the saddle-point approximation, the Lagrange multipliers, α and β, take on their definitions of the chemical potential and reciprocal temperature.

Evaluating the saddle-point equations for the neutrons,

$$N = \sum_k \left[1 - \frac{(e_k - \lambda)}{E_k} \tanh(\beta E_k/2)\right] \qquad \text{The Number Equation,}$$

$$E_N = \sum_k e_k \left[1 - \frac{(e_k - \lambda)}{E_k} \tanh(\beta E_k/2)\right] \qquad \text{The Energy Equation.}$$

The entropy at the saddle-point may be evaluated using the Number and Energy equations and the expression given by

$$S_N = 2 \sum_k \ell n[1 + \exp(-\beta E_k)] + 2\beta \sum_k \frac{E_k}{1 + \exp(\beta E_k)} \; .$$

Similar expressions hold for the protons. With these equations the density of states may be evaluated for an arbitrary nucleus by the following procedure,

1) The Number and Gap equations are solved simultaneously for the pairing gap and chemical potential with the assumption of zero temperature ($\beta = \infty$) for both neutrons and protons. The energy equations are then evaluated after substituting these values to obtain the total ground-state energy, E_o,

$$E_o = E_{oN} + E_{oZ} \; .$$

2) The critical temperatures for the proton and neutron systems, the temperatures at and above which the pairing gaps are identically zero, are determined by assuming the pairing gaps to be zero and solving the Number and Gap equations simulataneously for β and λ. These values define the critical temperatures, $T_{N,cr}$ and $T_{Z,cr}$.

3) For an arbitrary specific temperature, $T < T_{cr}$, the Number and Gap equations must be solved for both the neutrons and protons to determine the pairing gaps and chemical potentials. If $T > T_{cr}$, only the Number equation needs to be solved for λ. With these values, the total energy and the entropy may be evaluated as well as the other functions required to evaluate the density-of-states expression.

With all of the necessary quantities known for a specific temperature, the density is given in the saddle-point approximation by

$$\rho(E,N,Z) = \frac{\exp(S_N + S_Z)}{(2\pi)^{3/2}\, D^{1/2}} \quad ,$$

where E is the excitation energy, defined as the difference between the total energy evaluated at this temperature and the ground-state energy, E_o, S_N and S_Z are the entropy expressions for neutrons and protons, and D is the determinant of the second derivatives of the partition function, Ω, evaluated at this temperature and the values of λ and Δ determined in step #3,

$$D = \left[\frac{\partial^2 \Omega_N}{\partial \alpha_N^2}\right] D_Z + \left[\frac{\partial^2 \Omega_Z}{\partial \alpha_Z^2}\right] D_N \quad ,$$

where

$$D_N = \begin{vmatrix} \dfrac{\partial^2 \Omega_N}{\partial \alpha_N^2} & \dfrac{\partial^2 \Omega_N}{\partial \alpha_N \partial \beta} \\ \dfrac{\partial^2 \Omega_N}{\partial \beta \partial \alpha_N} & \dfrac{\partial^2 \Omega_N}{\partial \beta^2} \end{vmatrix} \quad .$$

A similar expression holds for the proton term, D_Z.

The above expression for the density of states involves states of all spins and parities. In Appendix E, the decomposition of this expression into a parity and angular momentum dependent form

is presented. A quantity of importance for the angular momentum dependent form is the spin cutoff parameter, σ. In the model of Moretto, this quantity is given by

$$\sigma_N^2 = \frac{1}{2} \sum_k m_k^2 \cdot \mathrm{sech}(\beta E_k/2) \quad ,$$

where m_k is the spin projection of the k^{th} single-particle neutron state. A similar expression holds for the protons. The spin cutoff parameter for the entire nucleus is then given by

$$\sigma^2 = \sigma_N^2 + \sigma_Z^2 \quad .$$

With this definition, the angular momentum dependent form of Appendix E may be used with the Moretto expression for the total density of states.

To evaluate the various infinite sums over single-particle states, a bit of digression is in order. In its most general form, the ground-state gap equation is written

$$\Delta_k = \frac{1}{2} \sum_{k'} \frac{\langle kk|G|k'k'\rangle}{E_{k'}} \cdot \Delta_{k'} \quad ,$$

where Δ_k is the pairing gap for the k^{th} level and $\langle kk|G|k'k'\rangle$ is the pairing interaction matrix element between nucleon pairs in levels k and k'. The gap equation is trivially satisfied if $\Delta_k = 0$ for all k. Making the standard assumption that $\Delta_k = \Delta_{k'}$ for all k and k', an overall Δ may be removed. It must be remembered, however, that $\Delta = 0$ is always a solution to the gap equation. To make the assumption that the matrix element is constant, with a value, G, a corresponding assumption must be made as to how the sum should be

terminated. The matrix element goes to zero for values of k and k' corresponding to states differing in energy by very much. Removing this term from the sum leaves

$$\sum_k \frac{1}{E_k}$$

which diverges. Any prescription for evaluating G then goes hand-in-hand with a statement as to how the sums should be terminated. Such prescriptions have been made by Nix [40] and by Nilsson et al. [60]. The Nix procedure has been used by Seeger and Howard [9] in the mass formula work, described in Appendix A. This shall be discussed later.

With the assumptions made with respect to G and Δ, use of the Moretto density expression requires that one first determine whether or not there exists a nonzero solution to the gap equation, which is now written,

$$\frac{2}{G} = \sum_k \frac{1}{E_k} \quad .$$

In order to determine whether or not there exists a ground-state pairing gap, Moretto suggests the following procedure [26]. Ground-state even-odd mass differences indicate pairing gaps to be given approximately by,

$$\Delta_o = (11 \pm 1)/\sqrt{A} \quad \text{MeV} \quad ,$$

where A is the mass number. Hence, a small value of Δ_o may be assumed, say 0.2 MeV, and the number equation solved at zero

temperature to determine the chemical potential. Using these values, the sum of the gap equation may be evaluated and compared to 2/G. If the sum is greater than 2/G, a larger value of Δ_o is needed and the number and gap equations must be solved simultaneously. If the sum is less than 2/G, a smaller value of Δ_o is needed and $\Delta_o = 0$ is assumed. Such $\Delta_o = 0$ cases occur at shell closures.

The procedure for truncating the sums is most simple for the case of $T \geq T_{cr}$ since there is no gap equation to satisfy. For this case, the sums may be truncated at a value of k approximately equal to the maximum number of particles to be treated, higher terms contributing negligibly.

For $T < T_{cr}$, the procedure is somewhat more complicated. Nilsson et al.[60] give

$$G/A = 19.2 \pm 7.4\left[(N-Z)/A\right] \quad ,$$

where the plus sign holds for the protons and the minus sign holds for the neutrons. With this prescription, only terms with k-values in the range

$$N/2 - \sqrt{15N} \leq k \leq N/2 + \sqrt{15N}$$

are allowed in the neutron sums and similarly for the protons. This prescription is recommended for nuclei of mass 190 and above. Also recommended are oscillator strengths for the conversion of the dimensionless energies of the single-particle states into energy dimensioned values, V,

$$V = 41/A^{1/3}\left[1 \pm 1/3(N-Z)/A\right] \text{ MeV} \quad .$$

In this expression, the minus sign applies for the protons and a plus sign for the neutrons.

A set of rules for terminating the sums and determining G also comes with the mass formula of Seeger and Howard [9]. For the pairing strength, G, the following expression is used,

$$\frac{1}{G} = g \cdot \ell n \left\{ \left[\left(\frac{n}{g\,\overline{\Delta}} \right)^2 + 1 \right]^{\frac{1}{2}} + \left(\frac{n}{g\,\overline{\Delta}} \right) \right\} \quad .$$

The quantities g and $\overline{\Delta}$ are identified in Appendix A as the smooth density of single-particle states at the Fermi energy and the the ground-state pairing gap, respectively. The value of $\overline{\Delta}$ used here was taken to be the empirically observed value,

$$\overline{\Delta}_N = \frac{10.5 \text{ MeV}}{(1.6N + 10)^{1/6}} \quad ,$$

$$\overline{\Delta}_Z = \frac{10.5 \text{ MeV}}{(8Z/3 - 50/3)^{1/6}} \quad ,$$

where the N and Z-subscripts refer to the values used for the neutrons and protons. It should be noted that these relations are empirically observed for nuclei along the β- stability line. Their use for the neutron-rich fission fragments is a source of potential error. The n which appears in the G-equation refers to the number of levels included in the sums, the value of k at which the sums are terminated, given by

$$n = \begin{cases} N \text{ or } Z & \text{for N or Z even} \\ N+1 \text{ or } Z+1 & \text{for N or Z odd} \end{cases}$$

The values of n, G, g, and $\overline{\Delta}$ are given independently for the neutrons and protons. Also given by Seeger and Howard [9] are oscillator strengths, different from those of Nilsson et al. [60],

$$V_N = 35.37/A^{1/3} \text{ MeV} \qquad V_Z = 31.08/A^{1/3} \text{ MeV}$$

One last difference between the Nilsson and Seeger and Howard prescriptions is the maximum number of levels used for the $T \geq T_{cr}$ cases. Nilsson et al. recommend that the sums be terminated at k = 150. Since this has been determined to be adequate for masses 190 and above, it seems reasonable to scale this value for the mass region of interest in this work and k = 120 is taken as the maximum value for the high temperature region.

The original version of the Moretto code for the calculation of densities was used for heavy masses. As an illustration of the sensitivity of the computed densities to the two prescriptions for evaluating G, the sum limits, the maximum number of levels, and the oscillator strengths, each of these prescriptions was changed, one at a time, and the change in the various computed quantities noted. The results are shown in Table 13 for two nuclei, starting with the Nilsson prescription and ending with that of Seeger and Howard. These results are presented merely as an illustration since it makes no sense to assume part of the prescription from one source and the other part from another source. The point to be made is that while the density may be quite accurately evaluated by this method, the results are quite sensitive to errors in the input models. For this

reason, it is important to have an independent check on the model in the mass region in which it is to be used. For the fission fragments, the Seeger and Howard [9] prescription is taken with the successful mass formula offered as supporting evidence.

Odd particle numbers present a problem in this theory. In the absence of pairing, the ground-state number equation becomes,

$$N = \sum_k \left[1 - \frac{e_k - \lambda}{|e_k - \lambda|} \right] = \sum_k n_k \quad .$$

The terms in this equation are

$$n_k = \begin{cases} 0 & e_k > \lambda \\ 2 & e_k \leq \lambda \end{cases} ,$$

i.e., this is an even particle number theory. To apply the theory to the case of odd particle numbers, Huizenga and Bekhami [13] introduce the so-called "sliding energy scale". The observation is made that the ground-state of an odd particle system already possesses one quasi-particle (unpaired particle) relative to the neighboring even particle number systems. This allows it to reach the same density of states at one quasi-particle energy, E_k, less than that of the even system below with one particle less. The sliding energy scale is applied by computing the density as prescribed and shifting the energy corresponding to that density by the energy of the ground-state quasi-particle. This assumption has been investigated in the vicinity of mass number 60 and found to give good agreement with measured densities [13].

At low temperature, the saddle-point approximation used to evaluate the density fails. This manifests itself as a local minimum in the density at low excitation. This is a problem only at the lowest excitations and is less significant for odd particle numbers than for even since the location of the minimum is shifted off of the scale. The saddle-point approximation has been checked by comparing its predictions to those of combinatorial calculations and found to give errors of about 20% at 5 MeV excitation and 1% at 20 MeV excitation.

Another peculiarity of the saddle-point approximation is the discontinuity in the temperature at the critical temperature,

$$\frac{1}{T} = \frac{\partial \ell n \rho}{\partial E} = \frac{\partial}{\partial E}\left[S - \frac{1}{2}\ell n(D)\right] \quad .$$

The saddle-point approximation introduces the determinant of second derivatives of the partition function which is discontinuous at the critical temperature. The discontinuity is small, typically a few percent [11], and is the type of error encountered when the number of particles is not sufficiently large that the statistical limit, $N >> \ell n(N)$, is achieved.

The formalism presented here allows the evaluation of the nuclear density-of-states expression to be performed at high accuracy. However, the number of fission fragments to be treated is large and, allowing for the possible variation in the nuclear shapes, the computational task is enormous. Another simplification

is possible which considerably reduces the computational chore with little loss in accuracy.

As presented, the entire density model may be written in terms of independent proton and neutron contributions. The only difference in the computed densities, say, for a fixed number of neutrons, comes about through the oscillator strength, V_n, and its $A^{1/3}$ term. If the step in which the dimensionless energies of the Nilsson model are converted into energy dimensioned quantities is bypassed, the thermodynamic functions required to evaluate the density may be computed once and for all for that particular particle number and type and the set of Nilsson levels required as input. (Shape dependencies are implicit in the Nilsson levels.) The density-of-states expression may then be assembled after a table look-up of the required values of these thermodynamic functions,

$$\rho(T) = \frac{\exp\left[S_N(T_N) + S_Z(T_Z)\right]}{(2\pi)^{3/2}\left[\left.\frac{\partial^2\Omega_N}{\partial\alpha_N^2}\right|_{T_N} \cdot D_Z + \left.\frac{\partial^2\Omega_Z}{\partial\alpha_Z^2}\right|_{T_Z} \cdot D_N\right]^{1/2}} ,$$

where

$$T_Z = T/V_Z$$

$$T_N = T/V_N$$

$$D_N = V_N^2 \cdot D_N(T_N)$$

$$D_Z = V_Z^2 \cdot D_Z(T_Z) \quad .$$

The quantity, $D_N(T_N)$ denotes the determinant of the matrix of

second derivatives of the neutron partition function, Ω_N, with respect to the dimensionless reciprocal temperature, $\beta_N = 1/T_N$, and chemical potential, α_N, which is dimensionless by definition. A similar expression describes $D_Z(T_Z)$. The corresponding excitation energy is given by

$$E(T) = V_N \cdot E_N(T_N) + V_Z \cdot E_Z(T_Z) \quad ,$$

where E_N and E_Z are dimensionless if dimensionless Nilsson energies are used to compute them.

The computational savings may be realized by noting that, in general, 350 or so fragment pairs occur in a given yield calculation and that, for each fragment pair, at least ten shape combinations may be considered. This would then require 3500 evaluations of the density-of-states expression for each yield calculation. Using the dimensionless procedure described here and noting that the yield calculation requires about 110 different neutron numbers and about 55 different proton numbers, the dimensionless evaluation requires about 6500 evaluations for all of the possible shapes to be considered. After this is done, no further evaluations are necessary. Noting that about 60 good yield evaluations were performed, not counting those that failed for various reasons, the savings was considerable.

The thermodynamic functions needed in the evaluation of the density of states were computed dimensionlessly on a dimensionless

temperature grid. The resulting functions are smooth in the dimensionless temperature and cubic splines were used to interpolate their values at the temperatures, T_N and T_Z. The actual grid used spanned the range

$$0.028 \leq T_N \leq .463 \qquad 0.028 \leq T_Z \leq .463$$

in steps of 0.015. Comparison of evaluations of the density of states computed with the dimensionless scheme and the exact method showed very good agreement, typically to four significant figures, with the worst error occurring at low temperatures. For excitation energies greater than 1.0 MeV, the worst error observed was less than 1%. Also needed in the yield evaluation via the saddle-point approximation is the derivative, dE/dT. Spline interpolation of this quantity also gave better than 1% agreement with exact evaluation.

Splines were generated and saved for Nilsson levels corresponding to the 39 most prolate shapes considered by Seeger and Howard [9], shown in Figure 1. Only values of $\varepsilon \geq 0$ were used and, for each ε, only the three smallest values of ε_4 were used. Particle numbers in the range

$$20 \leq Z \leq 80 \qquad 36 \leq N \leq 120$$

were assumed. This defines the range of particle numbers and space of allowed shapes assumed to describe the scission-point fragments in the yield calculations performed.

APPENDIX E

The Analytical Density of States Expression

The nuclear density-of-states expression of Appendix D may be evaluated analytically if it is assumed that the single-particle states of the constituent nucleons are uniformly spaced in energy. The resulting expression, first proposed by Bethe [16], has been applied to the problem of predicting values of the observed neutron resonance spacings by Gilbert and Cameron [17]. The expression is derived in References 17 and 58. The treatment given here is a summary of the treatment given in Reference 17.

The assumption of equidistant spacing of the single-particle states gives the single-particle state density for neutrons, g_N,

$$g_N = \frac{N}{e_F} \quad ,$$

where N is the number of neutrons and e_F is the Fermi energy, defined by

$$N = \int_0^{e_F} g_N(E)\, dE \quad .$$

A similar expression holds for the protons. This assumption allows the entropy and derivatives of the partition function to be directly evaluated, giving

$$\rho(E,M) = \frac{\exp(\pi^2 g/3\beta)}{(2\pi)^2\left[\pi^2 g^4 \langle m^2\rangle/(12\beta^6)\right]^{1/2}} \quad ,$$

where β is the reciprocal temperature. The M dependence appears in β as will be shown below. The presence of the terms M and $\langle m^2\rangle$

results from the inclusion of the z-components of the nuclear spin, M, and the single-particle states, m, into the partition function. The nuclear spin is accompanied by a corresponding chemical potential, α_M, in the partition function and the single-particle m-values sum to M. Also assumed in this expression is the equality of the neutron and proton single-particle state densities,

$$g_N = g_Z = \frac{1}{2} g \quad .$$

The density parameter, a, is defined as

$$a = \frac{\pi^2 g}{6} \quad .$$

In the derivation, the expression for the excitation energy, U, relative to the energy of the fully degenerate ground-state, which introduces the M-dependence, is given by

$$U = \frac{M^2}{2<m^2>g} + \frac{a}{\beta^2} \quad .$$

This expression may be solved for β giving

$$\frac{1}{\beta} = \sqrt{\frac{U}{a}\left(1 - \frac{M^2}{2<m^2>Ug}\right)} \quad .$$

Defining the spin cutoff parameter, σ^2, as

$$\sigma^2 = g<m^2>/\beta \simeq g<m^2>\sqrt{\frac{U}{a}} \quad ,$$

the density-of-states may be written

$$\rho(U,M) = \frac{1}{12\sqrt{2}} \frac{\exp(2\sqrt{aU} - M^2/2\sigma^2)}{a^{1/4}U^{5/4}\sigma} \quad .$$

Gilbert and Cameron give an expression for σ^2,

$$\sigma^2 = 0.0888 \sqrt{aU}\, A^{2/3} \quad .$$

In using this formula, the energy, U, has been defined as the excitation energy, the energy of the system relative to that of the fully degenerate ground-state. This would be the ordinary ground-state of the nucleus were it not for the presence of the residual pairing interaction, not present in the highly excited nucleus this formula is supposed to describe. If X_o denotes the energy of the ground-state in the absence of pairing and E_o denotes the energy of the ground-state in the presence of pairing, the two energies are related by

$$X_o - E_o = P \quad ,$$

where P is the pairing interaction energy. If E is the energy of the nucleus, the excitation energy to be used in the formula, U, is given by

$$U = E - X_o = E - E_o - P \quad .$$

The quantity, $E - E_o$, is the usual definition of the excitation energy, E^*. Hence, in using the formula with the standard definition of the excitation energy, $U = E^* - P$ is the energy to use.

In this form, the density-of-states expression is not very useful, the appearance of the unobservable spin projection, M, appearing explicitly. One may, however, extract from this expression the angular momentum dependent density-of-states expression which may be integrated over all angular momenta to give the total density-

of-states expression. This expression is most easily obtained by integrating over M to get the total density-of-states, $\rho(E)$,

$$\rho(E) = \int_{-\infty}^{\infty} \rho(E,M)\, dM = \frac{\sqrt{\pi}}{12} \frac{\exp(2\sqrt{aU})}{a^{1/4} U^{5/4}} \quad ,$$

so that

$$\rho(E,M) = \frac{\rho(E)}{\sigma\sqrt{2\pi}} \exp\left(\frac{-M^2}{2\sigma^2}\right) \quad .$$

The angular momentum dependent form must be extracted, however, since it is necessary for the modeling of the density parameter, described in Appendix F.

For a given value of M, the M-dependent density contains states of all angular momenta, J, with $J \geq M$. Denoting the contributing nuclear states by $|J,M\rangle$, consider the densities, $\rho(U,M=J)$ and $\rho(U,M=J+1)$. Terms which appear in $\rho(U,M=J)$ are

$$|J,J\rangle,\ |J+1,J\rangle,\ |J+2,J\rangle,\ldots. \quad ,$$

and in $\rho(U,M=J+1)$,

$$|J+1,J+1\rangle,\ |J+2,J+1\rangle,\ |J+3,J+1\rangle,\ldots.$$

For every state, $|J+n,M\rangle$, there is a state, $|J+n,M-1\rangle$, where n=1,2 and so on. The difference, $\rho(U,M=J) - \rho(U,M=J+1)$ contains only the terms, $|J,M=J\rangle$. Therefore, the density of states of $|J,M=J\rangle$ is

$$\rho(E,J,M=J) = \frac{\rho(E)}{\sqrt{2\pi\sigma^2}} \left\{ \exp\left(\frac{-J^2}{2\sigma^2}\right) - \exp\left(\frac{-(J+1)^2}{2\sigma^2}\right) \right\}$$

$$\simeq \frac{\rho(E)}{\sqrt{2\pi\sigma^2}} \left\{ \left(\frac{2J+1}{2\sigma^2}\right) \exp\left(\frac{-(J+1/2)^2}{2\sigma^2}\right) \right\} \quad .$$

Each of these states is (2J+1)-fold degenerate. This expression is used in the modeling of the density parameter in Appendix F.

No mention has been made so far of the parity of the various states in these results. The density-of-states expression derived includes states of all parity. At high excitation energy, the number of states of even and odd parity, denoted by π = even and π = odd, are assumed to be equal. Hence, the density of states of a given parity is related to the above expressions by introducing an overall factor of 1/2. For example,

$$\rho(E,\pi=\text{even}) = \rho(E,\pi=\text{odd}) = \frac{1}{2}\rho(E) \quad .$$

This point shall also be important in the modeling of Appendix F.

Gilbert and Cameron sought an expression for the density of states for use over the entire range of excitation energies to be used in calculations of the capture processes. The expression derived diverges at low energies. They proposed the inclusion of the empirically observed behavior of the density at low excitation,

$$\rho_L(E) = \frac{1}{T}\exp\left(\frac{E - E_o}{T}\right) \quad ,$$

where the L-subscript denotes low excitation energy and E_o and T, the temperature, are constants. This form is then coupled to the higher excitation form, derived above, in such a way that the density may be described continuously as a function of energy. To do this, they defined a crossover energy, E_x, at which the two formulas join smoothly,

$$\rho_L(E_x) = \rho_H(E_x) \qquad \rho_L'(E_x) = \rho_H'(E_x) \quad .$$

The H-subscript denotes the high excitation form based upon the equidistant spacing assumption and the prime (′) denotes differentiation with respect to energy. These two conditions define the low excitation form constants, T and E_o,

$$\frac{1}{T} = \sqrt{\frac{a}{U}} - \frac{5}{4U} \quad ,$$

$$E_o = E_x - T \ln[T\rho_H(E_x)] \quad .$$

In defining the temperature, T, here, the total density-of-states expression has been used. With these forms and a data set describing nuclei at both high and low excitation energies, a model for the density parameter, a, was determined and an expression for the cross-over energy, E_x, was given. The crossover energy was found to occur at

$$E_x = 2.5 + 150/A + P \quad ,$$

where P is the pairing correction energy and all quantities are given in MeV. This formula was determined by finding a value of E_x for each nucleus that best fit both the low and high excitation energy data. The formula reproduced the E_x values thus determined to about ±200 keV.

One of the objectives of the work of Gilbert and Cameron [17] was to model the density parameter, a, to include the observed effect of nuclear shells upon the density. They found that the predicted and measured values were in better agreement if the density parameter was assumed to be of the form,

$$a/A = p_1 + p_2 S \quad ,$$

where S is the shell correction to the nuclear mass and p_1 and p_2 are constants to be determined. This model is further discussed in Appendix F. One may see, however, that in order to use this expression for the density, a set of single-particle energies, S and P, are needed. Before the introduction of the Strutinsky procedure [38], the method for determining these energies was ill-defined. However, with two empirically adjustable parameters for each nucleus, a great degree of flexibility exists to improve the agreement between predicted and measured values of the density while maintaining the simplicity of the equidistant model.

A first order correction may be made to the assumption of equidistant spacing of the single-particle levels without losing the analytical form for the density expression. This has been proposed for use in the problem of predicting observed resonance spacings by Kataria et al. [21]. In this treatment, the single-particle spectrum is written as a Fourier series,

$$g(\varepsilon) = \sum_m g_m \cos(m\omega\varepsilon - \phi_m) \quad ,$$

where ε is the energy of the single-particle states, ω is the fundamental frequency of oscillation of the spectrum, and ϕ_m is a phase term. Dropping all but the m=0 and m=1 terms from the expansion, they give expressions for the entropy, S, and the excitation, U, by

$$S = 2aT + \left(\frac{\Delta_s}{T}\right)\left[\frac{\pi^2\omega^2T^2\cosh(\pi\omega T)}{\sinh^2(\pi\omega T)} - \frac{\pi\omega T}{\sinh(\pi\omega T)}\right] \quad ,$$

$$U = aT^2 + \Delta_s \left[\frac{\pi^2\omega^2T^2\cosh(\pi\omega T)}{\sinh^2(\pi\omega T)} - 1 \right] \quad ,$$

the density parameter is again denoted by a and T is the temperature, determined by solving the excitation energy equation. The energy, U, again differs from the nuclear excitation energy by the pairing energy, P, and, to avoid confusion, the shell correction term has been written as Δ_s. These expression are to be used with the high excitation energy form of the analytical density expression with S being the argument of the exponential. To determine the model parameters by fitting, the J-dependent form must be used. The spin cutoff parameter used in the model is given by

$$\sigma^2 = \frac{I_{rigid}}{h^2}\left(\frac{S}{2a}\right) \quad ,$$

$$I_{rigid} = \frac{2}{5} M R^2 \quad .$$

where M is the nuclear mass, R is the radius of a spherical nucleus of that mass, h is Planck's constant, and I_{rigid} denotes the rigid-body moment of inertia. Note that these expressions asymptotically assume the Gilbert and Cameron [17] values,

$$T \simeq \sqrt{\frac{U}{a}} \qquad S \simeq 2\sqrt{aU} \quad ,$$

ω is assumed to behave as $\omega_o A^{1/3}$ with ω_o in the range 0.15 to 0.2 . The density parameter is assumed to be of the form,

$$a/A = \gamma(1. - \beta B_s/A^{1/3}) \quad ,$$

with γ and β constants to be determined and B_s being the ratio of the surface area of the nucleus relative to a spherical nucleus

of a spherical nucleus of the same volume. Note that, through the B_s term, this model introduces deformation in a natural way, a feature not present in the Gilbert and Cameron [17] model. This is an important point in this work since, in general, the fission fragments are highly deformed at the scission-point and the single-particle correction energies are also shape dependent.

Each of the models presented here shall be examined in Appendix F and their parameters determined and discussed.

APPENDIX F

The Density Parameter

The observed neutron resonance spacing, $< D >$, provides an experimental measure of the level density,

$$\rho = \frac{1}{< D >} \quad .$$

In the mass range 70 to 165, 99 values of $< D >$ are available[18] from s-wave neutron capture measurements with a corresponding excitation energy of the compound nucleus formed of one neutron separation energy. With this data, one may assume a model for the density parameter, a, to be used in the analytical density-of-states model of Appendix E, and determine its parameters by fitting.

Single-particle shell and pairing energies, S and P, appear in the analytical density models and must be known before fitting can begin. In principle, these are the Strutinsky correction terms described in Appendix A. Since the analytical density expression predates the Strutinsky procedure, various empirical sets of these energies have evolved and are generally used with this model.

The first set of single-particle energies was determined by Cameron and Elkin[(61)] and was used by Gilbert and Cameron[17] in their model. The procedure for determining these is described in Appendix G. In determining their model for the density parameter, Gilbert and Cameron found it necessary to devide their data into two sets, one corresponding to nuclei with spherical

ground-state shapes and one corresponding to nuclei with deformed ground-state shapes. They chose a model with a linear dependence of the density parameter upon the shell correction energy. The model was otherwise assumed to be proportional to the mass number, A. Fitting then gave,

$$a/A = 0.00917\,S + 0.142 \qquad \text{undeformed}$$

$$a/A = 0.00917\,S + 0.120 \qquad \text{deformed}$$

Later, Cameron and Brancazio[20] concluded that the required separation into deformed and undeformed groups was the result of an improper determination of the single-particle terms. They redetermined the model with the result,

$$a/A = 0.143 + 0.0091\,(S - 0.23\,D)$$

where S was the old shell term and D is the difference in the number of neutrons or protons in the nucleus in question from that of the nearest spherical closed shell nucleus.

Cook et al.[18] took the Gilbert and Cameron model and empirically adjusted the S and P values to improve the agreement between predicted and measured values of $\langle D \rangle$. The P values were taken by Kataria et al.[21] in the determination of their model, also described in Appendix E. Their shell terms were, however, determined independently by using the liquid-drop part of the Seeger and Howard mass formula[9] and experimental masses[50] to give

$$\Delta_s = m_{exp} - m_{ld} - P_{Cook}$$

Here, m_{ld} is the liquid-drop portion of the Seeger and Howard[9] mass formula, P_{Cook} is the paring term as given by Cook et al.[18], m_{exp} is the experimentally measured mass[50], and Δ_s is the shell correction energy.

Fitting was performed to detemine models for the density parameter using several of these published data sets. For the disussion that is to follow, the two data sets appearing in Tables 14 and 15 are used. The data in Table 14 is determined from the Kataria prescription and the data in Table 15 is taken from the mass formula work of Appendix A. These two data sets are chosen to compare the results achieved with the empirically determined energies with those given by the Strutinsky prescription of Appendix A. The conclusions are not changed by the use of any of the other data sets mentioned.

In the fitting procedure, several models are to be considered. Needed is some criterion for determining the preference for one model over another. The quality of fit is indicated by the sum of squares of the residual errors, SS,

$$SS = \sum_{\text{data, } i} \left[f_i - f_{ci}(\vec{p}) \right]^2$$

where f_i is the i^{th} datum and $f_{ci}(\vec{p})$ is the calculated value of the i^{th} datum, dependent upon model parameters, $\vec{p}$.

As the number of parameters in the model increases, SS decreases, in general. The criterion for determining the signifi-

cance of an additional parameter is provided by analysis of variance techniques[62]. This is done by testing simple hypotheses. Assume that a p-parameter model has been determined from n data points giving a sum of squares of SS1. If one wishes to determine the significance of q of these parameters, the q parameters are set to zero and the model redetermined for the remaining parameters, giving a sum of squares, SS2. In general, SS2 is greater than SS1. One then forms the F-statistic,

$$F = \frac{\frac{SS2 - SS1}{q}}{\frac{SS1}{n-p}} ,$$

the ratio of the variance per gegree of freedom attributable to the q hypotheses and the variance per degree of freedom of the residual fit. This ratio is distributed as $F_{q,n-p}$, the F-statistic with q and n-p degrees of freedom. If the hypotheses are valid, the q parameters will add little to the quality of fit, SS2, and a low value of F will be obtained. If the hypotheses are not valid, SS2 will increase such that a larger value of F is obtained. For a given value of F, the power of the test is given by α,

$$\alpha = \int_F^\infty F_{q,n-p}(x)\, dx$$

The power of the test is related to the conifidence level for rejection by

$$\text{confidence} = 1 - \alpha$$

In general, 95% is taken as the confidence level for solid rejection of a hypothesis, or $\alpha = 0.05$. The hypothesis that q of the parameters are insignificant(zero) is then rejected if

$$F \geq F_{q,n-p,\alpha} \quad ,$$

where values of $F_{q,n-p,\alpha}$ are taken from standard tables[62]. The determination of a model for the density parameter, a, of the analytical density model may now begin.

In s-wave neutron capture by a nucleus, the parity, π, of the target nucleus is presumed to be a good quantum number. With a target nucleus of spin, J_o, either of two states may be formed in the compound nucleus, $J_o \pm 1/2$, with only the $J = 1/2$ state being formed for a spinless target. The predicted value of the observed neutron resonance spacing, $\langle D \rangle$, is then given by

$$\begin{aligned} \frac{1}{\langle D \rangle} &= \rho(E_x, J) \\ &= \rho(E_x, J_o+1/2, \pi) + \rho(E_x, J_o-1/2, \pi) \\ &= \frac{1}{2}\left[\rho(E_x, J_o+1/2) + \rho(E_x, J_o-1/2)\right] \quad . \end{aligned}$$

As a starting point, consider the model originally proposed by Bethe[16],

$$a = p_1 A \quad ,$$

where A is the mass number of the compound nucleus. Using a standard Marquardt fitting algorithm[63] and data from Table 15,

$$p_1 = .27712 \qquad SS = 4.135 \times 10^8 \quad .$$

Gilbert and Cameron suggested the inclusion of a shell energy correction term, S,[17]

$$a = p_1 A(1 - p_7 S) \quad .$$

Refitting yields

$$p_1 = .25317 \qquad p_7 = .11713 \qquad SS = 3.151 \times 10^8$$

The hypothesis, $p_7 = 0$, may now be tested to determine the significance of p_7. Forming the F-statistic,

$$F = \frac{\dfrac{4.135 \times 10^8 - 3.151 \times 10^8}{1}}{\dfrac{3.151 \times 10^8}{99-2}} = 30.3$$

since there are 99 data points in Table 15. Consulting a table of values of $F_{2,97,.05}$[62] gives $F_{2,97,.05} = 3.95$. The hypothesis, $p_7 = 0$, may then be rejected at greater than 95% confidence.

Ignatyuk et al.[19] pointed out that the shell effects present in the ground-state tend to wash out with incresing excitation energy. To include this effect, they proposed a model of the form,

$$a = \hat{a}\left[1 - F(U)\cdot S/U\right] \qquad F(U) = 1 - \exp(-p_7 U) \quad ,$$

where U is the excitation energy reduced by the pairing energy and $\hat{a}$ is a polynomial is A. Assuming this model with $\hat{a} = p_1 A$,

$$p_1 = .27012 \qquad p_7 = .16279 \qquad SS = 3.099 \times 10^8 \quad .$$

a slight improvement in the quality of fit over that given with the Gilbert and Cameron model. The two models with the shell term are not related by a simple hypothesis and an F-statistic can not

be formed. Model selection becomes subjective at this point. The wash-out feature of the Ignatyuk model[19] is desireable and is therefore kept.

Continuing with the Ignatyuk form for the shell term dependence, the following general form for $\hat{a}$ is tested,

$$\hat{a} = p_1 A + p_2 A^2 + p_3 A^3 + p_4 A^4 + p_5 A \left[1 - (-)^Z\right] + p_6 A \left[1 - (-)^N\right],$$

where N and Z are the number of neutrons and protons in the compound nucleus. Note that the terms p_5 and p_6 allow pairing effects in the a-parameter. Of particular interest here is the question of possible error in the pairing energy term, P. If such errors are present, the parameters, p_5 and p_6, should compensate somewhat. The extent to which these parameters are significant gives an indication of even-odd behavior in the density parameter from this, or any other, source.

The parameters of this proposed model are determined by fitting and the significance determined by comparison of the quality of fit to other models connected by simple hypotheses through a F-test. The results of the fitting and testing are tabulated here. The quantity, F_{crit}, denotes the values of $F_{q,n-p,.05}$ taken from Reference 62.

Case	p_i allowed	F-test relative to	SS x 10^{-8}	n-p	q	F	F_{crit}
0	1,7	———	3.099	—— reference case ——			
1	1,2,7	case 0	1.150	96	1	163.5	3.95
2	1,2,5,6,7	case 1	1.146	94	2	.16	3.10
3	1,2,3,7	case 1	1.020	95	1	12.1	3.95
4	1,2,3,4,7	case 3	1.011	94	1	.84	3.95
5	1,2,3,5,6,7	case 3	1.027	93	2	<0	

The parameters of case 3 give the best fit without introduction of insignificant parameters. Of note here is the apparent lack of sensitivity of the model to the pairing terms, p_5 and p_6.

In the modeling of the density expression of Kataria et al.[21], the same procedure is used. A different quality of fit indicator is suggested also, differing in a rather fundamental way from that used previously. Since the observed values of the resonance spacings vary over some three orders of magnitude, a more pleasing overall fit may be achieved by fitting logarithms of the predicted and measured values. This gives, as a measure of the quality of fit, the sum of the squares of logarithms of the ratio of computed and measured values. The model error, by this assumption, is given in terms of an overall multiplicative factor rather than and additive factor. The coefficient, β, in the Kataria model can not be determined very well since there is such little variation in the values of B_s in Table 15. Theoretically, $\beta \simeq 1$ is expected[21]. This is a hypothesis which may be tested. In each of the models postulated below, fitting was performed for both of the cases, $\beta = 0$ and

$\beta = 1$. The F-test may then be applied to the hypothesis, $\beta = 0$.

To compare the model of Gilbert and Cameron[17] to that of Kataria[21], only subjective choices may be made since the models are not connected by simple hypotheses. Recall, however, that the Kataria model is expected to be an improvement over the Gilbert and Cameron model. For the purpose of comparison, each of the models is tested with each of the two data sets, Tables 14 and 15, and for the two quality-of-fit indicators, denoted here by ϕ_{ss} and $\phi_{\ell n}$,

$$\phi_{ss} = \sum_{data} \left(D_{measured} - D_{calculated} \right)^2$$

$$\phi_{\ell n} = \sum_{data} \left[\ell n \left(\frac{D_{calculated}}{D_{measured}} \right) \right]^2$$

The results of the the eight possible combinations are summarized in Table 16.

Regarding the β parameter of the Kataria model, three of the four models indicated no preference for this parameter, i.e., the hypothesis, $\beta = 0$, could not be rejected with confidence. The remaining test indicated a clear loss in quality of fit with $\beta = 1$. The ω_o parameter of the Kataria model is to be in the range of 0.15 to 0.2. Three of the four tests then give undesirably large values of this parameter. Overall, the best results appear to come from the empirically adjusted parameters of Table 14. Using $\phi_{\ell n}$ as the quality of fit indicator gives a larger number of computed values within an overall multiplicative factor of two of the mea-

sured values in the range,

$$2 \geq \frac{D_{calculated}}{D_{measured}} \geq \frac{1}{2} \quad .$$

This may reflect the adjustment of the S and P terms performed by Cook et al.[18]. Worthy of note here are the predictions of the numerical density expression(Appendix D) made by Huizenga et al.[14,15]. With no adjustable parameters and no explicit shell and pairing energies, the numerical model achieves predictions of comparable quality for both spherical and deformed nuclei.

The quantity denoted $\hat{a}^{-1}$ in Table 16 is also noteworthy. It represents the value of the polynomial part of the a-model devided by the mass number, A, and averaged over the data set, i.e., excluding shell effects, $a \approx A/\hat{a}^{-1}$. The indication is that

$$4 \leq \hat{a}^{-1} \leq 7 \quad .$$

Computing densities with the numerical model of Appendix D and solving for the density parameter of the analytical model gives

$$8 \leq \hat{a}^{-1} \leq 12$$

with an average of 9.5. It has been argued that $\hat{a}^{-1} = 20$ should be used with the analytical model in computing fission product yields[1]. The basis for this statement is unknown and the indication here is that it is wrong.

The pairing terms, p_5 and p_6, appear to be of significance with both data sets. No conclusion can then be drawn regarding the presence of a error introduced by using the entire pairing energy in Table 15 rather than a correction-type pairing term.

In summary, the comparison of computed and measured values of <D> does not indicate the periodic level scheme to be a great improvement over the equidistant spacing scheme. Comparison of the predictions of the analytical model to those of the numerical model over a wide range of excitation energies gives some indication of the validity of the assumed $e^{2\sqrt{aU}}$ dependence and the adjustment necessary to obtain agreement not only with the <D> measurements, but also with values of the density at higher excitation energies than those at which the measurement of <D> was made. Tests on the β-parameter of the model of Kataria et al.[21] were inconclusive leaving open the question of the effect of deformation on the density parameter. If one must use the analytical model for the prediction of <D> , the best results are obtained using the empirically adjusted P values of Cook et al. and the shell energy prescription of Kataria et al., as in Table 14. It should be noted that these are determined from measurements on nuclei lying near the line of β-stability. The question of extrapolating this model into the neutron-rich region remains open. Again, the numerical density model of Appendix D avoids all of these questions.

APPENDIX G

The Single-Particle Shell and Pairing Energies

In order to improve the quality of mass formulas, Cameron and Elkin[61] attempted to extract single-particle energies, S, the nuclear correction term, and P, the pairing energy, from measured masses. To do this they define a correction term for each mass, C(N,Z),

$$C(N,Z) = m_{exp}(N,Z) - m_{ld}(N,Z) \quad ,$$

where $m_{exp}(N,Z)$ is a measured mass, and m_{ld} is the mass predicted by a liquid-drop mass formula. The object is to decompose C(N,Z) into individual contributions from shell and pairing effects for neutrons and protons independently,

$$C(N,Z) = C(N) + C(Z) = S(N) + P(N) + S(Z) + P(Z) \quad .$$

The general procedure for the determination of the S and P values is to minimize the sum,

$$\sum_{data} \left[m_{exp}(N,Z) - m_{ld}(N,Z) - S(N) - P(N) - S(Z) - P(N) \right]^2 \quad .$$

However, for each "known," m_{exp}, four "unknowns" are introduced and there are more "unknowns" than equations. To circumvent this problem and simplify the algebra, difference equations are formed. Letting $\delta(C)i$ and $\delta^2 C(i)$ be defined as

$$\delta C(i) = C(i) - C(i-1)$$

$$\delta^2 C(i) = C(i) - 2C(i-1) + C(i-2)$$

where i may be N or Z, the following difference equations, with values of h and k, may be formed,

$$h = (1/2)\delta^2 C(i) = (1/2)[\delta C(i)+\delta C(i-2)] - \delta C(i-1)$$

$$= (1/2)\delta^2 S(i) + (1/2)[\delta P(i)+\delta P(i-2)] - \delta P(i-1)$$

$$= (1/2)\delta^2 S(i) + (1/2)[P(i)-P(i-3)] - (3/2)[P(i-1)-P(i-2)]$$

$$k = -(1/2)\delta^2 C(i+1)$$

$$= -(1/2)\delta^2 S(i+1) -(1/2)[P(i+1)-P(i-2)] + (3/2)[P(i)-P(i-1)]$$

To guarantee a unique solution, the assumptions are made that for odd particle numbers, i, P(i) = 0, and that the shell terms vary smoothly between closed shells such that $\delta^2 S(i) = 0$. These assumptions reduce the number of unknowns and simplify the set of difference equations to be solved. The P(i) are then given, for even i, by solving the following set of equations,

$$h = -\frac{3}{2} P(i-1) - \frac{1}{2} P(i-3)$$

$$k = -\frac{1}{2} P(i+1) - \frac{3}{2} P(i-1)$$

The S(i) are then given, for even i, by

$$S(i) = C(i) - P(i) \quad .$$

For odd i,

$$P(i) = 0$$

$$S(i) = C(i) \quad .$$

By this procedure, Cameron and Elkin[61] determined their set of shell and pairing correction energies.

Cook et al.[18] later addressed the problem of shell and pairing corrections in order to improve the agreement between the measured and

predicted values of neutron resonance spacings. They empirically adjusted the Cameron and Elkin values as necessary to improve the agreement. In their work, the values S and P were constrained to sum to the constant determined by Cameron and Elkin,

$$[S(i) + P(i)]_{Cook} = [S(i) + P(i)]_{Cameron\text{-}Elkin} = C(i) \quad .$$

The Cook data set thus determined appears to be the most widely used with the analytical density expression, the improved fit offered as justification for the adjustment.

This method of determining single-particle correction energies predates the Strutinsky procedure[38] and is still in widespread use. The Strutinsky procedure, as described by Nix,[40] predicts S and P values with the same physical significance. In Appendix A, the mass formula of Seeger and Howard[9] is discussed. In it the shell correction energy is computed and may be used with the analytical density expression. The pairing energy is not a correction, in the Strutinsky sense, but represents the total energy attributed to the pairing interaction, i.e., it includes the smooth Strutinsky pairing term also. As such, it may not be suitable for use in the analytical density expression. To allow for this error, the density parameter model of Appendix F was allowed to exhibit even-odd fluctuations.

APPENDIX H

The Extraction of Shape Parameters

The fragment shapes are given in terms of the Nilsson parameters, ε and ε_4, by Nix [40]

$$R_\varepsilon(\theta) = \frac{R_o}{\lambda_\varepsilon}\left\{\frac{1 - \frac{1}{3}\varepsilon + \frac{2}{3}\varepsilon P_2(\cos\theta_t)}{1 - \frac{2}{3}\varepsilon P_2(\cos\theta_t) + 2\,\varepsilon_4 P_4(\cos\theta_t)}\right\}^{1/2} ,$$

where

$$\cos(\theta_t) = \left\{\frac{1 - \frac{2}{3}\varepsilon}{1 + \frac{1}{3}\varepsilon - \varepsilon\cos^2(\theta)}\right\}^{1/2}\cos(\theta) ,$$

where λ_ε is a volume preserving factor. A more transparent expression is given by expanding the nuclear radius in Legendre Polynomials,

$$R_\alpha(\theta) = R_o/\lambda_\alpha\left[1 + \alpha_2 P_2(\cos\theta) + \alpha_4 P_4(\cos\theta)\right] .$$

The term, λ_α, is also a volume preserving factor. The coefficients, α_i, may be extracted from the Nix expression by evaluating the integrals,

$$\alpha_2 = \frac{5}{2}\cdot\frac{\lambda_\alpha}{\lambda_\varepsilon}\int_{-1}^{1} R_\varepsilon(\theta)\, P_2(\cos\theta)\, d(\cos\theta) ,$$

$$\alpha_4 = \frac{9}{2}\frac{\lambda_\alpha}{\lambda_\varepsilon}\int_{-1}^{1} R_\varepsilon(\theta)\, P_4(\cos\theta)\, d(\cos\theta) .$$

Seeger and Howard [9] give approximate values of these coefficients,

$$\alpha_2 = \frac{2}{3}\varepsilon + \frac{5}{63}\varepsilon^2 + \frac{2}{21}\varepsilon\varepsilon_4 + \frac{50}{231}\varepsilon_4^2 ,$$

$$\alpha_4 = -\varepsilon + \frac{12}{35}\varepsilon^2 - \frac{50}{231}\varepsilon\cdot\varepsilon_4 + \frac{243}{1001}\varepsilon_4^2 \quad .$$

All yield calculations were performed using the Nix expression to give the nuclear center-to-tip distances, needed to evaluate the Coulomb energy. For illustration, α's computed by the above integrals appear in Table 1. Other terms appearing there for comparison are AA, the exact center-to-tip distance, $R_\varepsilon(\theta=0)$, and AAP, the center-to-tip distance given by the two term Legendre expansion, $R_\alpha(\theta=0)$. Both are given in terms of R_o. The term, AAP, is the volume preserving factor, λ_α.

APPENDIX I

The Energy Available for Prompt Neutron Emission

The prompt neutrons are assumed to be emitted from the fission fragments after scission. The amount of energy in internal excitation determines the probability of neutron emission. At scission, the fragments are excited by an energy, E, and have an amount of energy, D, involved in shape deformation. As the shape relaxes to that of the ground-state, the deformation energy is fed into internal degrees of freedom giving the energy available for prompt neutron emission, E_n, by

$$E \leq E_n \leq E + D$$

The rate at which the deformation energy is converted into internal excitation is then important. If the time is long relative to the time required for the emission of a neutron, the neutrons will appear to come from a nucleus of excitation less than E + D. If the relaxation time is short, the neutrons will appear to come from a more highly excited nucleus. A estimation of the relevant time is presented and discussed here.

The nucleus is treated as a viscous vibrator with inertial parameter, M, spring constant, K, and dissipation coefficient, η. Assuming the shape to be described by a single deformation coordinate, α, the Lagrangian describing the motion is,

$$L = T - V = (1/2)M\dot{\alpha}^2 - (1/2)K\alpha^2 \quad ,$$

and the Rayleigh dissipation function is

$$(1/2)\eta\dot{\alpha}^2$$

The equation of motion is

$$M\ddot{\alpha} + \eta\dot{\alpha} + K\alpha = 0. \quad .$$

Assuming the intitial conditions, $\alpha(0) = \alpha_o$ and $\dot{\alpha}(0) = 0.$, the solution is

$$\alpha(t) = \alpha_o \exp(-\gamma t)[\cos(\omega t) + \left(\frac{\gamma}{\omega}\right)\sin(\omega t)] \quad ,$$

where

$$\gamma = \eta/2M \quad \omega^2 = \omega_o^2 - \gamma^2 \quad \omega_o^2 = K/M \quad .$$

Davies, Nix, and Sierk[10] give, for ellipsoidal-shaped liquid-drops,

$$\eta = 4\pi(R_o^3/c^2)\mu \qquad M = \frac{1}{5}[\,1 + (R_o/c)^3\,]\,M_o$$

where

R_o = relaxed nuclear radius = $r_o A^{1/3}$

c = semi-major axis length

M_o = rest mass = $A\,m_n$

$\mu = 3 \times 10^{10}$ Poise

m_n = one mass unit = 931 MeV/(speed of light)^2

1 Poise = 10^{-33} MeV-sec/fm^3

A = mass number .

The value of r_o is taken from the mass formula work of Appendix A,

$r_o = 1.2254$ fm. .

Estimates of the damping time may then be made.

From Table 1, it may be seen that values of c range from 1.0 to 1.6 times R_o. For the heaviest nuclei of interest here, $A \simeq 150$, γ is approximately 2.0×10^{21} sec^{-1}. This gives a characteristic damping time of 5.0×10^{-22} sec. Vandenbosch and Huizenga[32] report a characteristic time for the emission of neutrons from the

fragments of about 10^{-20} sec. Hence, it appears that the shape may be relaxed before a neutron is emitted. The implication for this work is that all of the deformation energy should be included as excitation energy of the nucleus from which the first neutron is emitted.

A related quantity in this regard, leading to the opposite conclusion, is the kinetic energy of the prompt neutrons as given in the yield calculation. According to Vandenbosch and Huizenga[32], the average laboratory kinetic energy of the neutrons is about 2 MeV. Of this, approximately 2/3 MeV is the result of the center-of-mass to laboratory transformation. In the yield calculation, the center-of-mass neutron kinetic energy was recorded. For $^{235}U(n_{th},f)$, the value is about 1.5 MeV, about 0.2 MeV higher than that indicated by Vandenbosch and Huizenga. An estimate of the error indicated in the fragment excitation energy may be made. The neutron kinetic energy in the center-of-mass of the fragment, T_n, is related to the temperature of the nucleus, T, by

$$T_n \simeq 2\,T \quad .$$

The nuclear temperature is related to the excitation energy, E_x, approximately, by

$$T \propto \sqrt{E_x} \quad .$$

Then,

$$dT_n = \frac{1}{2}\left(\frac{T_n}{E_x}\right) dE_x$$

For E_x = 12 MeV, an average computed for $^{235}U(n_{th},f)$,

and $T_n = 1.5$ MeV, $dT_n \simeq 0.2$ MeV implies that $dE_x \simeq 3.2$ MeV, a value typical of the deformation energy of the fragments in the vicinity of the mass peaks. The inclusion of the deformation energy in the calculation of the emission of the first neutron may then be in error. This point should be kept in mind in using the computed fission product mass-chain yields. As indicated in Appendix J, the problem of prompt neutron emission is an area for potentially great improvement in this model.

APPENDIX J

Prompt Neutrons

Two methods are offered to estimate the number of prompt neutrons emitted from the highly excited fission fragments and to relate the computed fission fragment yields to the measured fission product yields. The spectrum of neutrons emitted from an excited nucleus is assumed to be given by a simple evaporation model,

$$P(k) = \left(\frac{k}{T^2}\right)\exp(-k/T)$$

where P(k) is the probability of emitting a neutron of kinetic energy, k, from a nucleus excited by an energy, E, to a temperature, T. This particular probability distribution gives an average value of the kinetic energy of $2T$. In emitting a neutron, the nucleus cools by an energy of $S_1 + 2T$, where S_1 is the neutron separation energy of the emitting nucleus. The simplest assumption, valid at high excitation energies, is that the nucleus will emit a neutron of kinetic energy, $2T$, if it is energetically possible, i.e., if $E \geq S_1 + 2T$. The procedure may be repeated for the product nucleus until emission of further neutrons is energetically impossible. The remaining energy may be assumed to appear as prompt gamma-ray energy. This method is called the 2T-model in the text.

In the next treatment, it is noted that the spectrum has a finite upper limit, $k = E - S_1$. If S_2 is the neutron separation energy of the product nucleus, emission of a neutron of kinetic energy, $k > E - S_1 - S_2$, will result in a product nucleus too cool to emit another neutron. Any neutron emitted with energy less than this results in a product nucleus with sufficient excitation energy to emit another neutron. The probability of terminating the neutron emission sequence with the emission of one more neutron, P_{stop}, is then given by

$$P_{stop} = C \int_{E-S_1-S_2}^{E-S_1} \left(\frac{k}{T^2}\right) \exp(-k/T)\, dk \quad .$$

The probability of continuing the sequence, P_{go}, is given by

$$P_{go} = 1 - P_{stop} \quad .$$

C is the normalization constant given by integrating the spectrum to its upper limit, $E - S_1$.

For each case, an average neutron kinetic energy may be computed and recorded. This is used to give the average excitation of the product nucleus and the average neutron kinetic energy for the neutrons emitted from that fragment, necessary to compute ν_p. Once neutron emission is no longer possible, determined by $P_{go} < 10^{-3}$, the remaining energy is assumed to appear as prompt gamma-ray energy. This treatment is called the Simple Cascade Model in the text.

The treatments suggested here for computation of the

prompt neutron number and kinetic energy is not meant as a definitive answer to the problem, but is offered as an estimate of the relationship between fission fragment and fission product yields. A more realistic treatment must properly address the problems of gamma decay competition with neutron emission in the later stages of decay and the rate at which deformation energy at the scission-point is dissipated, producing internal excitation energy which may lead to prompt neutron emission. Both of these problems are left open for further improvement. A careful treatment should improve the estimates of both ν_p and the neutron kinetic energy.

EP	EP4	ALAMP	ALPHA2	ALPHA4	AAP	AA
-.35	-.08	1.011	-.2211	.1122	.8812	.8559
-.30	-.08	1.009	-.1903	.1037	.9056	.8847
-.25	-.08	1.006	-.1592	.9639E-01	.9314	.9147
-.20	-.08	1.004	-.1278	.9051E-01	.9587	.9462
-.15	-.08	1.003	-.9599E-01	.8606E-01	.9874	.9792
-.10	-.08	1.002	-.6385E-01	.8309E-01	1.018	1.014
-.05	-.08	1.001	-.3135E-01	.8167E-01	1.049	1.050
0.00	-.08	1.001	.1532E-02	.8185E-01	1.083	1.089
.05	-.08	1.001	.3481E-01	.8370E-01	1.117	1.130
.10	-.08	1.002	.6849E-01	.8729E-01	1.154	1.173
.15	-.08	1.003	.1026	.9269E-01	1.191	1.219
.20	-.08	1.005	.1371	.9997E-01	1.231	1.269
.25	-.08	1.008	.1721	.1092	1.272	1.321
.30	-.07	1.011	.2073	.1093	1.303	1.358
.35	-.06	1.014	.2431	.1113	1.336	1.396
.40	-.05	1.018	.2795	.1156	1.370	1.435
.45	-.04	1.023	.3166	.1222	1.406	1.476
.50	-.03	1.029	.3543	.1313	1.444	1.520
.55	-.02	1.035	.3928	.1431	1.484	1.565
.60	-.01	1.042	.4320	.1578	1.525	1.613
-.35	-.04	1.010	-.2229	.7495E-01	.8432	.8271
-.30	-.04	1.008	-.1921	.6574E-01	.8669	.8538
-.25	-.04	1.006	-.1609	.5786E-01	.8921	.8817
-.20	-.04	1.004	-.1293	.5137E-01	.9187	.9108
-.15	-.04	1.002	-.9744E-01	.4633E-01	.9469	.9413
-.10	-.04	1.001	-.6521E-01	.4278E-01	.9765	.9732
-.05	-.04	1.000	-.3261E-01	.4079E-01	1.008	1.007
0.00	-.04	1.000	.3634E-03	.4042E-01	1.041	1.042
.05	-.04	1.000	.3373E-01	.4174E-01	1.075	1.079
.10	-.04	1.001	.6751E-01	.4482E-01	1.111	1.119
.15	-.04	1.002	.1017	.4972E-01	1.149	1.160
.20	-.04	1.004	.1363	.5653E-01	1.188	1.205
.25	-.04	1.007	.1714	.6533E-01	1.229	1.252

Table 1: Approximate realationship between the parameters of the Nilsson model[41], EP and EP4, and those of a collective radial expansion in Legendre polynomials, ALPHA2 and ALPHA4, described in Appendix H. The Nilsson parameters here correspond to those taken by Seeger and Howard in the mass formula determination[9]. Other quantities appearing here are described in Appendix H.

EP	EP4	ALAMP	ALPHA2	ALPHA4	AAP	AA
.30	-.03	1.009	.2070	.6541E-01	1.261	1.285
.35	-.02	1.013	.2432	.6762E-01	1.294	1.319
.40	-.01	1.017	.2801	.7212E-01	1.330	1.355
.45	0.00	1.022	.3177	.7906E-01	1.367	1.392
.50	.01	1.027	.3560	.8862E-01	1.406	1.431
.55	.02	1.034	.3950	.1010	1.448	1.472
.60	.03	1.041	.4348	.1164	1.490	1.516
-.35	0.00	1.010	-.2243	.3834E-01	.8059	.8005
-.30	0.00	1.007	-.1933	.2852E-01	.8291	.8255
-.25	0.00	1.005	-.1620	.2006E-01	.8536	.8515
-.20	0.00	1.003	-.1303	.1300E-01	.8797	.8786
-.15	0.00	1.002	-.9827E-01	.7411E-02	.9074	.9069
-.10	0.00	1.001	-.6589E-01	.3337E-02	.9366	.9365
-.05	0.00	1.000	-.3314E-01	.8456E-03	.9675	.9675
0.00	0.00	1.000	-.1110E-13	-.8993E-14	1.000	1.000
.05	0.00	1.000	.3353E-01	.8690E-03	1.034	1.034
.10	0.00	1.001	.6748E-01	.3525E-02	1.070	1.070
.15	0.00	1.002	.1018	.8043E-02	1.108	1.108
.20	0.00	1.004	.1366	.1450E-01	1.147	1.148
.25	0.00	1.006	.1719	.2299E-01	1.188	1.191
.30	.01	1.009	.2080	.2316E-01	1.220	1.221
.35	.02	1.012	.2447	.2555E-01	1.255	1.253
.40	.03	1.016	.2821	.3032E-01	1.291	1.286
.45	.04	1.021	.3202	.3766E-01	1.330	1.320
.50	.05	1.027	.3591	.4776E-01	1.370	1.355
.55	.06	1.033	.3987	.6082E-01	1.413	1.393
.60	.07	1.040	.4392	.7708E-01	1.458	1.432
-.35	.04	1.010	-.2253	.2252E-02	.7694	.7758
-.30	.04	1.007	-.1941	-.8143E-02	.7919	.7992
-.25	.04	1.005	-.1626	-.1717E-01	.8160	.8236
-.20	.04	1.003	-.1308	-.2476E-01	.8416	.8489
-.15	.04	1.002	-.9855E-01	-.3087E-01	.8688	.8753
-.10	.04	1.001	-.6598E-01	-.3543E-01	.8977	.9029

Table 1, continued.

EP	EP4	ALAMP	ALPHA2	ALPHA4	AAP	AA
-.05	.04	1.000	-.3302E-01	-.3837E-01	.9283	.9317
0.00	.04	1.000	.3313E-03	-.3964E-01	.9605	.9618
.05	.04	1.000	.3408E-01	-.3916E-01	.9945	.9934
.10	.04	1.001	.6826E-01	-.3686E-01	1.030	1.027
.15	.04	1.002	.1029	-.3264E-01	1.068	1.062
.20	.04	1.004	.1379	-.2644E-01	1.107	1.099
.25	.04	1.006	.1734	-.1816E-01	1.148	1.138
.30	.05	1.009	.2099	-.1787E-01	1.182	1.165
.35	.06	1.012	.2472	-.1526E-01	1.217	1.194
.40	.07	1.016	.2852	-.1016E-01	1.254	1.225
.45	.08	1.021	.3239	-.2366E-02	1.294	1.256
.50	.09	1.027	.3634	.8315E-02	1.336	1.289
.55	.10	1.033	.4037	.2211E-01	1.380	1.323
.60	.11	1.040	.4448	.3927E-01	1.427	1.359
-.35	.08	1.010	-.2260	-.3342E-01	.7333	.7527
-.30	.08	1.008	-.1946	-.4439E-01	.7553	.7747
-.25	.08	1.005	-.1629	-.5395E-01	.7789	.7976
-.20	.08	1.004	-.1308	-.6206E-01	.8041	.8214
-.15	.08	1.002	-.9836E-01	-.6866E-01	.8310	.8461
-.10	.08	1.001	-.6554E-01	-.7368E-01	.8595	.8719
-.05	.08	1.001	-.3234E-01	-.7705E-01	.8899	.8988
0.00	.08	1.001	.1272E-02	-.7870E-01	.9219	.9269
.05	.08	1.001	.3529E-01	-.7856E-01	.9558	.9563
.10	.08	1.002	.6974E-01	-.7654E-01	.9916	.9871
.15	.08	1.003	.1046	-.7257E-01	1.029	1.019
.20	.08	1.004	.1400	-.6656E-01	1.069	1.054
.25	.08	1.007	.1758	-.5840E-01	1.110	1.089
.30	.09	1.009	.2129	-.5796E-01	1.144	1.115
.35	.10	1.013	.2507	-.5510E-01	1.180	1.142
.40	.11	1.017	.2892	-.4963E-01	1.219	1.170
.45	.12	1.022	.3286	-.4135E-01	1.259	1.199
.50	.13	1.028	.3687	-.3004E-01	1.303	1.229
.55	.14	1.034	.4097	-.1546E-01	1.348	1.261
.60	.15	1.041	.4516	.2654E-02	1.397	1.294

Table 1, continued.

Table 2: Comparison of the calculated and measured values of the total kinetic energy, TKE, prompt neutron number determined by assuming the 2T prompt neutron treatment of Appendix J, NUP, and the total prompt gamma energy, EGAMMA, for $^{235}U(n_{th},f)$. This calculation assumes the analytical density of states expression with ε as the only shape variable. Reference values for this reaction are[8,25],

TKE = 169.9 MeV

NUP = 2.4

EGAMMA = 6.96 MeV

Cases considered are 1) Cook[18] S and P values and Garvey-Kelson[24] ground-state masses; 2) Seeger and Howard[9] S and P values and ground-state masses; 3) Seeger and Howard S and P values and Garvey-Kelson ground-state masses.

CASE	QUANTITY	GMAX	YMAX	SUM
1	TKE	166.6	169.5	170.6
	NUP	2.96	2.81	2.80
	EGAMMA	6.07	5.26	4.72
2	TKE	168.9	170.6	171.4
	NUP	2.91	2.75	2.89
	EGAMMA	7.32	6.82	5.32
3	TKE	166.1	168.9	170.1
	NUP	3.27	2.95	2.99
	EGAMMA	7.04	6.92	5.51

	$^{233}U(n_{th},f)$		$^{235}U(n_{th},f)$		$^{239}Pu(n_{th},f)$		$^{235}U(n+14,f)$		$^{238}U(n+14,f)$		$^{252}Cf(sf)$	
	GMAX	YMAX	GMAX	YMAX	GMAX	YMAX	GMAX	YMAX	GMAX	YMAX	GMAX	YMAX
ν_p	2.69	2.94	2.81	3.02	3.18	3.34	4.71	4.91	4.79	4.92	3.96	4.12
cool	7.43	7.47	7.22	7.26	7.44	7.59	7.50	7.69	7.00	7.15	7.38	7.39
$\overline{\nu}_p$	2.49		2.40		2.87		4.37		4.43		3.76	
$\Delta\nu_p$	0.3	0.45	0.41	0.61	0.31	0.47	0.34	0.54	0.36	0.49	0.20	0.36
E_γ	5.00	5.39	4.75	5.12	5.41	6.10	4.85	5.05	4.40	4.83	6.10	5.73
$\overline{E}_\gamma$	7.60		6.96		7.78		6.96		6.28		8.60	
ΔE	-1.1	-1.2	0.74	2.62	-0.1	1.90	0.40	2.30	0.67	2.10	-1.0	-.02
TKE	170.4	168.1	169.6	167.7	177.1	175.2	168.8	166.7	168.9	167.2	181.3	184.5
$\overline{TKE}$	168.7		169.6		176.0		169.6		170.0		185.7	
ΔTKE	1.7	-0.6	0.	-1.9	1.0	-0.8	-0.8	-2.9	1.1	2.8	-0.7	-1.2
G	18.45	16.63	18.75	16.78	21.63	19.11	32.29	29.36	30.77	27.40	24.97	22.86

Table 3: Energy accounting for yields computed with the $\delta(Z)$ parameters of Table 5. Quantities appearing are ν_p, the prompt neutron number, E_γ, the total prompt gamma energy, cool, the total energy of de-excitation associated with each prompt neutron, TKE, the total fragment kinetic energy, and G, the scission-point energy release. Quantities with a bar above denote ENDF/B[8] values. Quantities preceeded by a Δ denote direct or inferred deviation from ENDF/B values. All energies in MeV.

	GMAX			YMAX				
	Δ_{ucd}	σ	Δ_z	Δ_{ucd}	σ	Δ_z		Light-product only, Δ_{ucd}
								GMAX / YMAX
$^{233}U(n_{th},f)$	.290	.462±.024	.668	.264	.460±.021	.698	Fragments	
$^{235}U(n_{th},f)$	.319	.462±.024	.835	.261	.458±.021	.262		
$^{239}Pu(n_{th},f)$	.283	.484±.024	.663	.259	.469±.019	.541		
$^{235}U(n+14,f)$	.224	.521±.015	.315	.190	.508±.013	.172		
$^{238}U(n+14,f)$	.246	.520±.016	.007	.195	.506±.014	.038		
$^{252}Cf(sf)$	.210	.512±.016	.353	.210	.492±.014	.277		
$^{233}U(n_{th},f)$	.529	.466±.033	.451	.579	.478±.043	.480	Products	.746 / .676
$^{235}U(n_{th},f)$	.548	.470±.033	.548	.588	.469±.031	.563		.796 / .678
$^{239}Pu(n_{th},f)$	.624	.494±.033	.352	.656	.483±.030	.298		.849 / .754
$^{235}U(n+14,f)$	.919	.527±.025	.116	.956	.516±.024	.049		1.041 / .945
$^{238}U(n+14,f)$	.923	.525±.023	.040	.947	.513±.023	.089		1.053 / .935
$^{252}Cf(sf)$	.771	.522±.026	.212	.801	.500±.027	.152		.970 / .926

Table 4: Independent yield parameters of the Gaussian model assuming $\delta(Z)$ parameters of Table 5. $\Delta_{ucd} = Z_p - Z_{ucd}$, σ = width of Gaussian, Δ_z = even-Z pairing enhancement, redefined here as $\exp(\Delta_z)-1$. All quantities are mass-chain yield weighted averages except those denoted "Light-product only" which are averaged over only those chains of mass less than or equal to one half of the mass of the fissioning system.

DZ	233U-TH	235U-TH	239PU-TH	235U-14	238U-14	252CF-S
0	5.000	5.000	5.000	5.000	5.000	5.000
1	5.145	5.178	4.879	5.186	5.163	5.038
2	5.140	5.162	5.302	5.060	5.067	5.370
3	5.598	5.535	5.442	5.445	5.427	5.418
4	5.686	5.692	5.735	5.464	5.445	5.519
5	5.880	5.951	5.783	5.724	5.731	5.378
6	5.890	5.935	5.933	5.630	5.595	5.501
7	6.144	6.128	5.735	5.819	5.706	5.458
8	5.999	5.946	5.769	5.609	5.499	5.624
9	5.994	5.967	5.656	5.676	5.635	5.503
10	5.986	5.950	5.816	5.614	5.553	5.770
11	6.184	6.160	5.802	5.873	5.769	5.672
12	6.245	6.227	6.046	5.884	5.758	5.846
13	6.555	6.511	6.127	6.173	6.085	5.790
14	6.613	6.583	6.372	6.194	6.158	6.076
15	6.711	6.644	6.420	6.325	6.375	6.114
16	6.764	6.671	6.565	6.319	6.273	6.459
17	6.951	6.845	6.600	6.595	6.533	6.524
18		6.828	6.858	6.544	6.496	6.718
19			6.939	7.231	7.044	6.754
20				7.827	7.662	7.482
P	-.048	-.054	-.053	-.077	-.083	-.072
k_o	27.5	28.0	28.0	25.0	25.2	27.0

Table 5: GMAX $\delta(Z)$ parameters determined by fitting to ENDF/B[8] charge lumped yields for the six reactions considered. DZ is the deviation of the charge from the symmetric split value, Z_{sym}, $DZ = Z_{sym} - Z$. P is the magnitude of the even-odd fluctuation about the smooth Z behavior. The energy constrained to remain in prescission kinetic energy, k_o, is given in MeV.

DZ	233U-TH	235U-TH	239PU-TH	235U-14	238U-14	252CF-S
0	5.000	5.000	5.000	5.000	5.000	5.000
1	5.107	5.138	4.876	5.127	5.087	4.989
2	5.120	5.152	5.234	5.010	5.008	5.224
3	5.472	5.454	5.338	5.258	5.243	5.141
4	5.527	5.535	5.542	5.147	5.134	5.324
5	5.759	5.783	5.447	5.377	5.358	5.248
6	5.741	5.747	5.605	5.286	5.241	5.398
7	5.896	5.899	5.510	5.514	5.455	5.349
8	5.788	5.795	5.663	5.410	5.356	5.545
9	5.917	5.902	5.589	5.593	5.550	5.517
10	5.925	5.902	5.748	5.543	5.481	5.761
11	6.116	6.097	5.742	5.784	5.694	5.699
12	6.195	6.169	6.006	5.803	5.710	5.904
13	6.511	6.466	6.094	6.122	6.050	5.844
14	6.564	6.507	6.343	6.078	6.069	6.116
15	6.708	6.632	6.357	6.339	6.311	6.162
16	6.759	6.665	6.562	6.281	6.259	6.503
17	6.933	6.830	6.582	6.562	6.516	6.518
18		6.803	6.840	6.529	6.467	6.783
19			6.888	7.216	7.028	6.821
20				7.795	7.671	7.530
P	-.051	-.051	-.061	-.086	-.077	-.070
k_o	27.5	28.0	28.0	25.0	25.2	27.0

Table 5, continued: YMAX $\delta(Z)$ parameters.

DA	233U-TH	235U-TH	239PU-TH	235U-14	238U-14	252CF-S
0	5.063	5.059	4.940	5.062	5.071	5.169
1	5.060	5.099	4.954	5.101	5.081	5.044
2	5.087	5.109	4.961	5.092	5.101	5.150
3	5.170	5.139	5.198	5.128	5.116	5.292
4	5.242	5.218	5.306	5.132	5.139	5.346
5	5.252	5.280	5.279	5.193	5.177	5.331
6	5.482	5.297	5.486	5.119	5.333	5.458
7	5.600	5.498	5.489	5.374	5.396	5.436
8	5.600	5.708	5.535	5.460	5.444	5.469
9	5.737	5.684	5.662	5.475	5.501	5.463
10	5.745	5.754	5.722	5.533	5.548	5.468
11	5.766	5.846	5.735	5.628	5.586	5.461
12	5.819	5.861	5.837	5.634	5.644	5.454
13	5.867	5.900	5.843	5.666	5.661	5.450
14	5.854	5.985	5.852	5.683	5.664	5.411
15	5.945	5.977	5.868	5.685	5.659	5.443
16	6.005	5.994	5.841	5.693	5.656	5.465
17	5.993	6.019	5.863	5.707	5.653	5.466
18	6.068	6.022	5.825	5.706	5.646	5.512
19	6.063	6.056	5.803	5.741	5.622	5.530
20	6.075	6.049	5.784	5.730	5.600	5.539
21	6.066	6.044	5.728	5.719	5.587	5.560
22	6.026	6.005	5.739	5.671	5.572	5.558
23	6.046	5.939	5.714	5.633	5.572	5.574
24	5.952	5.982	5.618	5.651	5.581	5.570
25	6.032	5.938	5.739	5.638	5.596	5.632

Table 6: GMAX $\delta(A)$ parameters extracted from Table 5 values assuming an even-odd Z term of -0.059 fm. DA is the deviation of the mass number from that of the symmetric split, A_{sym}, $DA = A_{sym} - A$. The energy constrained to remain in prescission kinetic energy, k_o, is given in MeV.

DA	233U-TH	235U-TH	239PU-TH	235U-14	238U-14	252CF-S
26	6.036	6.006	5.749	5.674	5.615	5.624
27	6.053	6.049	5.772	5.745	5.643	5.704
28	6.113	6.055	5.851	5.753	5.687	5.716
29	6.179	6.115	5.901	5.819	5.717	5.723
30	6.184	6.245	5.894	5.891	5.739	5.735
31	6.302	6.239	5.973	5.906	5.793	5.775
32	6.420	6.291	6.037	5.947	5.846	5.790
33	6.381	6.394	6.051	6.043	5.906	5.803
34	6.491	6.392	6.182	6.048	6.012	5.851
35	6.550	6.473	6.258	6.119	6.108	5.954
36	6.577	6.600	6.255	6.193	6.141	5.954
37	6.669	6.604	6.327	6.205	6.200	6.023
38	6.660	6.639	6.431	6.252	6.233	6.105
39	6.686	6.606	6.430	6.264	6.279	6.100
40	6.680	6.671	6.479	6.304	6.311	6.182
41	6.814	6.637	6.499	6.303	6.325	6.352
42	6.812	6.729	6.536	6.381	6.342	6.362
43	6.817	6.760	6.525	6.467	6.368	6.423
44	6.887	6.739	6.652	6.439	6.423	6.545
45	6.873	6.783	6.668	6.529	6.455	6.528
46	6.892	6.887	6.671	6.560	6.497	6.587
47			6.794	6.562	6.565	6.650
48			6.900	6.601	6.714	6.713
k_o	27.5	28.0	28.0	25.0	25.2	27.0

Table 6, continued: GMAX δ(A) parameters.

DA	233U-TH	235U-TH	239PU-TH	235U-14	238U-14	252CF-S
0	5.058	5.061	4.938	5.061	5.052	5.013
1	5.061	5.072	4.945	5.064	5.048	4.988
2	5.052	5.097	4.949	5.064	5.042	5.053
3	5.154	5.101	5.127	5.068	5.049	5.117
4	5.165	5.209	5.177	5.072	5.067	5.093
5	5.197	5.284	5.206	5.111	5.087	5.162
6	5.376	5.260	5.390	5.096	5.137	5.185
7	5.388	5.394	5.365	5.173	5.165	5.186
8	5.437	5.535	5.402	5.174	5.181	5.204
9	5.576	5.482	5.457	5.200	5.190	5.244
10	5.573	5.594	5.444	5.209	5.201	5.241
11	5.596	5.661	5.482	5.255	5.224	5.267
12	5.685	5.636	5.503	5.244	5.260	5.300
13	5.707	5.720	5.502	5.312	5.286	5.300
14	5.717	5.781	5.509	5.331	5.298	5.311
15	5.798	5.771	5.537	5.341	5.306	5.332
16	5.805	5.807	5.542	5.355	5.325	5.347
17	5.805	5.828	5.549	5.423	5.350	5.352
18	5.832	5.798	5.569	5.415	5.384	5.401
19	5.833	5.839	5.581	5.453	5.402	5.428
20	5.839	5.851	5.579	5.464	5.413	5.432
21	5.846	5.847	5.602	5.474	5.427	5.483
22	5.851	5.855	5.625	5.478	5.445	5.534
23	5.860	5.846	5.620	5.521	5.470	5.529
24	5.870	5.887	5.650	5.542	5.494	5.579
25	5.968	5.876	5.672	5.554	5.517	5.657

Table 6, continued: YMAX $\delta(A)$ parameters.

DA	233U-TH	235U-TH	239PU-TH	235U-14	238U-14	252CF-S
26	5.967	5.960	5.684	5.600	5.540	5.638
27	5.990	5.990	5.702	5.655	5.565	5.700
28	6.050	5.993	5.789	5.661	5.605	5.736
29	6.140	6.047	5.828	5.728	5.647	5.739
30	6.129	6.193	5.832	5.815	5.694	5.766
31	6.252	6.188	5.937	5.821	5.753	5.828
32	6.351	6.236	6.044	5.876	5.816	5.843
33	6.327	6.344	6.022	5.995	5.885	5.857
34	6.451	6.337	6.151	5.996	5.965	5.903
35	6.562	6.419	6.221	6.065	6.029	5.986
36	6.542	6.550	6.214	6.117	6.077	5.986
37	6.621	6.540	6.290	6.139	6.128	6.062
38	6.638	6.568	6.394	6.158	6.174	6.165
39	6.663	6.573	6.382	6.262	6.216	6.157
40	6.677	6.662	6.422	6.273	6.256	6.233
41	6.810	6.631	6.485	6.292	6.291	6.386
42	6.801	6.724	6.521	6.341	6.321	6.374
43	6.820	6.744	6.519	6.409	6.340	6.454
44	6.869	6.732	6.637	6.395	6.387	6.557
45	6.856	6.769	6.653	6.496	6.428	6.560
46	6.874	6.863	6.653	6.545	6.475	6.596
47			6.773	6.534	6.538	6.710
48			6.870	6.587	6.705	6.784
k_o	27.5	28.0	28.0	25.0	25.2	27.0

Table 6, continued: YMAX δ(A) parameters.

	$^{233}U(n_{th},f)$		$^{235}U(n_{th},f)$		$^{239}Pu(n_{th},f)$		$^{235}U(n+14,f)$		$^{238}U(n+14,f)$		$^{252}Cf(sf)$	
	GMAX	YMAX	GMAX	YMAX	GMAX	YMAX	GMAX	YMAX	GMAX	YMAX	GMAX	YMAX
ν_p	2.69	2.93	2.82	3.01	3.21	3.35	4.72	4.93	4.80	4.95	3.95	4.12
cool	7.46	7.47	7.23	7.25	7.50	7.58	7.57	7.67	7.03	7.14	7.41	7.38
$\overline{\nu}_p$	2.49		2.40		2.87		4.37		4.43		3.76	
$\Delta\nu_p$	0.20	0.44	0.42	0.61	0.34	0.48	0.35	0.56	0.37	0.52	0.19	0.36
E_γ	5.10	5.46	4.83	5.15	5.47	6.05	4.90	4.78	4.44	4.81	6.12	5.71
$\overline{E}_\gamma$	7.60		6.96		7.78		6.96		6.28		8.60	
ΔE	-1.0	1.12	0.87	2.57	0.30	-1.7	0.59	2.12	0.80	2.30	-1.0	-.20
TKE	170.4	168.2	169.6	167.8	177.2	175.2	168.8	167.0	169.0	167.2	185.2	184.6
$\overline{TKE}$	168.7		169.6		176.0		169.6		170.0		185.7	
ΔTKE	1.7	-0.5	0.	-1.8	1.2	-0.8	-0.8	2.6	-1.0	-2.8	-0.5	-1.1
G	18.50	16.64	18.81	16.79	21.63	19.13	32.39	29.43	30.88	27.51	24.95	22.92

Table 7: Energy accounting for yields computed with the $\delta(A)$ parameters of Table 6. Quantities appearing are ν_p, the prompt neutron number, E_γ, the total prompt gamma energy, cool, the total energy of de-excitation associated with each prompt neutron, TKE, the total fragment kinetic energy, and G, the scission-point energy release. Quantities with a bar above denote ENDF/B[8] values. Quantities preceeded by a Δ denote direct or inferred deviation from ENDF/B values. All energies in MeV.

	GMAX			YMAX				Light-product only, Δ_{ucd}	
	Δ_{ucd}	σ	Δ_z	Δ_{ucd}	σ	Δ_z		GMAX	YMAX
$^{233}U(n_{th},f)$	.391	.463±.021	.524	.399	.453±.016	.591	Fragments		
$^{235}U(n_{th},f)$	.405	.462±.018	.700	.381	.454±.018	.709			
$^{239}Pu(n_{th},f)$	.321	.494±.020	.646	.368	.474±.012	.523			
$^{235}U(n+14,f)$	.316	.525±.021	.454	.334	.507±.012	.374			
$^{238}U(n+14,f)$	.318	.523±.017	.152	.332	.505±.014	.160			
$^{252}Cf(sf)$	.307	.512±.016	.356	.367	.492±.015	.322			
$^{233}U(n_{th},f)$	.529	.474±.028	.431	.576	.468±.031	.404	Products	.806	.849
$^{235}U(n_{th},f)$	.549	.470±.034	.438	.586	.476±.039	.376		.884	.794
$^{239}Pu(n_{th},f)$	.630	.498±.033	.266	.658	.486±.027	.278		.900	.860
$^{235}U(n+14,f)$	.921	.530±.029	.343	.962	.514±.024	.196		1.125	1.077
$^{238}U(n+14,f)$	.925	.525±.024	.197	.954	.512±.026	.163		1.126	1.063
$^{252}Cf(sf)$	.770	.521±.024	.167	.803	.496±.026	.172		1.068	1.074

Table 8: Independent yield parameters of the Gaussian model assuming $\delta(A)$ parameters of Table 6. $\Delta_{ucd} = Z_p - Z_{ucd}$, σ = width of the Gaussian, Δ_z = even-Z pairing enhancement, redefined here as $\exp(\Delta_z)-1$. All quantities are mass-chain yield weighted averages except those denoted "Light-product only" which are averaged over only those chains of mass less than or equal to one half of the mass of the fissioning system.

Table 9: Coefficients of the δ(A or Z) formula determined by fitting over the six sets appearing in Tables 5 and 6. The form determined is

$$\delta(y) = f_o + f_2x^2 + f_3x^3 + f_4x^4 + f_5x^5 + f_6x^6 + g_o(-)^Z$$

where y is A or Z and x is A_{sym} - A or Z_{sym} - Z. Standard deviation for all fits is .17. All quantities are in fm. Estimated k_o for use here is 26.8 MeV

	GMAX δ(Z)	YMAX δ(Z)	GMAX δ(A)	YMAX δ(A)
f_o	4.9626	4.9749	5.0336	5.0220
f_2	1.3740E-01	8.8966E-02	1.8313E-02	1.0537E-02
f_3	-3.6844E-02	-2.4254E-02	-1.8376E-03	-1.0306E-03
f_4	3.9233E-03	2.7002E-03	7.2840E-05	4.1576E-05
f_5	-1.8512E-04	-1.3278E-04	-1.2735E-06	-7.3924E-07
f_6	3.2365E-06	2.4061E-06	8.2215E-09	4.8280E-09
g_o	-.059	-.060	-.059(input)	-.060(input)

	$^{233}U(n_{th},f)$		$^{235}U(n_{th},f)$		$^{239}Pu(n_{th},f)$		$^{235}U(n+14,f)$		$^{238}U(n+14,f)$		$^{252}Cf(sf)$	
	GMAX	YMAX	GMAX	YMAX	GMAX	YMAX	GMAX	YMAX	GMAX	YMAX	GMAX	YMAX
ν_p	2.65	2.83	2.74	2.86	3.13	3.30	4.76	4.97	4.84	5.04	4.20	4.31
cool	7.63	7.35	7.24	7.09	7.32	7.49	7.51	7.75	6.94	7.17	7.29	7.33
$\overline{\nu}_p$	2.49		2.40		2.87		4.37		4.43		3.76	
$\Delta\nu_p$	0.16	0.34	0.34	0.46	0.26	0.43	0.39	0.60	0.41	0.61	0.44	0.55
E_γ	4.45	4.90	4.23	4.57	5.26	6.01	4.92	5.04	4.44	4.98	6.68	5.44
$\overline{E}_\gamma$	7.60		6.96		7.78		6.96		6.28		8.60	
ΔE	-1.9	-0.2	-0.3	-0.9	-0.6	1.40	0.90	2.80	1.00	3.10	1.30	0.90
TKE	172.4	169.4	170.8	168.4	175.9	174.4	168.1	166.6	167.4	166.2	182.8	183.8
$\overline{TKE}$	167.4		169.6		176.0		169.6		170.0		185.7	
ΔTKE	5.0	2.0	1.2	-1.2	-0.1	-1.6	-1.5	-3.0	-2.6	-3.8	-2.9	-1.8
G	16.99	15.07	17.23	15.38	21.37	19.34	33.07	30.35	32.01	28.83	27.08	24.02

Table 10: Energy accounting for yields computed with the $\delta(A)$ parameters of Table 9, determined by fitting to the $\delta(A)$ parameters of the six cases considered. Quantities appearing are ν_p, the prompt neutron number, E_γ, the total prompt gamma energy, cool, the total energy of de-excitation associated with each prompt neutron, TKE, the total fragment kinetic energy, and G, the scission-point energy release. Quantities with a bar above denote ENDF/B[8] values. Quantities preceeded by a Δ denote direct or inferred deviation from ENDF/B values. All energies in MeV.

	GMAX			YMAX				Light-product only, Δ_{ucd}	
	Δ_{ucd}	σ	Δ_z	Δ_{ucd}	σ	Δ_z		GMAX	YMAX
$^{233}U(n_{th},f)$	.338	.469±.029	.606	.416	.452±.013	.441	Fragments		
$^{235}U(n_{th},f)$	.363	.463±.026	.726	.415	.454±.016	.426			
$^{239}Pu(n_{th},f)$	.402	.486±.020	.651	.410	.474±.013	.502			
$^{235}U(n+14,f)$	.328	.521±.019	.619	.346	.513±.011	.394			
$^{238}U(n+14,f)$	.364	.517±.019	.346	.350	.511±.014	.164			
$^{252}Cf(sf)$	.319	.517±.019	.521	.373	.498±.013	.304			
$^{233}U(n_{th},f)$	.520	.470±.033	.441	.557	.471±.032	.276	Products	.824	.818
$^{235}U(n_{th},f)$	.532	.473±.039	.430	.558	.475±.038	.230		.850	.818
$^{239}Pu(n_{th},f)$	.614	.496±.032	.282	.647	.487±.027	.264		.921	.878
$^{235}U(n+14,f)$	.929	.529±.027	.367	.971	.519±.025	.231		1.138	1.089
$^{238}U(n+14,f)$	.932	.519±.026	.465	.972	.513±.023	.232		1.149	1.083
$^{252}Cf(sf)$	.817	.525±.027	.433	.839	.501±.025	.176		1.075	1.091

Table 11: Independent yield parameters of the Gaussian model assuming $\delta(A)$ parameters of Table 9. $\Delta_{ucd} = Z_p - Z_{ucd}$, σ = width of the Gaussian, Δ_z = even-Z pairing enhancement, redefined here as $\exp(\Delta_z) - 1$. All quantities are mass-chain yield weighted averages except those denoted "Light-product only" which are averaged over only those chains of mass less than or equal to one half of the mass of the fissioning system.

Table 12: Independent yield parameters of the Gaussian model, extracted from ENDF/B[8] data. Δ_{ucd} is the deviation of Z_p from the UCD value for the light mass product, only, σ is the width of the Gaussian, and Δ_z is the even-Z paring enhancement, redefined here as $\exp(\Delta_z)-1$. All quantities are chain-yield weighted averages.

Reaction	Δ_{ucd}	σ	Δ_z
$^{233}U(n_{th},f)$	1.039	.595±.011	.305
$^{235}U(n_{th},f)$	1.077	.598±.021	.464
$^{239}Pu(n_{th},f)$	1.118	.595±.011	.258
$^{235}U(n+14,f)$	1.234	.596±.011	.035
$^{238}U(n+14,f)$	1.187	.593±.013	.077
$^{252}Cf(sf)$	1.234	.593±.011	.107

QUANTITY	START	SUM LIMITS	LEVELS MAX	G	V
GN	.28543	.26015	.26015	.89425	.18631
GP	.31698	.28070	.28070	1.0663	.19520
DN0	1.9778	1.5916	1.5916	15.0468	.8078
DP0	1.9219	1.5098	1.5098	14.6462	.9436
TCN	1.102	.9075	.9075	7.8675	.4862
TCP	1.041	.8033	.8033	7.6176	.4944
LNC	49.585	49.606	49.606	48.076	41.518
LPC	44.104	44.218	44.218	42.559	34.727
E0N	1483.2	1483.8	1483.8	1382.1	1239.6
E0P	1071.3	1072.5	1072.5	976.1	841.3
LN(.245)	-.379	-.915	-.915	8.509	-.651
LN(1.063)	13.51	14.49	14.45	-.957	17.60
LN(2.045)	26.07	26.07	26.07	-4.76	32.49

A = 71 Z = 32

Table 13: The effect of cumulative change upon the various computed quantities of the numerical desity-of-states expression of Appendix D. Quantities appearing here are GN and GP, the neutron and proton interaction strengths, DN0 and DP0, the neutron and proton ground-state pairing gaps, TCN and TCP, the neutron and proton critical temperatures, LNC and LPC, the neutron and proton chemical potentials at the critical temperature, E0N and E0P, the ground-state energies of the neutron and proton systems, and the value of the logarithm of the density-of-states expression evaluated at the three temperatures shown. All energies are in MeV. The column marked "START" shows values obtained using the prescription of Nilsson, et. al.[60]. Column headings then show changes in the tabulated quantities as the prescription of Seeger and Howard[9] is assumed. The last column gives values obtained with the pure Seeger and Howard prescription. The transition illustrated here is described in Appendix D.

QUANTITY	START	SUM LIMITS	LEVELS MAX	G	V
GN	.10848	.10848	.10848	.41500	.06527
GP	.12425	.12425	.12425	.55871	.07722
DN0	1.5291	1.7466	1.7466	17.5674	.8179
DP0	1.3251	1.3859	1.3859	16.9606	.6297
TCN	.7897	.9116	.9116	9.1246	.4178
TCP	.7118	.7441	.7441	8.7447	.3392
LNC	51.676	51.660	51.660	49.712	42.137
LPC	40.989	40.989	40.989	39.679	33.059
E0N	3807.4	3805.9	3805.9	3464.5	3105.7
E0P	2127.8	2127.5	2127.5	1858.3	1715.3
LN(.161)	-.783	-.462	-.462	6.326	-.600
LN(1.019)	37.94	37.94	37.94	-.765	43.23
LN(2.039)	66.20	66.20	61.14	-5.56	82.22

A = 165 Z = 68

Table 13, continued: Effect of cumulative changes of the prescription for evaluateing the numerical density-of-states expression of Appendix D.

D	A	Z	S	EX	P	J	ERR
320.00	70	31	-.874	7.655	-.280	1.5	90.00
190.00	72	31	-1.643	6.522	.040	1.5	50.00
2000.00	71	32	-1.785	7.420	.880	0.0	800.00
3900.00	73	32	-1.982	6.782	1.200	0.0	1500.00
77.00	74	32	-1.656	10.200	2.790	4.5	9.00
8500.00	75	32	-1.260	6.506	1.410	0.0	4500.00
8000.00	77	32	-1.591	6.073	1.600	0.0	800.00
87.30	76	33	-1.482	7.329	.010	1.5	11.40
200.00	75	34	-2.423	8.028	1.370	0.0	350.00
1200.00	77	34	-1.887	7.419	1.580	0.0	600.00
150.00	78	34	-2.478	10.497	3.080	.5	40.00
4500.00	79	34	-2.493	6.961	1.770	0.0	1000.00
1600.00	81	34	-.749	6.702	1.360	0.0	600.00
6900.00	83	34	.405	5.928	1.520	0.0	1100.00
61.00	80	35	-2.525	7.883	.160	1.5	13.00
52.00	82	35	-.573	7.604	-.250	1.5	14.00
1100.00	86	37	1.072	8.651	.040	2.5	200.00
1800.00	88	37	1.688	6.081	.050	1.5	600.00
350.00	85	38	-1.190	8.526	1.080	0.0	120.00

Table 14: Data used in modeling the density parameter for the analytical density-of-states expression described in Appendix E. Quantities appearing are D, the observed resonance spacing, in eV, taken from Cook, et. al.[18], A and Z, the mass and charge of the compound nucleus, S, the shell correction energy, in MeV, given as prescribed by Kataria, et. al.[21], EX, the excitation energy at which D was measured, in MeV, P, the pairing correction energy as given by Cook, et. al., in MeV, J, the spin of the target nucleus, and ERR, the experimental error in the measurement of D, in eV.

D	A	Z	S	EX	P	J	ERR
2100.00	87	38	.856	8.428	1.240	0.0	1000.00
210.00	88	38	2.645	11.114	2.170	4.5	80.00
12000.00	89	38	2.027	6.365	1.250	0.0	2000.00
1600.00	90	39	2.072	6.859	.300	.5	400.00
3300.00	91	40	2.105	7.204	1.100	0.0	800.00
250.00	92	40	1.545	8.636	1.710	2.5	50.00
3400.00	93	40	1.207	6.733	.590	0.0	1100.00
3300.00	95	40	-.200	6.474	1.220	0.0	900.00
1100.00	97	40	.028	5.586	.440	0.0	300.00
36.00	94	41	.671	7.230	-.240	4.5	4.60
100.00	96	42	-.421	9.155	2.590	2.5	40.00
1200.00	97	42	-.733	6.819	1.300	0.0	500.00
120.00	98	42	-1.671	8.643	2.690	2.5	60.00
790.00	99	42	-1.092	5.927	.520	0.0	550.00
400.00	101	42	-1.838	5.399	1.090	0.0	75.00
26.00	100	43	-1.146	6.765	-.420	4.5	5.00
200.00	100	44	-.831	9.674	2.670	2.5	50.00
15.00	102	44	-1.155	9.220	1.950	2.5	4.00
10.30	104	45	-.835	7.001	-.160	.5	2.00
11.10	106	46	-1.321	9.561	2.640	2.5	1.70
50.00	108	47	-.375	7.269	-.130	.5	12.00
19.10	110	47	-.811	6.806	-.100	.5	3.80
34.00	112	48	-.503	9.396	2.020	.5	6.00
200.00	113	48	-.691	6.544	1.130	0.0	75.00
27.00	114	48	-1.032	9.041	2.700	.5	3.00
7.10	114	49	-.703	7.275	.360	4.5	1.20
9.50	116	49	-.546	6.784	.170	4.5	2.40
140.00	113	50	.516	7.747	.830	0.0	50.00
320.00	115	50	.071	7.547	1.350	0.0	90.00
50.00	116	50	-.406	9.562	2.920	.5	20.00
250.00	117	50	.171	6.947	1.160	0.0	40.00
65.00	118	50	.069	9.326	2.530	.5	15.00
730.00	119	50	.648	6.485	.810	0.0	180.00
62.00	120	50	.692	9.105	2.330	.5	12.00
240.00	121	50	.542	6.173	1.490	0.0	50.00
400.00	123	50	1.786	5.947	1.200	0.0	150.00
250.00	125	50	3.003	5.732	1.370	0.0	75.00
13.00	122	51	.347	6.807	.220	2.5	2.00
30.00	124	51	1.588	6.467	-.070	3.5	13.00
130.00	123	52	.094	6.934	1.270	0.0	8.00

Table 14, continued.

D	A	Z	S	EX	P	J	ERR
33.00	124	52	.337	9.424	2.600	.5	9.00
46.00	126	52	1.355	9.117	2.420	.5	11.00
550.00	129	52	3.729	6.165	.780	0.0	125.00
5700.00	131	52	5.698	5.925	.700	0.0	800.00
19.00	128	53	1.815	6.826	.100	2.5	5.00
21.00	130	53	3.089	6.461	-.270	3.5	6.00
31.00	132	54	3.324	8.937	1.920	1.5	1.00
500.00	136	54	6.803	7.992	2.050	1.5	100.00
20.70	134	55	3.397	6.892	-.260	3.5	4.70
120.00	131	56	.727	7.495	1.300	0.0	40.00
380.00	135	56	2.815	6.975	.850	0.0	100.00
35.00	136	56	3.182	9.107	2.390	1.5	9.00
3800.00	137	56	4.316	6.899	1.200	0.0	2400.00
460.00	138	56	5.074	8.612	2.250	1.5	240.00
9600.00	139	56	4.530	4.724	.950	0.0	3400.00
41.00	139	57	4.199	8.778	1.250	5.0	6.00
110.00	140	57	3.782	5.162	-.050	3.5	20.00
3000.00	141	58	3.193	5.429	1.150	0.0	1000.00
1000.00	143	58	1.720	5.156	1.190	0.0	200.00
83.80	142	59	2.140	5.844	.680	2.5	12.10
19.00	144	60	1.262	7.819	2.610	3.5	9.00
25.00	146	60	.702	7.566	1.900	3.5	9.00
5.70	148	61	1.243	5.903	-.410	3.5	1.50
7.90	148	62	.513	8.142	2.090	3.5	1.30
3.22	150	62	.693	7.987	1.930	3.5	.53
24.00	151	62	.920	5.597	.810	0.0	10.00
1.30	152	62	1.289	8.259	1.910	1.5	.50
60.00	153	62	1.703	5.868	.850	0.0	20.00
.72	152	63	.821	6.306	-.290	2.5	.14
1.30	154	63	1.839	6.438	-.250	2.5	.40
1.99	156	64	1.893	8.537	1.890	1.5	.32
75.00	157	64	2.594	6.361	.710	0.0	19.00
6.10	158	64	2.386	7.938	1.910	1.5	1.60
4.30	160	65	2.834	6.376	.010	1.5	.78
2.55	162	66	2.897	8.197	1.570	2.5	.38
42.00	163	66	3.381	6.273	.560	0.0	6.00
9.60	164	66	3.181	7.655	1.750	2.5	1.60
5.67	166	67	3.429	6.244	.220	3.5	.74
7.10	163	68	2.095	6.904	.690	0.0	1.20
17.00	165	68	3.092	6.650	.320	0.0	5.00

Table 14, continued.

D	A	Z	S	UX	J	ERR	BS
320.00	70	31	-3.174	6.493	1.5	90.00	1.004495
190.00	72	31	-2.354	6.308	1.5	50.00	1.005016
2000.00	71	32	-3.203	5.898	0.0	800.00	1.005286
3900.00	73	32	-2.541	5.573	0.0	1500.00	1.005641
77.00	74	32	-2.109	7.030	4.5	9.00	1.005016
8500.00	75	32	-1.399	5.432	0.0	4500.00	1.006268
8000.00	77	32	-2.847	3.473	0.0	800.00	1.001236
87.30	76	33	-2.160	6.856	1.5	11.40	1.006965
200.00	75	34	-3.685	5.730	0.0	350.00	1.007165
1200.00	77	34	-2.531	5.480	0.0	600.00	1.007901
150.00	78	34	-3.705	6.138	.5	40.00	1.003000
4500.00	79	34	-3.137	4.796	0.0	1000.00	1.001987
1600.00	81	34	-1.392	4.732	0.0	600.00	1.001186
6900.00	83	34	.404	4.276	0.0	1100.00	1.000546
61.00	80	35	-3.833	6.473	1.5	13.00	1.001837
52.00	82	35	-1.835	6.594	1.5	14.00	1.001186
1100.00	86	37	.232	7.668	2.5	200.00	1.000636
1800.00	88	37	.821	5.559	1.5	600.00	1.000301
350.00	85	38	-2.160	6.576	0.0	120.00	1.001066

Table 15: Data used in modeling the density parameter for the analytical density-of-states expression described in Appendix E. Quantities appearing are D, the observed resonance spacing, in eV, taken from Cook, et. al.[18], A and Z, the mass and charge of the compound nucleus, S, the shell correction energy, in MeV, UX, the excitation energy at which D was measured, reduced by subtracting the pairing energy, in MeV, J, the spin of the target nucleus, ERR, the experimental error in the measurement of D, in eV, and BS, the ratio of the surface area of the compound nucleus to that of a spherical nucleus of the same volume. The energies S and UX and the term BS were computed with the Seeger and Howard mass formula[9], described in Appendix A.

D	A	Z	S	UX	J	ERR	BS
2100.00	87	38	.484	6.879	0.0	1000.00	1.000481
210.00	88	38	2.419	8.706	4.5	80.00	1.000000
12000.00	89	38	1.234	4.927	0.0	2000.00	1.000222
1600.00	90	39	.989	6.684	.5	400.00	1.000576
3300.00	91	40	.658	5.079	0.0	800.00	1.000234
250.00	92	40	-1.283	4.366	2.5	50.00	1.000000
3400.00	93	40	-2.094	2.921	0.0	1100.00	1.000000
3300.00	95	40	-2.356	3.152	0.0	900.00	1.000171
1100.00	97	40	-3.610	2.139	0.0	300.00	1.001676
36.00	94	41	-1.073	5.525	4.5	4.60	1.000316
100.00	96	42	-2.740	3.895	2.5	40.00	1.000000
1200.00	97	42	-2.178	3.655	0.0	500.00	1.000160
120.00	98	42	-3.042	4.212	2.5	60.00	1.000000
790.00	99	42	-2.816	3.273	0.0	550.00	1.001491
400.00	101	42	-1.740	4.016	0.0	75.00	1.005531
26.00	100	43	-2.294	5.094	4.5	5.00	1.001641
200.00	100	44	-2.110	5.103	2.5	50.00	1.000000
15.00	102	44	-5.355	2.694	2.5	4.00	1.000000
10.30	104	45	-1.868	5.487	.5	2.00	1.003255
11.10	106	46	-2.595	5.444	2.5	1.70	1.001147
50.00	108	47	-1.352	5.850	.5	12.00	1.003305
19.10	110	47	-1.662	5.422	.5	3.80	1.004181
34.00	112	48	-2.799	5.042	.5	6.00	1.001397
200.00	113	48	-1.777	4.208	0.0	75.00	1.003075
27.00	114	48	-1.862	5.412	.5	3.00	1.002760
7.10	114	49	-1.966	4.718	4.5	1.20	1.001540
9.50	116	49	-1.469	4.807	4.5	2.40	1.002051
140.00	113	50	-.803	4.825	0.0	50.00	1.000000
320.00	115	50	-1.149	4.558	0.0	90.00	1.000000
50.00	116	50	-1.168	5.922	.5	20.00	1.000000
250.00	117	50	-1.230	4.186	0.0	40.00	1.000423
65.00	118	50	-2.166	4.539	.5	15.00	1.000000
730.00	119	50	-1.114	3.779	0.0	180.00	1.000328
62.00	120	50	-2.356	3.616	.5	12.00	1.000000
240.00	121	50	-.848	3.244	0.0	50.00	1.000210
400.00	123	50	-1.197	1.800	0.0	150.00	1.000000
250.00	125	50	.498	2.023	0.0	75.00	1.000000
13.00	122	51	-.538	5.207	2.5	2.00	1.001361
30.00	124	51	.413	5.083	3.5	13.00	1.001133
130.00	123	52	-.936	4.889	0.0	8.00	1.002110

Table 15, continued.

D	A	Z	S	UX	J	ERR	BS
33.00	124	52	-1.019	5.672	.5	9.00	1.001369
46.00	126	52	-.909	4.700	.5	11.00	1.000535
550.00	129	52	-.473	1.651	0.0	125.00	1.000000
5700.00	131	52	2.596	2.662	0.0	800.00	1.000000
19.00	128	53	.407	5.757	2.5	5.00	1.001880
21.00	130	53	-.208	4.063	3.5	6.00	1.000201
31.00	132	54	-1.534	2.890	1.5	1.00	1.000000
500.00	136	54	5.866	5.702	1.5	100.00	1.000000
20.70	134	55	-.880	3.530	3.5	4.70	1.000000
120.00	131	56	-1.337	5.290	0.0	40.00	1.003227
380.00	135	56	-1.636	2.597	0.0	100.00	1.000000
35.00	136	56	.131	4.364	1.5	9.00	1.000000
3800.00	137	56	2.575	4.457	0.0	2400.00	1.000113
460.00	138	56	4.140	5.785	1.5	240.00	1.000000
9600.00	139	56	2.733	2.116	0.0	3400.00	1.000000
41.00	139	57	3.569	7.380	5.0	6.00	1.000000
110.00	140	57	2.167	3.577	3.5	20.00	1.000000
3000.00	141	58	1.791	2.842	0.0	1000.00	1.000000
1000.00	143	58	-.502	1.619	0.0	200.00	1.000000
83.80	142	59	1.238	4.248	2.5	12.10	1.000146
19.00	144	60	-.857	2.812	3.5	9.00	1.000000
25.00	146	60	-2.806	2.018	3.5	9.00	1.000000
5.70	148	61	.116	4.943	3.5	1.50	1.004575
7.90	148	62	-1.117	4.335	3.5	1.30	1.001528
3.22	150	62	.291	5.138	3.5	.53	1.006030
24.00	151	62	1.761	5.139	0.0	10.00	1.008680
1.30	152	62	2.426	6.107	1.5	.50	1.009845
60.00	153	62	3.141	5.442	0.0	20.00	1.010949
.72	152	63	1.361	6.231	2.5	.14	1.008854
1.30	154	63	2.696	6.473	2.5	.40	1.010804
1.99	156	64	3.166	6.821	1.5	.32	1.011117
75.00	157	64	3.063	5.540	0.0	19.00	1.012016
6.10	158	64	2.830	5.879	1.5	1.60	1.011783
4.30	160	65	2.852	6.315	1.5	.78	1.012662
2.55	162	66	2.886	6.714	2.5	.38	1.012018
42.00	163	66	3.003	5.789	0.0	6.00	1.012256
9.60	164	66	3.239	6.480	2.5	1.60	1.012435
5.67	166	67	3.271	6.311	3.5	.74	1.013201
7.10	163	68	2.110	6.403	0.0	1.20	1.011275
17.00	165	68	2.793	6.399	0.0	5.00	1.012080

Table 15, continued.

Model	ϕ	Data Table	ϕ-best	$\hat{a}^{-1}$	ω_o	β	Polynomial form	Systematics
1. Kataria	SS	14	1.214×10^8	6.730	.1987	inc	1-term	no
2. Kataria	SS	15	1.963×10^8	5.227	.3566	0	4-term with pairing	no
3. Kataria	ℓn	14	56.49	7.003	.2136	inc	4-term with pairing	no
4. Kataria	ℓn	15	150.5	6.367	.3086	inc	4-term with pairing	yes
5. GC	SS	14	1.058×10^8	6.214	-	-	2-term	yes
6. GC	SS	15	1.150×10^8	3.936	-	-	3-term	yes
7. GC	ℓn	14	57.03	7.093	-	-	4-term with pairing	no
8. GC	ℓn	15	166.3	6.201	-	-	4-term with pairing	yes

Table 16: Results of fitting described in Appendix F for the analytical density-of-states models. Indicated are the model type, either that of Kataria, et. al.[21] or Gilbert and Cameron[17], denoted GC, the form of the function indicating quality of fit, ϕ, either the sum of squares (SS) or sum of squares of logarithms, (ℓn), the data table from which the energies were taken, the value of the quality-of-fit function corresponding to the best model, ϕ-best, the reciprocal of $\hat{a}$, $\hat{a}^{-1}$, the value of ω_o in the Kataria model, a quantity not present in the Gilbert and Cameron model, the preferred value of β, either 0 or 1, in the Kataria model, inc denoting an inconclusive result, the form of the polynomial part of the density parameter, a, and whether or not the even-odd pairing terms were significant, and whether or not systematic errors were observed in the final model predictions.

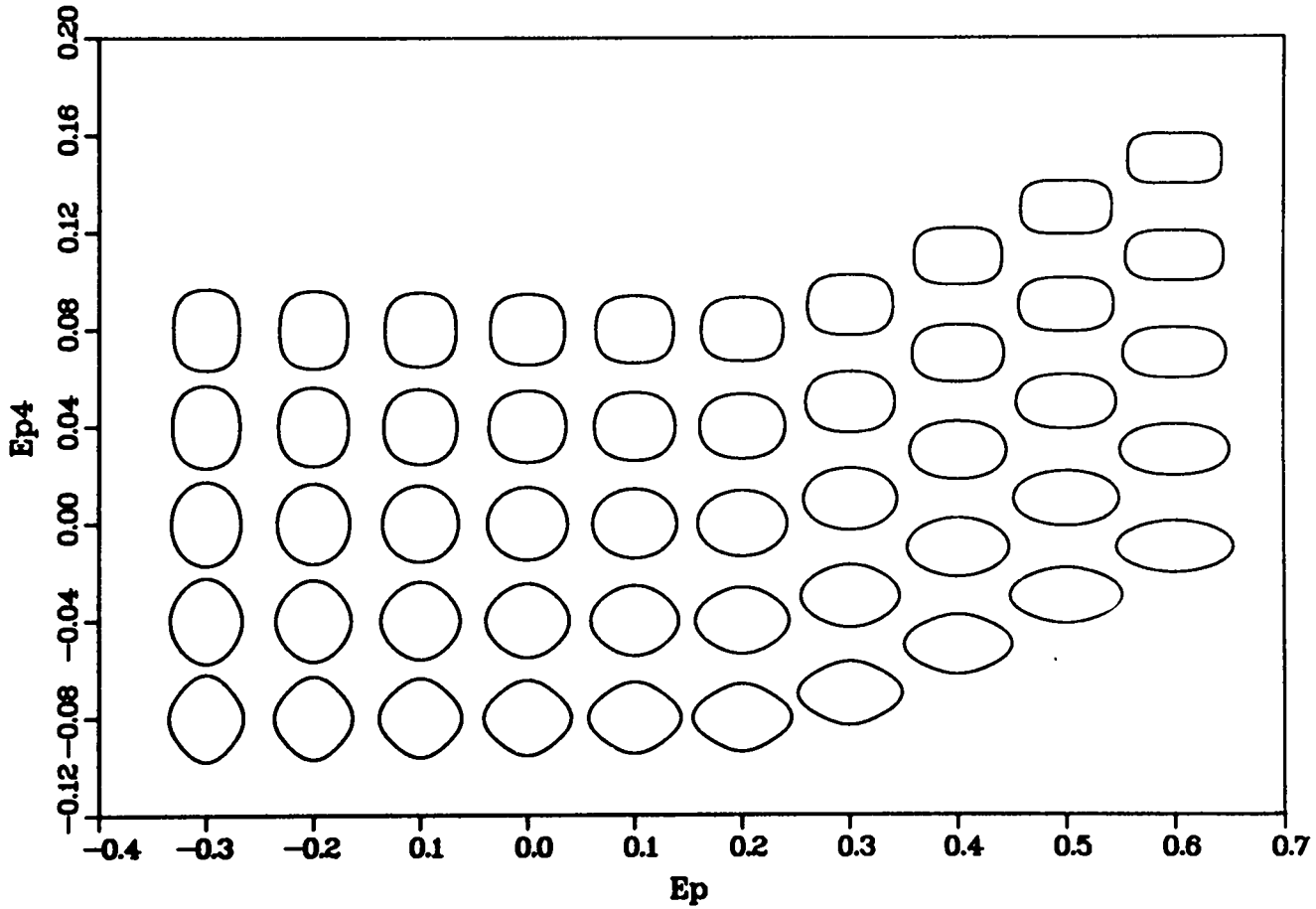

Figure 1: The space of allowed shapes considered in the mass formula of Appendix A. Actual grid step size is 0.05 in the ε degree of freedom with ε values extending to -0.35. These shapes were generated with the Nix expression[40] of Appendix H.

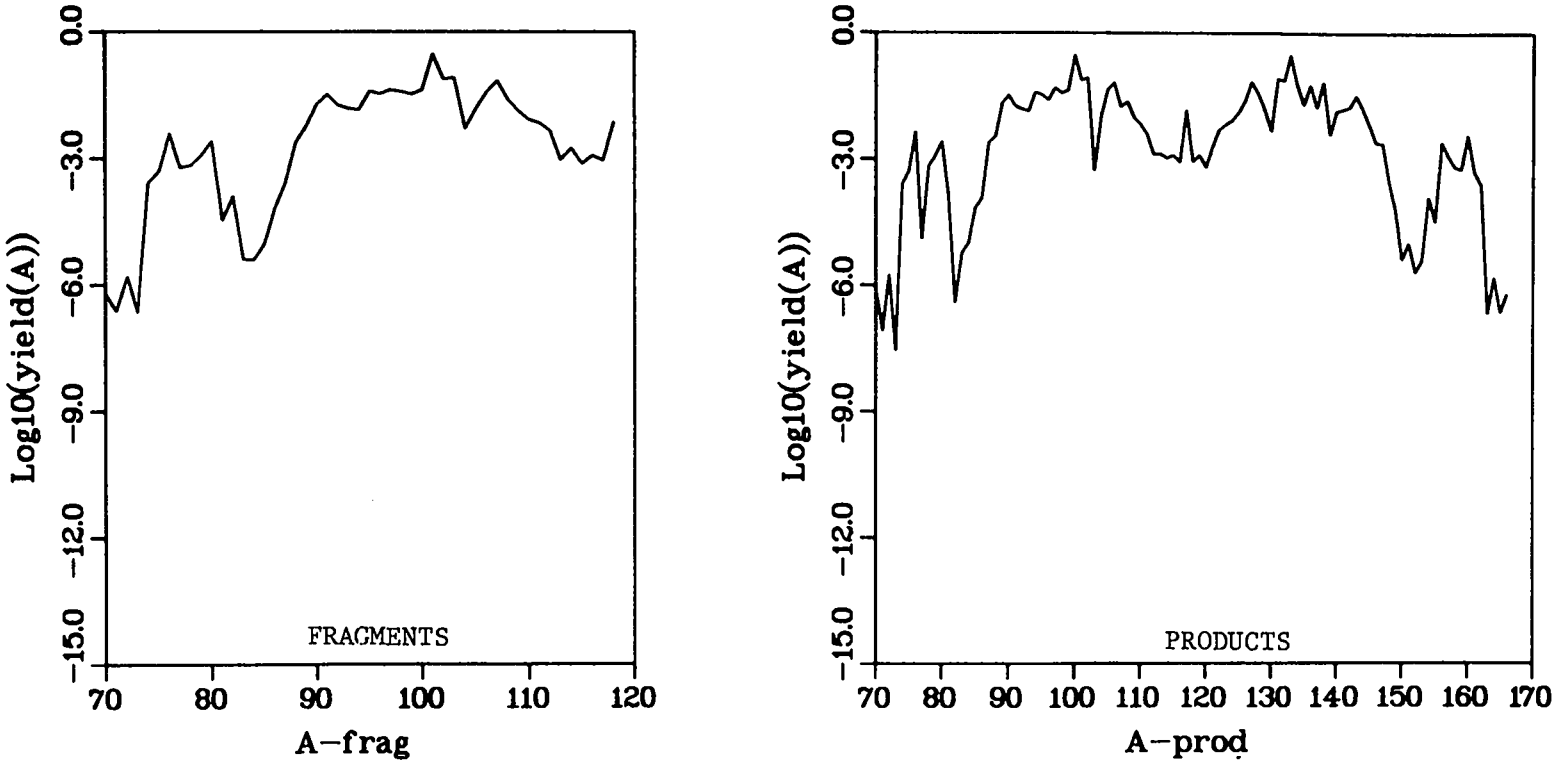

Figure 2: GMAX mass chain yields for fragments and products. Products are determined assuming a 2 T neutron treatment. The analytical model is assumed with the Cook[18] S and P values and a-model. The ground-state mass is assumed to be given by Garvey-Kelson recursion relations[24]. The spacing parameter, δ, is assumed to be constant for all masses, δ = 3 fm.

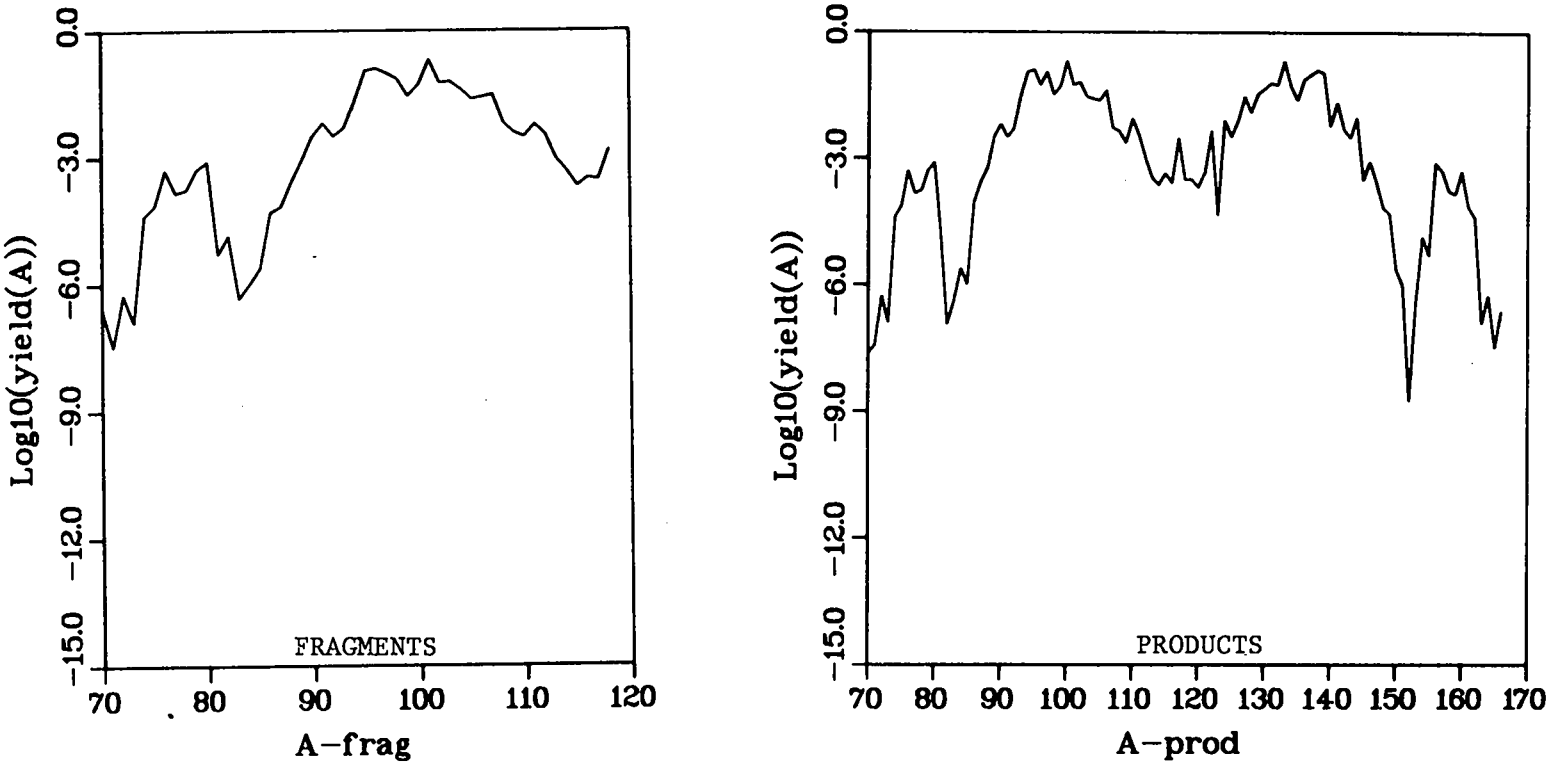

Figure 3: YMAX mass chain yields for fragments and products. Products are determined assuming a 2 T neutron treatment. The analytical model is assumed with the Cook[18] S and P values and a-model. The ground-state mass is assumed to be given by Garvey-Kelson recursion relations[24]. The spacing parameter, δ, is assumed to be constant for all masses, δ = 3 fm.

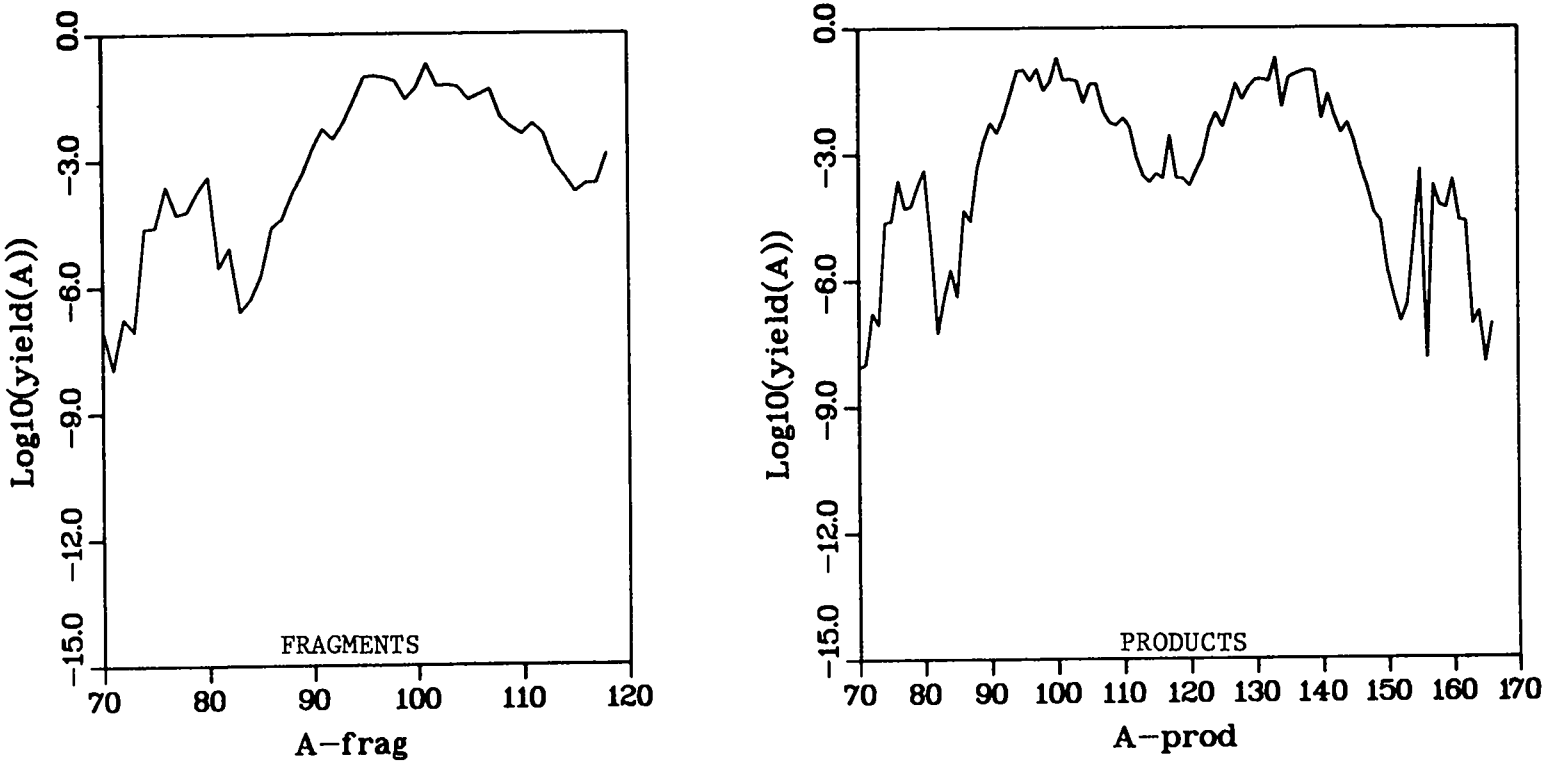

Figure 4: SUM mass chain yields for fragments and products. Products are determined assuming a 2 T neutron treatment. The analytical model is assumed with the Cook[18] S and P values and a-model. The ground-state mass is assumed to be given by Garvey-Kelson recursion relations[24]. The spacing parameter, δ, is assumed to be constant for all masses, δ = 3 fm.

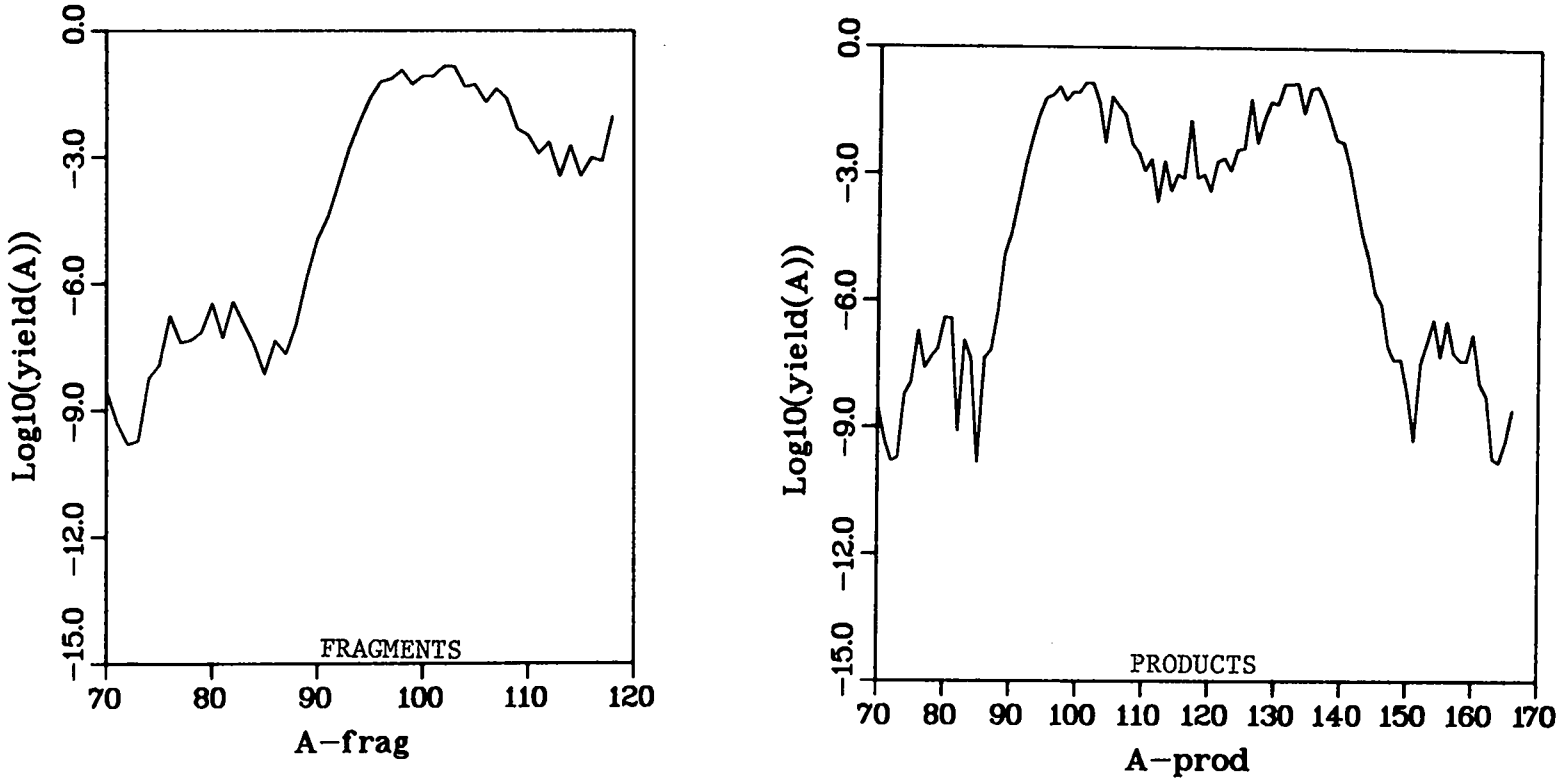

Figure 5: GMAX mass chain yields for fragments and products. Products are determined assuming a 2 T neutron treatment. The analytical model is assumed with the Seeger[9] S and P values and a-model. The ground-state mass is assumed to be given by Garvey-Kelson recursion relations[24]. The spacing parameter, δ, is assumed to be constant for all masses, δ = 3 fm.

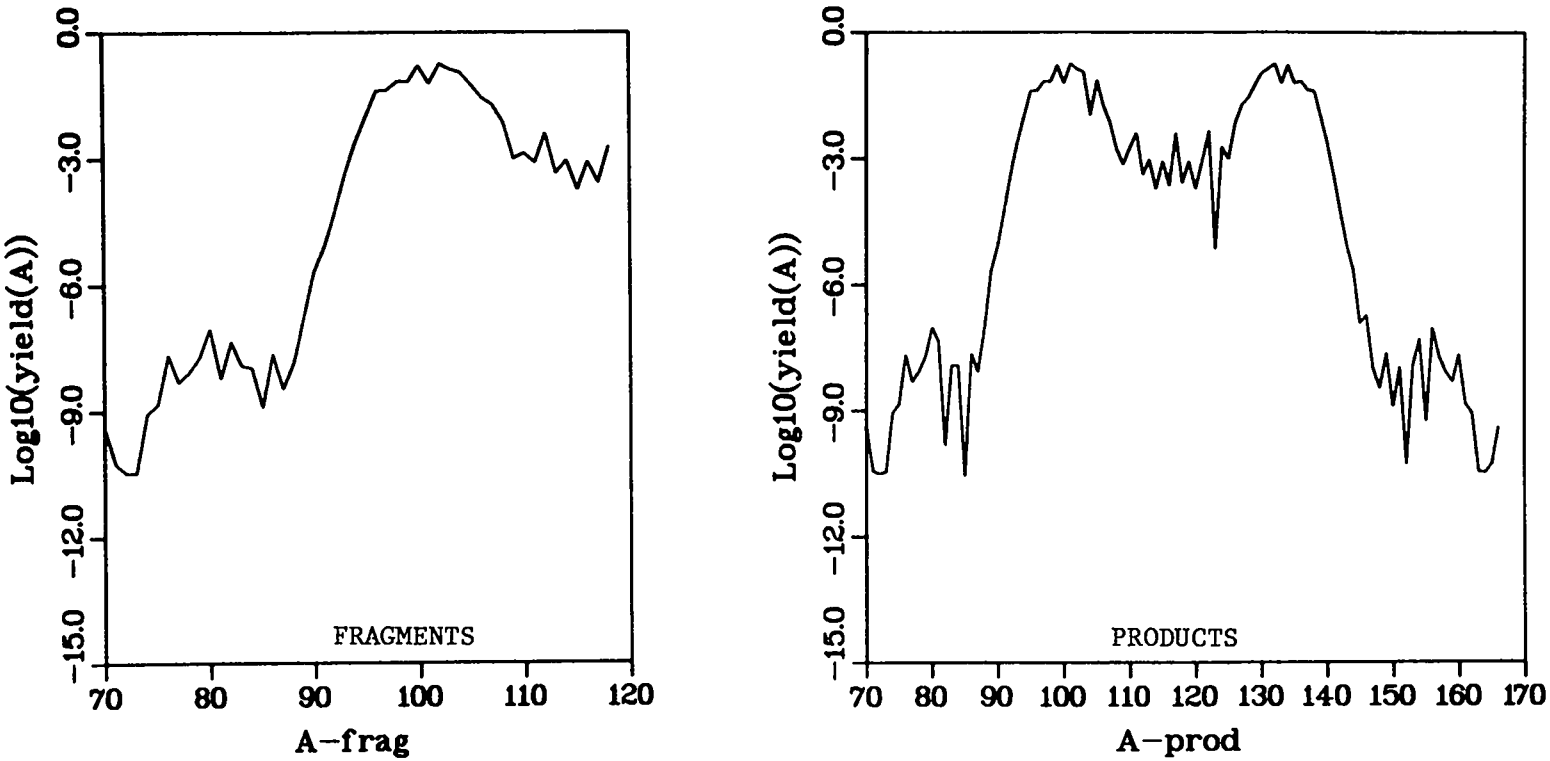

Figure 6: YMAX mass chain yields for fragments and products. Products are determined assuming a 2 T neutron treatment. The analytical model is assumed with the Seeger[9] S and P values and a-model. The ground-state mass is assumed to be given by Garvey-Kelson recursion relations[24]. The spacing parameter, δ, is assumed to be constant for all masses, δ = 3 fm.

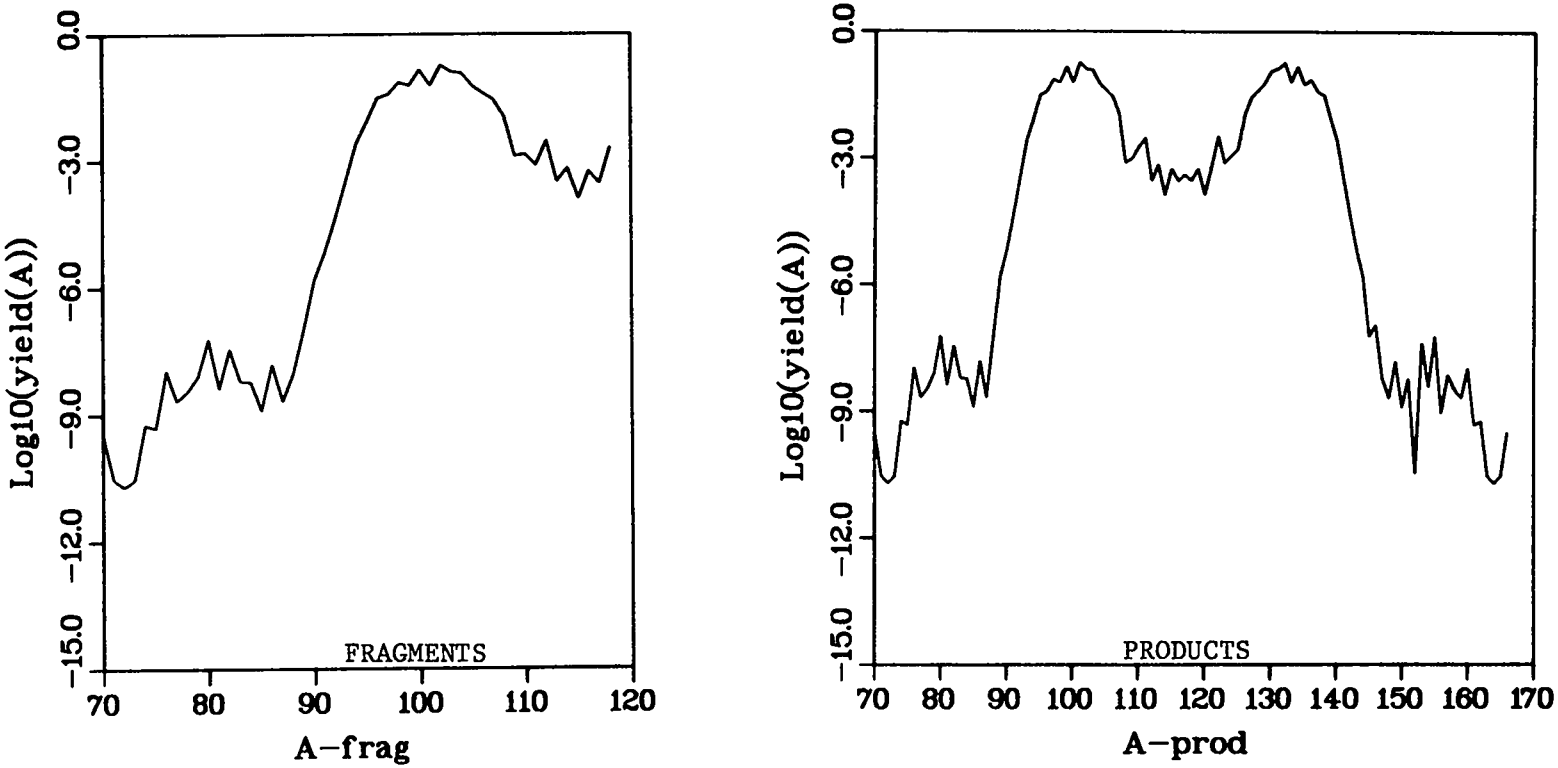

Figure 7: SUM mass chain yields for fragments and products. Products are determined assuming a 2 T neutron treatment. The analytical model is assumed with the Seeger[9] S and P values and a-model. The ground-state mass is assumed to be given by Garvey-Kelson recursion relations[24]. The spacing parameter, δ, is assumed constant for all masses, δ = 3 fm.

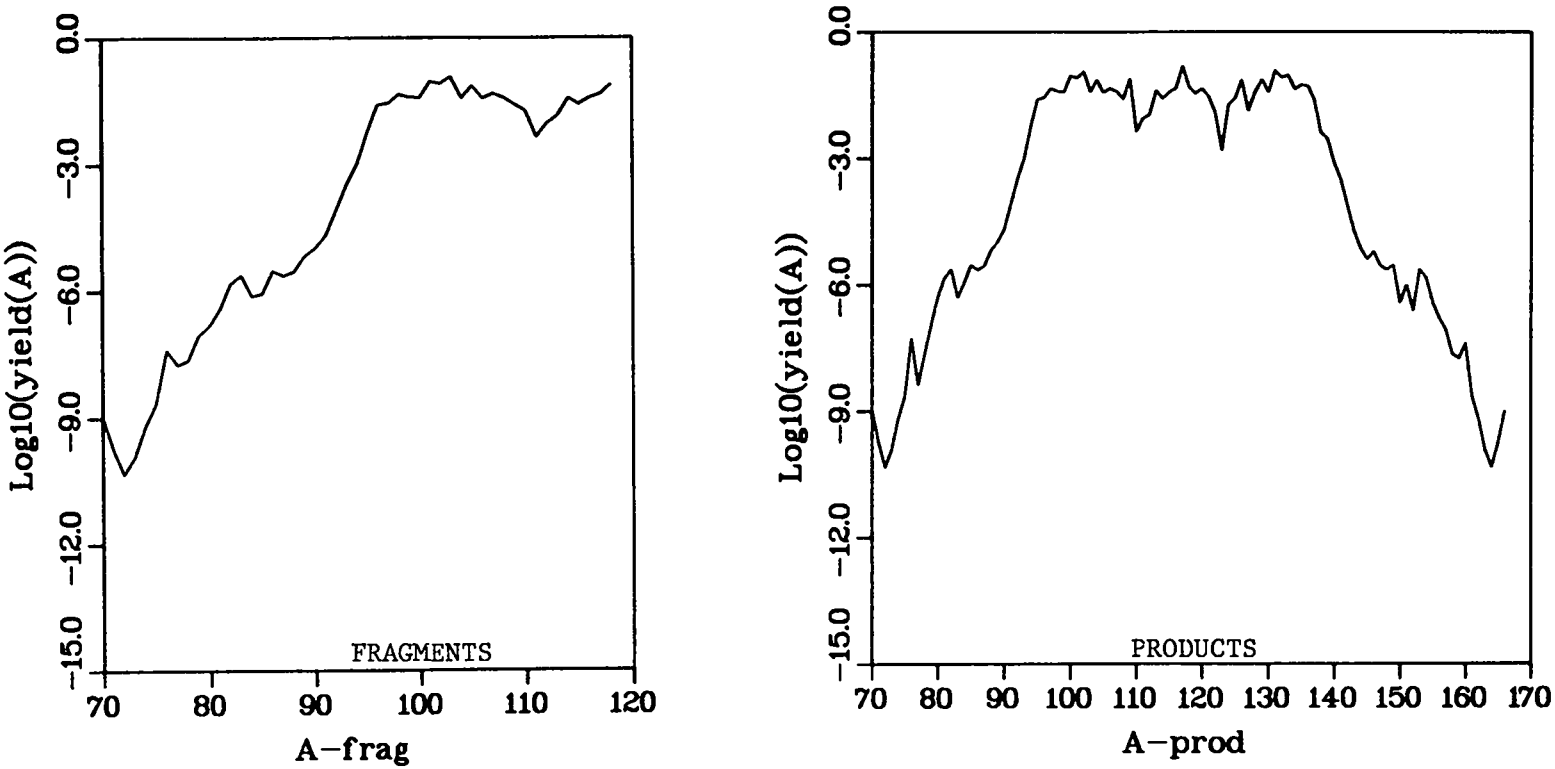

Figure 8: GMAX mass chain yields for fragments and products. Products are determined assuming a 2 T neutron treatment. The analytical model is assumed with Seeger[9] S and P values, a-model, and ground state masses. The spacing parameter, δ, is assumed constant for all masses, δ = 3 fm.

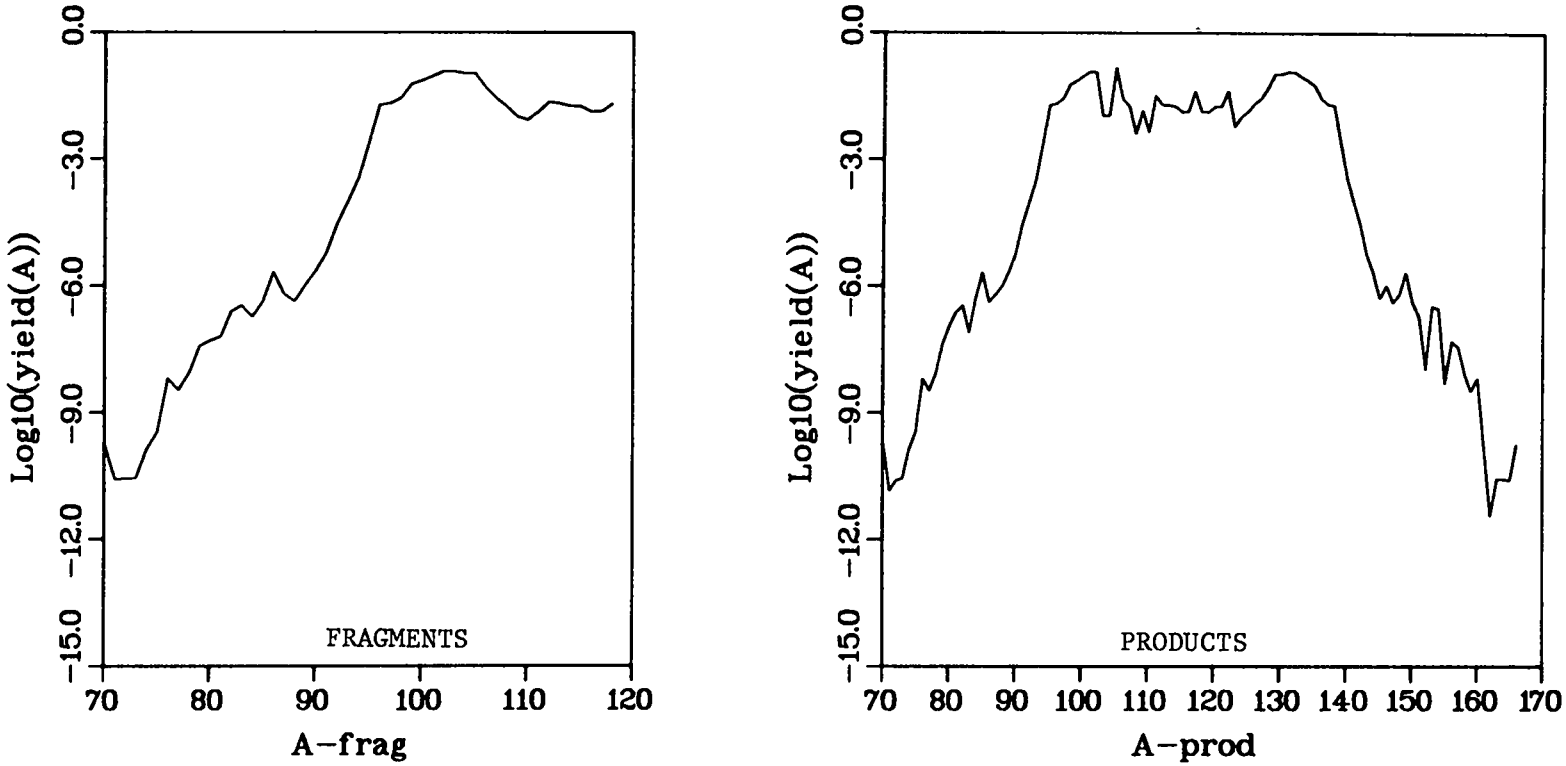

Figure 9: YMAX mass chain yields for fragments and products. Products are determined assuming a 2 T neutron treatment. The analytical model is assumed with Seeger [9] S and P values, a-model, and ground-state masses. The spacing parameter, δ, is assumed constant for all masses, δ = 3 fm.

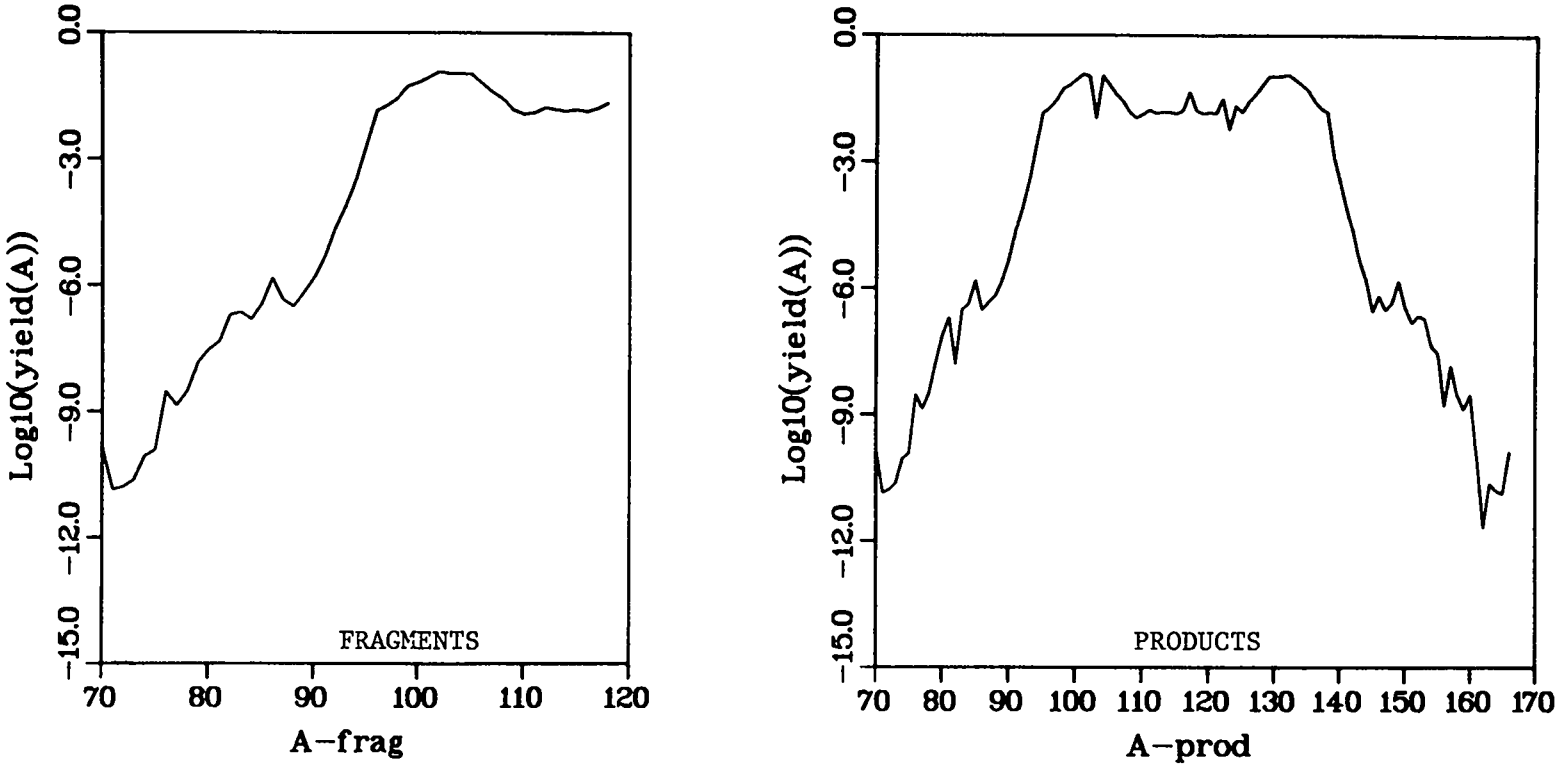

Figure 10: SUM mass chain yields for fragments and products. Products are determined assuming a 2 T neutron treatment. The analytical model is assumed with Seeger[9] S and P values, a-model, and ground-state masses. The spacing parameter, δ, is assumed constant for all masses, δ = 3 fm.

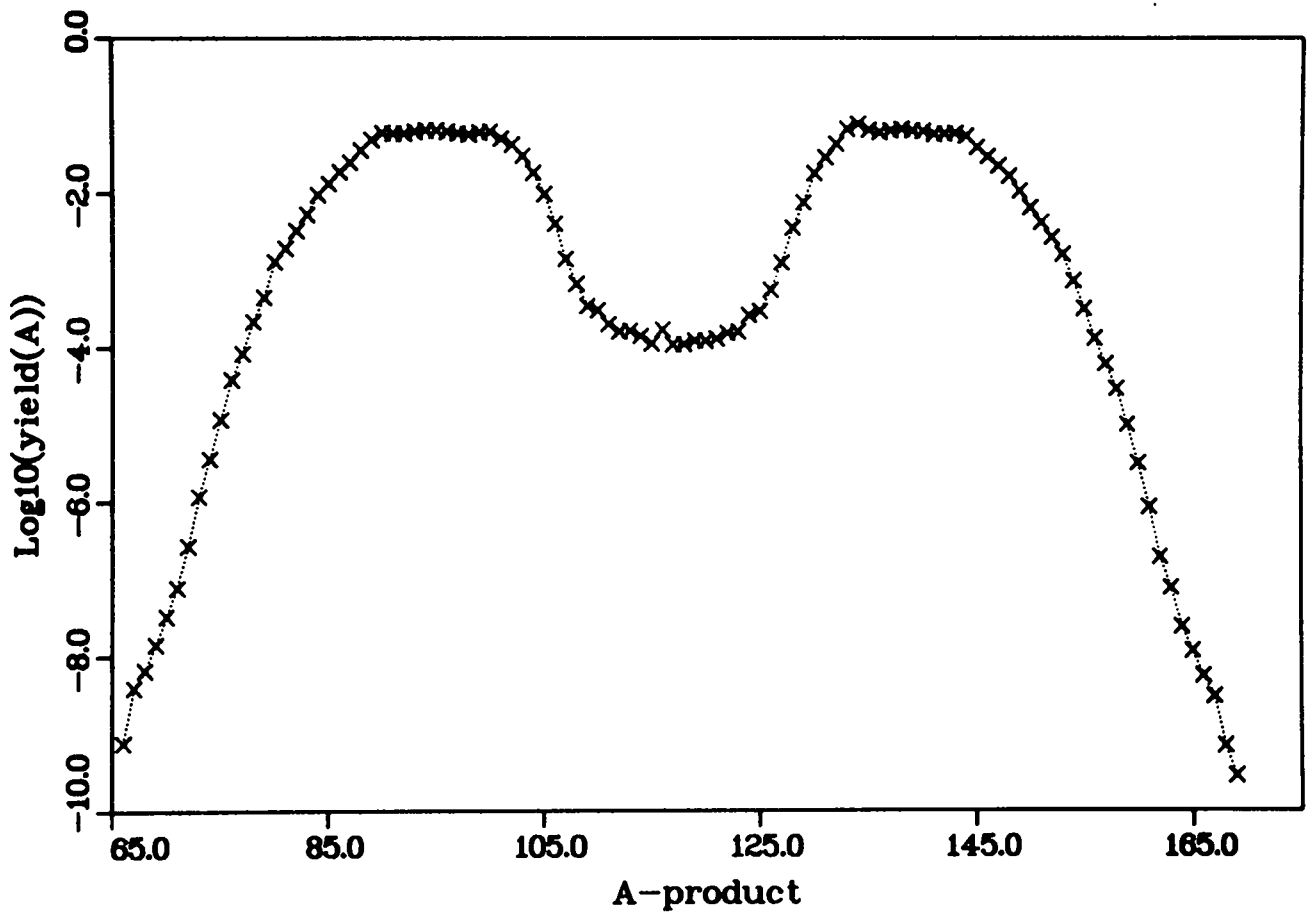

Figure 11: Mass chain yields for $^{235}U(n_{th},f)$ as given by Reference 8.

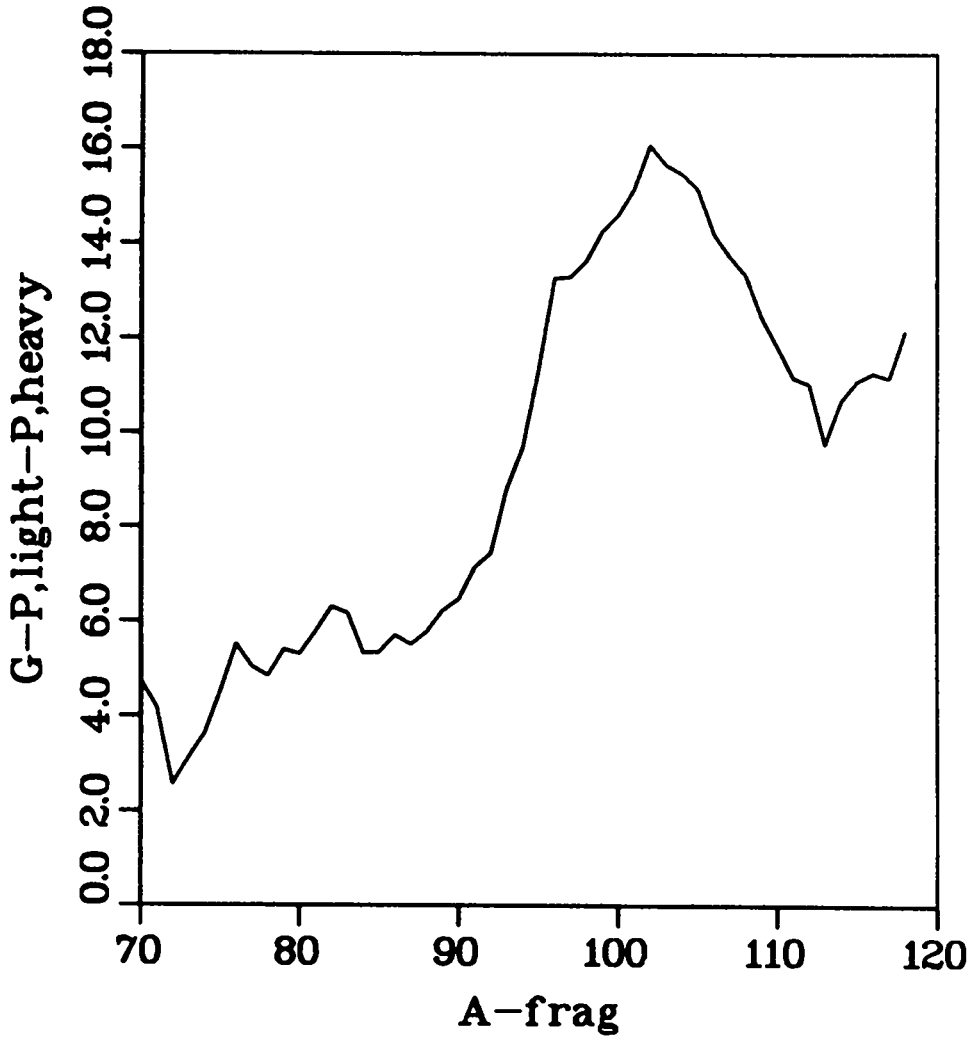

Figure 12: The G-energy shifted by the sum of the pairing energies for the yield shown in Figure 8. The values shown here are averaged over charge for fixed fragment mass.

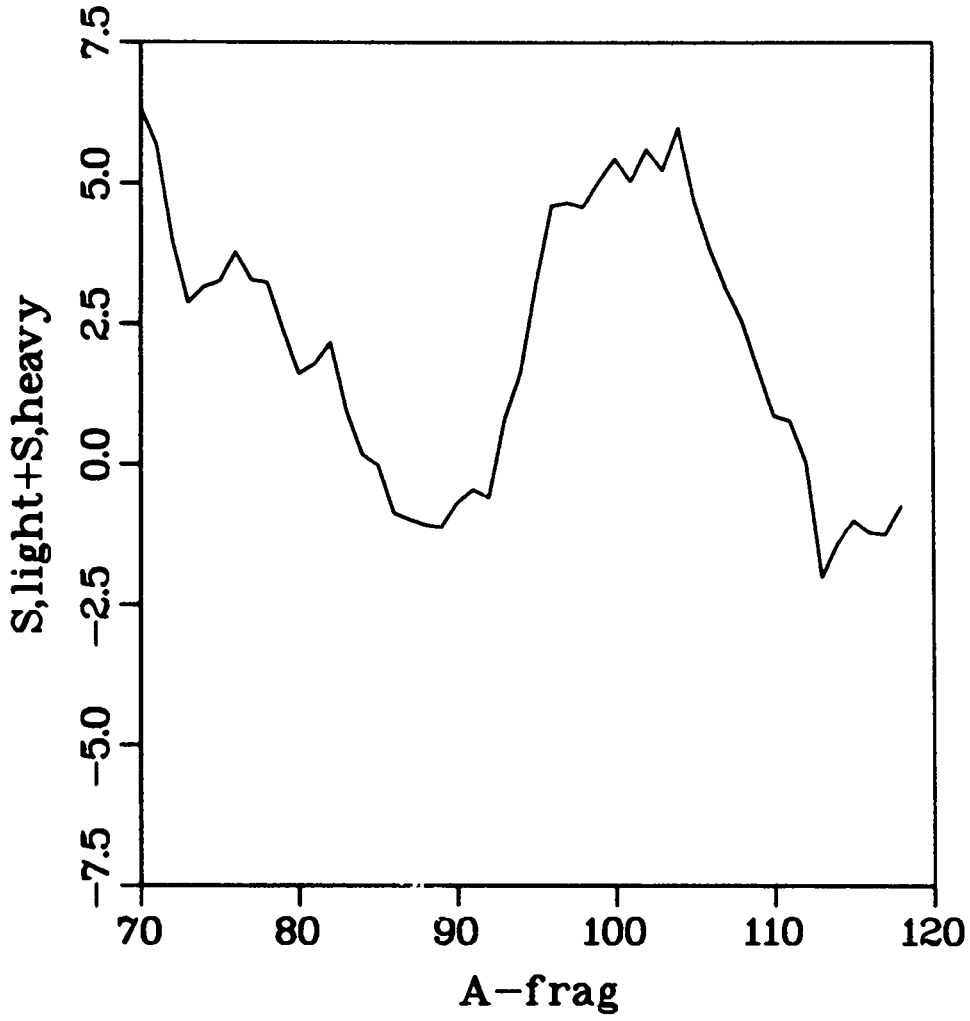

Figure 13: The sum of the shell terms for the yield shown in Figure 8. The values shown here are averaged over charge for fixed mass.

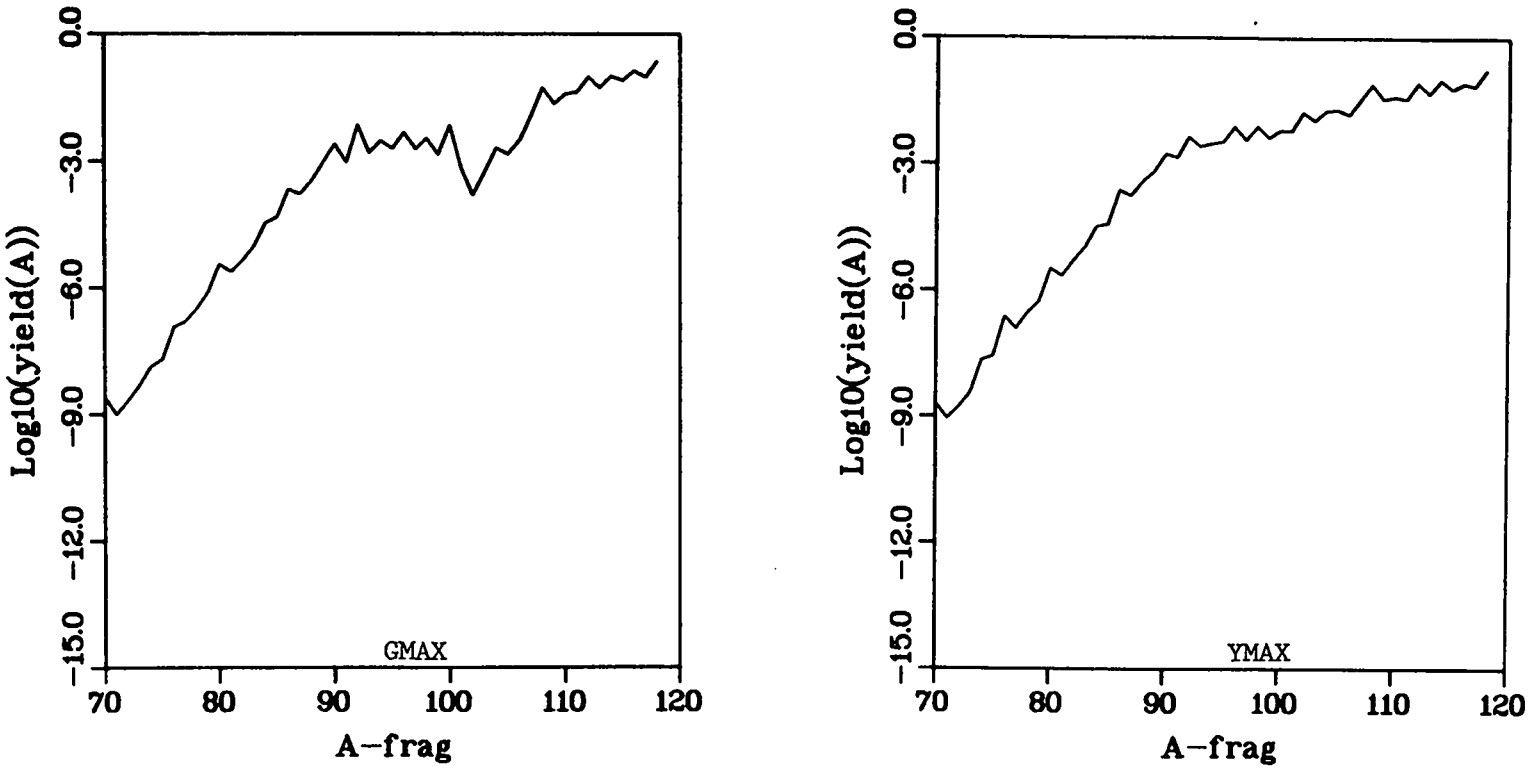

Figure 14: Fission fragment yields for $^{235}U(n_{th},f)$ assuming the spacing parameter, δ, to be constant, δ = 3 fm.

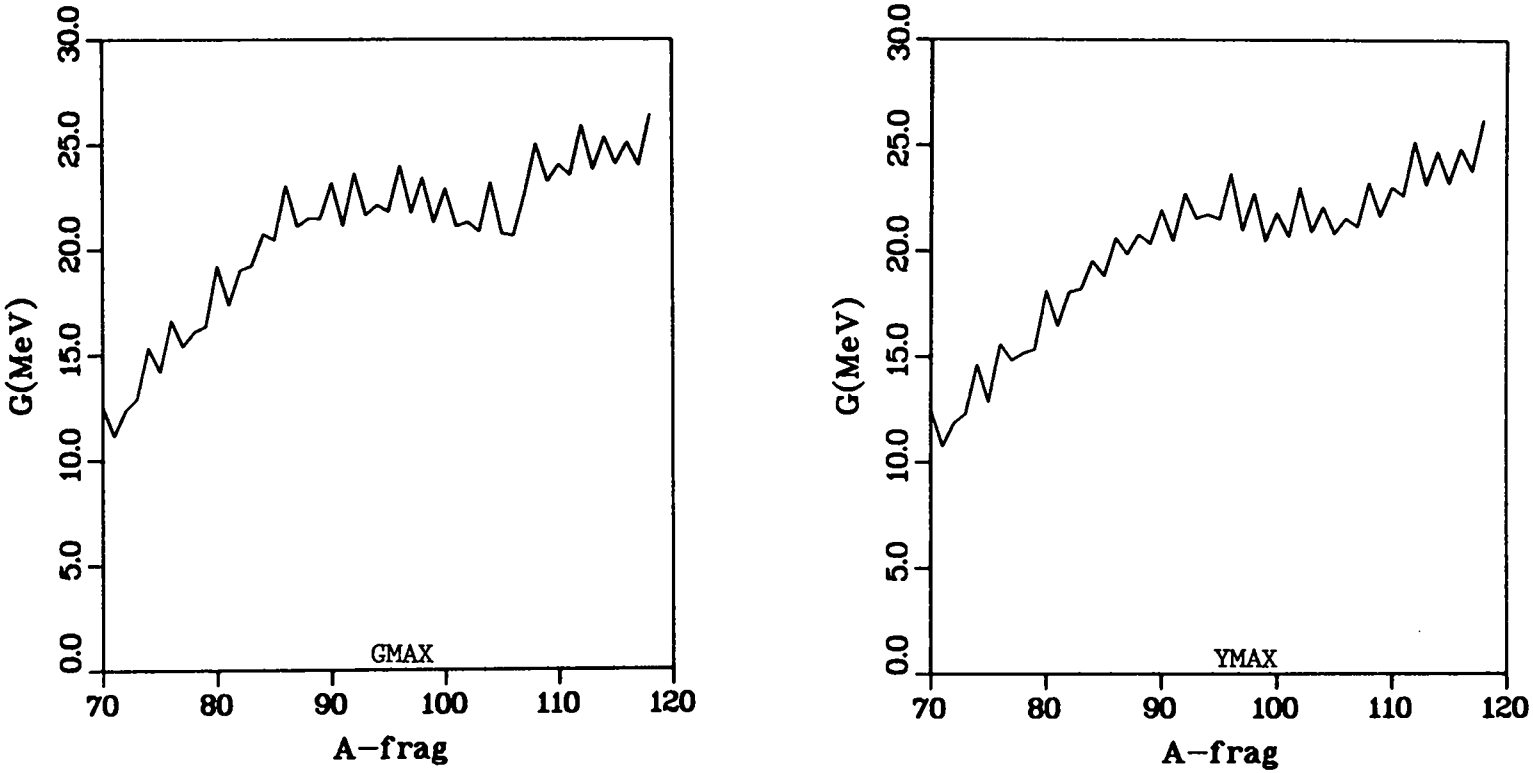

Figure 15: G energies, averaged over charge, for yields shown in Figure 14.

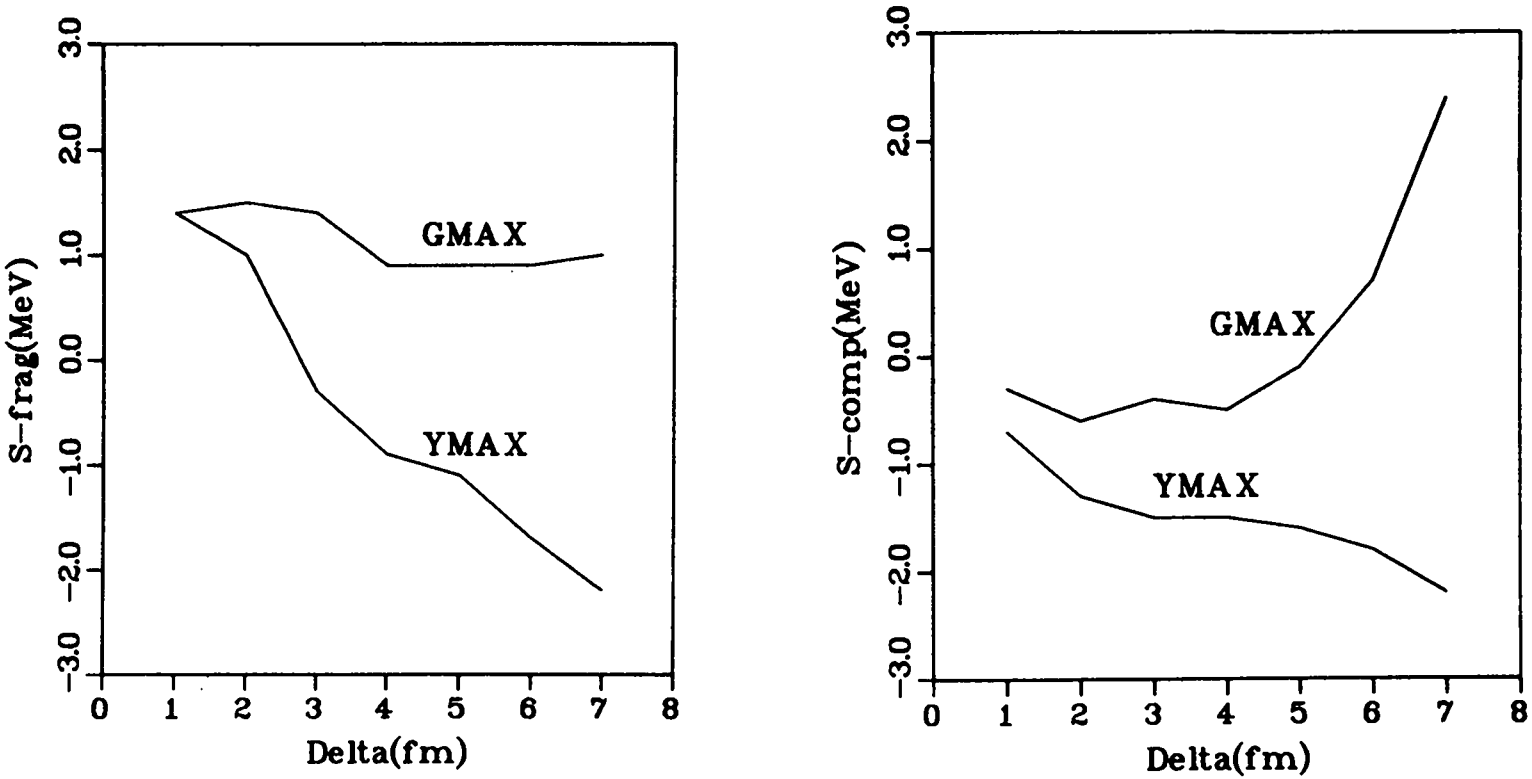

Figure 16: Integral values of the single-particle shell correction energies, S, for the light fragment and its heavy compliment for fixed values of the spacing parameter, δ.

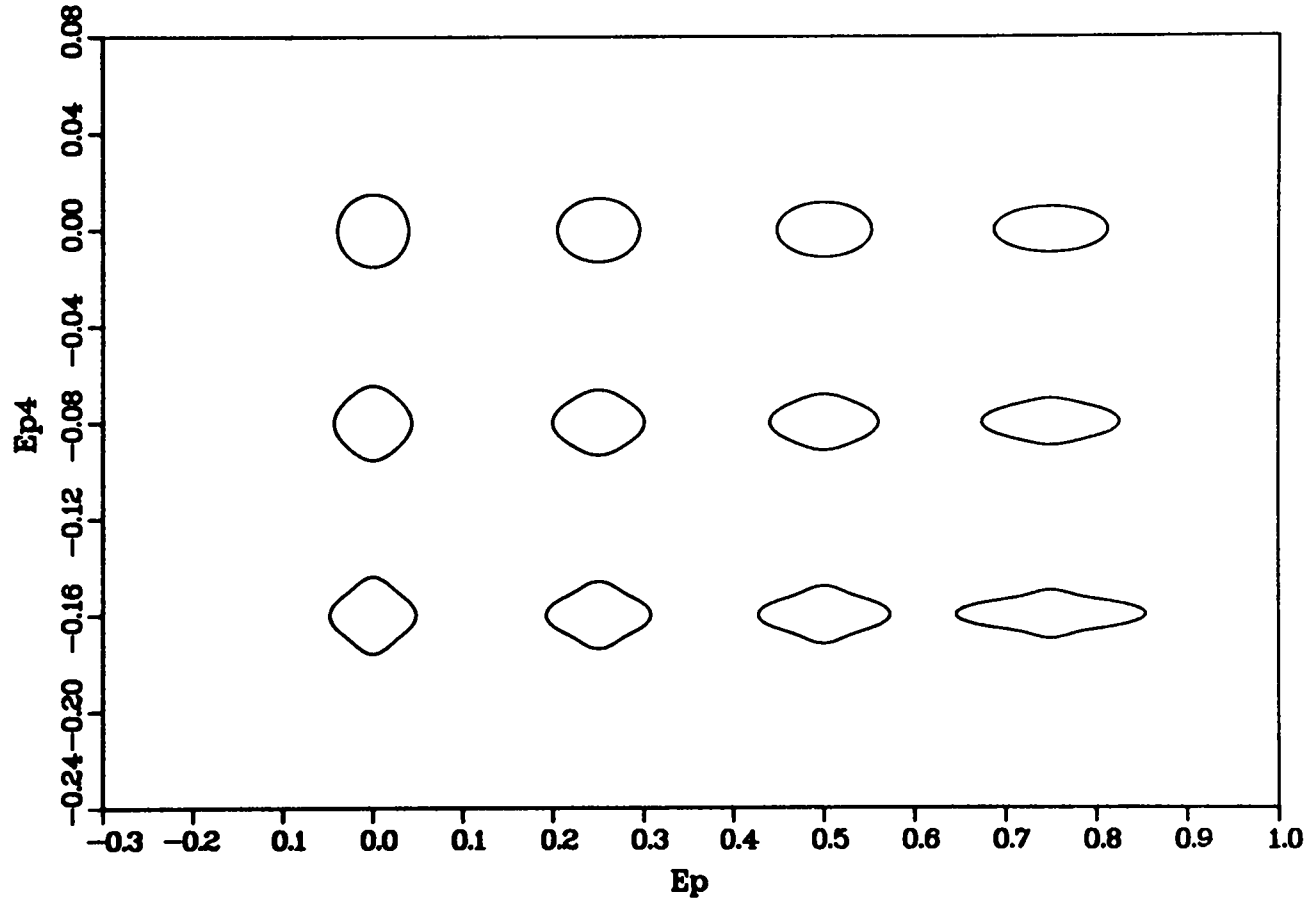

Figure 17: Shapes given by extending the maximum value of ε_4 in the space of allowed shapes. These shapes were generated with the Nix expression[40] of Appendix H.

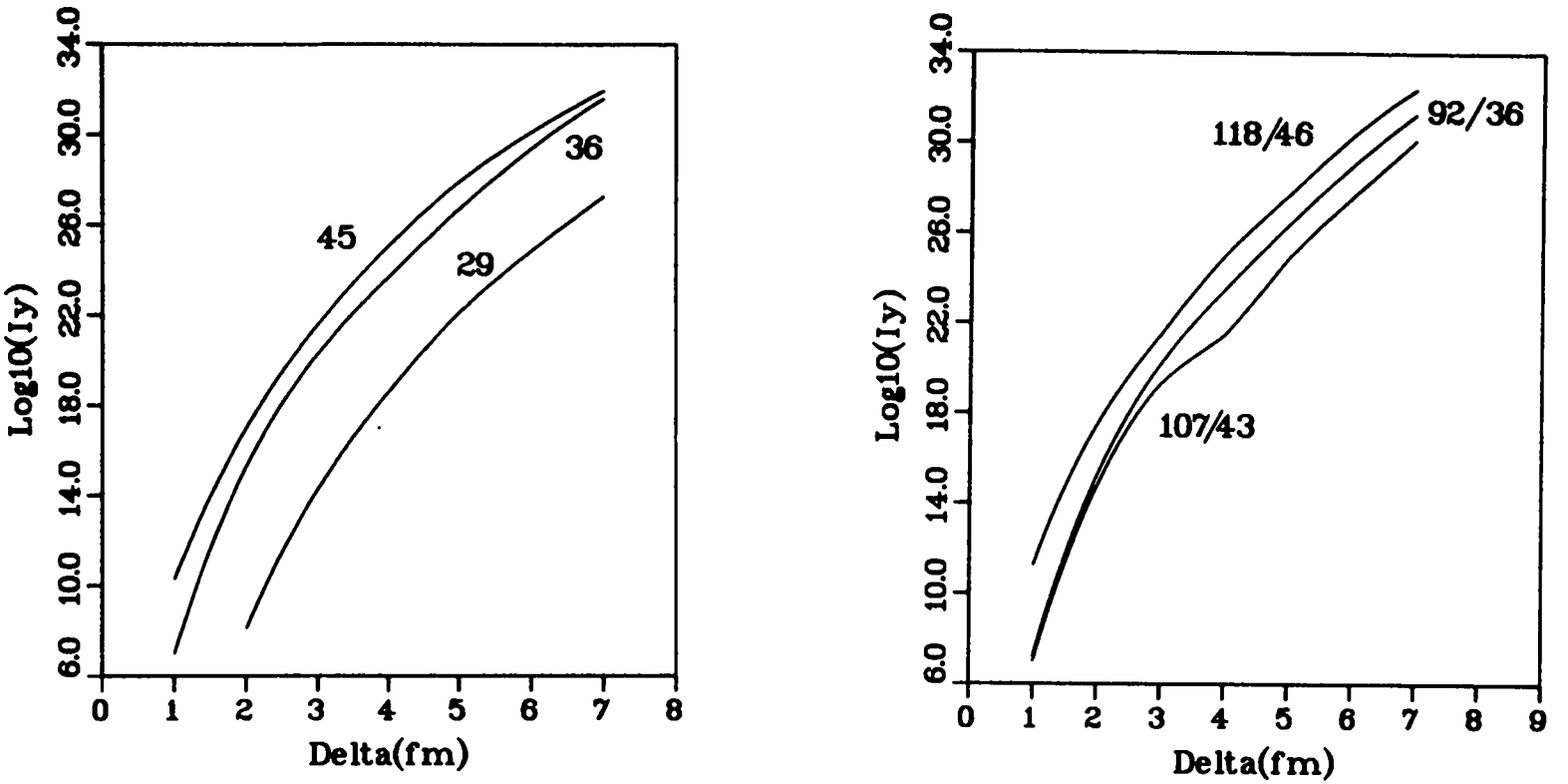

Figure 18: Behavior of yield integrals with spacing parameter, δ. Shown on the left are the "charge-lumped" integrals, obtained by summing over all masses for a given fixed charge, with each curve labeled by the charge number. Those on the right show the integrals' behaviors for a few individual fragments, labeled by the fragment mass and charge as A/Z. Note the effect of a change of shape in the curve labeled 107/43. These curves correspond to GMAX shapes.

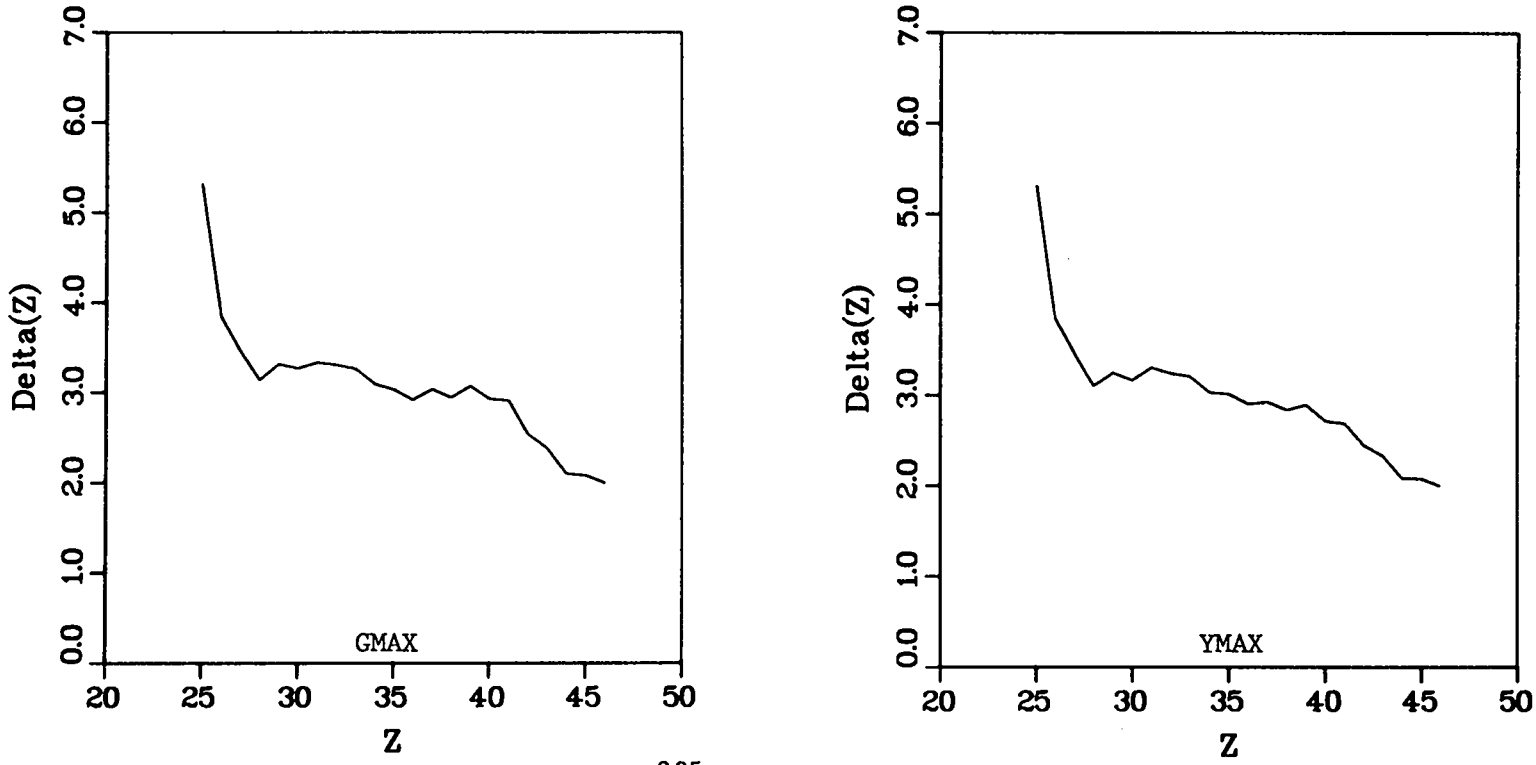

Figure 19: δ(Z) families obtained for $^{235}U(n_{th},f)$ assuming δ(Z=46) = 2 fm.

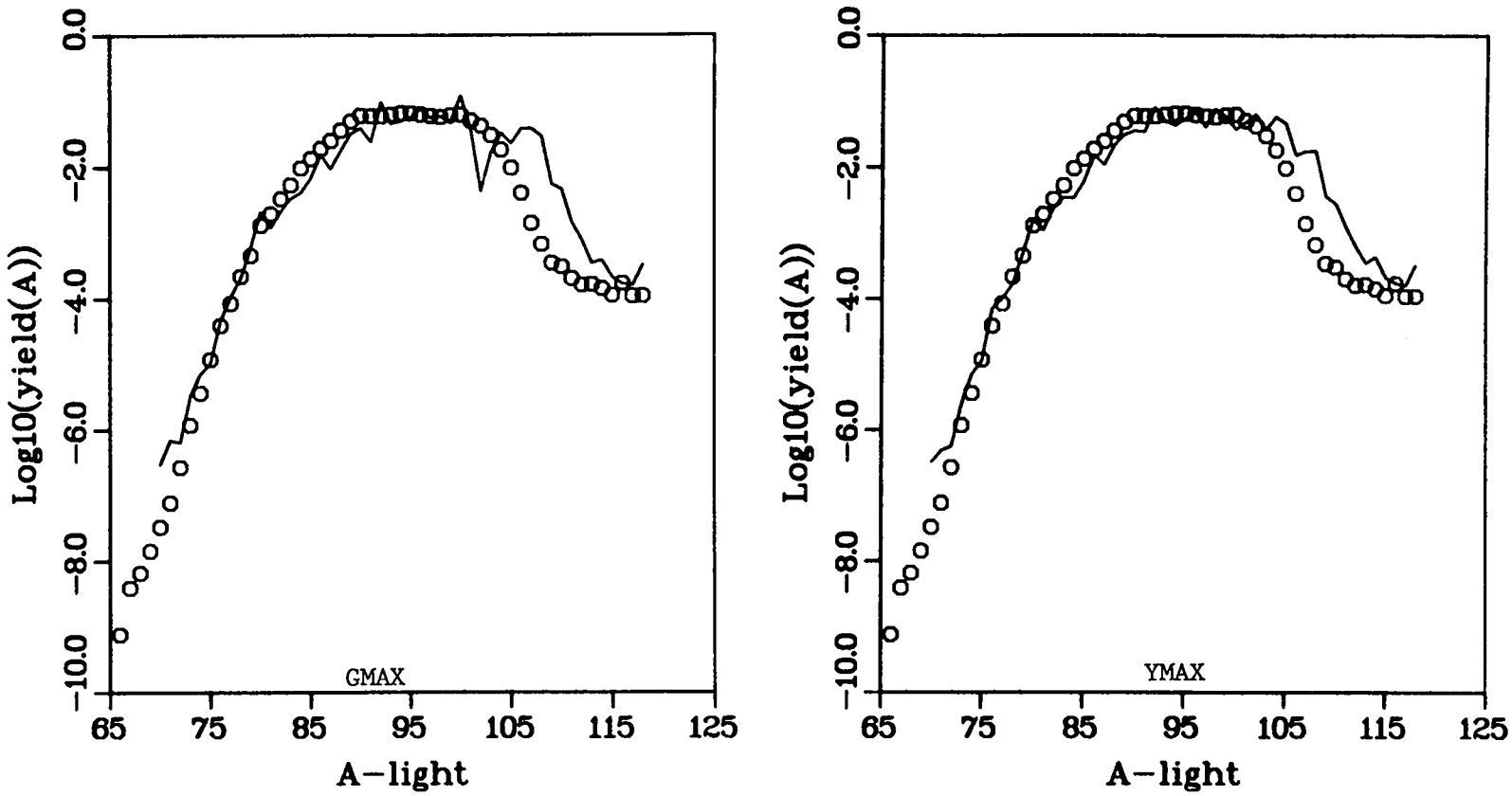

Figure 20: Fission fragment yields for $^{235}U(n_{th},f)$ assuming $\delta(Z)$ as in Figure 19. Circles are fission product yields from Reference 8, shown here for comparison.

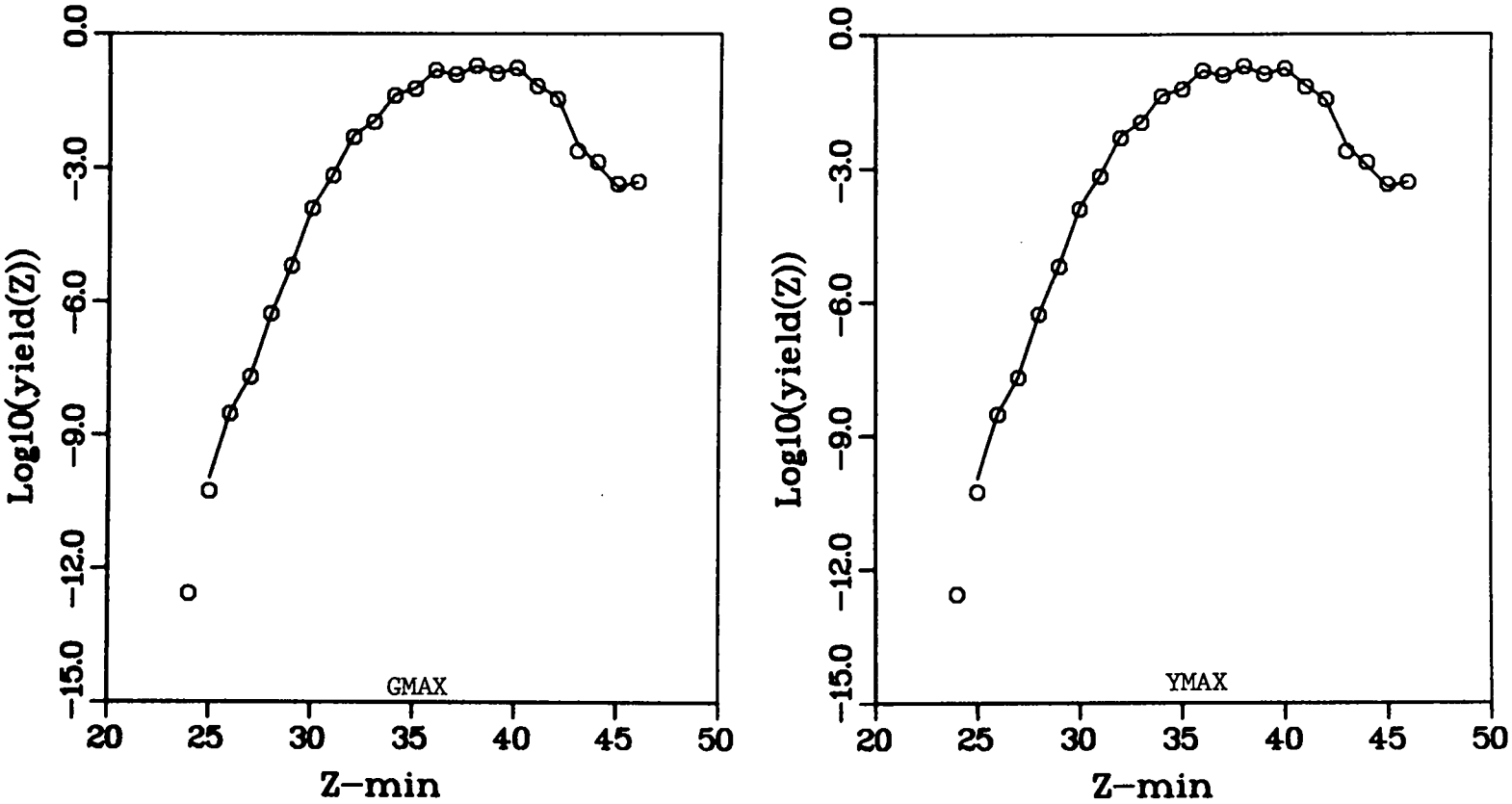

Figure 21: Charge yields for $^{235}U(n_{th},f)$ assuming $\delta(Z)$ parameters of Figure 19. Circles are measured yields from Reference 8.

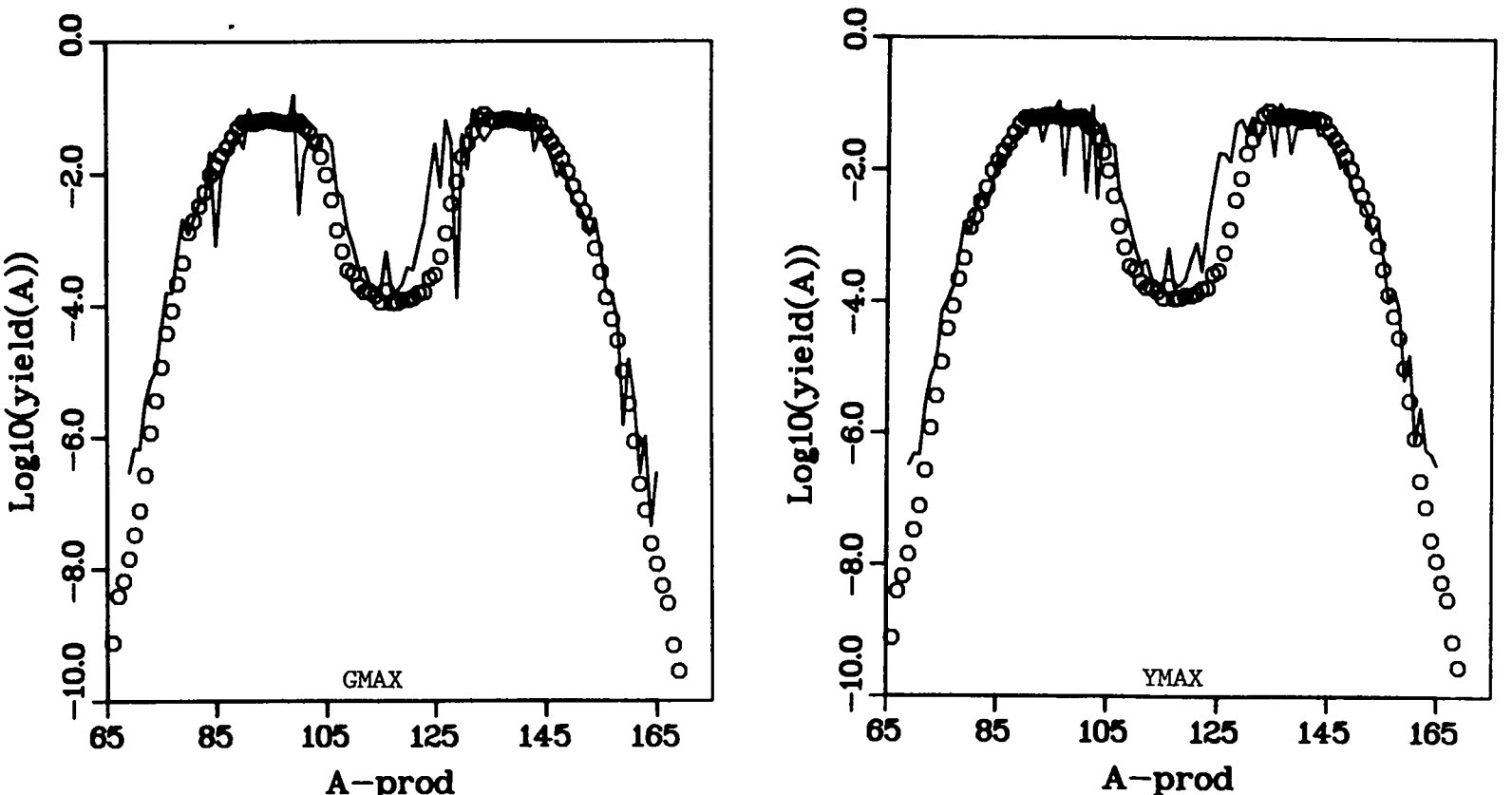

Figure 22: Fission product yields for $^{235}U(n_{th},f)$ assuming $\delta(Z)$ parameters of Figure 19 and a 2 T neutron treatment. Circles are measured yields from Reference 8.

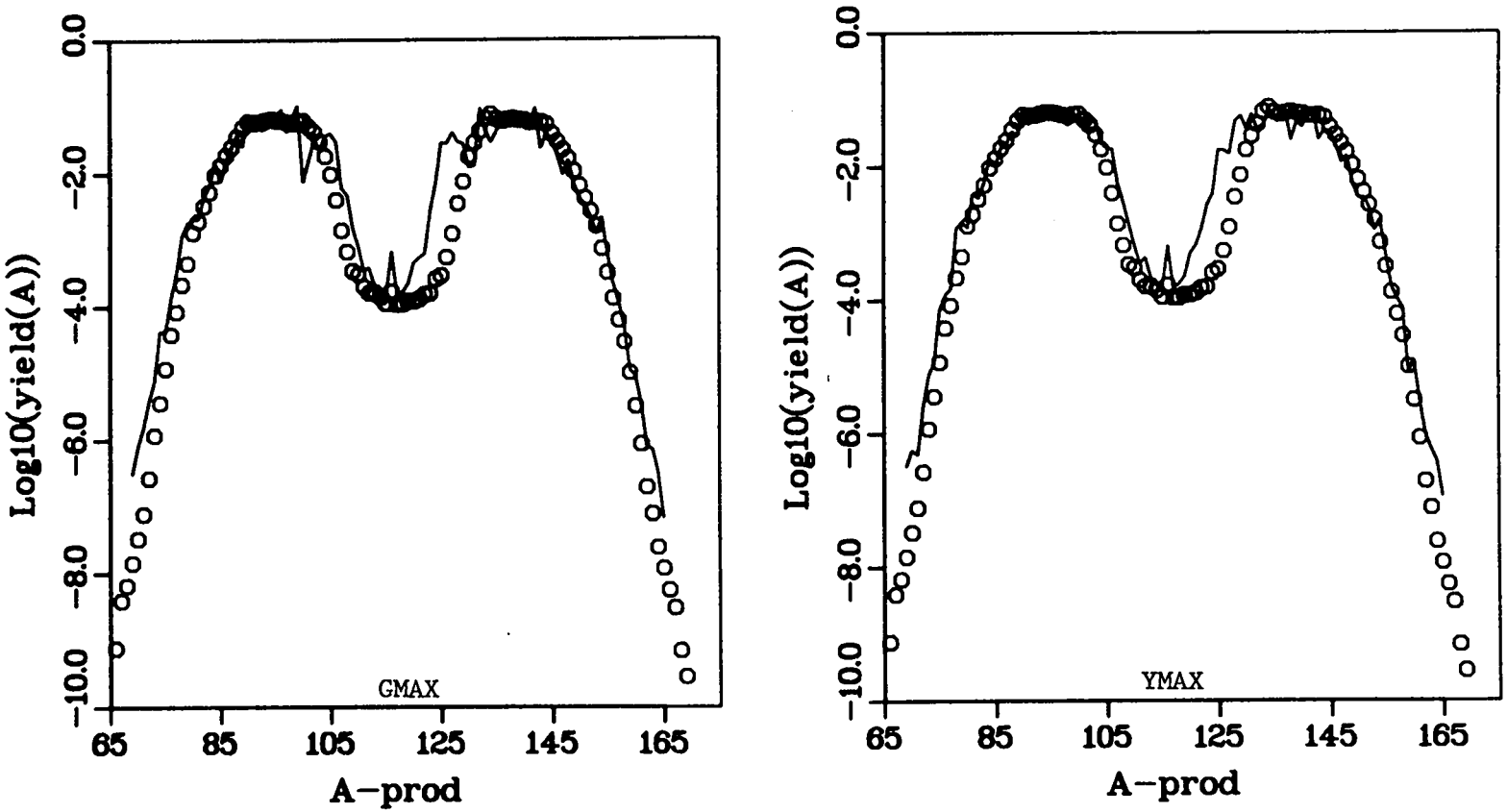

Figure 23: Fission product yields for $^{235}U(n_{th},f)$ assuming $\delta(Z)$ parameters of Figure 19 and a simple cascade neutron treatment. Circles are measured yields from Reference 8. Yields computed with this neutron treatment are to be compared to those given by the 2 T treatment of Figure 22.

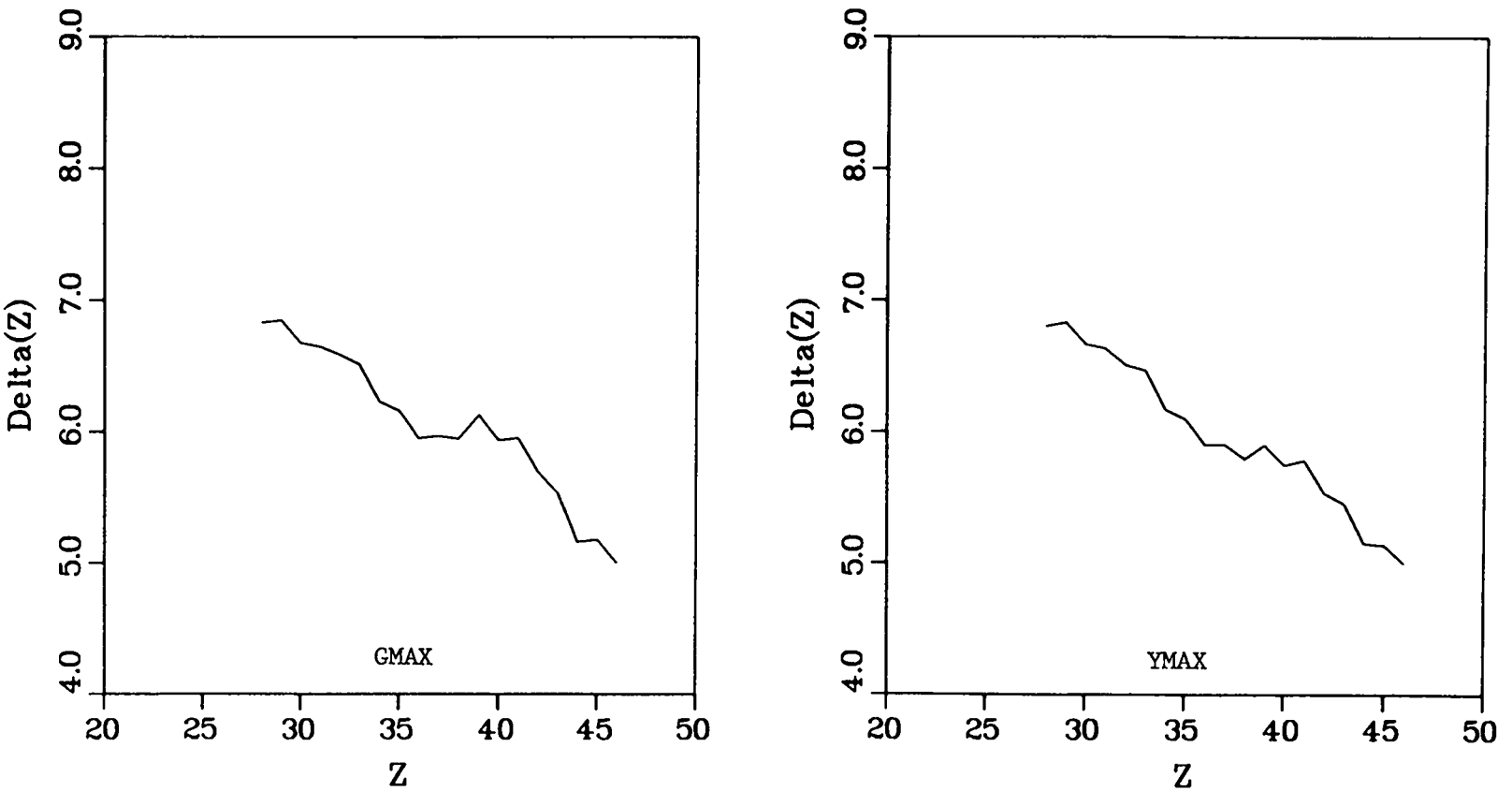

Figure 24: Spacing parameter, $\delta(Z)$, for $^{235}U(n_{th},f)$ assuming $\delta(Z=46)$ = 5 fm. and constraining 27.5 MeV to remain in k_o.

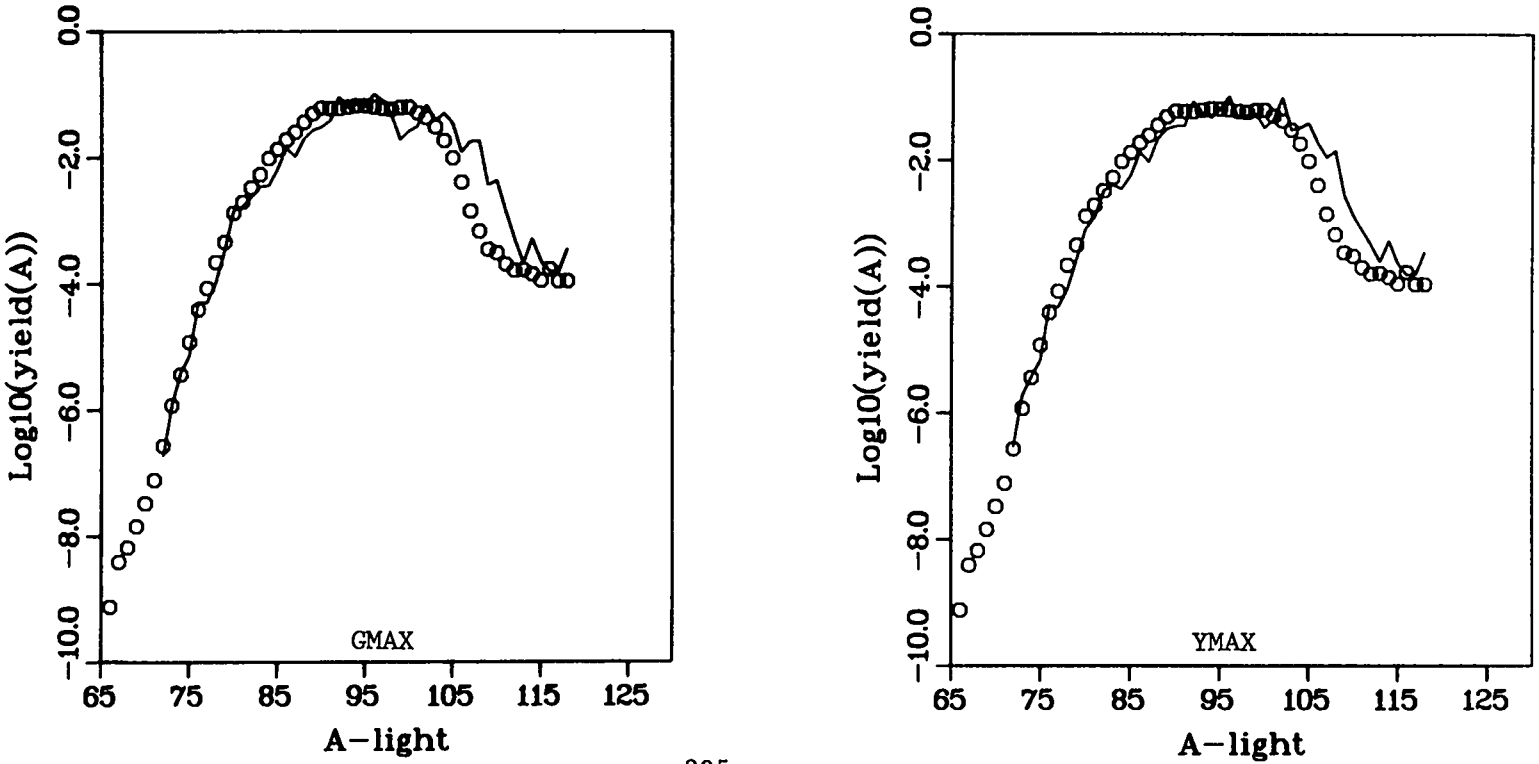

Figure 25: Fission fragment yields for $^{235}U(n_{th},f)$ assuming $\delta(Z)$ as given in Figure 24. Circles are fission product yields from Reference 8, shown here for comparison.

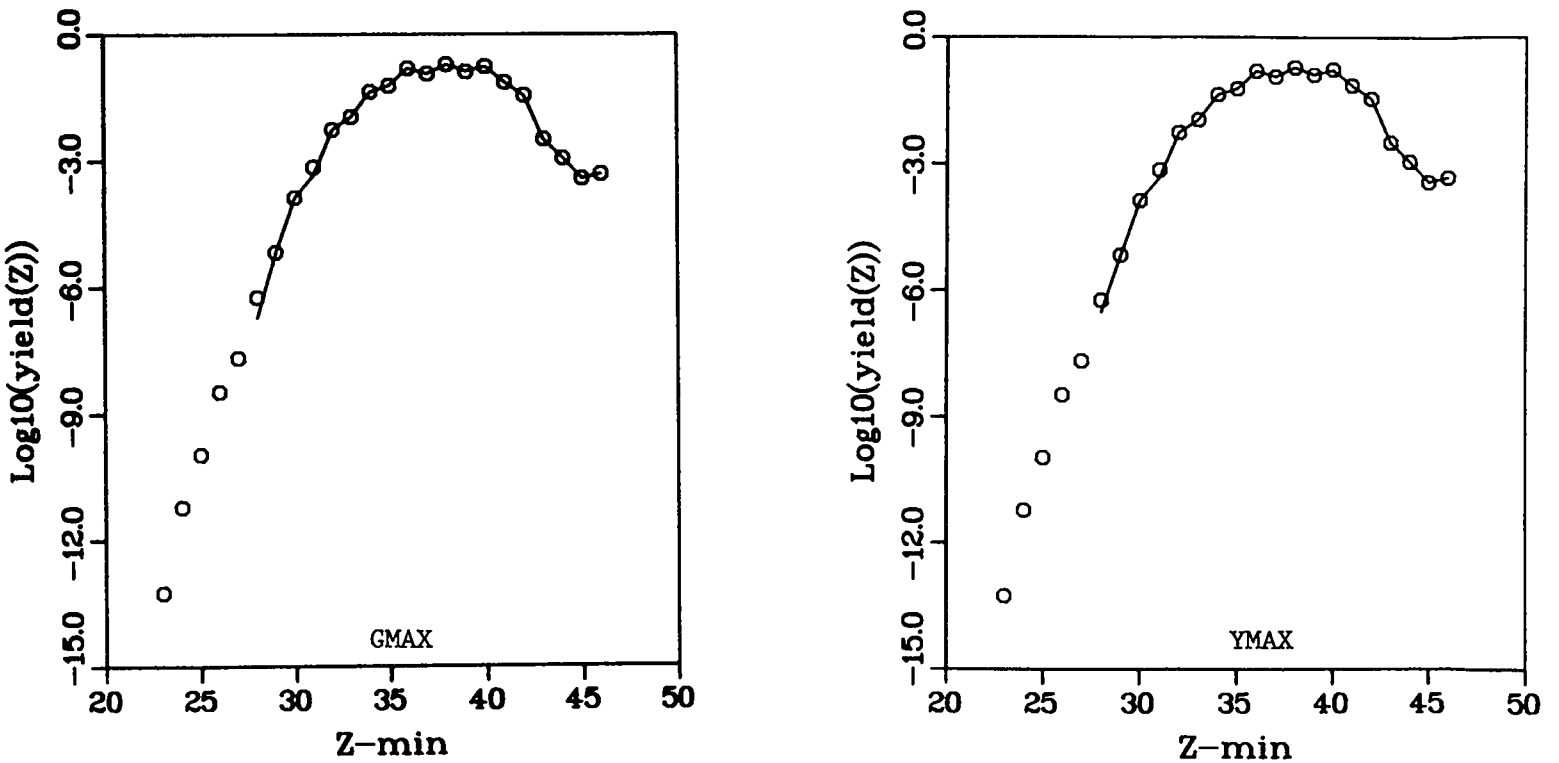

Figure 26: Charge yields for $^{235}U(n_{th},f)$ assuming $\delta(Z)$ as in Figure 24. Circles are measured yields from Reference 8.

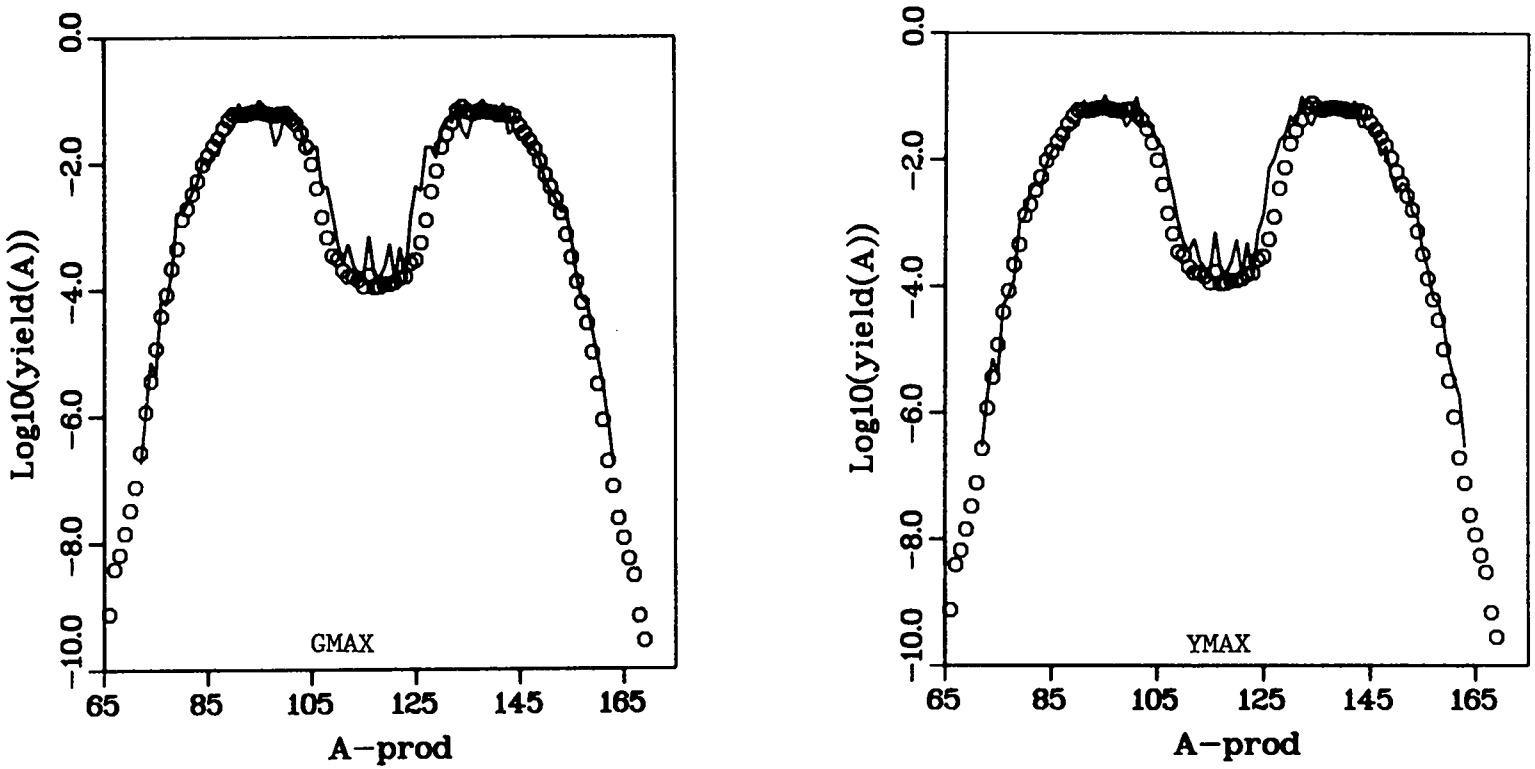

Figure 27: Fission product yields for $^{235}U(n_{th},f)$ assuming $\delta(Z)$ as in Figure 24 and a simple cascade neutron treatment. Circles are measured yields from Reference 8.

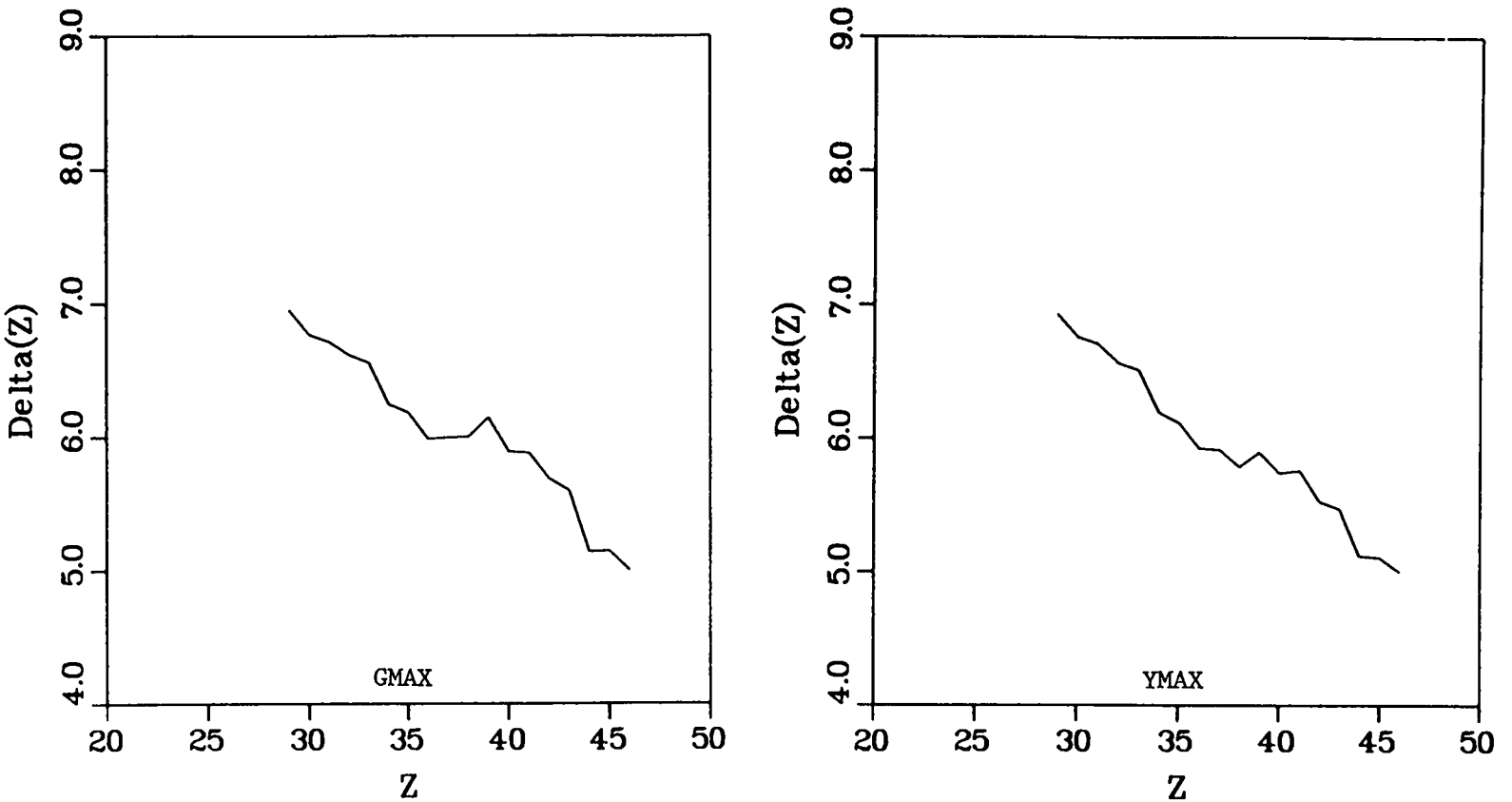

Figure 28: Spacing parameter, $\delta(Z)$, for $^{233}U(n_{th},f)$ assuming $\delta(Z=46)$ = 5 fm. and constraining 28.0 MeV to remain in k_o.

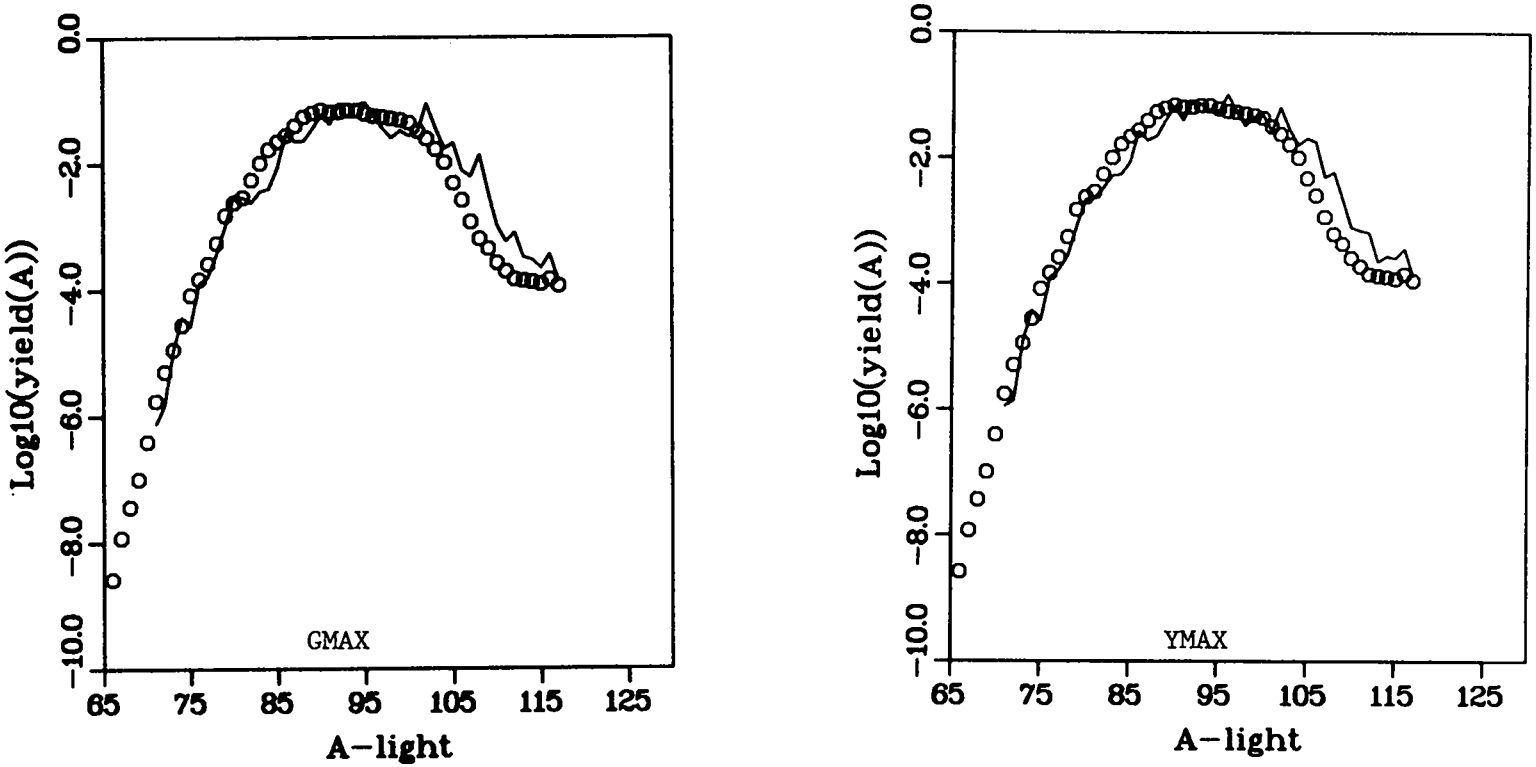

Figure 29: Fission fragment yields for $^{233}U(n_{th},f)$ assuming $\delta(Z)$ as in Figure 28. Circles are fission product yields from Reference 8, shown here for comparison.

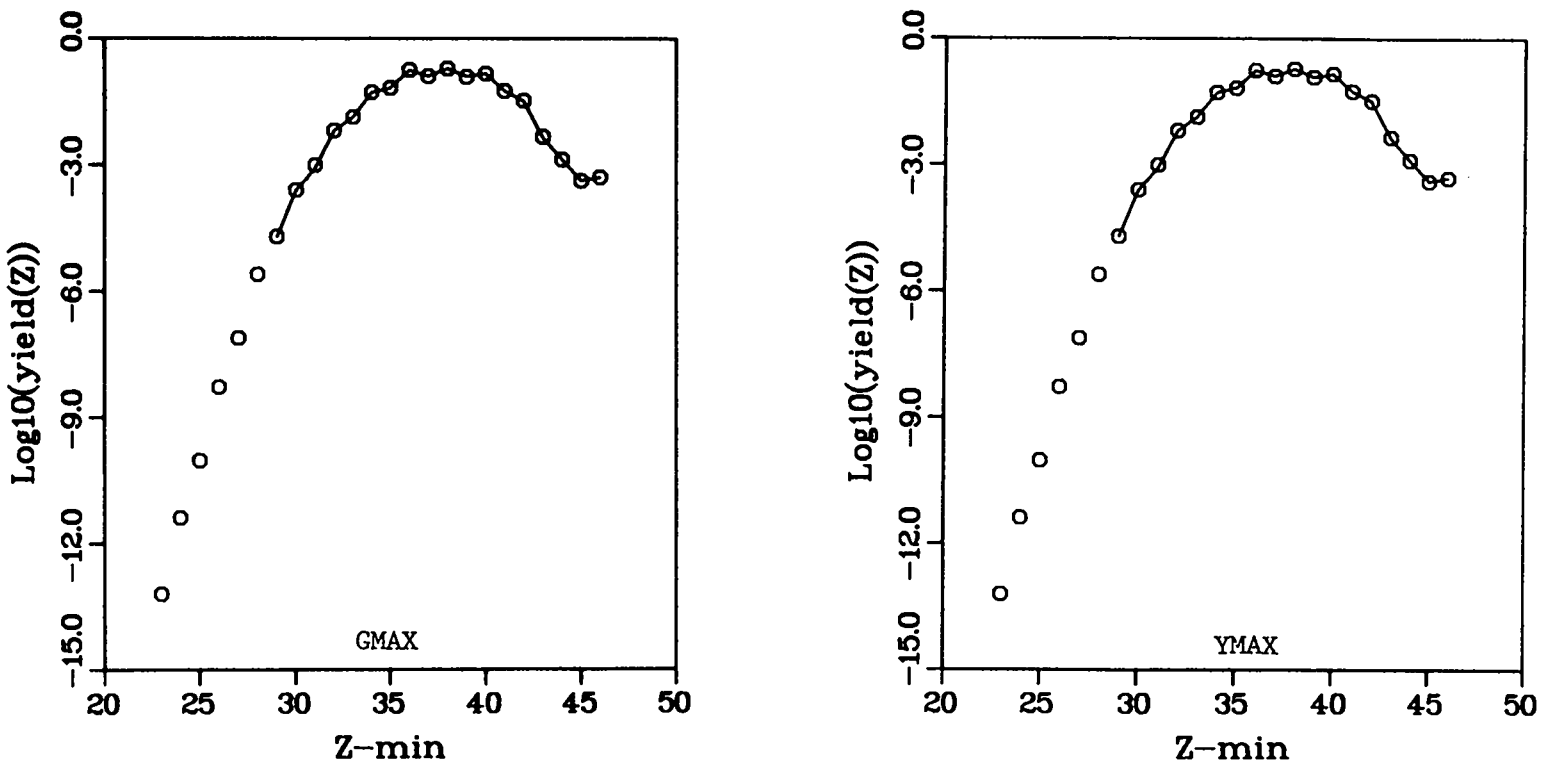

Figure 30: Charge yields for $^{233}U(n_{th},f)$ assuming $\delta(Z)$ as in Figure 28. Circles are measured yields from Reference 8.

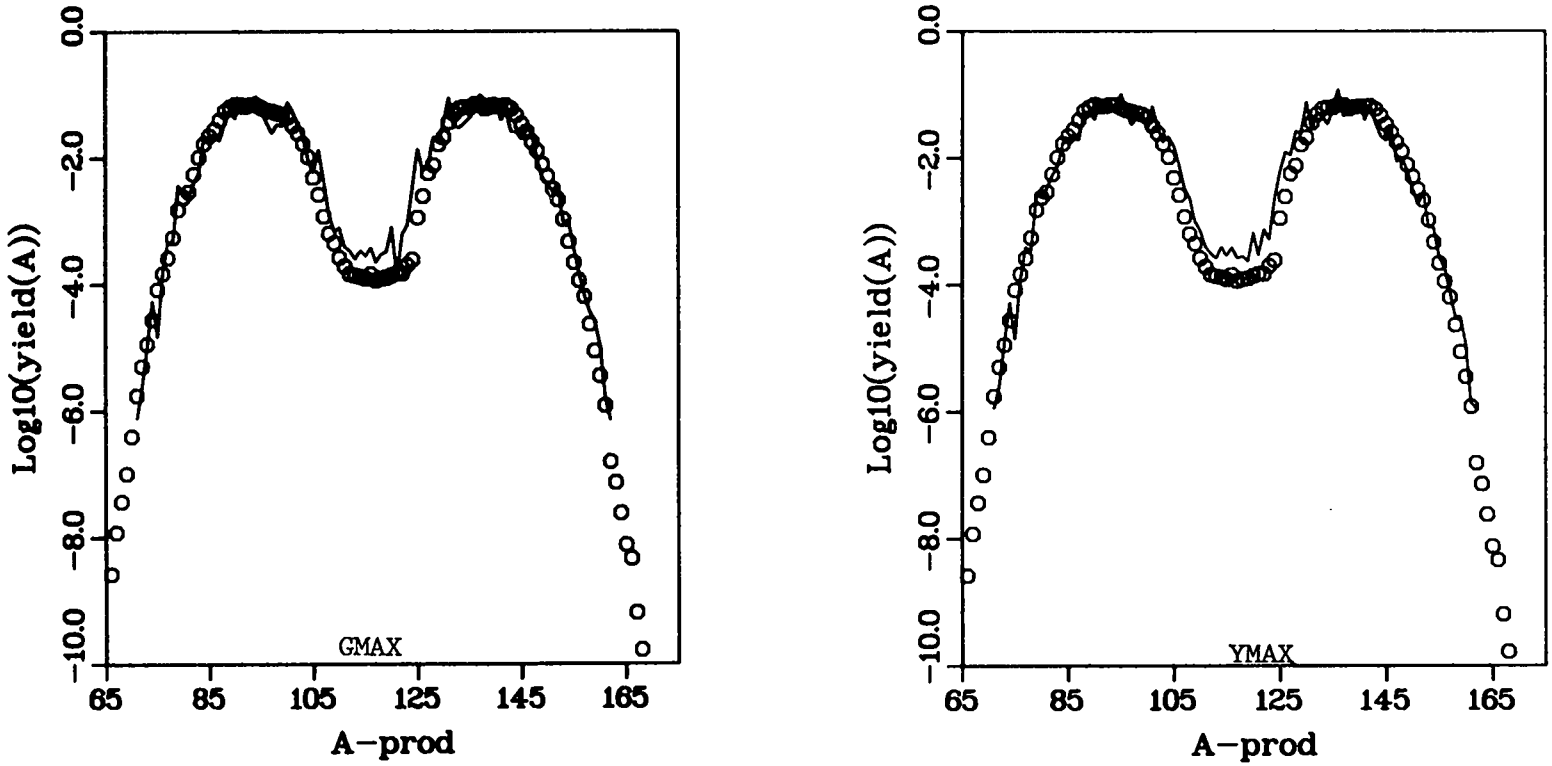

Figure 31: Fission product yields for $^{233}U(n_{th},f)$ assuming $\delta(Z)$ as in Figure 28 and a simple cascade neutron treatment. Circles are measured yields from Reference 8.

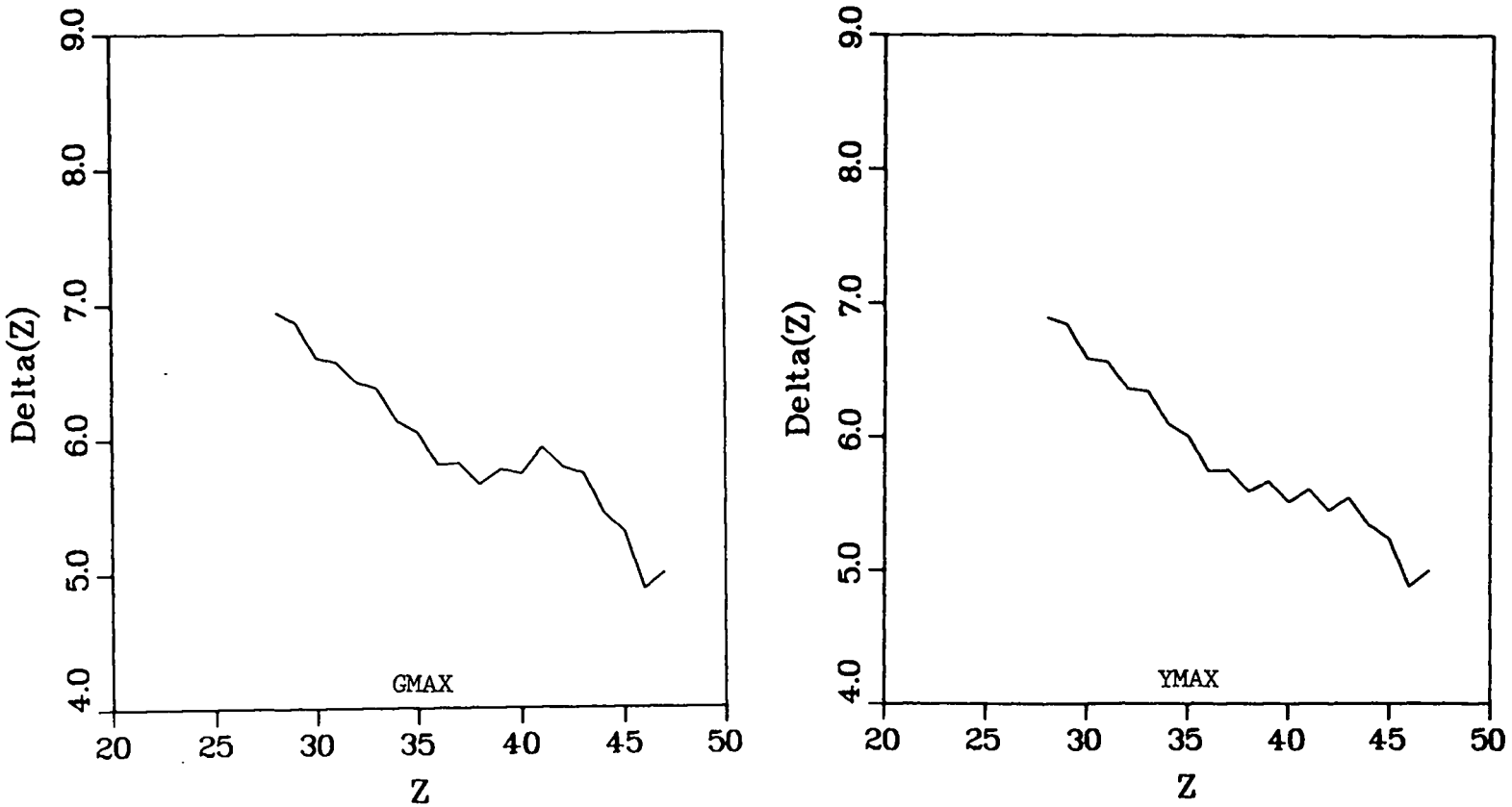

Figure 32: Spacing parameter, $\delta(Z)$, for $^{239}Pu(n_{th},f)$ assuming $\delta(Z=47)$ = 5 fm. and constraining 28.0 MeV to remain in k_o.

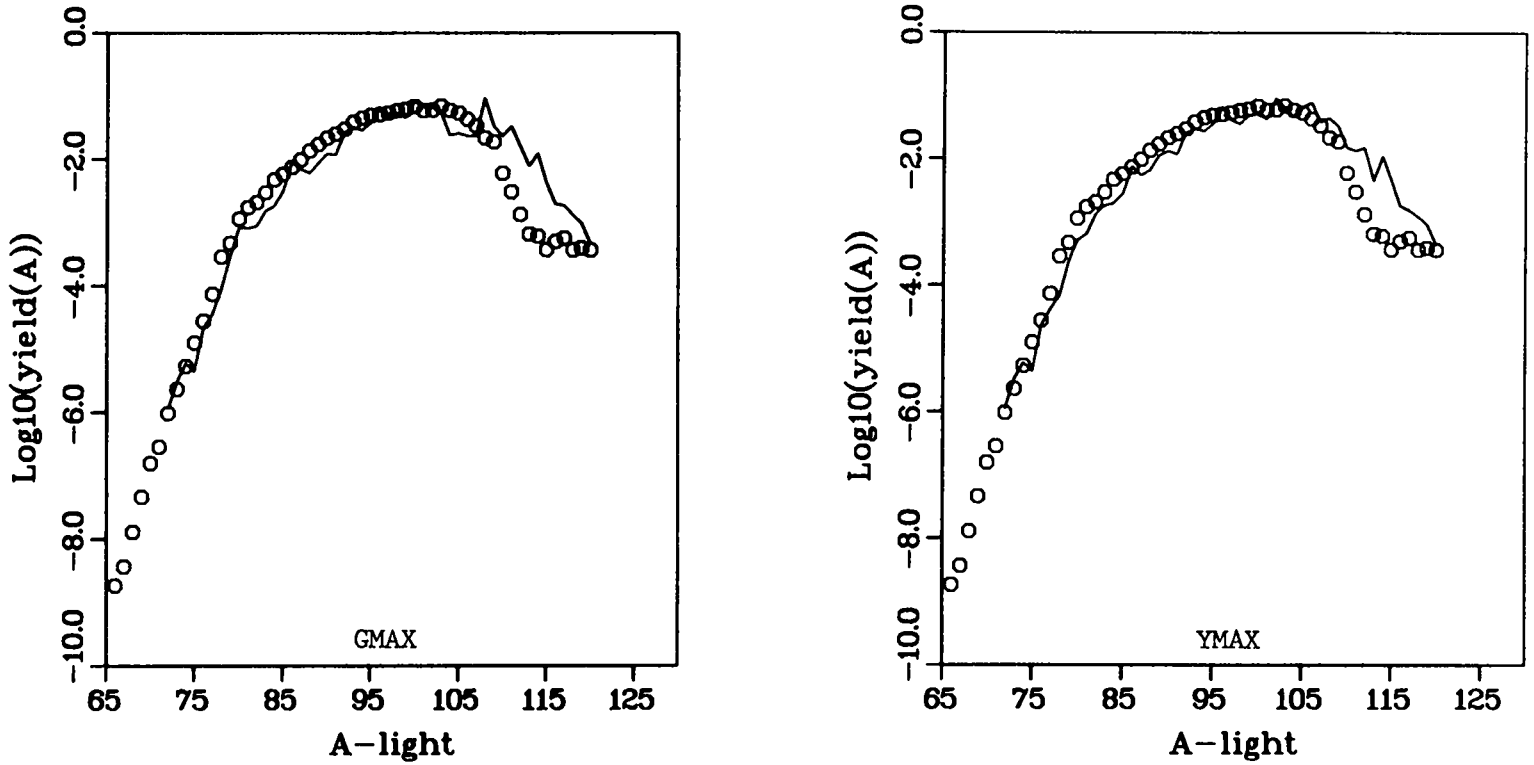

Figure 33: Fission fragment yields for $^{239}Pu(n_{th},f)$ assuming $\delta(Z)$ as in Figure 32. Circles are fission product yields from Reference 8, shown here for comparison.

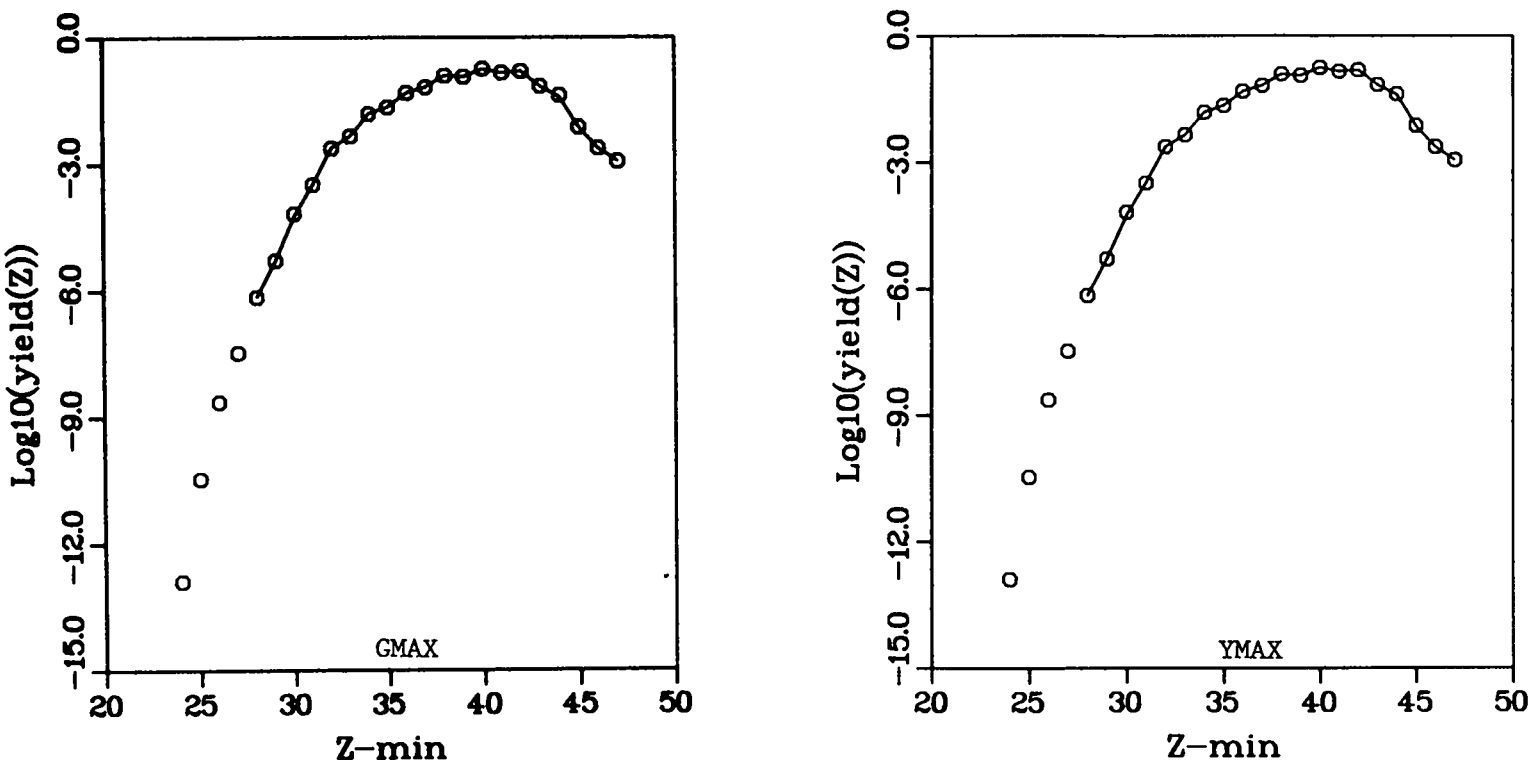

Figure 34: Charge yields for $^{239}Pu(n_{th},f)$ assuming $\delta(Z)$ as in Figure 32. Circles are measured yields from Reference 8.

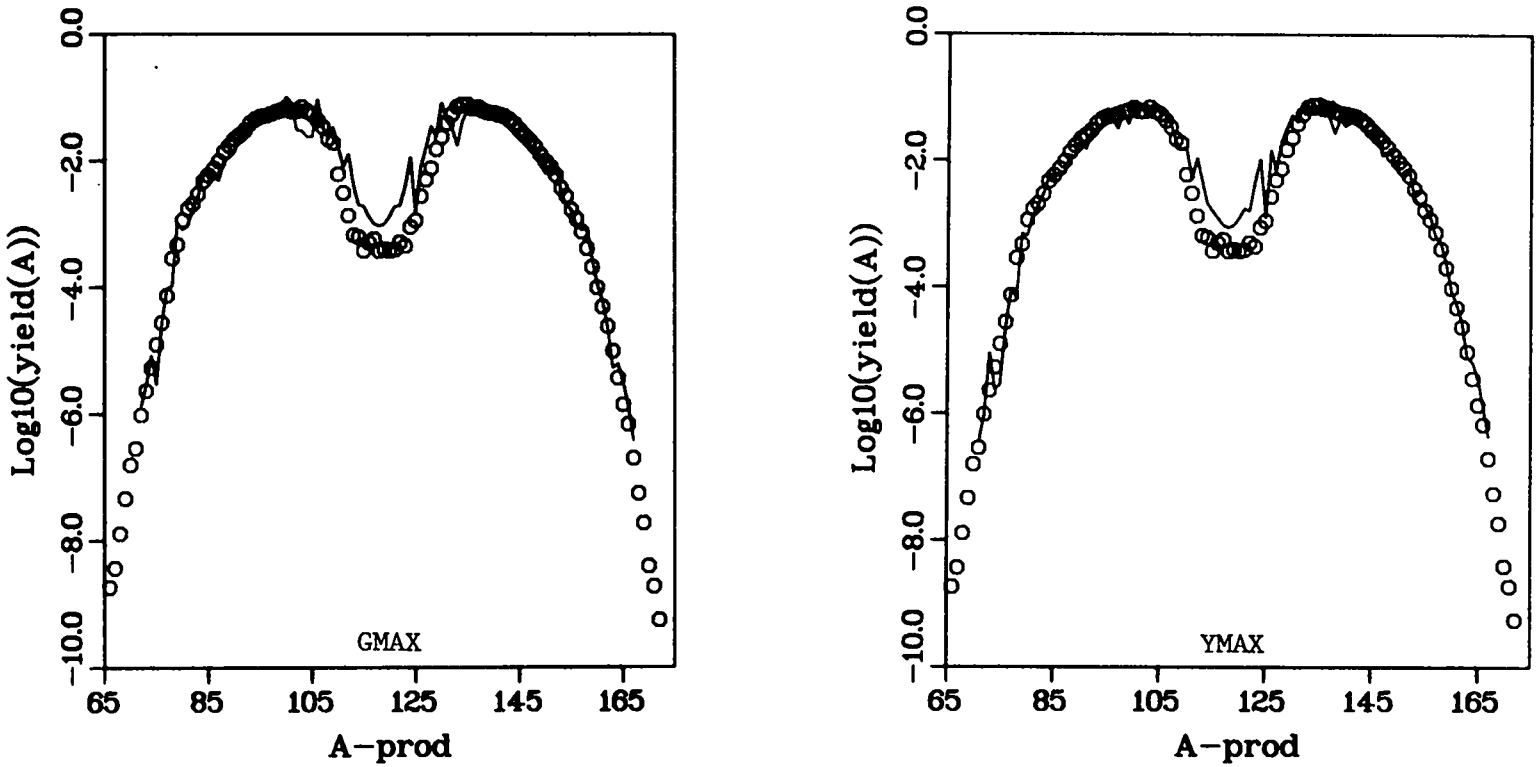

Figure 35: Fission product yields for $^{239}Pu(n_{th},f)$ assuming $\delta(Z)$ as in Figure 32 and a simple cascade neutron treatment. Circles are measured yields from Reference 8.

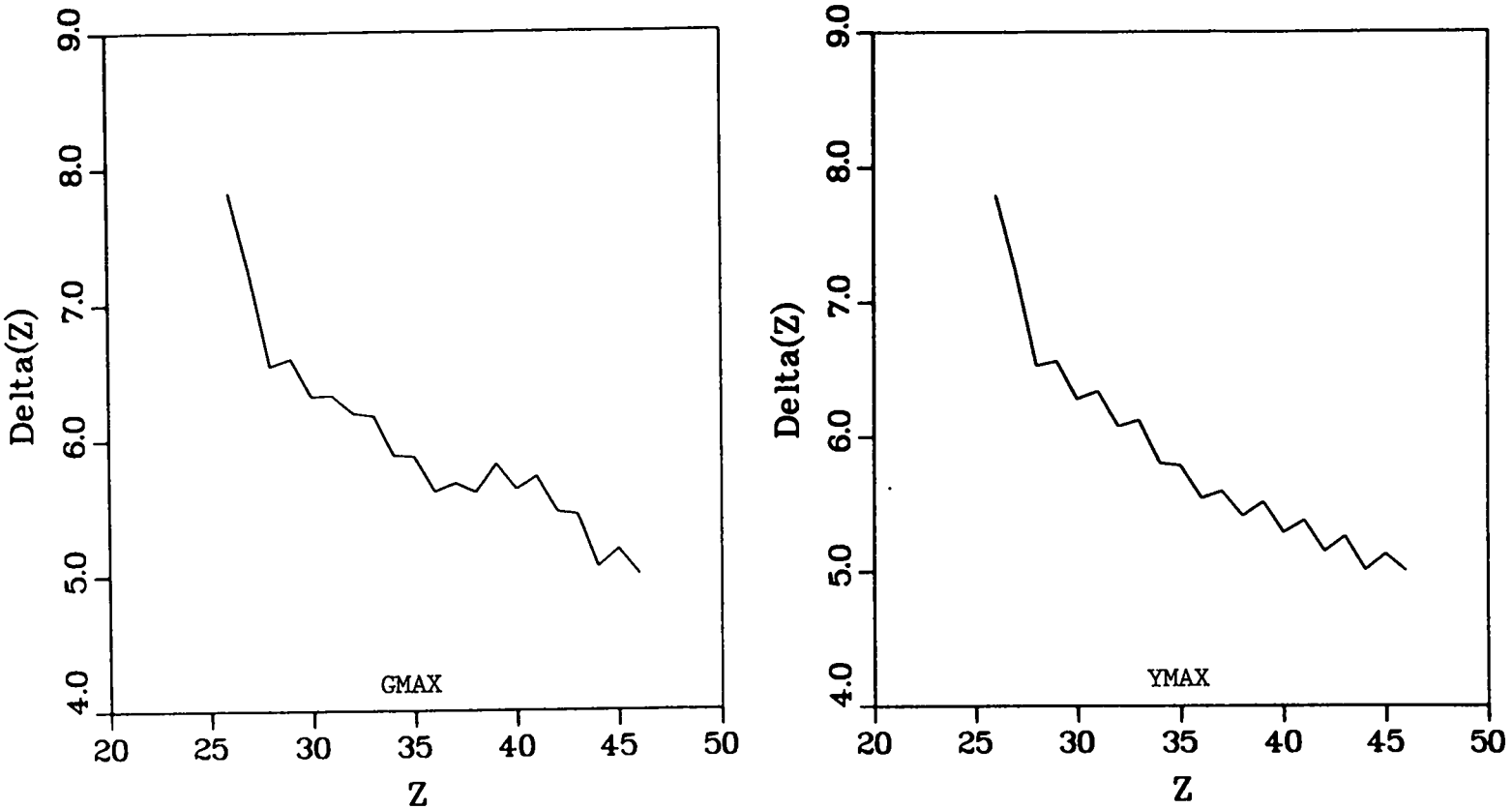

Figure 36: Spacing parameter, $\delta(Z)$, for $^{235}U(n+14,f)$ assuming $\delta(Z=46)$ = 5 fm. and constraining 25.0 MeV to remain in k_o.

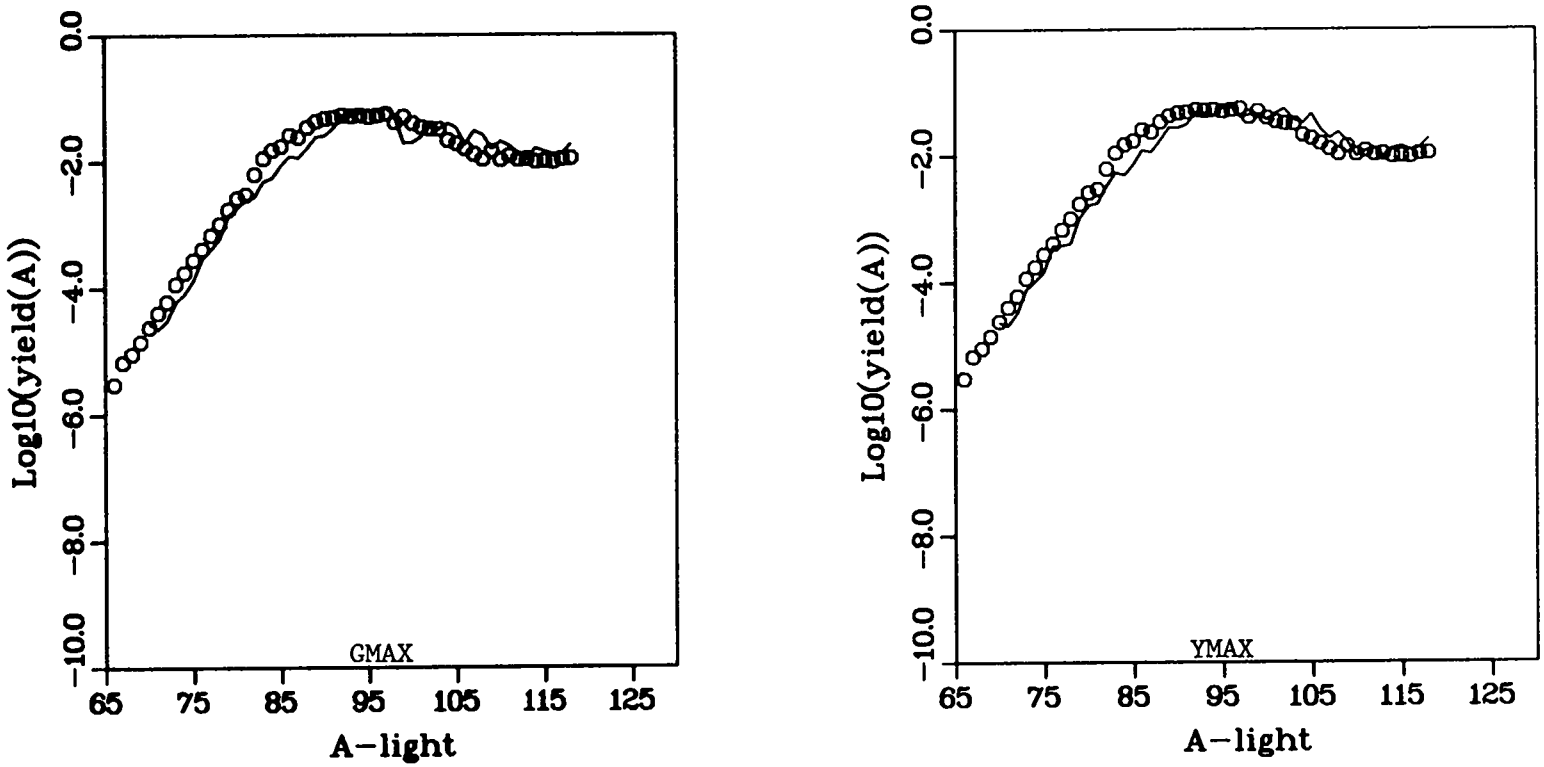

Figure 37: Fission fragment yields for $^{235}U(n+14,f)$ assuming $\delta(Z)$ as in Figure 36. Circles are fission product yields from Reference 8, shown here for comparison.

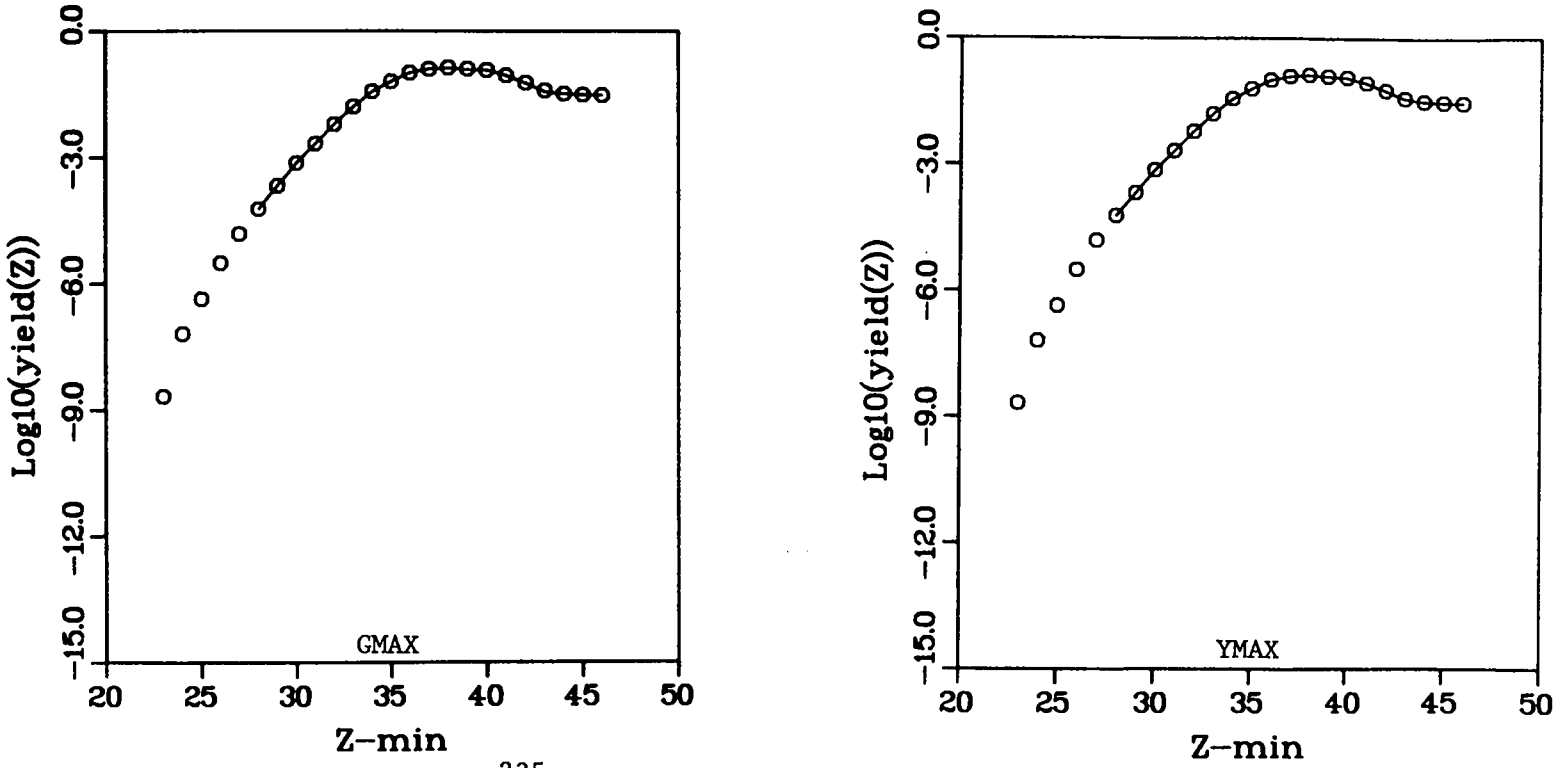

Figure 38: Charge yields for $^{235}U(n+14,f)$ assuming $\delta(Z)$ as in Figure 36. Circles are measured yields from Reference 8.

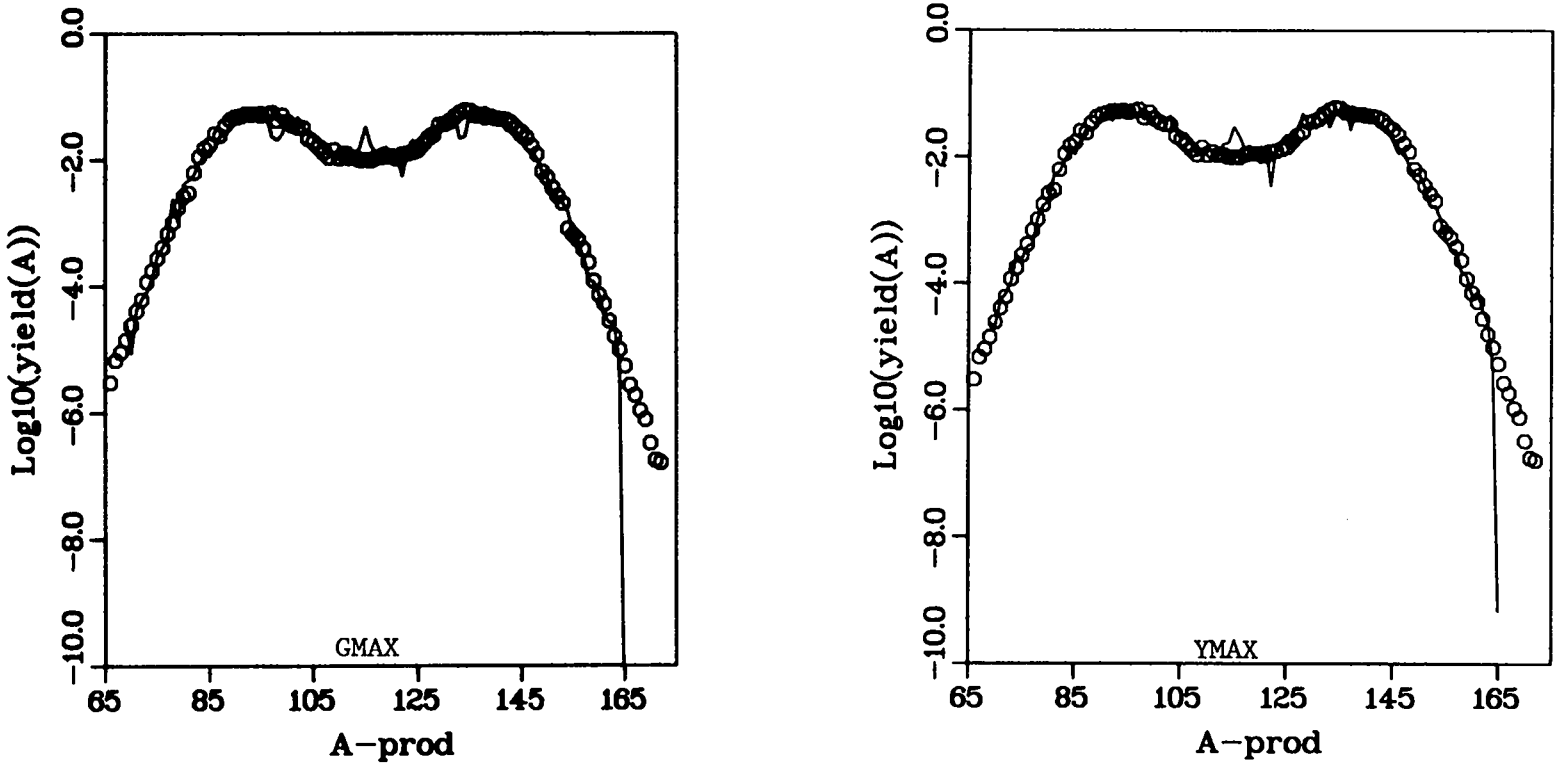

Figure 39: Fission product yields for $^{235}U(n+14,f)$ assuming $\delta(Z)$ as in Figure 36 and a simple cascade neutron treatment. Circles are measured yields from Reference 8.

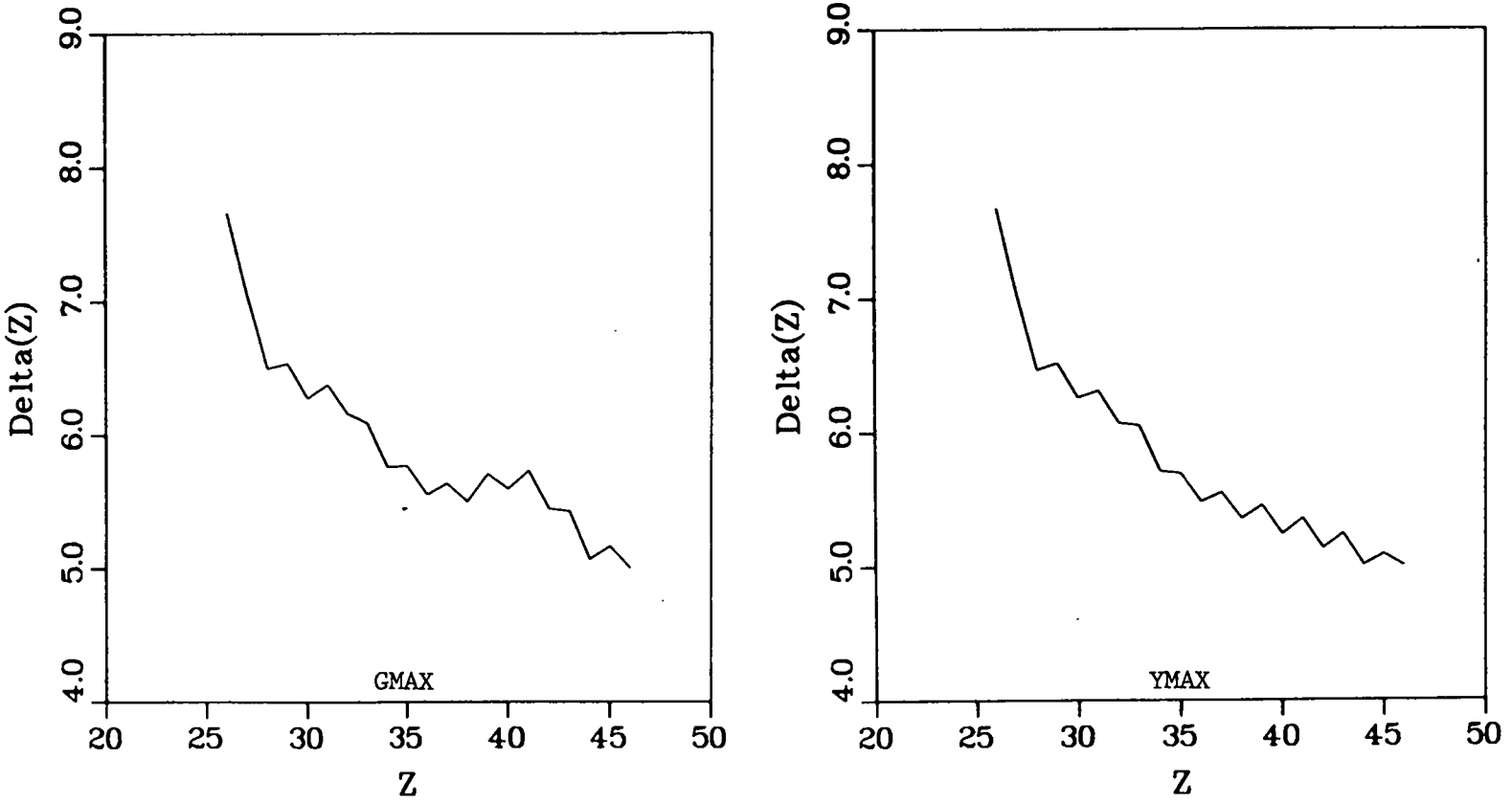

Figure 40: Spacing parameter, $\delta(Z)$, for $^{238}U(n+14,f)$ assuming $\delta(Z=46)$ = 5 fm. and constraining 25.2 MeV to remain in k_o.

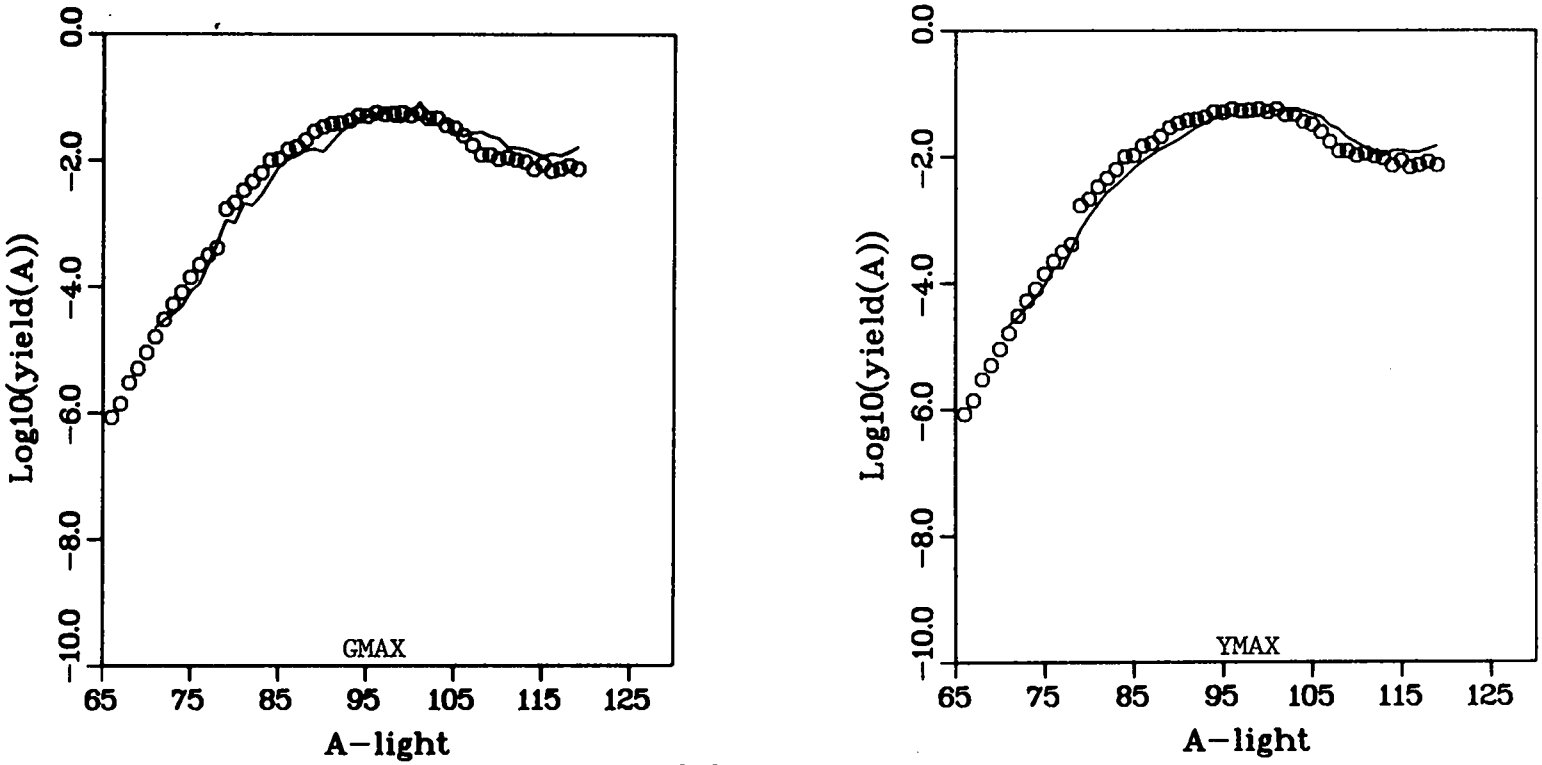

Figure 41: Fission fragment yields for $^{238}U(n+14,f)$ assuming $\delta(Z)$ as in Figure 40. Circles are fission product yields from Reference 8, shown here for comparison.

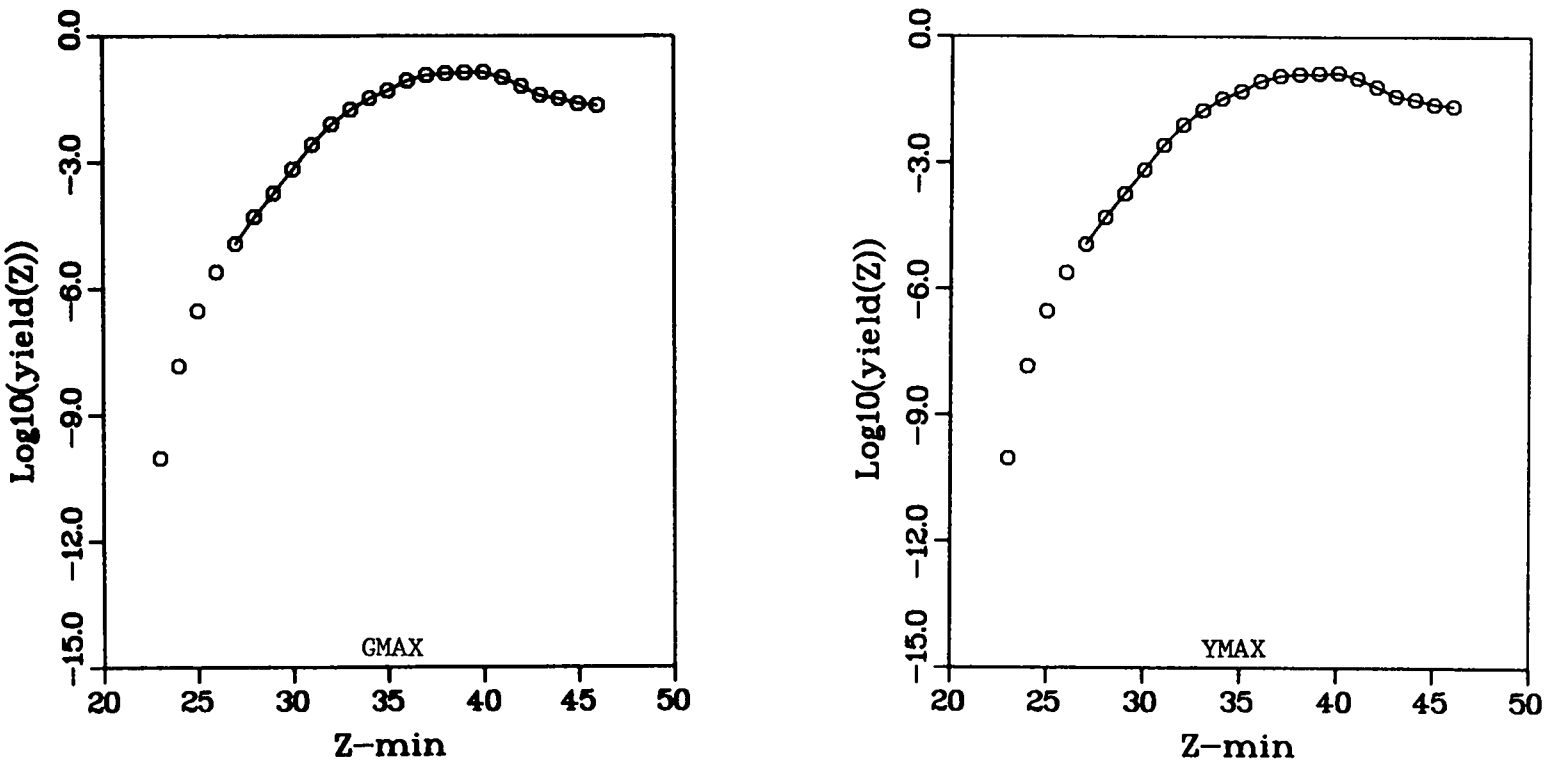

Figure 42: Charge yields for $^{238}U(n+14,f)$ assuming $\delta(Z)$ as in Figure 40. Circles are measured yields from Reference 8.

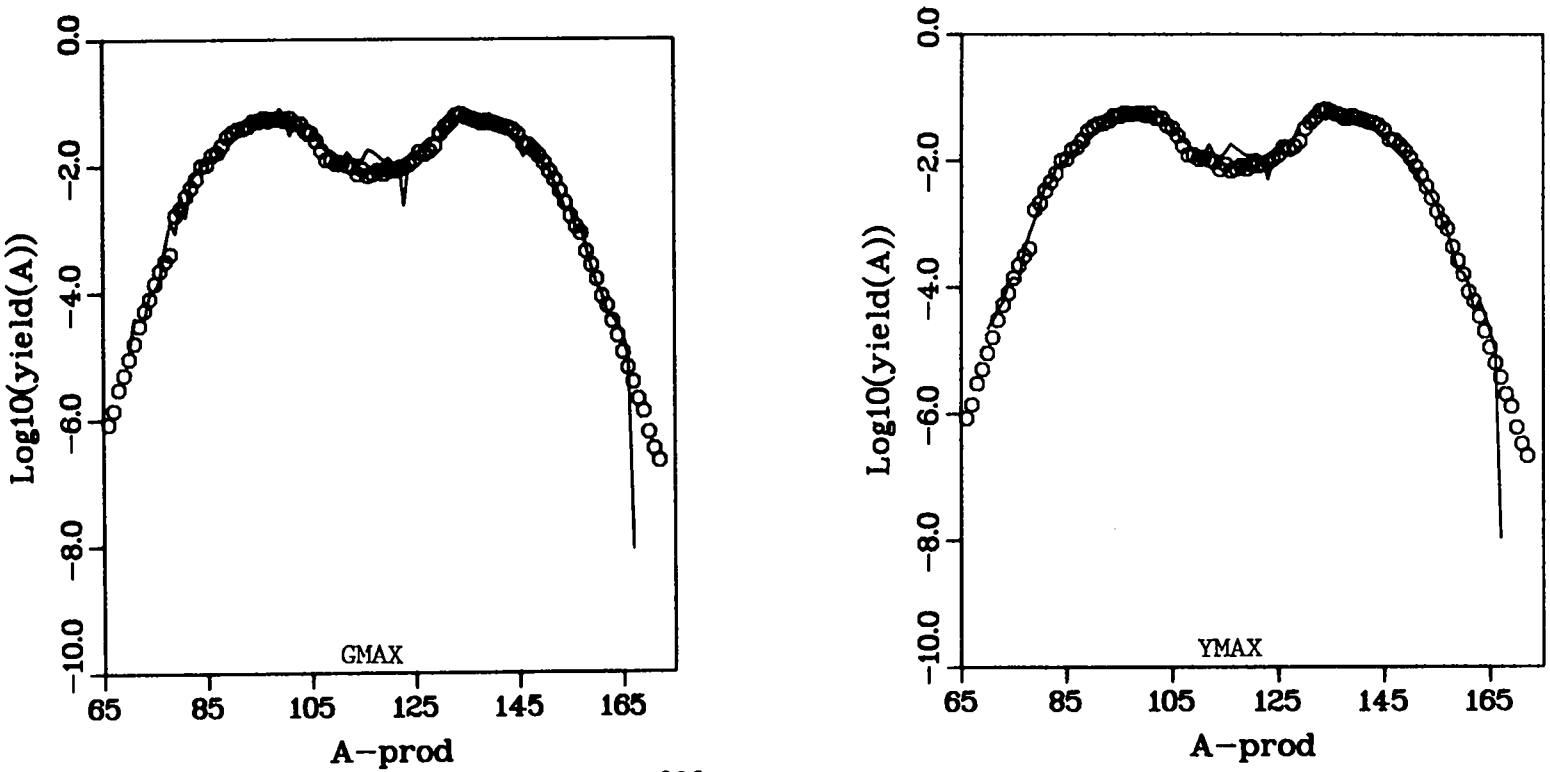

Figure 43: Fission product yields for $^{238}U(n+14,f)$ assuming $\delta(Z)$ as in Figure 40 and a simple cascade neutron treatment. Circles are measured yields from Reference 8.

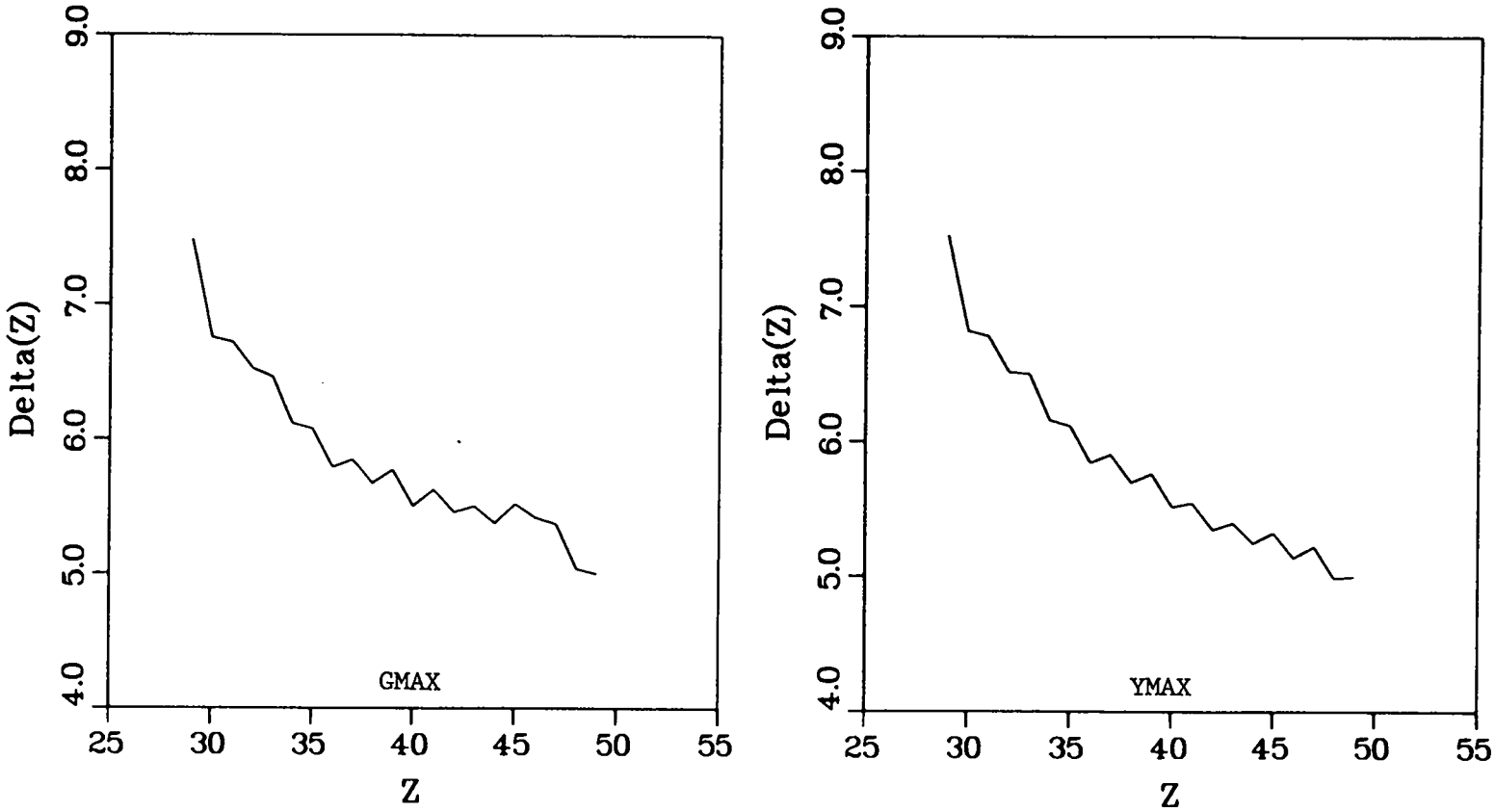

Figure 44: Spacing parameter, $\delta(Z)$, for $^{252}Cf(sf)$ assuming $\delta(Z=49) = 5$ fm. and constraining 27.0 MeV to remain in k_o.

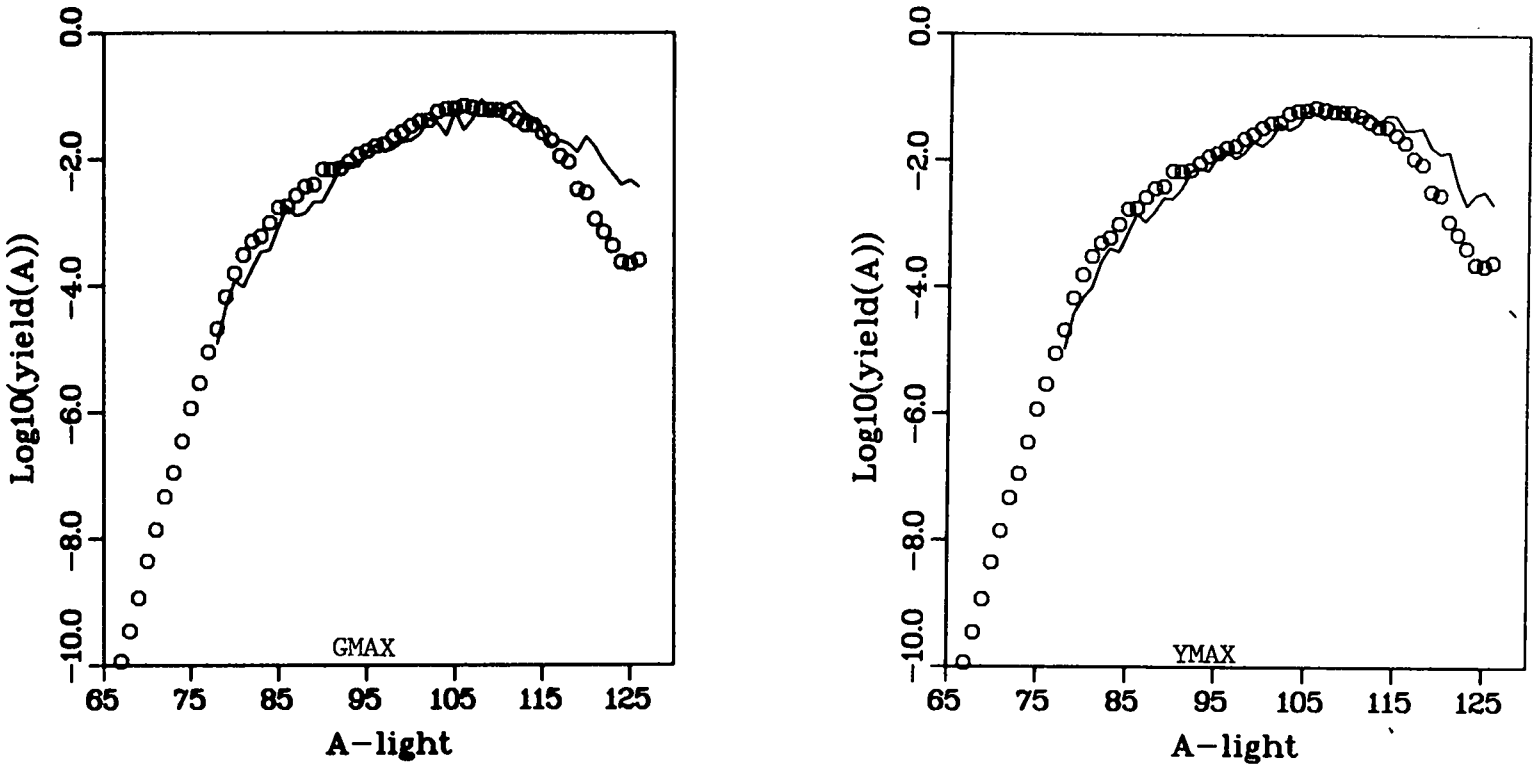

Figure 45: Fission fragment yields for ^{252}Cf(sf) assuming $\delta(Z)$ as in Figure 44. Circles are fission product yields from Reference 8, shown here for comparison.

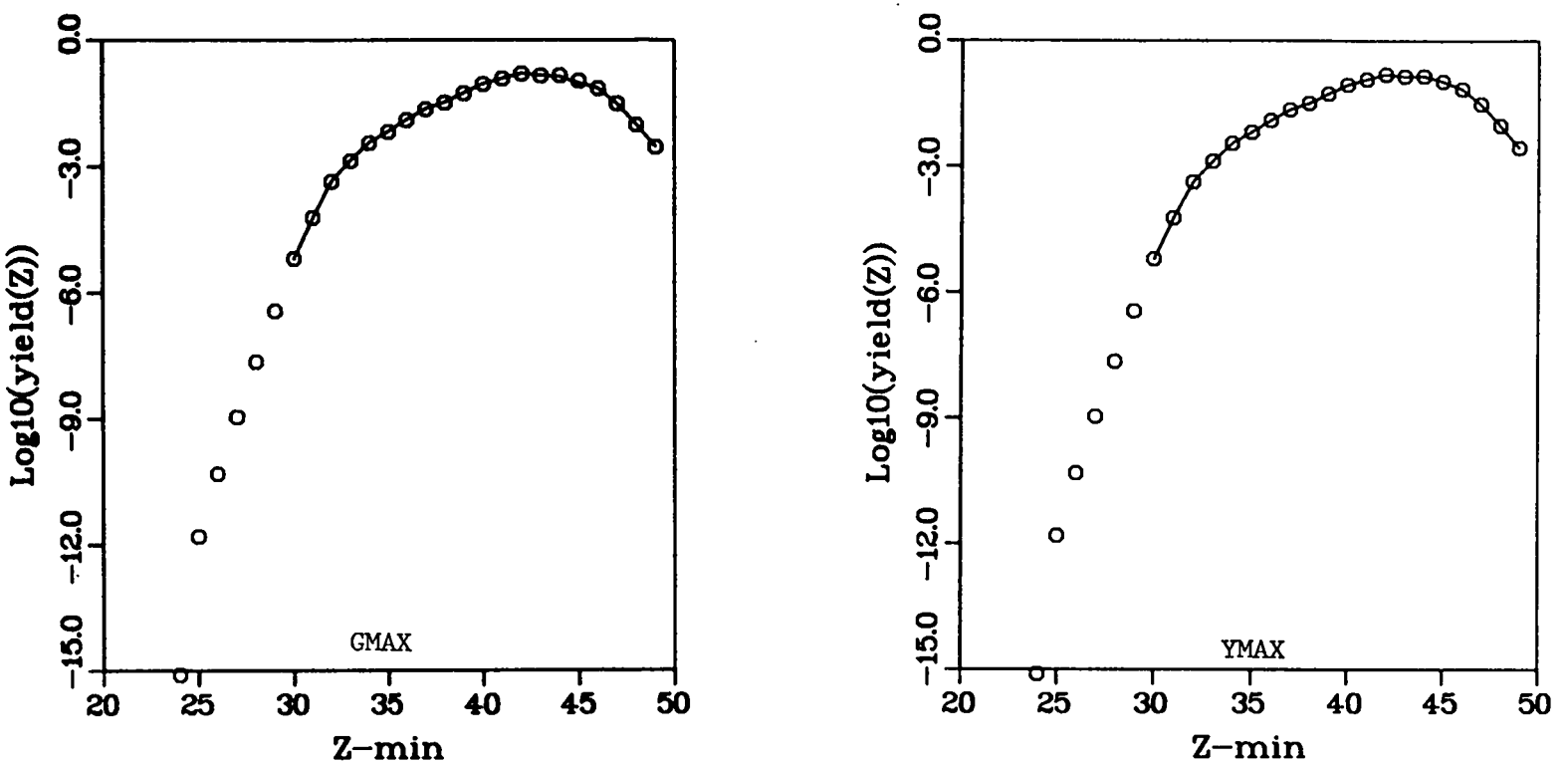

Figure 46: Charge yields for ^{252}Cf(sf) assuming $\delta(Z)$ as in Figure 44. Circles are measured yields from Reference 8.

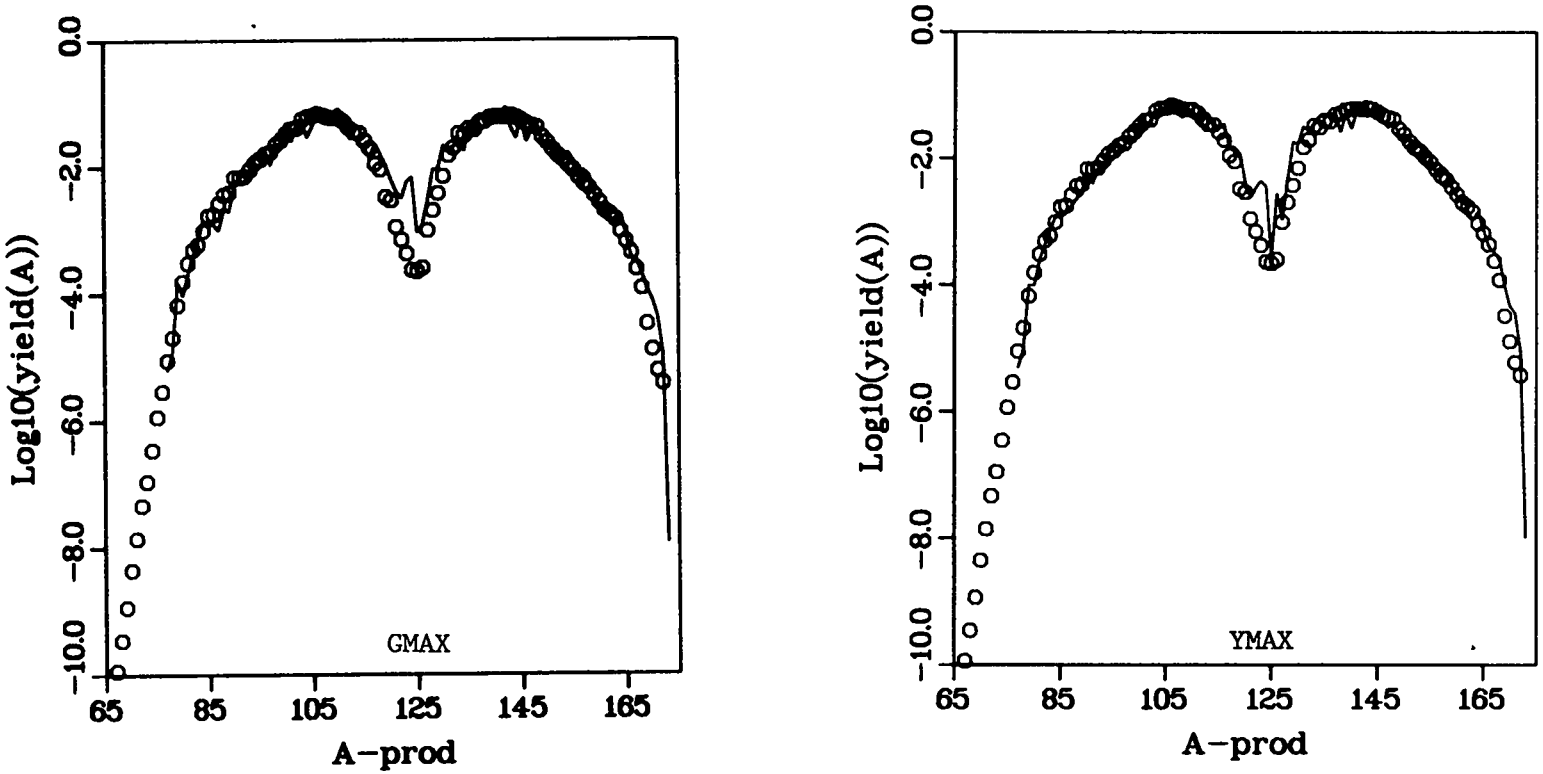

Figure 47: Fission product yields for $^{252}Cf(sf)$ assuming $\delta(Z)$ as in Figure 44 and a simple cascade neutron treatment. Circles are measured yields from Reference 8.

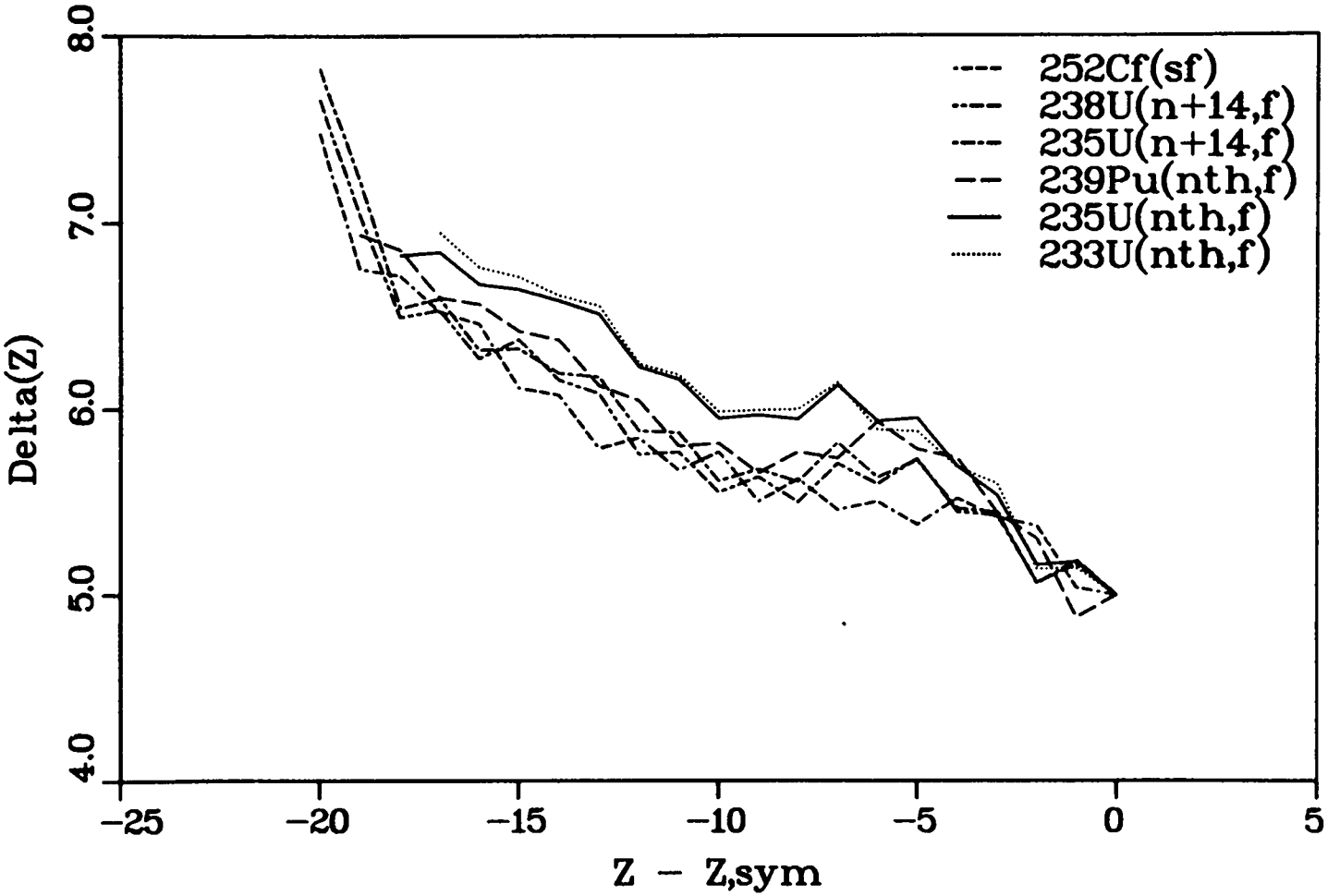

Figure 48: GMAX $\delta(Z)$ parameters for the six cases considered, in fm.

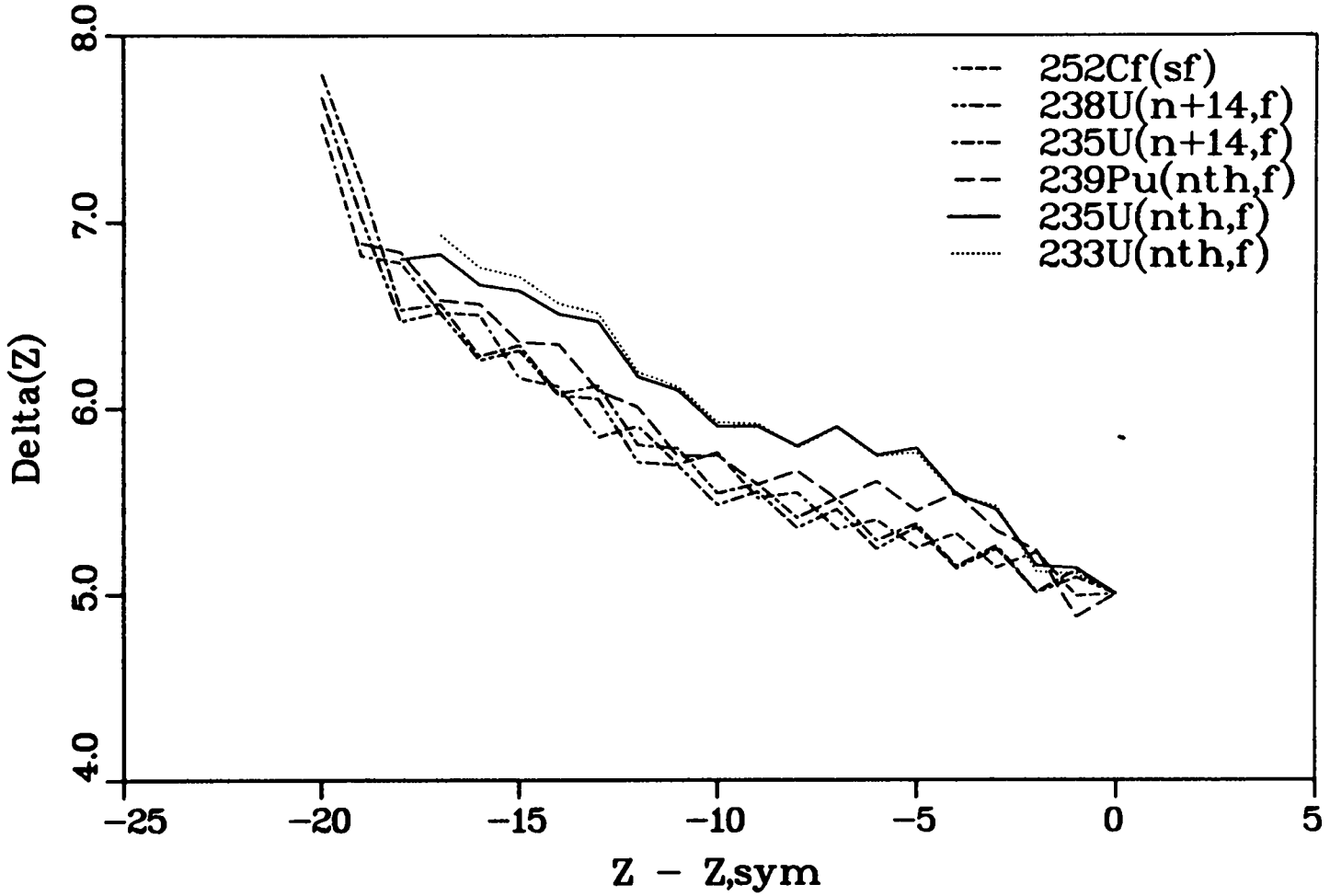

Figure 49: YMAX $\delta(Z)$ parameters for the six cases considered, in fm.

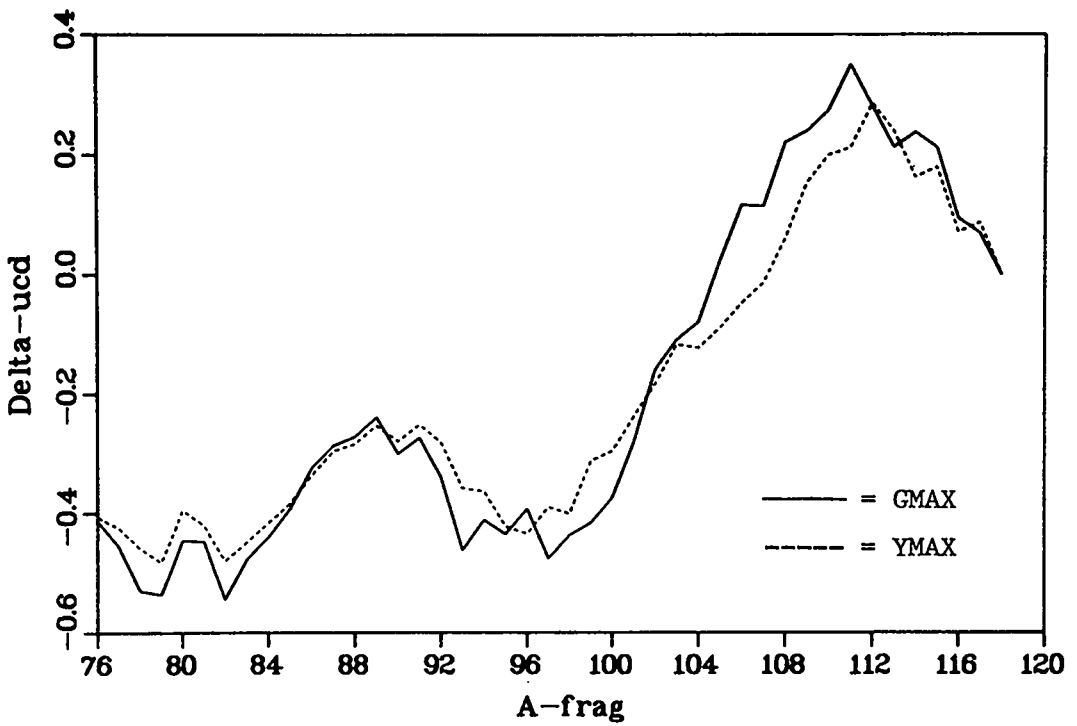

Figure 50: Deviation of computed fragment Z_p values from that predicted by UCD for $^{235}U(n_{th},f)$ assuming the $\delta(Z)$ parameters of Table 5. The quantity plotted is $Z_{ucd} - Z_p$.

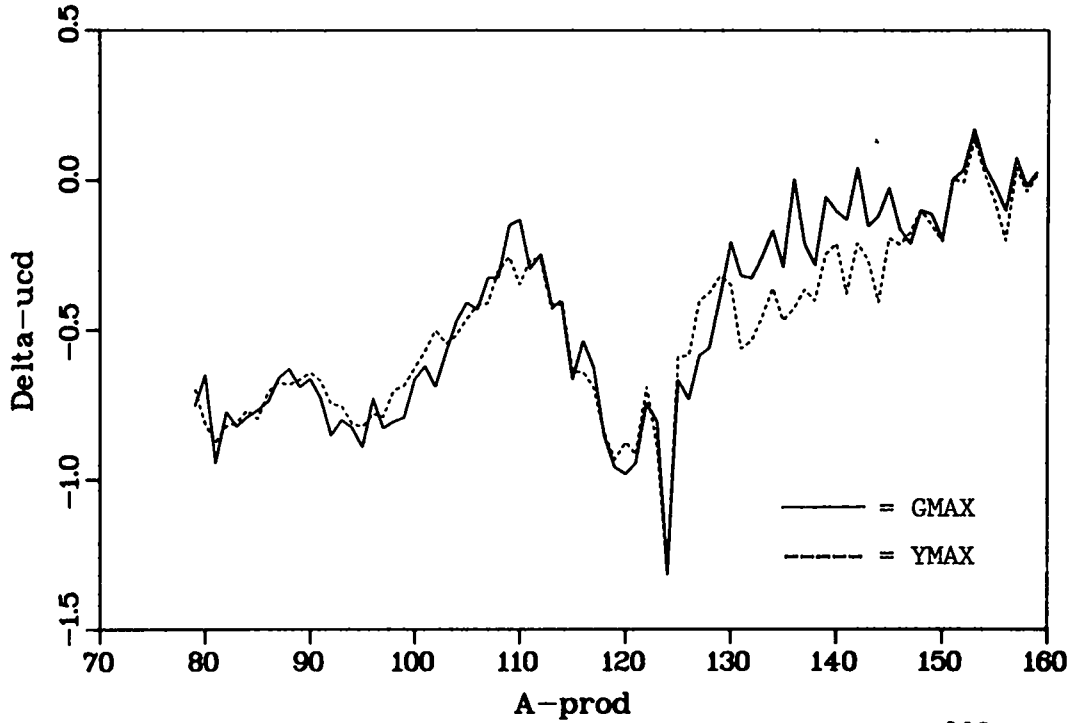

Figure 51: Deviation of computed Z_p values from the UCD prediction for $^{235}U(n_{th},f)$ assuming the $\delta(Z)$ parameters of Table 5. Quantity plotted is $Z_{ucd} - Z_p$.

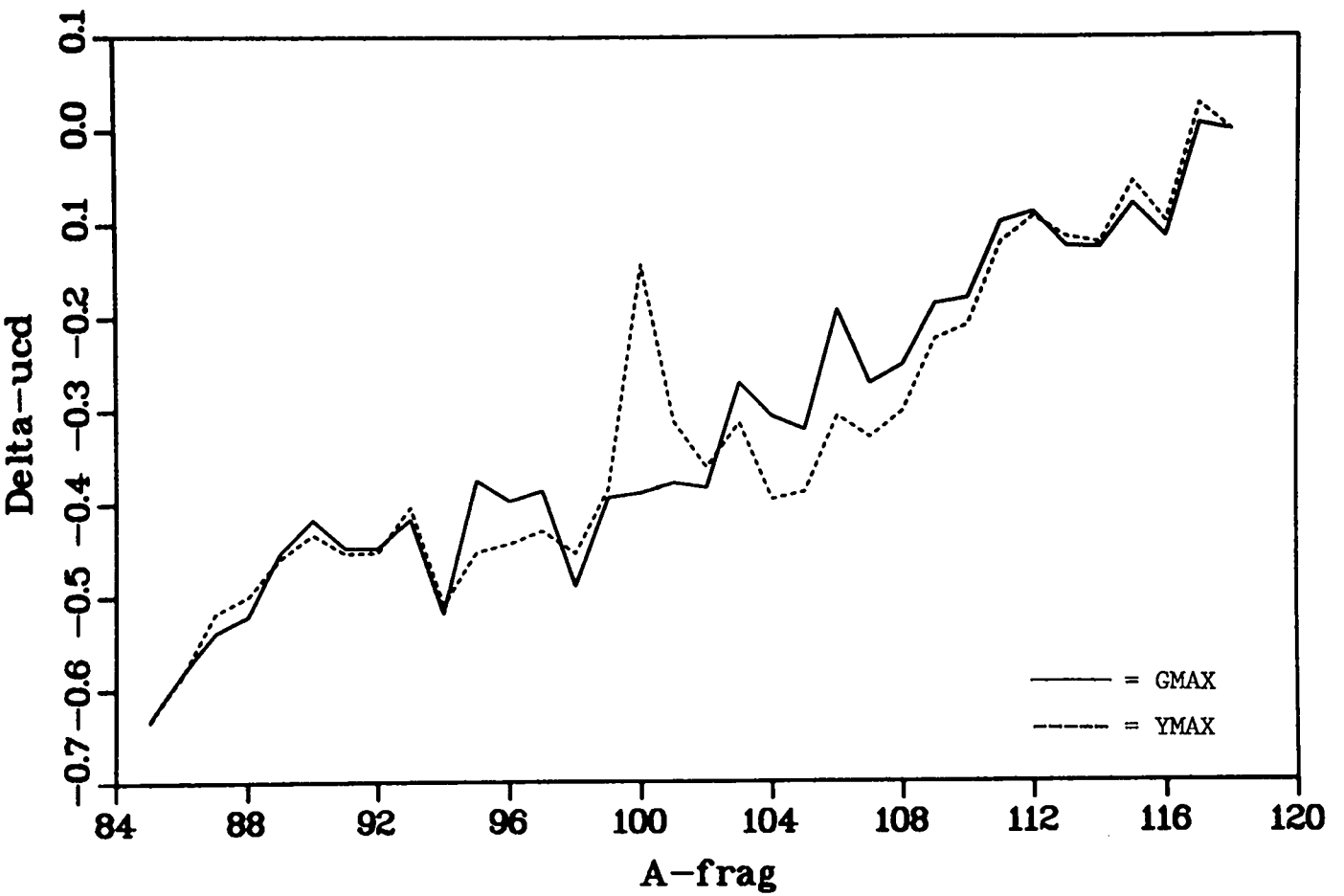

Figure 52: Deviation of fragment Z_p values from that predicted by UCD for $^{235}U(n_{th},f)$. Quantity plotted is $Z_{ucd} - Z_p$. This calculation assumes the spacing parameter constant, $\delta = 5$ fm.

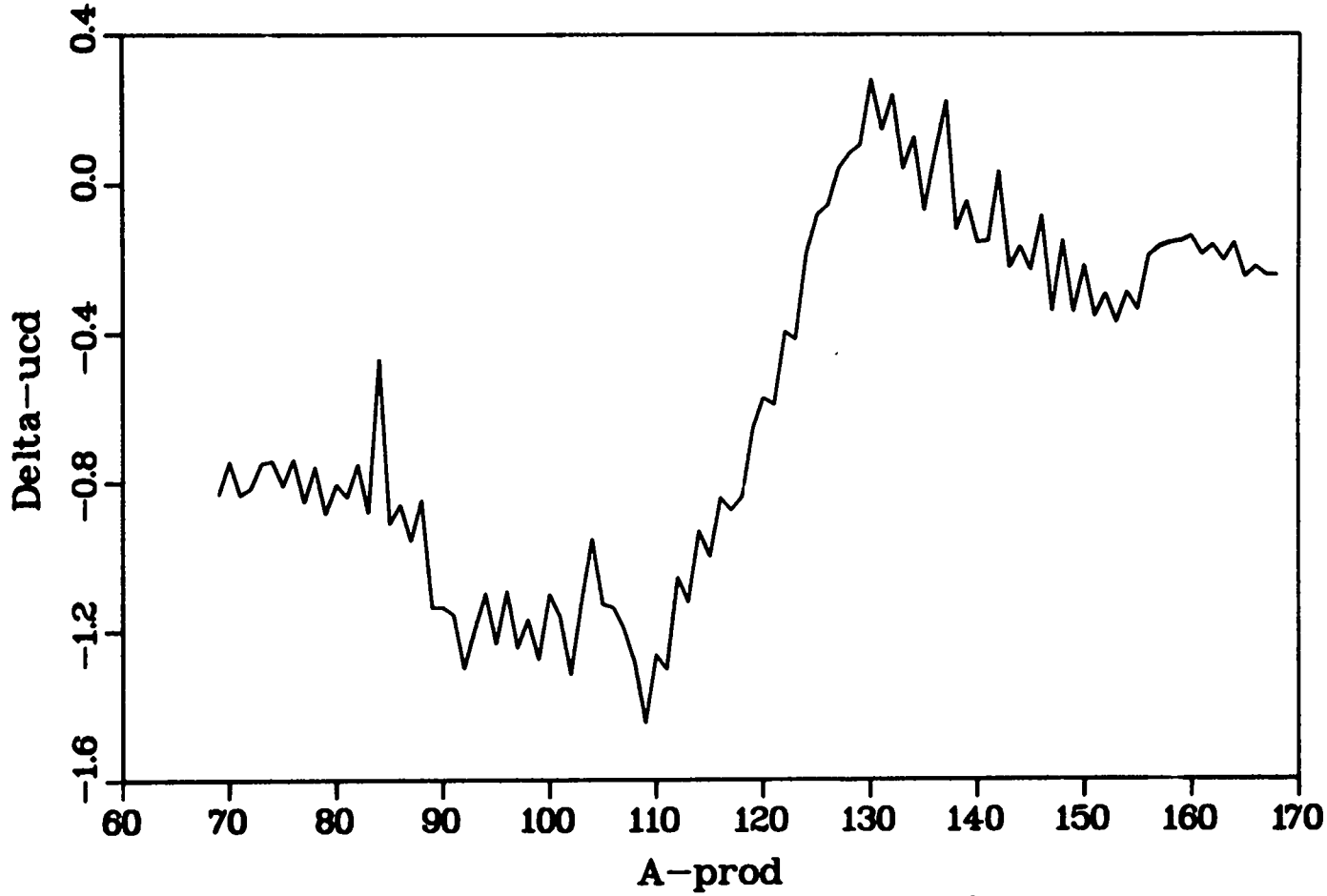

Figure 53: Deviation from UCD of yield data of Reference 8 for $^{235}U(n_{th},f)$. The quantity plotted is $Z_{ucd} - Z_p$.

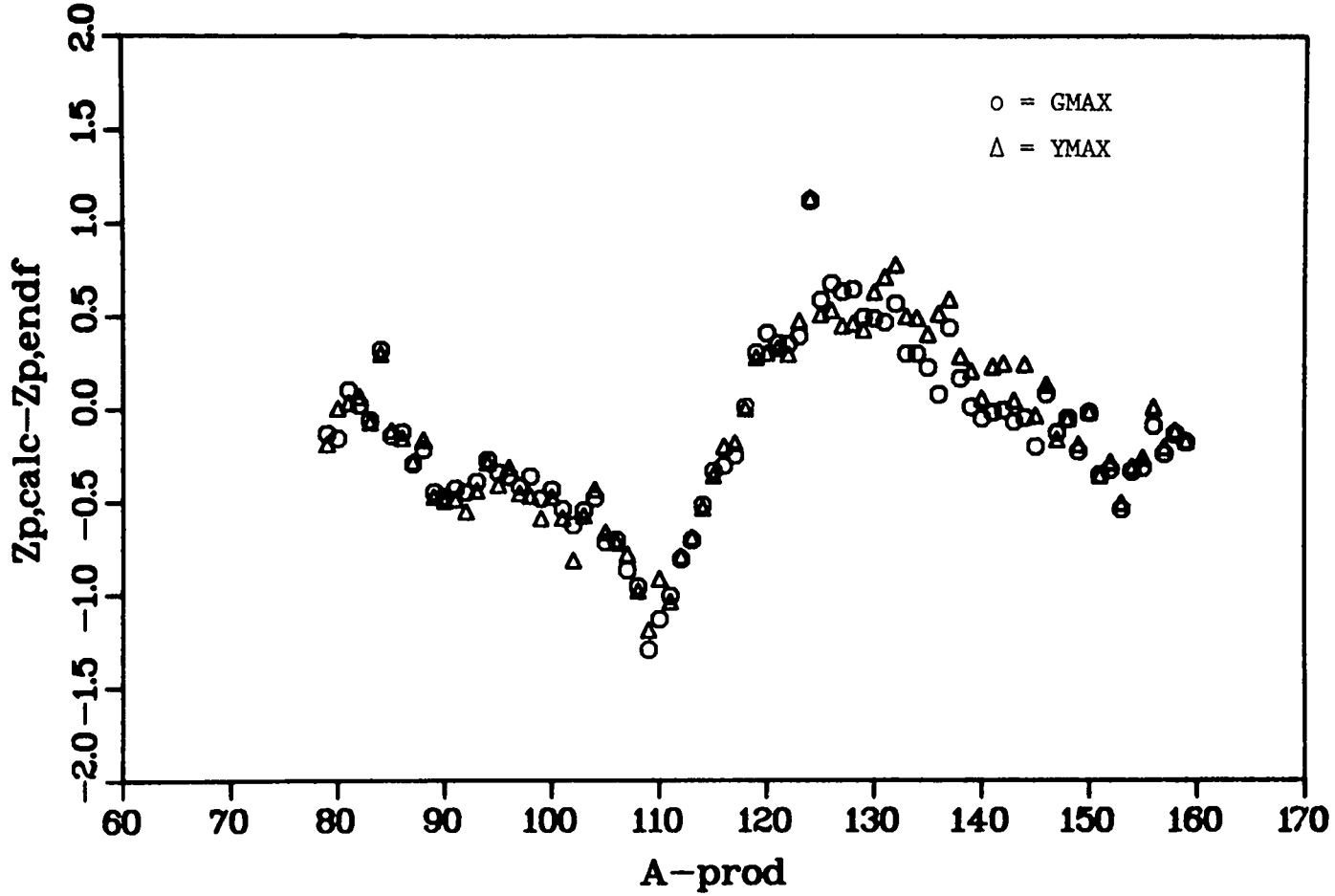

Figure 54: Deviation of Z_p values of data from Reference 8 from those computed assuming $\delta(Z)$ as given in Table 5 for the reaction $^{235}U(n_{th},f)$.

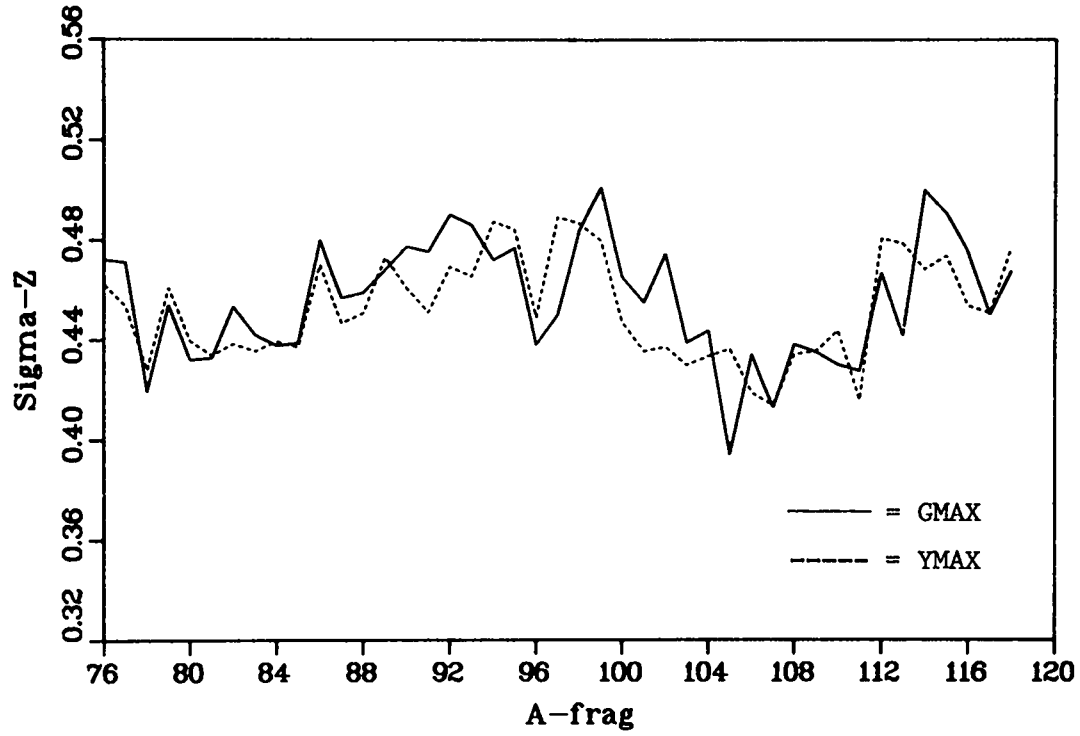

Figure 55: Gaussian width parameter, σ_z, for the fission fragment yields for $^{235}U(n_{th},f)$ assuming the $\delta(Z)$ parameters of Table 5.

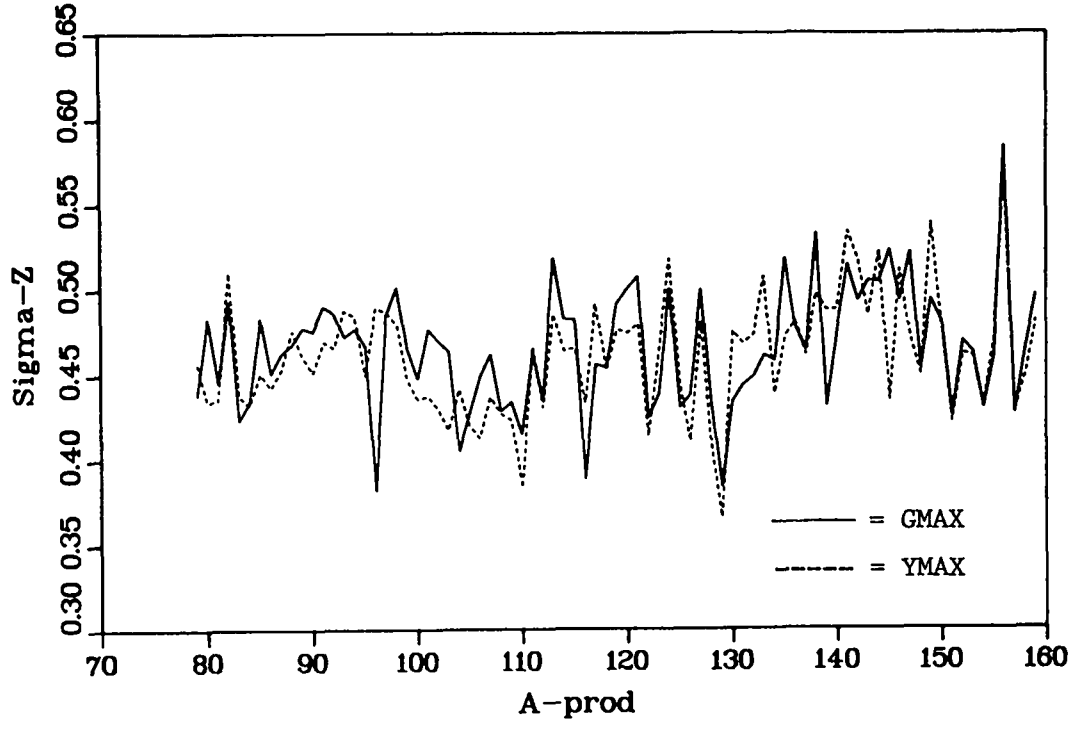

Figure 56: Gaussian width parameter, σ_z, for the reaction $^{235}U(n_{th},f)$ assuming the $\delta(Z)$ parameters of Table 5.

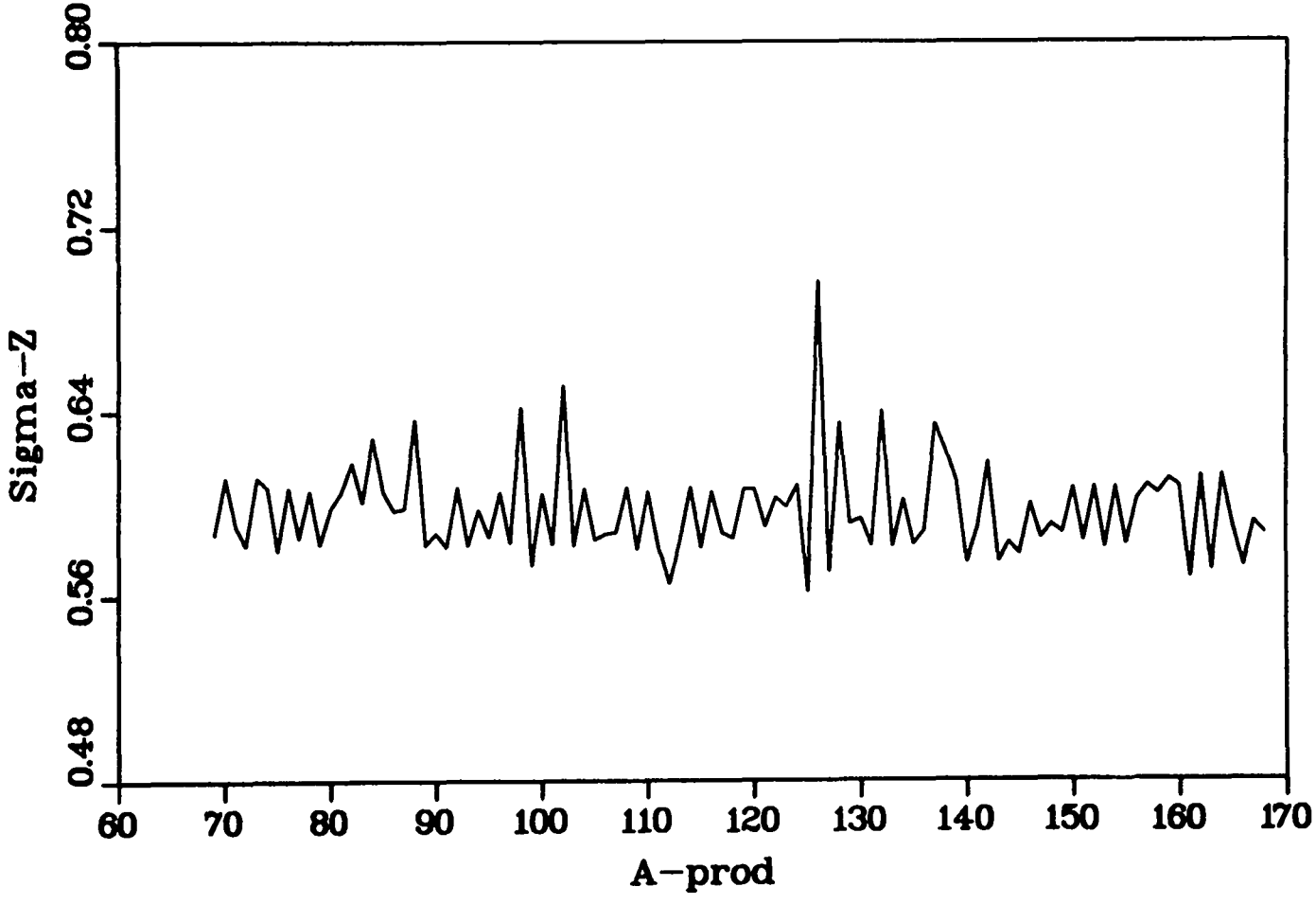

Figure 57: Gaussian width parameter, σ_z, for data from Reference 8 for $^{235}U(n_{th},f)$

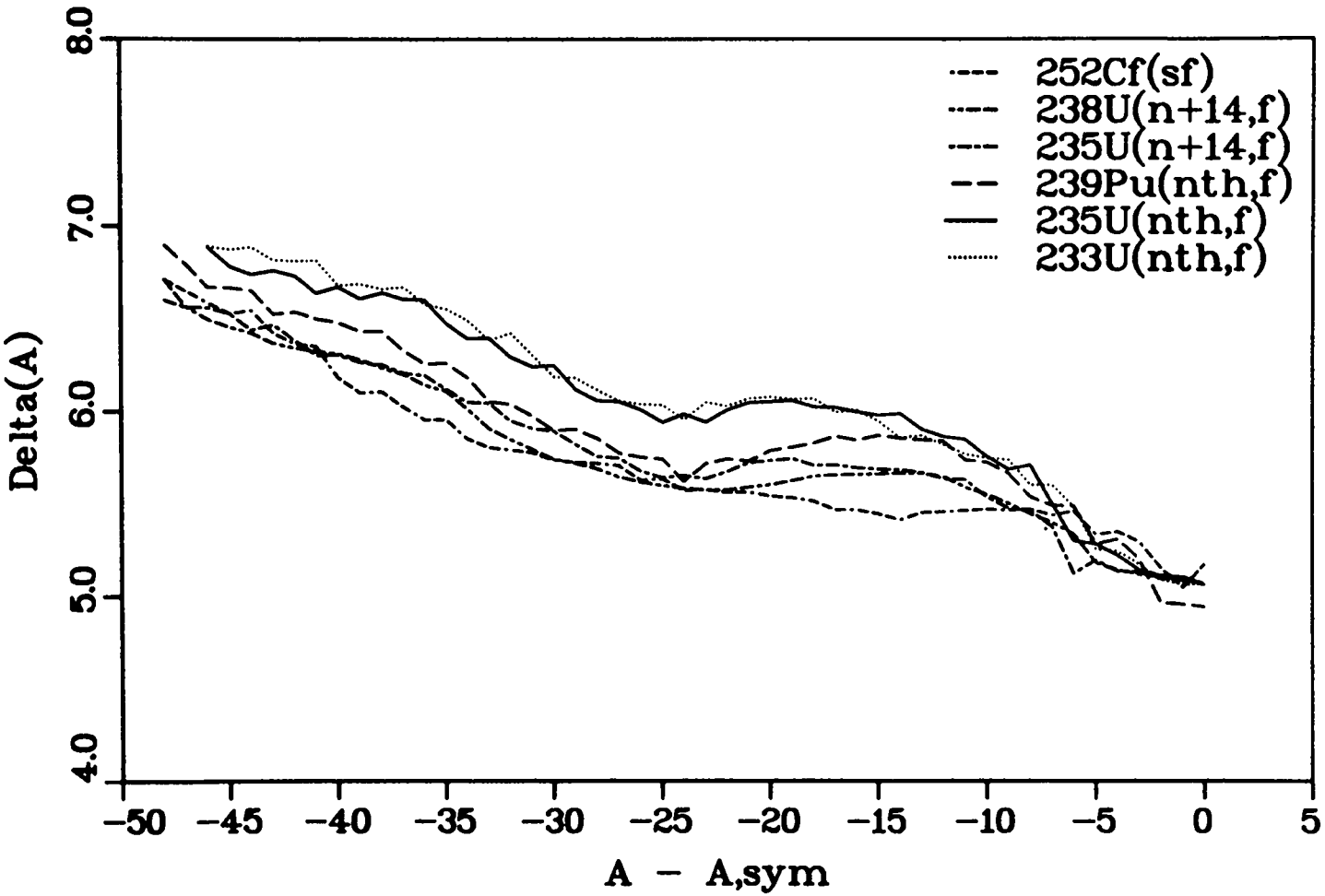

Figure 58: GMAX $\delta(A)$ parameters for the six cases considered, in fm.

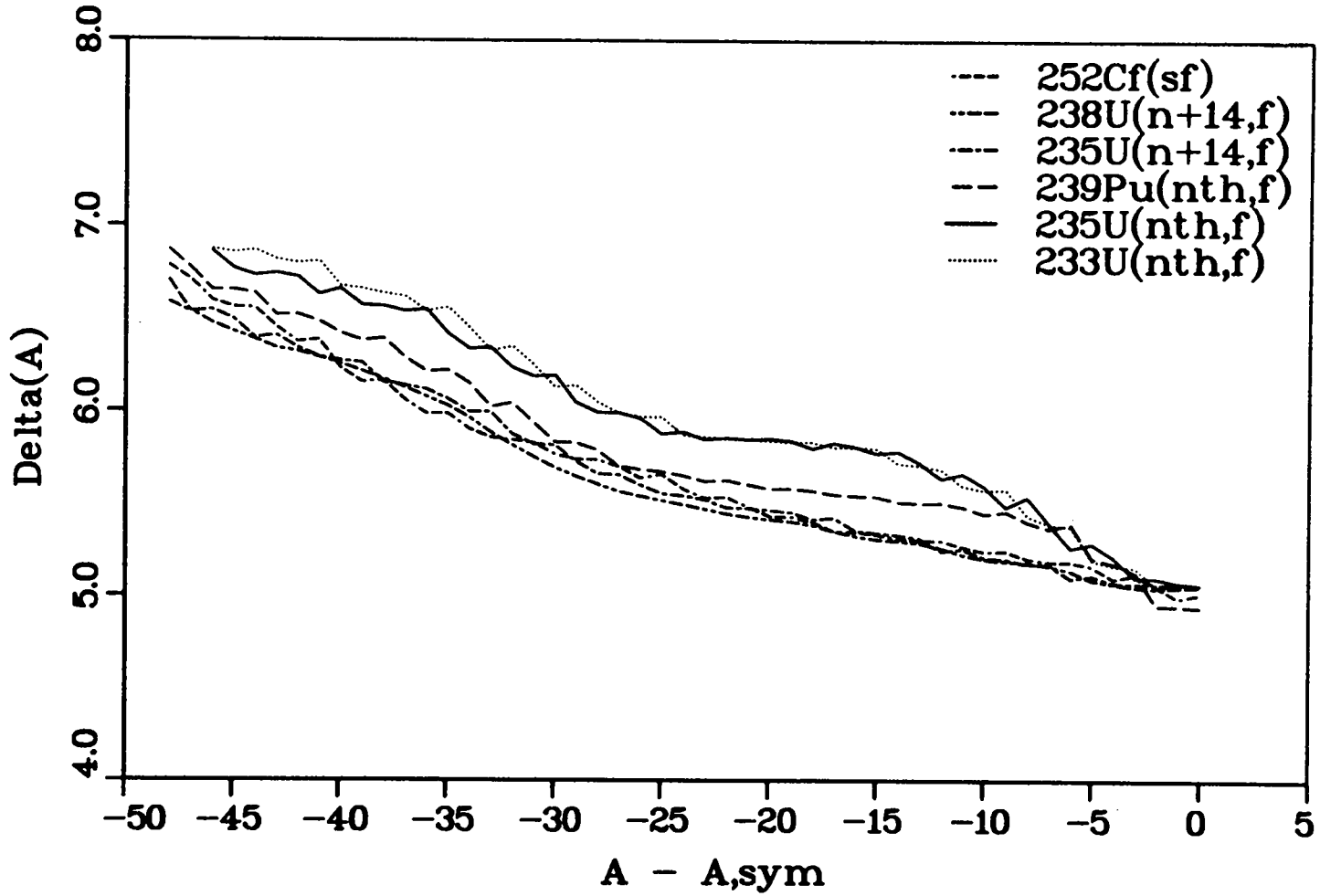

Figure 59: YMAX δ(A) parameters for the six cases considered, in fm.

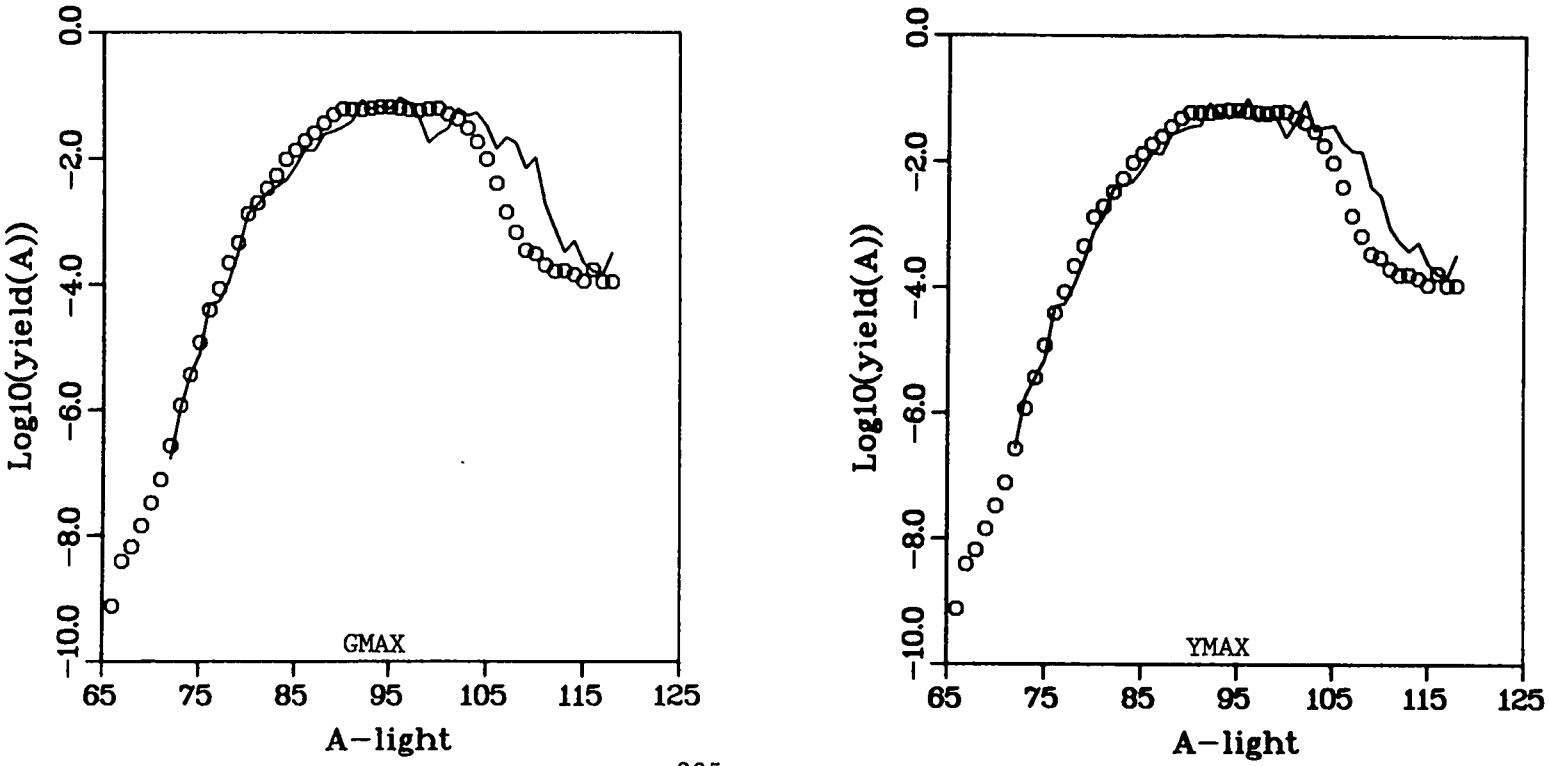

Figure 60: Fission fragment yields for $^{235}U(n_{th},f)$ assuming $\delta(A)$ parameters of Table 6. Circles are fission product yields from Reference 8, shown here for comparison. This calculation assumes 27.5 MeV constrained to remain in k_o

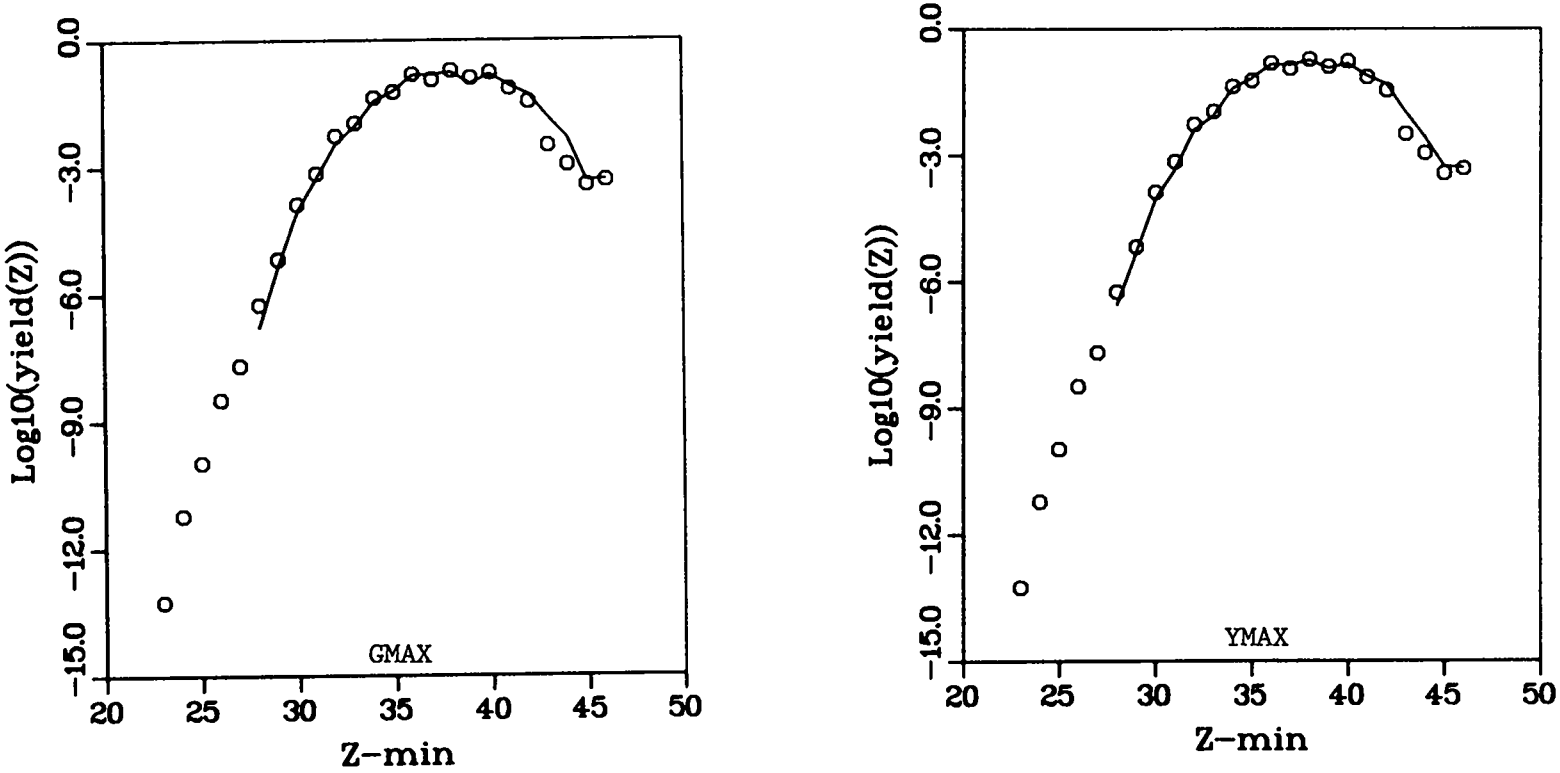

Figure 61: Charge yields for $^{235}U(n_{th},f)$ assuming $\delta(A)$ parameters of Table 6. Circles are measured yields from Reference 8. This calculation assumes 27.5 MeV constrained to remain in k_o.

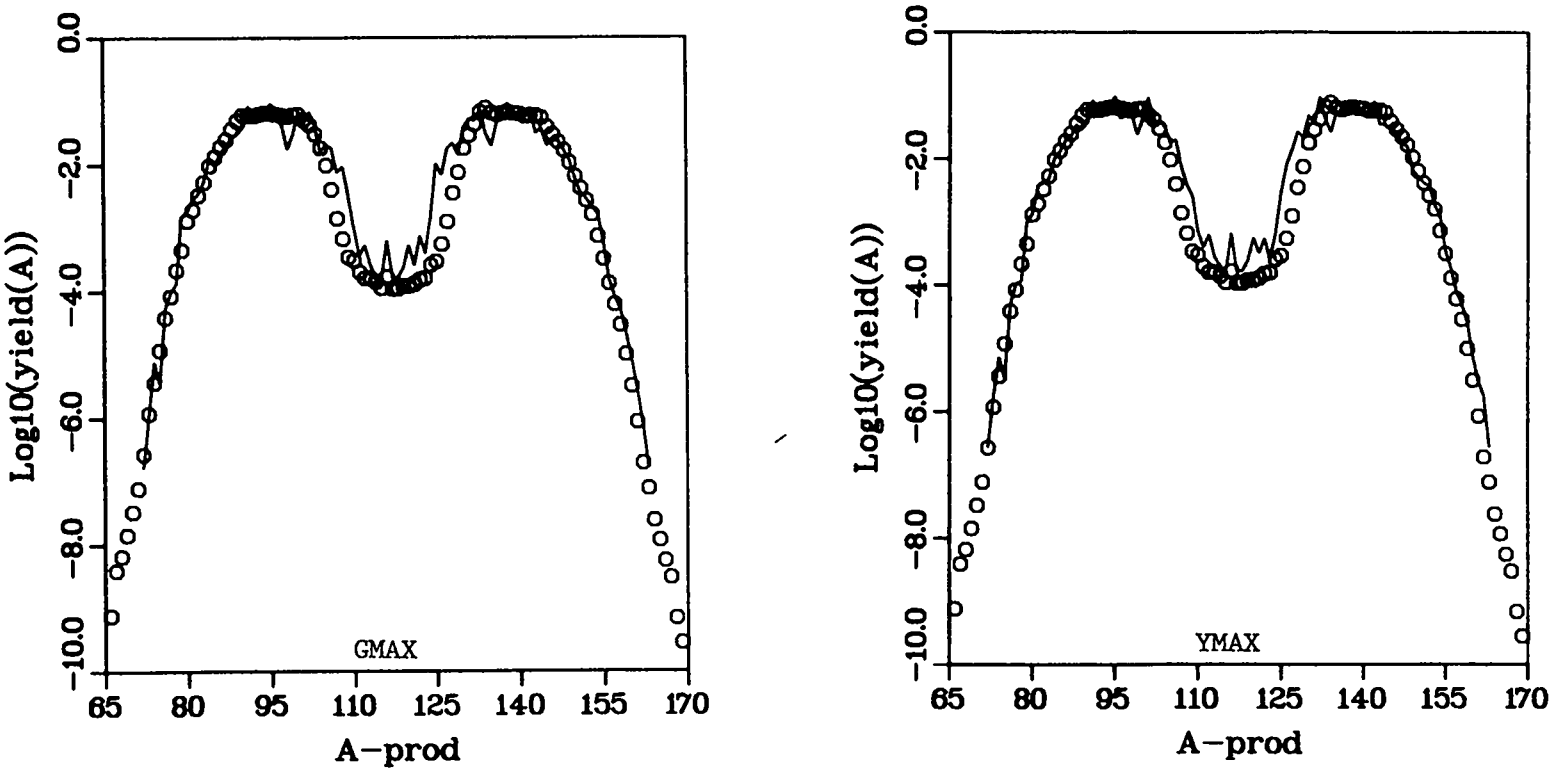

Figure 62: Fission product yields for $^{235}U(n_{th},f)$ assuming $\delta(A)$ parameters of Table 6 and a simple cascade neutron treatment. Circles are measured yields from Reference 8. This calcualtion assumes 27.5 MeV constrained to remain in k_o.

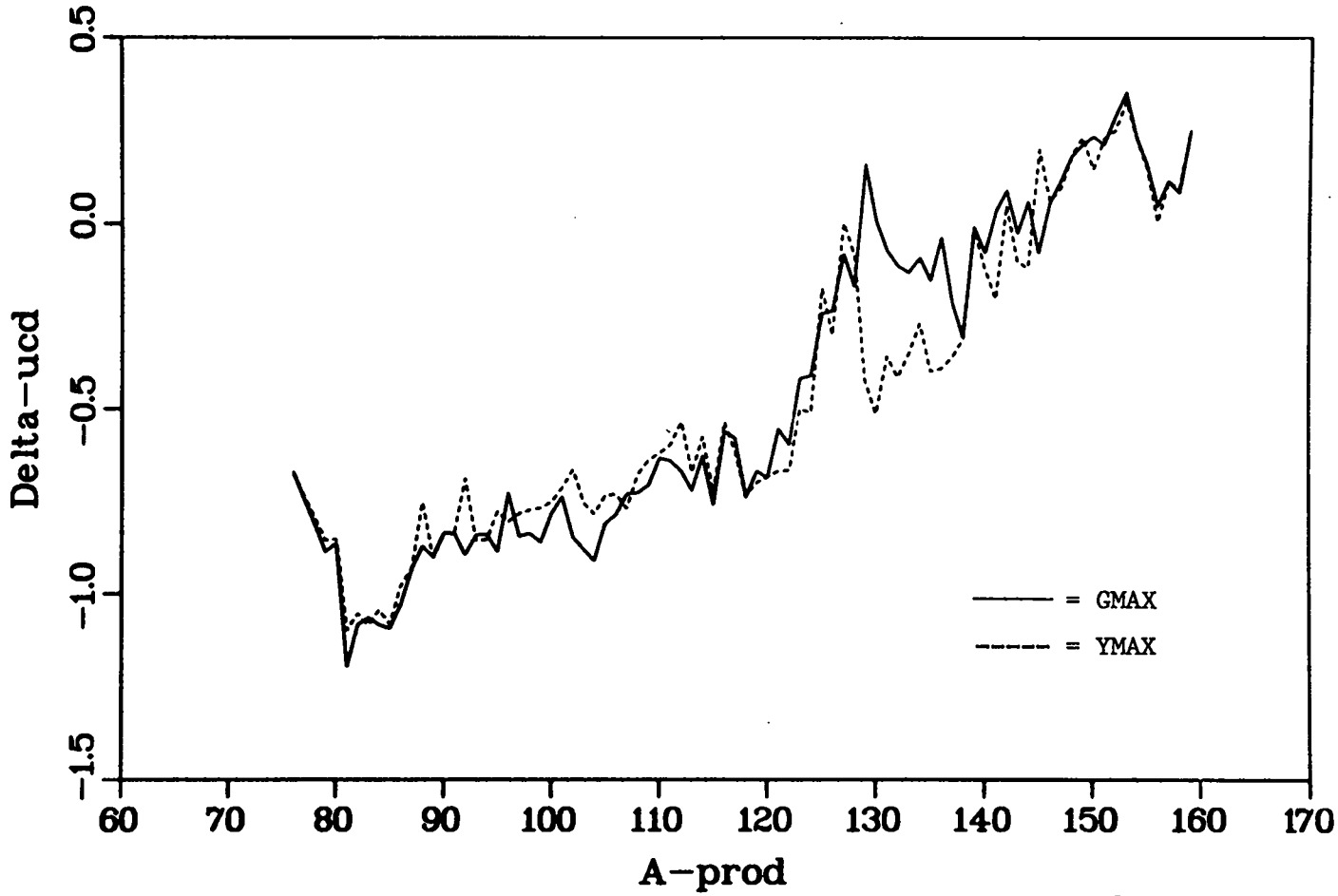

Figure 63: Deviation of computed Z_p values from the UCD prediction for $^{235}U(n_{th},f)$ assuming the $\delta(A)$ parameters of Table 6. Quantity plotted is $Z_{ucd} - Z_p$.

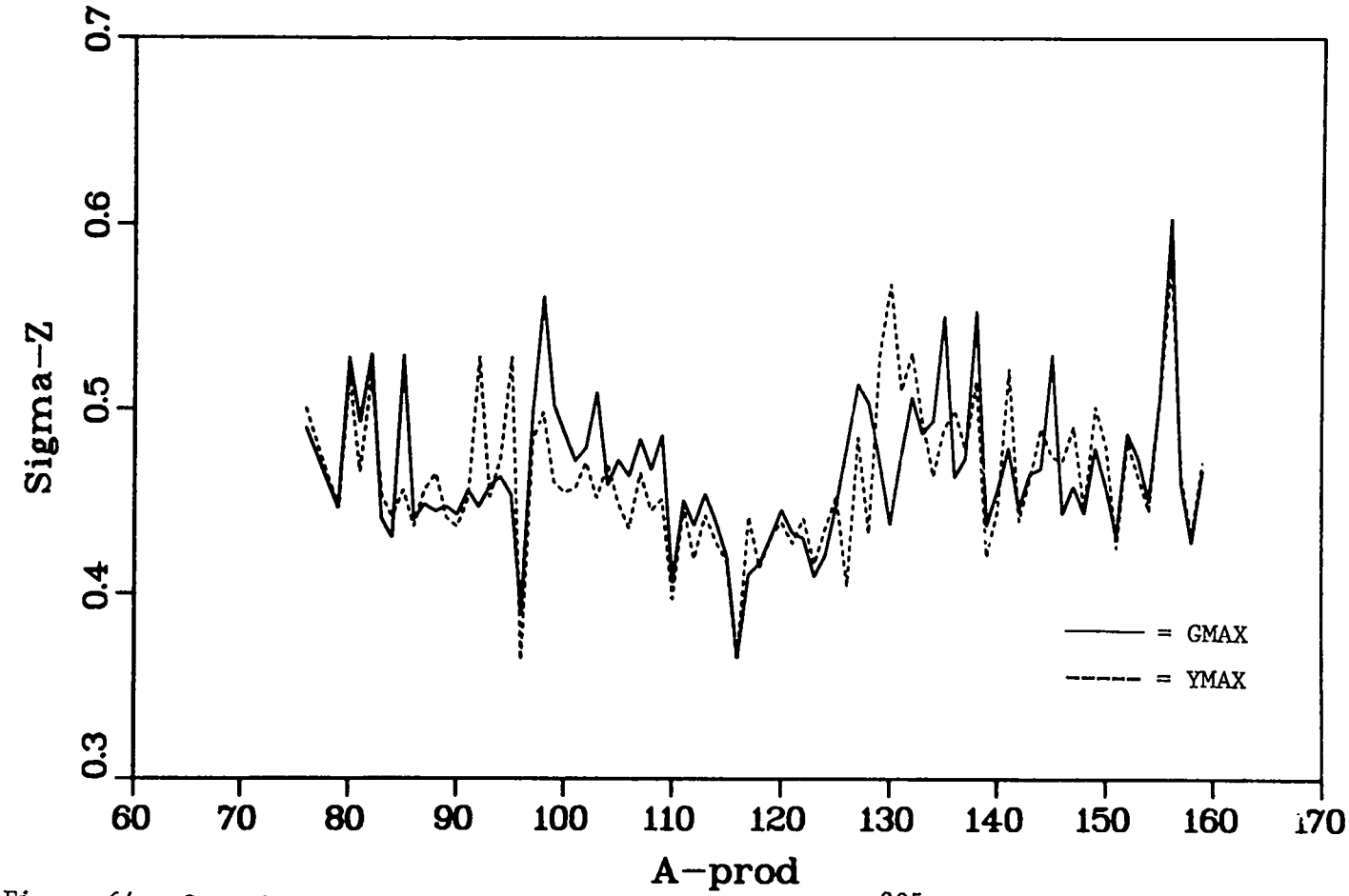

Figure 64: Gaussian width parameter, σ_z, for the reaction $^{235}U(n_{th},f)$ assuming the $\delta(A)$ parameters of Table 6.

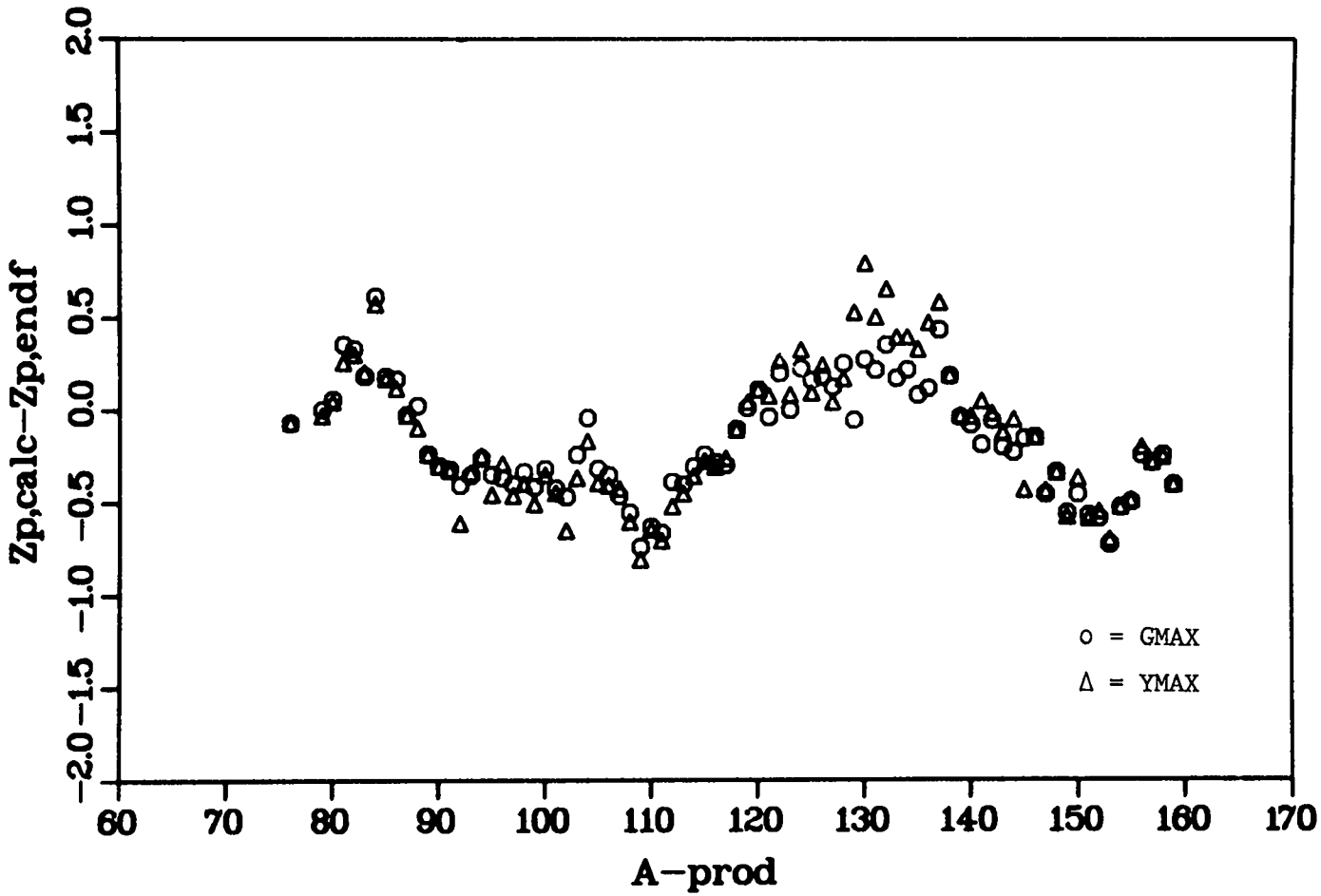

Figure 65: Deviation of Z_p values of data from Reference 8 from those computed assuming $\delta(A)$ parameters of Table 6 for the reaction $^{235}U(n_{th},f)$.

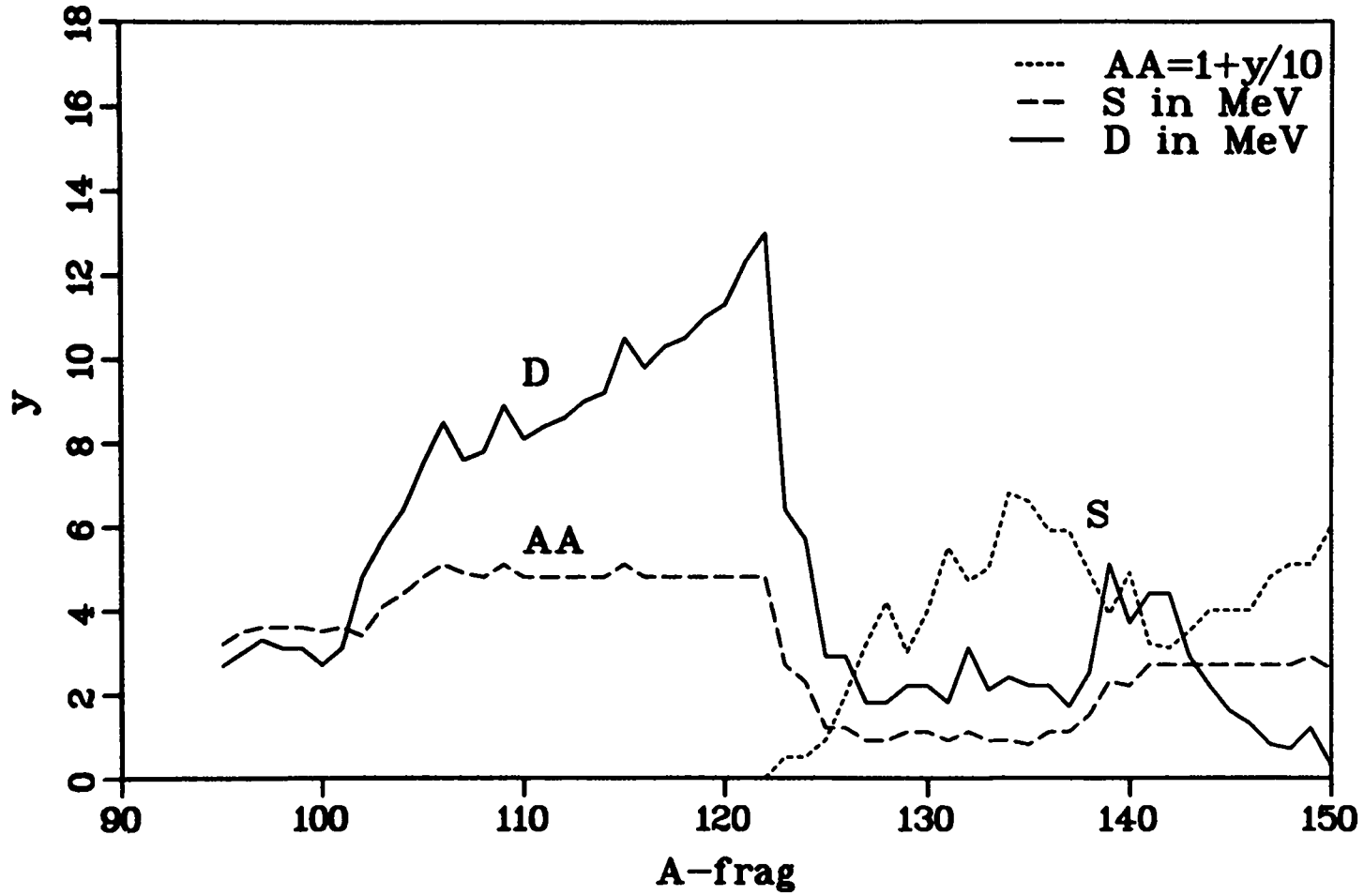

Figure 66: The deformation energy, D, total shell terms, S, and dimensionless semi-major axis length, AA, for $^{233}U(n_{th},f)$.

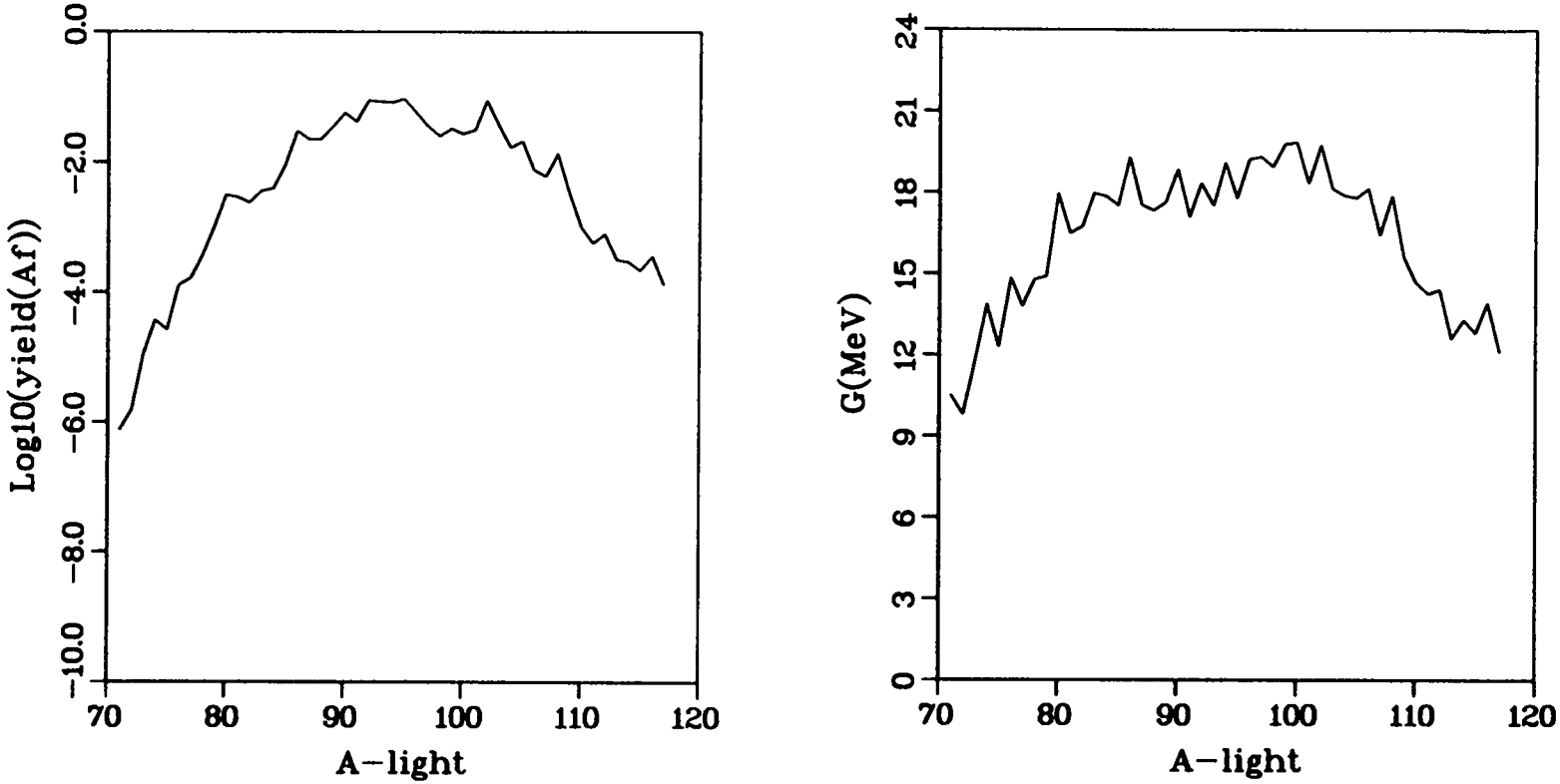

Figure 67: The fission fragment yield and G-energy for $^{233}U(n_{th},f)$.

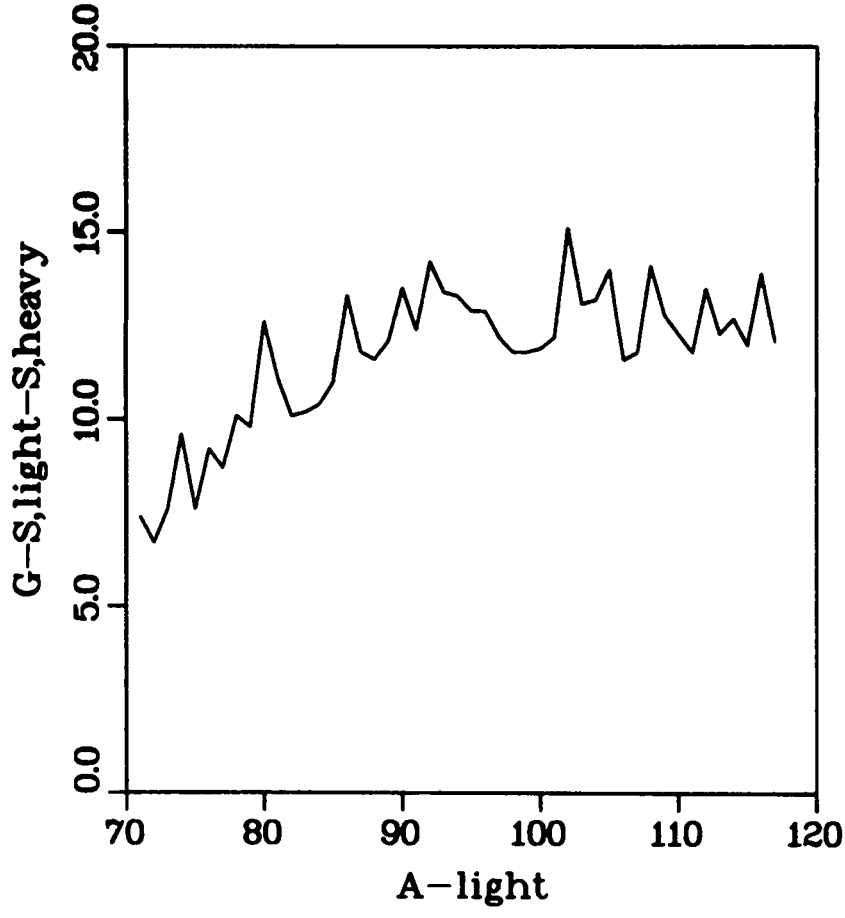

Figure 68: The G-energy shifted by the sum of the light and heavy fragment shell correction energies. These values are averaged over charge for fixed fragment mass.

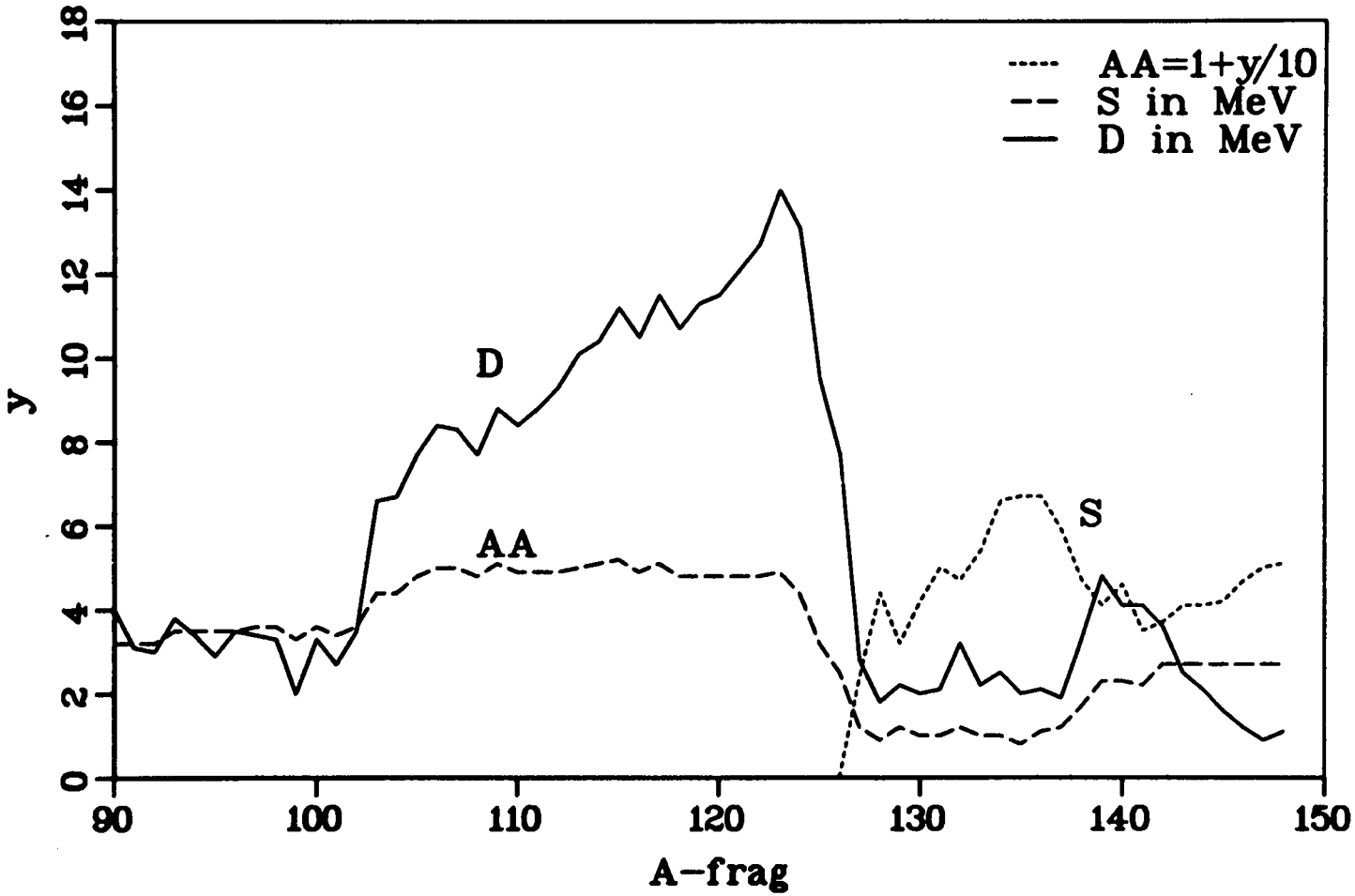

Figure 69: The deformation energy, D, total shell terms, S, and dimensionless semi-major axis length for $^{239}Pu(n_{th},f)$.

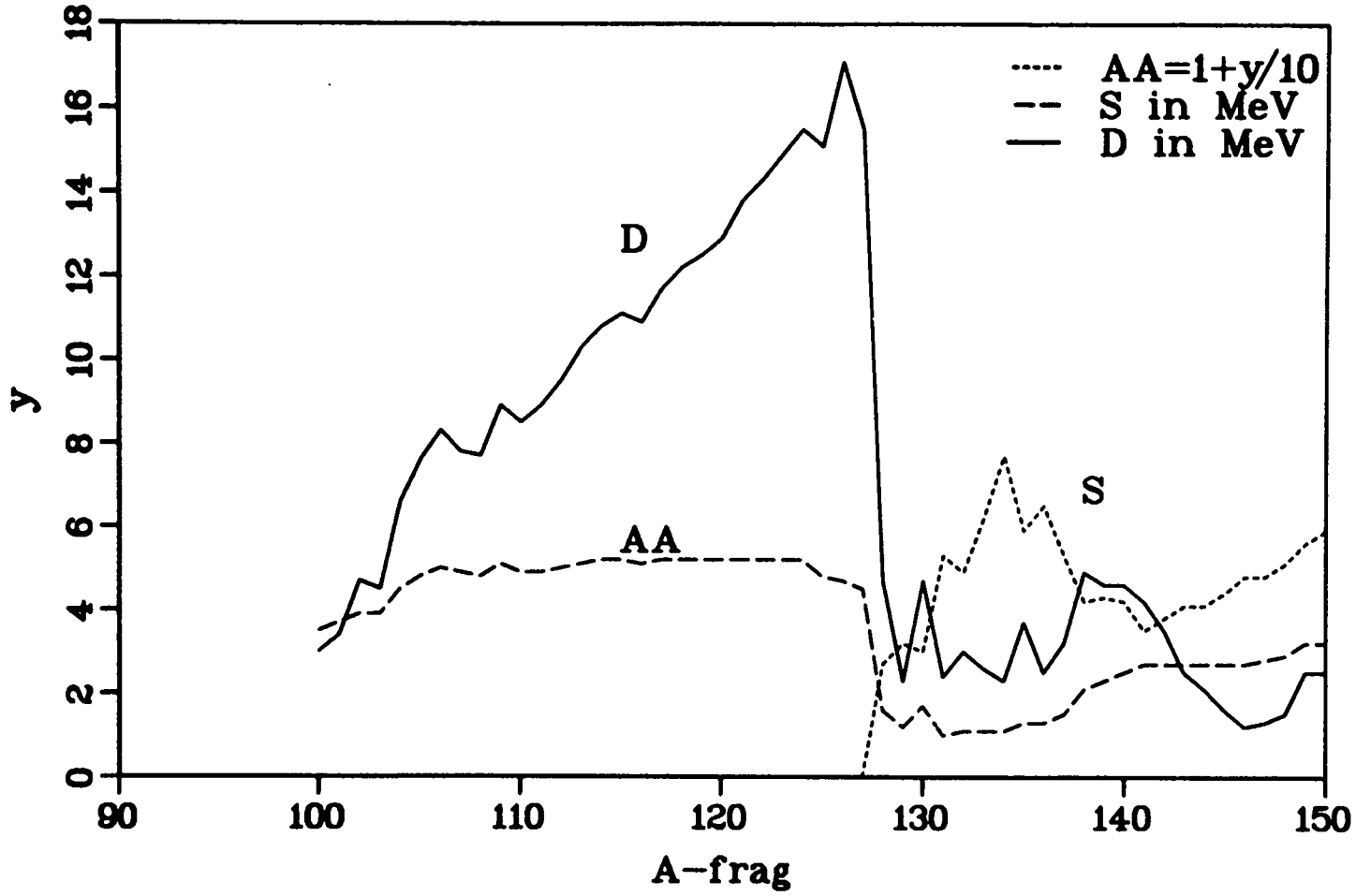

Figure 70: The deformation energy, D, total shell terms, S, and dimensionless semi-major axis length for ^{252}Cf(sf).

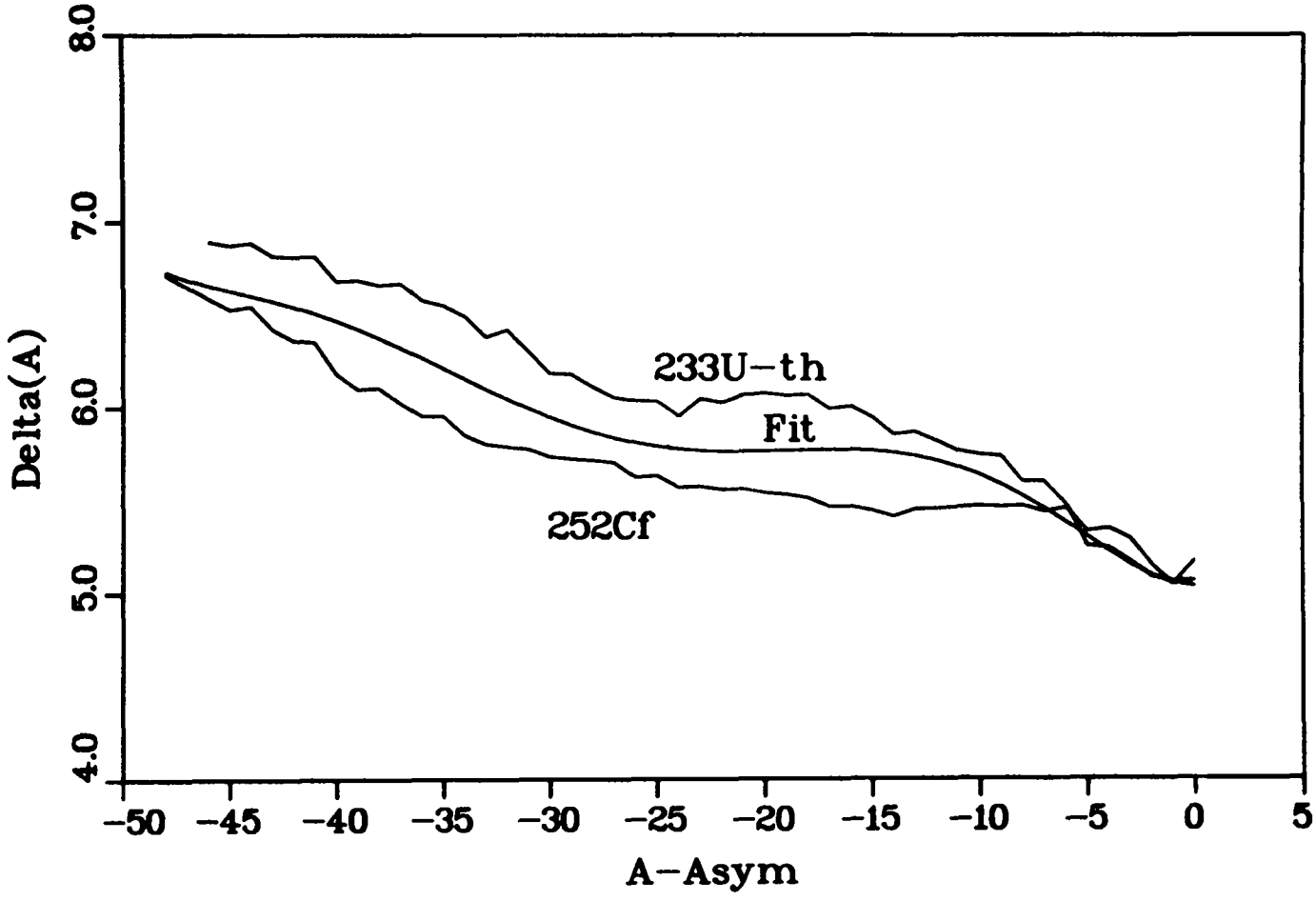

Figure 71: Comparison of the δ(A) formula of Table 9 with two of the input δ(A) sets of Table 6.

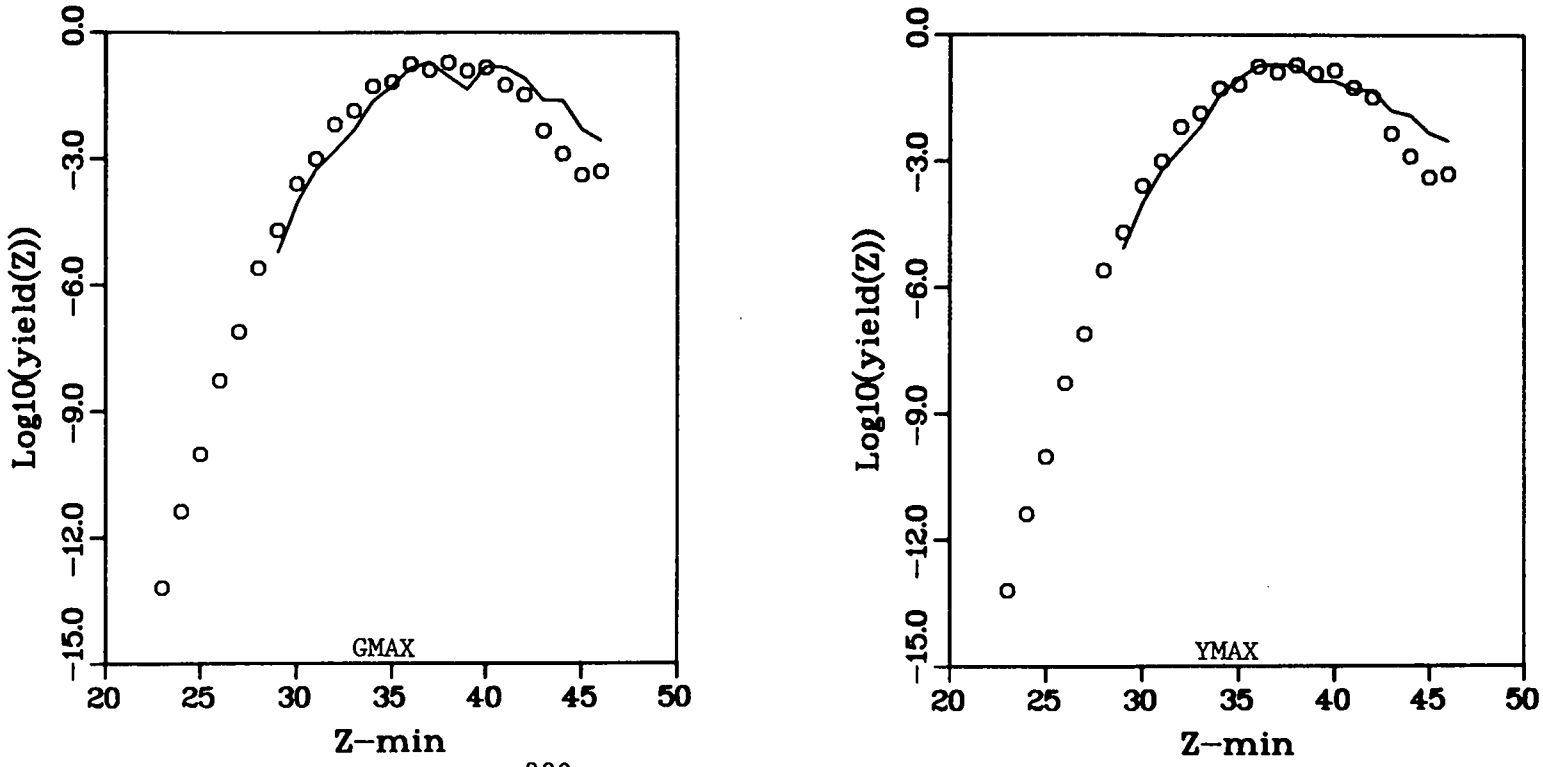

Figure 72: Charge yields for $^{233}U(n_{th},f)$ assuming $\delta(A)$ parameters of Table 9. Circles are measured yields from Reference 8. This calculation assumes 28.0 MeV constrained to remain in k_o.

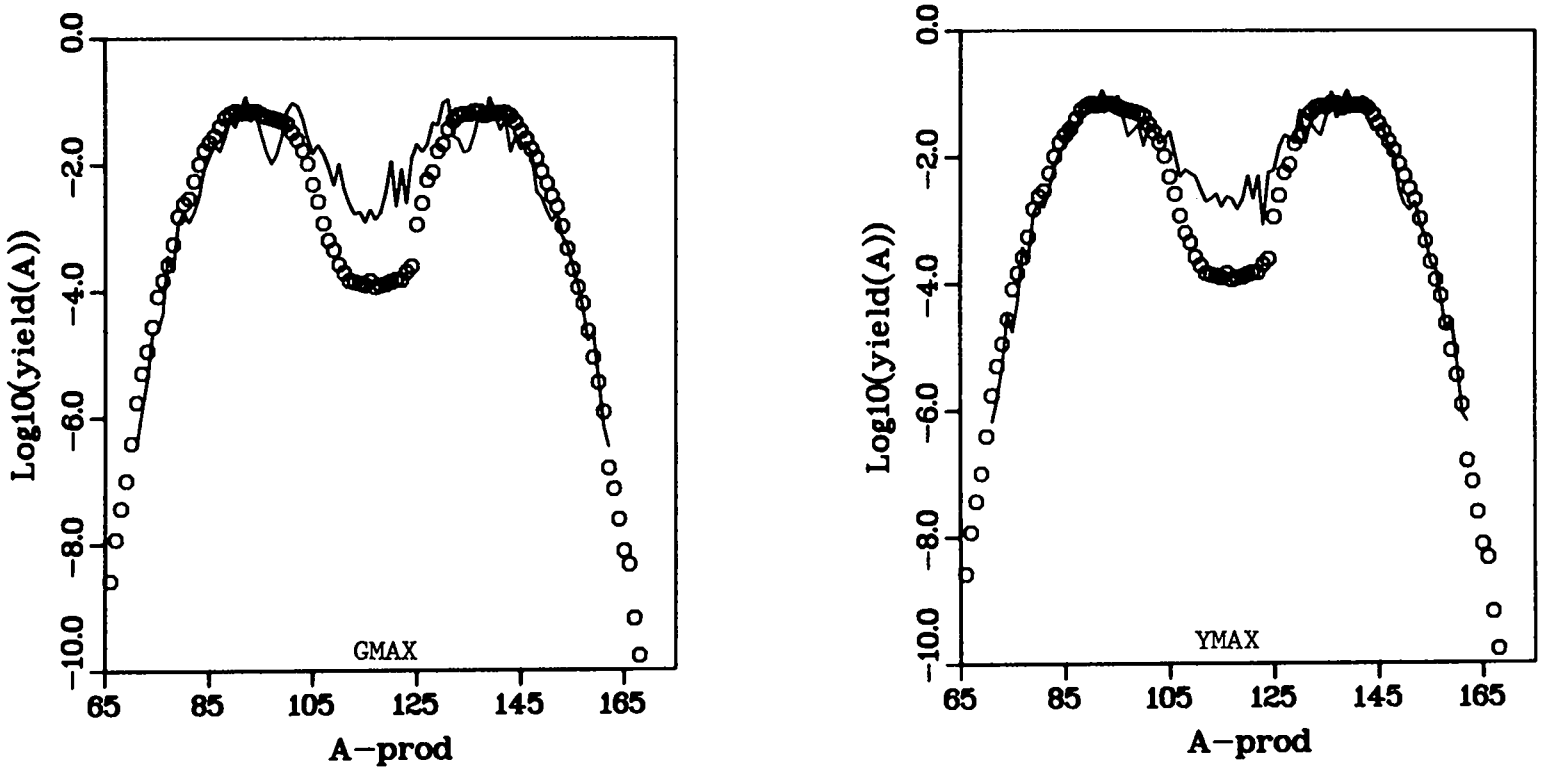

Figure 73: Fission product yields for $^{233}U(n_{th},f)$ assuming $\delta(A)$ parameters of Table 9. Circles are measured yields from Reference 8. This calculation assumes 28.0 MeV constrained to remain in k_o.

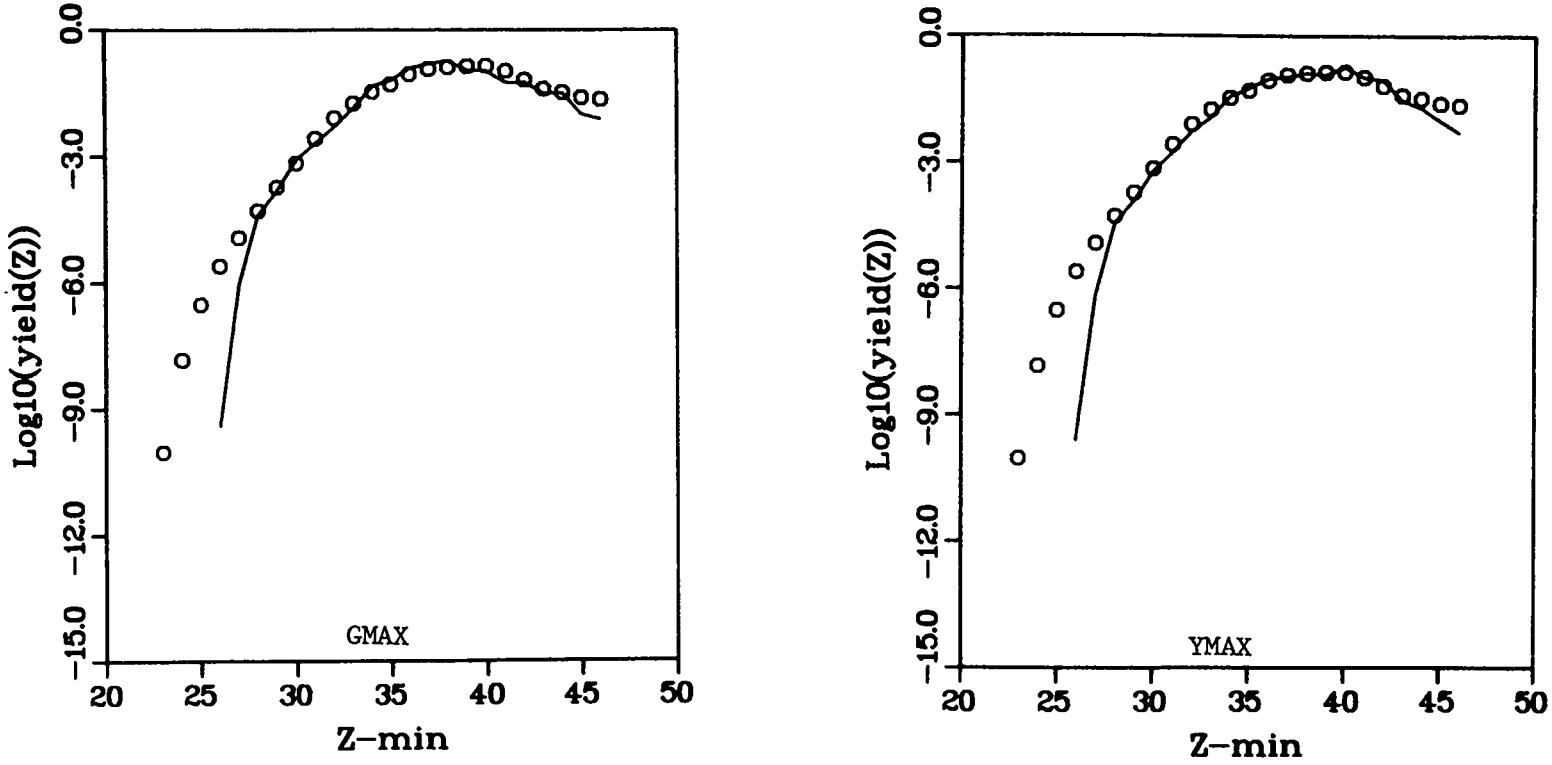

Figure 74: Charge yields for $^{238}U(n+14,f)$ assuming $\delta(A)$ parameters of Table 9. Circles are measured yields from Reference 8. This calculation assumes 25.2 MeV constrained to remain in k_o.

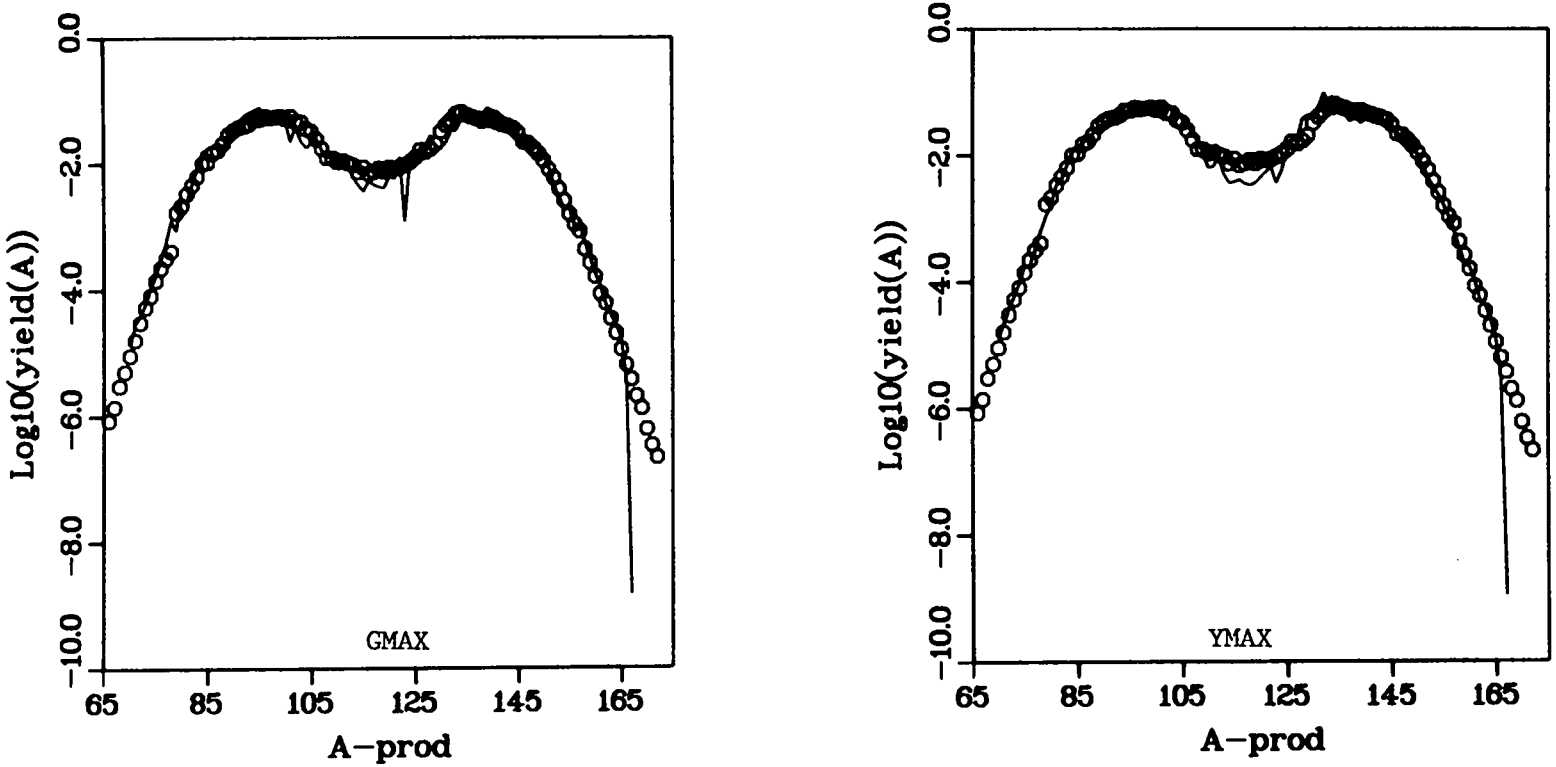

Figure 75: Fission product yields for $^{238}U(n+14,f)$ assuming $\delta(A)$ parameters of Table 9. Circles are measured yields from Reference 8. This calculation assumes 25.2 MeV constrained to remain in k_o

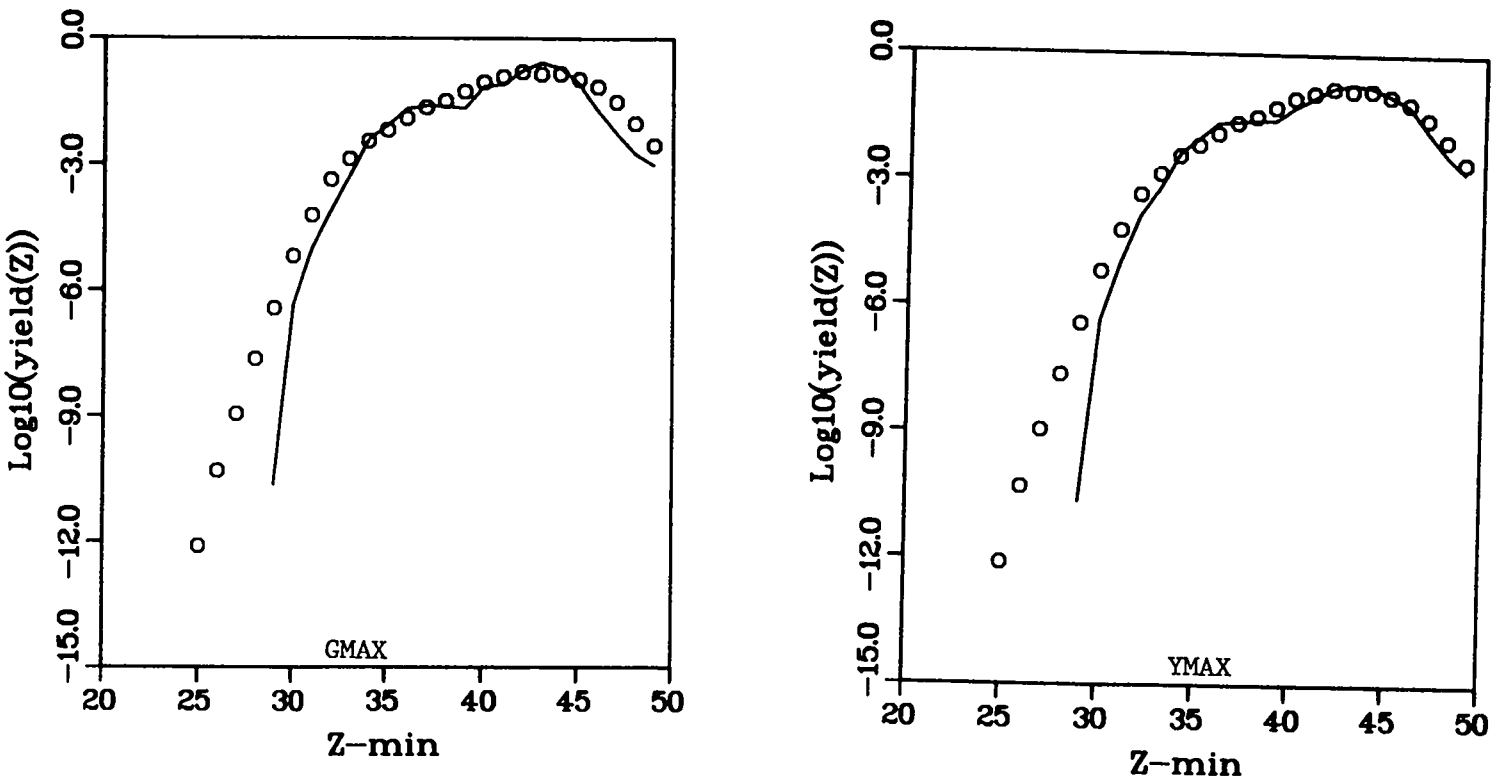

Figure 76: Charge yields for $^{252}Cf(sf)$ assuming $\delta(A)$ from Table 9. Circles are measured yields from Reference 8. This calculation assumes 27.0 MeV constrained to remain in k_o.

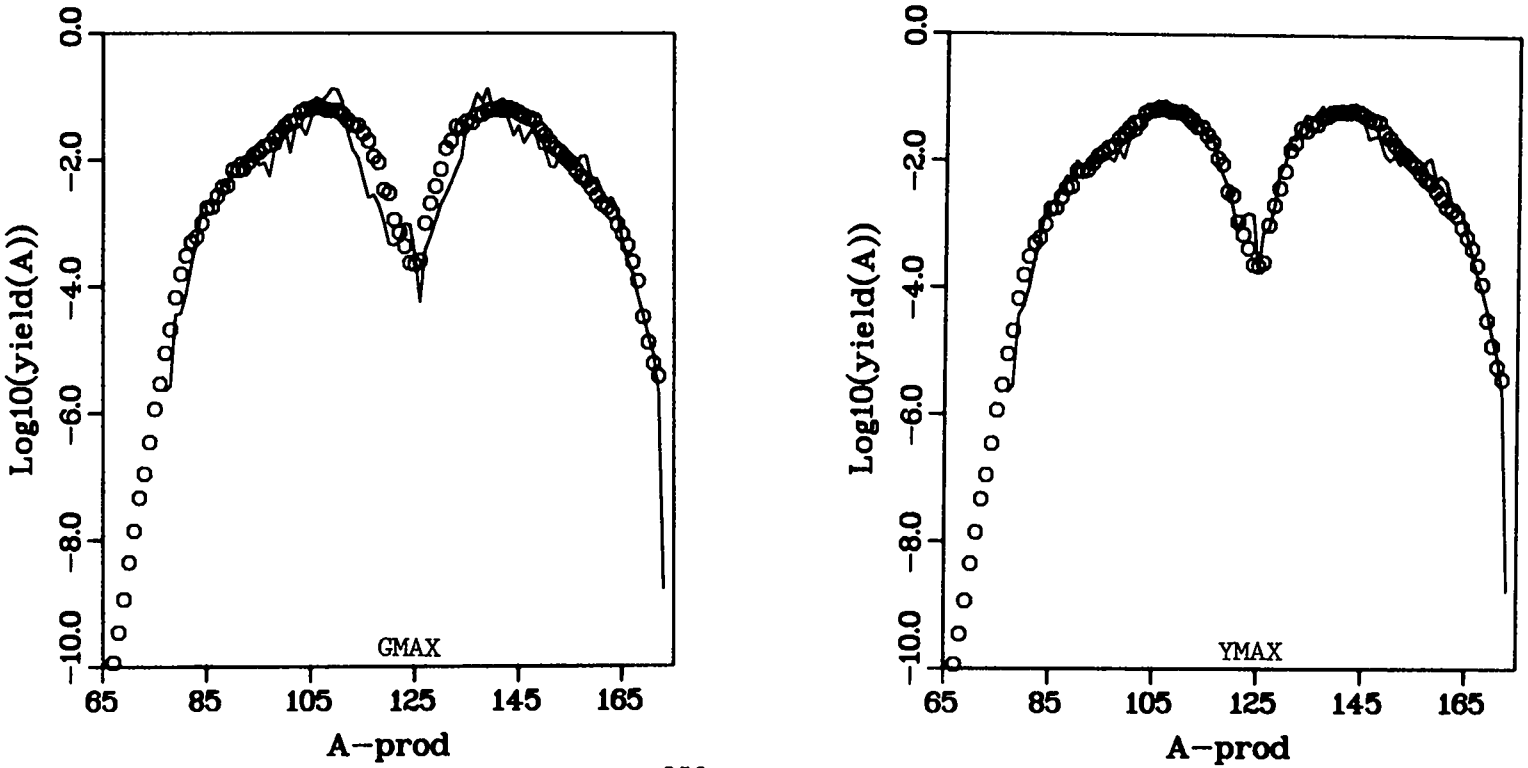

Figure 77: Fission product yields for ^{252}Cf(sf) assuming δ(A) from Table 9. Circles are measured yields from Reference 8. This calculation assumes 27.0 MeV constrained to remain in k_o.

REFERENCES

1. P. Fong, Statistical Theory of Nuclear Fission (Gordon and Breach, New York, 1969).

2. A. V. Ignatyuk, "Statistical Description of the Yields of the Fission Products," Yad. Fiz 9 (1969) 208.

3. H. Okamoto, H. Nakahara, and T. Nishi, "Statistical Calculation of Fission," J. Phys. Soc. Japan, 34 (1972) 588.

4. B. D. Wilkins, E. P. Steinberg, and R. R. Chasman, "Scission-point Model of Nuclear Fission Based upon Deformed Shell Effects," Phys. Rev. C14 (1976) 1832.

5. I. Kaplan, Nuclear Physics (Addison-Wesley, Reading, Mass., 1964).

6. E. Fermi, Nuclear Physics (University of Chicago Press, Chicago, 1974).

7. L. Wilets, Theories of Nuclear Fission (Clarendon Press, Oxford, 1964).

8. Fission Produce Decay Library of the Evaluated Nuclear Data File, Version V (ENDF/B-V), Los Alamos Scientific Laboratory unclassified release LA-UR-78-687, available from and maintained by the National Nuclear Data Center (NNDC) at Brookhaven National LAboratory.

9. P. A. Seeger and W. M. Howard, "Semi-empirical Atomic Mass Formula," Nucl. Phys. A238 (1975) 491.

10. K. Davies, A. Sierk, and J. R. Nix, "Effect of Viscosity on the Dynamics of Nuclear Fission," Phys. Rev. C13 (1976) 2385.

11. M. Sano and S. Yamasaki, "Phase Transition and Level Density of Atomic Nuclei," Prog. Theor. Phys. 29 (1963) 397.

12. L. G. Moretto, "Statistical Description of Deformation in Excited Nuclei and the Disappearance of Shell Effects with Excitation Energy," Nucl. Phys. A182 (1972) 641.

13. A. N. Behkami and J. R. Huizenga, "Comparison of Experimental Level Densities and Spin Cutoff Parameters with Microscopic Theory for Nuclei Near A=60," Nucl. Phys. A217 (1973) 78.

14. J. R. Huizenga, A. N. Behkami, J. S. Sventek, and R. W. Atcher, "Comparison of Neutron Resonance Spacings with Microscopic Theory for Spherical Nuclei," Nucl. Phys. A223 (1974) 577.

15. J. R. Huizenga, A. N. Nehkami, R. W. Atcher, J. S. Sventek, H. C. Britt, and H. Freiesleben, "Comparison of Neutron Resonance Spacings with Microscopic Theory for Nuclei with Static Deformation," Nucl. Phys. A223 (1974) 589.

16. H. A. Bethe, "An Attempt to Calculate the Number of Energy Levels of a Heavy Nucleus," Phys. Rev. 50 (1936) 332.

17. A. Gilbert and A. G. W. Cameron, "A Complete Nuclear Level Density Formula with Shell Corrections," Can. J. Phys. 43 (1965) 1446.

18. J. Cook, H. Ferguson, and A. Musgrove, "Nuclear Level Densities in Intermediate and Heavy Nuclei," Aust. J. Phys. 20 (1967) 477.

19. A. V. Ignatyuk, G. N. Smirenkin, and A. S. Tishin, "Phenomenological Description of the Energy Dependence of the Level Density Parameter," Sov. J. Nucl. Phys. 21 (1975) 255.

20 A. G. W. Cameron and P. J. Brancazio, "Relations Between Nuclear Levels Density Parameters and Shell Corrections," Can. J. Phys. 47 (1969) 1029.

21. S. K. Kataria, V. S. Ramamurthy, and S. S. Kapoor, "Semi-empirical Nuclear Level Density with Shell Effects," Phys. Rev. C18 (1978) 549.

22. P. G. Young and E. D. Arthur, "GNASH: A Preequilibrium Statistical Nuclear Model Code for Calculation of Cross Sections and Emission Spectra," Los Alamos Scientific LAboratory report LA-6947 (1977).

23. F. B. Hildebrand, Introduciton to Numerical Analysis (McGraw-Hill New York, 1974).

24. J. Janecke, "Updated Mass Predictions from the Garvey-Kelson Mass Relations," Atomic Data and Nuclear Data Tables 17 (1976) 455.

25. R. Sher, S. Fiarman, and C. Beck, "Fission Energy Release for 16 Fissioning Nuclides," unpublished (October 1976).

26. L. G. Moretto, Lawrence Berkeley Laboratory, personal communication.

27. K. Davies, S. Koonin, J. R. Nix, and A. Sierk, "Macroscopic and Microscopic Approaches to Nuclear Dissipation," Los Alamos Scientific Laboratory unpublished release LA-UR-75-5 (1975).

28. K. T. R. Davies, R. A. Managa, J. R. Nix, and A. J. Sierk, "Neck Rupture in Nuclear Fission," Phys. Rev. C16 (1977) 1890.

29. A. J. Sierk, S. E. Koonin, and J. R. Nix, "Modified One-Body Dissipation," Phys. Rev. C17 (1978) 646.

30. H. J. Krappe, J. R. Nix, and A. J. Sierk, "Unified Nuclear Potential for Heavy-Ion Scattering, Fusion, Fission, and Ground-State Masses and Deformation," Submitted to Phys. Rev. C.

31. A. J. Sierk, Los Alamos Scientific LAboratory, personal communication.

32. R. Vandenbosch and J. R. Huizenga, Nuclear Fission (Academic Press, New York, 1973).

33. H. G. Clerc, W. Lang, H. Wohlfarth, K. H. Schmitt, H. Schrader, K. E. Pferdenkaemper, and R. Jungman, "The Influence of Pairing and Nuclear Structure on the Thermal Neutron Induced Fission of ^{235}U," Institut fur Kernphysik, Technische Hochschule Darmstadt report IKDA 75/10 (1975).

34. R. B. Strittmatter, "Nuclide Yields for Thermal Fission of Uranium-235," Ph.D. Thesis, University of Illinois (1978).

35. D. G. Madland and T. R. England, "The Influence of Pairing on the Distribution of Independent Yield Strengths in Neutron-Induced Fission," Los Alamos Scientific Laboratory report LA-6430-MS (ENDF-240) (1976).

36. C. F. von Weisaecker, "Zur Theorie der Kernmassen," Z. Physik 96 (1935) 29.

37. W. D. Meyers and W. J. Swiatecki, "Nuclear Masses and Deformation," Nucl. Phys. 81 (1966) 1.

38. V. M. Strutinsky, "Shell Effects in Nuclear Masses and Deformations," Nucl. Phys. A95 (1967) 420.

39. J. Bardeen, L. N. Cooper, and J. R. Schrieffer, "Theory of Superconductivity," Phys. Rev. 108 (1957) 1175.

40. J. R. Nix, "Calculation of Fission Barriers in Heavy and Superheavy Nuclei," Annu. Rev. Nucl. Sci. 22 (1972) 66.

41. B. Nilsson, "Inclusion of a P -term in the Deformed Shell Model Potential," Nucl. Phys. A129 (1969) 445.

42. R. W. Hasse, "Studies in the Shape Dependence of the Droplet Model of Nuclei," Ann. Phys. (N.Y.) 68 (1971).

43. A. H. Wapstra and N. B. Gove, "The 1971 Mass Evaluation," Nucl. Data Tables 9 (1971) 265.

44. K. Aleklett, "Total β-decay Energies and Atomic Masses in Regions Far from β-stability," Chalmers Teknisha Hoegskols, Goetenborg (Sweden) Instituitionen foer Fysik report INIS-3836 (1977).

45. H. V. Groote, E. Hilfe, and K. Takehashi, "A New Semi-empirical Shell Correction to the Droplet Model," Atomic Data and Nucl. Data Tables 17 (1976) 418.

46. W. D. Myers, "Development of the Semi-empirical Droplet Model," Atomic Data and Nucl. Data Tables 17 (1976) 411.

47. M. Epherre, G. Audi, C. Thibault, R. Klapisch, G. Huber, F. Touchard, and H. Wollnik, "Direct Measurement of the Masses of Rubidium and Cesium Isotopes Far from Stability," Phys. Rev. C19 (1979) 1504.

48. J. R. Nix, Los Alamos Scientific Laboratory, personal communication.

49. P. A. Seeger, Los Alamos Scientific Laboratory, personal communication.

50. A. H. Wapstra and K. Bos, "A 1975 Midstream Atomic Mass Evaluation," Atomic Data and Nucl. Data Tables 17 (1976) 474.

51. J. O. Hirschfelder, C. F. Curtiss, and R. B. Bird, Molecular Theory of Gases and Liquids (John Wiley and Sons, New York, 1964).

52. J. R. Nix, "Studies in the Liquid-Drop Theory of Nuclear Fission," Ph.D. Thesis, University of California (1964).

53. M. Braak, J. Samgaard, A. S. Jensen, H. C. Pauli, V. M. Strutinsky, and C. Y. Wong, "Funny Hills: The Shell Correction Approach to Nuclear Shell Effects and Its Application to the Fission Process," Rev. Mod. Phys. 44 (1972) 320.

54. E. O. Fiset and J. R. Nix, "Calculation of Half-lives for Superheavy Nuclei," Nucl. Phys. A193 (1972) 647.

55. P. Armbruster, H. Labes, and K. Reichelt, "Investigation of the Primary Spins of the ^{235}U Fission Fragments," Z. Naturforsch 26 (1971) 512.

56. D. C. Aumann, W. Gueckel, E. Nirschl, and H. Zeising, "Independent Isomeric Yield Ratio of ^{148}Pm in Fission of teh Moderately Excited ^{236}U Compound Nucleus as A Measurement of Fragment Angular Momentum," Phys. Rev. C16 (1977) 254.

57. V. M. Strutinsky, "Angular Anisotropy of Gamma Quanta that Accompany Fission," J. Exp. Theor. Phys. (U.S.S.R.) 37 (1959) 861.

58. A. Bohr and B. R. Mottelson, Nuclear Structure (W. A. Benjamin, Reading, Mass., 1975).

59. G. P. Ford, "Calculation of Nuclear Level Densities for ^{56}Fe, ^{59}Co, ^{60}Ni, ^{61}Cu, ^{62}Ni, ^{63}Cu, and ^{65}Cu," Nucl. Sci. Eng. 66 No. 3 (1978) 334.

60. S. G. Nilsson, C. F. Tsang, A. Sobiczewski, Z. Zsmanski, S. Wycech, C. Gustafson, I. Lamm, P. Moeller, and B. Nilsson, "On the Nuclear Structure and Stability of Superheavy Elements," Nucl. Phys. A131 (1969) 1.

61. A. G. W. Cameron and R. M. Elkin, "Role of the Symmetry Energy in Atomic Mass Formulas," Can. J. Phys. 43 (1965) 1288.

62. N. R. Draper and H. Smith, Applied Regression Analysis (John Wiley and Sons, New York, 1966).

63. Y. Bard, Nonlinear Parameter Estimation (Academic Press, New York 1974).

☆ U.S. Government Printing Office: 1979 — 677—115/202

Printed in the United States of America. Available from
National Technical Information Service
US Department of Commerce
5285 Port Royal Road
Springfield, VA 22161

Microfiche $3.00

001-025	4.00	126-150	7.25	251-275	10.75	376-400	13.00	501-525	15.25
026-050	4.50	151-175	8.00	276-300	11.00	401-425	13.25	526-550	15.50
051-075	5.25	176-200	9.00	301-325	11.75	426-450	14.00	551-575	16.25
076-100	6.00	201-225	9.25	326-350	12.00	451-475	14.50	576-600	16.50
101-125	6.50	226-250	9.50	351-375	12.50	476-500	15.00	601-up	

Note: Add $2.50 for each additional 100-page increment from 601 pages up.